

# Role of mitochondrial morphology and metabolism in the regulation of cancer cell migration

Thesis submitted as requirement for the degree of  
Doctor of Philosophy  
**School of Biological Sciences**

Khatab R. Mawlood  
January 2019

**Declaration**

I confirm that this is my own work and the use of all material from other sources has been properly and fully acknowledged.

Signed: .....



## **Abstract**

Cancer metastasis is responsible for 90% of cancer deaths. It is well known that metabolic reprogramming, which is one of the hallmarks of cancer, plays an important role in increasing cancer cell migration and metastasis. Changes in mitochondrial morphology are thought to affect their function; however the mechanism is still unclear. Moreover, it is not known whether changes in mitochondrial morphology and their metabolism can affect cell migration or not. The overall aim of this study was to investigate the link between mitochondrial morphology and their metabolism with cancer cell migration.

Several factors such as different glucose levels, PGC-1 $\alpha$  activator, hydrogen peroxide, and anti-metabolic agents that can affect mitochondrial morphology has been used to investigate the effect of mitochondrial morphologic changes on their metabolism and cell migration. Furthermore, p66shc and TRAP1, the function of which are related to mitochondria, have been identified as novel components related to reprogramming metabolism and cell migration. Using confocal and time-lapse microscopy, as well as through measuring ATP production, lactate production, and estimation of ROS generation in MDA-MB-231 breast cancer cells, HT1080 fibrosarcoma cells, and HeLa cells.

This study has been found that mitochondria fragmentation induces metabolic reprogramming from oxidative phosphorylation to glycolysis, due to reducing mitochondrial inner membrane surface area which required for mitochondrial oxidative phosphorylation enzyme activity, which in turn led to increases in cancer cell migration. Inhibition of mitochondrial fragmentation using a mitochondrial division-1 inhibitor has led to significant decreases in glycolysis and cell migration.

This study has also shown that the function of pro-apoptotic p66shc and cytoprotective TRAP1 are correlated strongly to each other. Increasing the expression of p66shc can trigger metabolic reprogramming and enhance cancer cell migration, whereas, increasing TRAP1 expression inhibits apoptosis, which can be induced by activated p66shc.

In conclusion, mitochondrial fragmentation can alter cancer cell metabolism to glycolysis and activated p66shc is a main cause of this metabolic reprogramming, which controls cancer cell migration. In addition, TRAP1 and mitochondrial fragmentation can increase resistance to apoptosis induced by oxidative stress. This finding could be exploited in the development of new therapy for cancer treatment.

## Acknowledgements

I would like to start by express my profound gratitude to my supervisor Assoc. prof. Dr. Phil Dash for the patient guidance, support, encourages and advice he has provided throughout my time as his student. I have been extremely lucky to have a supervisor who cared so much about my work, and who responded to my questions and queries so promptly, this work would not have been possible without his inestimable help.

I would also like to thank all the members of staff at University of Reading who helped me. In particular I would like to thank my past lab members, Dr. Godwin Ponuwei, Dr. Kelsey Huang, Dr. Dhurgham Al-Fahad, and my current lab members: Miss Ana Wass, Mr Jonathan Rudge, Mr. Bander Al-Harbi and Mr. Salem Al-Harhi, as well as technical staff, Mrs Hong Lin, Mrs Hilary Loxton, and Dr. Graham Luke.

Appreciation is extended to the Ministry of Higher Education and Scientific Research / University of Soran, for the help and support during the study period.

I would like to extend my special thanks to my sponsor, the Higher Committee for Education Development in Iraq (HCED). Without their financial support and immediate help for different problems I encountered, this work would not have been achievable.

In closing, I would like to single out my dearest wife and my lovely children, Sara, Ghada, and Mohammed, for their understanding, patience and tremendous support during this study.

## Table of Contents

<b>Contents</b>	<b>Page</b>
Abstract.....	III
Acknowledgements.....	VI
Table of Contents.....	VII
List of Figures.....	XII
List of Tables.....	XVII
List of Abbreviations.....	XVIII
<b>Chapter One: General Introduction</b>	
1.1 Cancer .....	1
1.2 Cancer Metastasis.....	6
1.3 Cell Migration.....	7
1.4 Mitochondria.....	9
1.4.1 Mitochondrial structure and morphology.....	9
1.4.2 Mitochondrial dynamics.....	11
1.4.3 Mitochondrial morphology and function.....	12
1.4.4 Mitochondrial biogenesis.....	14
1.4.5 Mitochondrial mitophagy.....	14
1.4.6 Effect of glucose level on mitochondrial morphology .....	16
1.4.7 Effect of H <sub>2</sub> O <sub>2</sub> on mitochondrial morphology .....	17
1.4.8 Effect of PGC-1 $\alpha$ on mitochondrial morphology.....	17
1.4.9 Role of mitochondria in apoptosis.....	18
1.4.10 Inhibition of mitochondrial fragmentation with mdivi-1.....	24
1.5 Cancer cell metabolism.....	26
1.5.1 Aerobic glycolysis.....	26
1.5.2 Pentose phosphate pathway and its role in antioxidant response....	28
1.5.3 Targeting glycolysis with 3-Bromopyruvic acid.....	31
1.5.4 Oxidative phosphorylation in cancer cells.....	32
1.5.5 Targeting oxidative phosphorylation with Antimycin A.....	33
1.6 Pro-apoptotic protein p66shc.....	35
1.7 Role of p66shc in cancer cell metabolism and cell migration .....	38
1.8 Role of cytoprotective TRAP1 protein in cancer cells .....	39
1.9 Role of TRAP1 in cancer cells metabolism and cell migration.....	41
1.10 Link between p66shc and TRAP1.....	42
1.11 Effect of microenvironment on the mitochondrial morphology .....	42

1.12	Aim of the study.....	44
<b>Chapter Two: Material and Methods</b>		
2.1	Materials.....	46
2.1.1	Reagent and Kits.....	46
2.1.2	Preparation of stock solutions.....	49
2.2	Methods.....	49
2.2.1	Cell culture.....	49
2.2.2	Counting cells.....	50
2.2.3	Preparing cell lysates.....	50
2.2.4	Bradford Protein Assay.....	51
2.2.5	Sodium Dodecyl Sulphate-Polyacrylamide Gel Electrophoresis (SDS-PAGE) / Western Blot Analysis.....	53
2.2.5.1	Protein Running.....	53
2.2.5.2	Preparation of SDS-PAGE.....	54
2.2.5.3	SDS-PAGE buffers and reagents.....	55
2.2.6	Preparing collagen coated surfaces.....	56
2.2.7	Mitochondrial Staining.....	56
2.2.8	Immunostaining.....	57
2.2.9	Gene Knockdown with siRNA.....	58
2.2.10	Quantitative Real- Time PCR (qRT-PCR).....	58
2.2.11	Cell viability assay (MTT assay).....	60
2.2.12	Quantification of Reactive Oxygen Species (ROS).....	61
2.2.13	Quantification of L-Lactate production (Glycolysis).....	62
2.2.14	Quantification of ATP production.....	63
2.2.15	Time-lapse microscopy analysis.....	64
2.2.16	Confocal microscopy analysis.....	64
2.2.17	Measuring cancer cell migration.....	65
2.2.18	Measuring apoptosis.....	66
2.2.19	Quantifying p66shc.....	67
2.2.20	Statistical analysis.....	68
<b>Chapter Three: Investigating the impact of glucose levels on mitochondrial dynamics, metabolism, and cell migration in MDA-MB-231 cells</b>		
3.1	Introduction.....	69
3.2	Material and methods.....	74
3.2.1	Cell culture.....	74

3.2.2	Mitochondrial staining.....	74
3.2.3	Confocal microscopy images analysis.....	75
3.2.4	Quantitative Real- Time PCR (qRT-PCR).....	76
3.2.5	Western blot analysis.....	76
3.2.6	Measurement of glycolysis activity.....	76
3.2.7	Measurement of ATP.....	77
3.2.8	Measurement of intracellular ROS.....	78
3.2.9	Wound Healing Assay.....	78
3.2.10	Cell migration.....	79
3.3	Results.....	80
3.3.1	Effect of glucose level on the mitochondrial dynamics, metabolism, and cell migration.....	80
3.3.2	Effect of H <sub>2</sub> O <sub>2</sub> on mitochondrial dynamics, metabolism, and cell migration.....	91
3.3.3	Effect of inhibition mitochondrial fragmentation on mitochondrial metabolism, and cell migration.....	101
3.4	Discussion.....	109
3.4.1	Glucose levels affect mitochondrial morphology, metabolism, and cell migration.....	109
3.4.2	Hydrogen peroxide induces mitochondria fragmentation, changes metabolism, and increases cell migration.....	114
3.4.3	Mitochondrial division-1 inhibitor decreases mitochondrial fragmentation, glycolysis, and cell migration.....	116
 <b>Chapter Four: Investigating the impact of PGC-1<math>\alpha</math> on mitochondrial dynamics, cellular metabolism, and cell migration</b>		
4.1	Introduction.....	120
4.2	Material and Methods.....	122
4.2.1	Cell culture.....	122
4.2.2	Mitochondrial staining and analysis.....	122
4.2.3	Quantitative Real- Time PCR (qRT-PCR).....	122
4.2.4	Analysis of metabolism and ROS.....	123
4.2.5	Western blot analysis.....	123
4.2.6	Cell migration.....	123
4.3	Results.....	124
4.4	Discussion.....	148

## **Chapter Five: Investigating the effect of metabolism on mitochondrial dynamics and cell migration**

5.1	Introduction.....	158
5.1.1	Targeting glycolysis with 3-bromopyruvate.....	158
5.1.2	Targeting oxidative phosphorylation with Antimycin A.....	159
5.2	Material and Methods.....	159
5.2.1	Cell culture.....	159
5.2.2	Mitochondrial staining and analysis.....	160
5.2.3	Quantitative Real- Time PCR (qRT-PCR).....	160
5.2.4	Analysis of metabolism and ROS.....	160
5.2.5	Cell migration .....	160
5.3	Results.....	161
5.4	Discussion.....	174

## **Chapter Six: Role of p66shc and TRAP1 proteins in cancer cell migration.**

6.1	Introduction.....	180
6.2	Materials and Methods.....	184
6.2.1	Materials.....	184
6.2.2	Cell culture.....	184
6.2.3	siRNA Transfection.....	185
6.2.4	Immunostaining.....	186
6.2.5	Quantitative Real- Time PCR (qRT-PCR).....	186
6.2.6	Analysis of metabolism and ROS.....	187
6.2.7	Western Blotting.....	187
6.2.8	Apoptosis.....	187
6.2.9	Cell migration.....	187
6.3	Results.....	188
6.3.1	P66shc and TRAP1 gene silencing efficiency.....	188
6.3.2	Effect of silencing p66shc and/or TRAP1 genes on the activation p66shc in MDA-MB-231 cell.....	194
6.3.3	Effect of silencing p66shc and/or TRAP1 genes on apoptosis in MDA-MB-231 cells.....	196
6.3.4	Effect of silencing p66shc and/or TRAP1 genes on the intracellular ROS production.....	197
6.3.5	Effect of silencing p66shc and/or TRAP1 genes on cellular metabolism.....	199

6.3.6	Effect of silencing p66shc and/or TRAP1 genes on the cancer cell migration.....	204
6.4	Discussion.....	206
<b>Chapter Seven: Investigation role of mitochondria in 3D migration using Collagen gels, decellularised lung tissue, and Alvetex</b>		
7.1	Introduction.....	213
7.1.1	Collagen I gel as 3D cell culture.....	214
7.1.2	Alvetex scaffold as 3D cell culture.....	215
7.1.3	Decellularised lung tissue as 3D cell culture.....	216
7.2	Aim.....	216
7.3	Material and methods.....	217
7.3.1	3D collagen I gel cell culture.....	217
7.3.2	3D Alvetex cell culture.....	218
7.3.3	Decellularised lung tissue as 3D cell culture.....	219
7.4	Results.....	222
7.4.1	Impact of the glucose levels on the mitochondrial number in 3D cell culture.....	222
7.4.2	Impact of the glucose level on the mitochondrial dynamics in 3D cell culture.....	224
7.4.3	Impact of mitochondrial dynamics on 3D cell migration in MDA-MB-231.....	228
7.4.4	Impact of the mitochondrial division inhibitor on 3D cell migration	229
7.5	Discussion.....	230
<b>Chapter Eight: General Discussion</b> .....		
<b>References</b> .....		
		246

## List of Figures

### Chapter 1

	<b>Page</b>
Figure 1.1: The Hallmarks of cancer	2
Figure 1.2: Emerging hallmarks and enabling characteristics	2
Figure1.3: Sequential events of the metastatic cascade	7
Figure 1.4: Mechanism of cell migration	8
Figure 1.5: Basic mitochondrial structure	10
Figure 1.6: Mitochondrial fission and fusion	13
Figure 1.7: Mitochondrial morphology and activity depending on the conditions	15
Figure 1.8: Mitophagy process	16
Figure 1.9: Death receptor and mitochondrial pathways of apoptosis	22
Figure 1.10: Role of mitochondrial morphology in apoptosis	24
Figure 1.11: Mechanism of mdivi-1 inhibitor effect	25
Figure1.12: Aerobic glycolysis	27
Figure 1.13: A schematic representation shows the pentose phosphate pathway and it crosslink with glycolysis.	30
Figure 1.14: Scheme representation shows the role of NADPH in reducing of oxidized glutathione GSSG by glutathione reductase	30
Figure 1.15: Target site of Antimycin A in Electron Transport Chain	34
Figure 1.16: Organization of Shc A isoforms	35
Figure 1.17: Mechanism of p66shc activation and translocation to mitochondria	37
Figure 1.18: CypD control mitochondrial permeability transition pore opening	40

### Chapter 2

Figure 2.1: Data sheet shows a standard 96 well plate	52
Figure 2.2: Standard curve for protein with known concentrations and absorbance	52
Figure 2.3: Agarose gel electrophoresis	60

Figure 2.4: Yellow colour MTT tetrazolium changed to purple colour formazan in metabolic active cells	61
Figure 2.5: Mechanism of quantification intracellular ROS	62
Figure 2.6: Mechanism of L-Lactate quantification	63
Figure 2.7: Micrographs showing wound healing in MDA-MB-231 cells	66
Figure 2.8: Morphological changes of apoptotic cells enable differentiating them from other cells	67
<b>Chapter 3</b>	
Figure 3.1: Mechanism of inducing mitochondrial fragmentation in high glucose level	70
Figure 3.2: The illustration shows principle of glycolysis assay kit	77
Figure 3.3: Effect of glucose level on mitochondrial fragmentation in MDA-MB-231 cells	81
Figure 3.4: Micrographs showing the mitochondrial morphology	82
Figure 3.5: Quantification of mtDNA copy number in MDA-MB-231 cells grown in different glucose levels	83
Figure 3.6: Western blot showing the effect of glucose levels on the Drp1 protein expression in MDA-MB-231	84
Figure 3.7: Quantitation of ATP in MDA-MB-231 cells grown in different glucose levels	85
Figure 3.8: Lactate generation in MDA-MB-231 cells grown in different glucose levels	86
Figure 3.9: Wound healing assay to evaluate MDA-MB-231 cell migration in different glucose levels	87
Figure 3.10: Wound healing assay Micrographs showing the MDA-MB-231 cells under the effect of different glucose levels in DMEM medium	88
Figure 3.11: Impact of different glucose levels on cell migration in MDA-MB-231 cells	89
Figure 3.12: Reactive oxygen species (ROS) in MDA-MB-231 cells in different glucose levels	90
Figure 3.13: MTT assays showing the effect of H <sub>2</sub> O <sub>2</sub> on the cell viability in MDA-MB-231 cells	91

Figure 3.14: Effect of hydrogen peroxide (H <sub>2</sub> O <sub>2</sub> ) on mitochondrial fragmentation in MDA-MB- 231 cells	93
Figure 3.15: Micrographs showing the mitochondrial shape in MDA-MB-231 cells	94
Figure 3.16: Quantification of mtDNA copy number in MDA-MB-231 cells treated with different concentrations of H <sub>2</sub> O <sub>2</sub>	95
Figure 3.17: Effect of H <sub>2</sub> O <sub>2</sub> on ATP generation in MDA-MB-231cells	96
Figure 3.18: Effect of H <sub>2</sub> O <sub>2</sub> on lactate production in MDA-MB-231 cells	96
Figure 3.19: Wound healing assay of MDA-MB-231 cells treated with hydrogen peroxide (H <sub>2</sub> O <sub>2</sub> )	97
Figure 3.20: Wound healing assay Micrographs showing the MDA-MB-231 cells treated with hydrogen peroxide (H <sub>2</sub> O <sub>2</sub> )	98
Figure 3.21: Effect of Hydrogen peroxide (H <sub>2</sub> O <sub>2</sub> ) on the cell migration in MDA-MB-231 cells	99
Figure 3.22: Effect of H <sub>2</sub> O <sub>2</sub> on generation of Reactive oxygen species (ROS) in MDA-MB-231cells	100
Figure 3.23: Mechanism of mitochondrial fragmentation inhibition by Mdivi-1 inhibitor	101
Figure 3.24: Effect of mdivi-1 inhibitor on the mitochondrial morphology in MDA-MB-231 cells	103
Figure 3.25: Micrographs showing the effect of mdivi-1 inhibitor on the mitochondrial morphology in MDA-MB-231 cells	104
Figure 3.26: Quantification of mtDNA copy number in MDA-MB-231 cells treated with mdivi-1 inhibitor	105
Figure 3.27: Effect of mdivi-1 inhibitor on ATP production in MDA-MB-231 cell	106
Figure 3.28: Effect of mdivi-1 inhibitor on lactate production in MDA-MB-231 cell	106
Figure 3.29: Effect of mdivi-1 inhibitor on the ROS production in MDA-MB-231 cells	107
Figure 3.30: Impact of mdivi-1inhibitor on the cell migration in MDA-MB-231	108

## **Chapter 4**

Figure 4.1: Effect of ZLN005 on the mitochondrial dynamics in MDA-MB-231 cells	125
--	-----

Figure 4.2: Micrographs shows the changes in the mitochondrial morphology in MDA-MB-231 cells	126
Figure 4.3: Effect of ZLN005 on the mitochondrial morphology in MDA-MB-231 cells grown in low glucose medium	128
Figure 4.4: Micrographs showing mitochondrial hyper-fragmentation in MDA-MB-231 cells	129
Figure 4.5: Effect of ZLN005 on mitochondrial dynamics in MDA-MB-231 cell grown in high glucose level	131
Figure 4.6: Micrographs showing mitochondrial hyper-fragmentation in MDA-MB-231 cells	132
Figure 4.7: Quantification of mtDNA copy number in MDA-MB-231 cells treated ZLN005	134
Figure 4.8: Western blot showing the effect of ZLN005 on the PGC-1 $\alpha$ and Drp1 proteins expression	138
Figure 4.9: Effect of ZLN005 on ATP production in MDA-MB-231 cells	141
Figure 4.10: Effect of ZLN005 on lactate production in MDA-MB-231 cells	143
Figure 4.11: Effect of ZLN005 on the ROS production in MDA-MB-231 cells	145
Figure 4.12: Effect of ZLN005 on the cell migration in MDA-MB-231 cells	147
 <b>Chapter 5</b>	
Figure 5.1: MTT assays showing the cell viability after 24hrs treating cells with 3BrPA or AMA	161
Figure 5.2: Effect of 3-BrPA and AMA on the ROS production in MDA-MB-231cells	163
Figure 5.3: Effect of 3-BrPA on the mitochondrial morphology in MDA-MB-231 cells	165
Figure 5.4: Micrographs showing the mitochondrial morphology in MDA-MB-231 cells treated with 3BrPA	166
Figure 5.5: Effect of AMA on mitochondrial morphology in MDA-MB-231 cells	168
Figure 5.6: Micrographs showing the mitochondrial morphology in MDA-MB-231 cells treated with AMA	169
Figure 5.7: Impact of 3-BrPA and AMA on the mtDNA copy number in MDA-MB-231 cells	170

Figure 5.8: Quantification of ATP in MDA-MB-231 cells treated with 3-BrPA or AMA	171
Figure 5.9: Effect of 3-BrPA and AMA on lactate production in MDA-MB-231 cells	172
Figure 5.10: Effect of 3-BrPA and AMA on the cell migration in MDA-MB-231 cells	173
<b>Chapter 6</b>	
Figure 6.1: Impact of glucose on mitochondrial dynamics	181
Figure 6.2: Mitochondrial electron transport chain	183
Figure 6.3: Western blot of p66shc and/or TRAP1 proteins in MDA-MB-231 cells after 48hrs of silencing p66shc and TRAP1 genes	189
Figure 6.4: Western blot of p66shc and/or TRAP1 proteins in HT1080 cells after 48hrs of silencing p66shc and TRAP1 genes	191
Figure 6.5: Western blot of p66shc and/or TRAP1 proteins in HeLa cells after 48hrs of p66shc and TRAP1 genes knockdown	193
Figure 6.6: Effect of silencing p66shc and TRAP1 on the activation of protein p66shc in MDA-MB-231 cells	194
Figure 6.7: Microscopic images shows activated p66shc in MDA-MB-231 cells after 48hrs of silencing p66shc or/and TRAP1 genes	195
Figure 6.8: Effect of Silencing p66shc and TRAP1 genes on cell death in MDA-MB-231 cells	196
Figure 6.9: Effect of silencing p66shc or/and TRAP1 genes on the ROS production	198
Figure 6.10: Effect of silencing p66shc and/or TRAP1 genes on the ATP production	201
Figure 6.11: Effect of silencing p66shc and/or TRAP1 genes on lactate production	203
Figure 6.12: Effect of silencing p66shc and/or TRAP1 genes on the cell migration	205
<b>Chapter 7</b>	
Figure 7.1: Alvetex Scaffold	215
Figure 7.2: Decellularised rat lung tissue	219
Figure 7.3: Micrographs showing 3D image of MDA-MB-231 cells cultured in decellularised lung tissue	221

Figure 7.4: Quantification of mtDNA copy number in MDA-MB-231 cells cultured in different glucose levels and in different 3D cell cultures	223
Figure 7.5: Micrographs showing mitochondria in MDA-MB-231 cells cultured in different glucose levels on collagen gel	225
Figure 7.6: Micrographs showing mitochondria in MDA-MB-231 cells cultured in different glucose levels in Alvetex scaffold	226
Figure 7.7: Micrographs showing mitochondria in MDA-MB-231 cells cultured in different glucose level in decellularised lung tissue.	227
Figure 7.8: Effect of glucose level on 3D cell migration	228
Figure 7.9: Effect of mdivi-1 inhibitor on 3D cell migration	229

## **List of Tables**

### **Chapter 1**

	Page
Table 1.1: The caspase family in human	20
Table 1.2: Bcl-2 Family protein	21

### **Chapter 2**

Table 2.1: List of antibodies used in western blot protein analysis and in immunocytochemistry assay	48
Table 2.2: List of primers used in real-time qPCR	48

### **Chapter 6**

Table 6.1: The cell numbers used in the experiments	187
---	-----

## List of Abbreviations

ATP	Adenosine triphosphate
AIF	Apoptosis inducing factor
AMA	Antimycin A
ANOVA	Analysis of variance
ANT	Adenine nucleotide translator
Apaf-1	Apoptotic protease activating factor-1
BSA	Bovine serum albumin
BAX	BCL <sub>2</sub> -associated X protein
3BrPA	3-bromopyruvate
CIN	Chromosomal instability
Cyp D	Cyclophilin D
DMEM	Dulbecco's modified Eagle medium
DMSO	Dimethyl sulfoxide
Drp1	Dynamin-related protein1
DM	Diabetes mellitus
DCF	Dichlorodihydrofluorescein
deLung	Decellularised lung tissue
EMT	Epithelial-mesenchymal transition
ECM	Extracellular matrix
EDTA	Ethylene diamine tetra acetic acid
EGF	Epidermal growth factor
EMEM	Eagle's Minimum Essential Medium
ER	Endoplasmic reticulum
ETC	Electron transport chain
Fis1	Mitochondrial fission 1 protein
GAPDH	Glyceraldehyde 3-phosphate dehydrogenase

GLUTs	Glucose transporters
GSSG	Glutathione disulfide
GTP	Guanosine triphosphate
HKII	Hexokinase II
IAPs	Inhibitor of apoptosis proteins
IM	Inner membrane
IMM	Inner mitochondrial membrane
IMS	Intermembrane space
LDH A	Lactate dehydrogenase A
MAM	Mitochondria-associated endoplasmic reticulum membranes
MCTs	Monocarboxylate transporters
mdivi -1	Mitochondrial division inhibitor 1
Mff	Mitochondrial fission factor
Mfn1	Mitofusin 1
MMP	Matrix metalloproteinases
MnSOD	Manganese superoxide dismutase
MOMP	Mitochondrial outer membrane permeabilization
MTT	3-(4,5-Dimethylthiazol-2-Yl)-2,5-Diphenyltetrazolium Bromide
mPTP	Mitochondrial permeability transition pore
mtDNA	Mitochondrial DNA
OM	Outer membrane
OMM	Mitochondrial outer membrane
OPA1	Optic atrophy protein 1
OXPHOS	Oxidative phosphorylation
OD	Optical density
PDGF	Platelet-derived growth factor
PDH	Pyruvate dehydrogenase
PDK	Pyruvate dehydrogenase kinase

PFA	Paraformaldehyde
PFK-B	Phosphofructokinase
PGC-1 $\alpha$	Peroxisome proliferator-activated receptor gamma coactivator 1-alpha
PI	Protease inhibitors
PTB	Phosphotyrosine-binding domain
PTP	Permeability transition pore
PTPC	Permeability transition pore complex
PPP	pentose phosphate pathway
PVDF	Polyvinylidene difluoride
qPCR	Quantitative Polymerase chain reaction
RFU	Relative fluorescence units
RFU	Relative fluorescence unit
RIP1	Receptor-interacting protein 1
RIPA	Radio-immuno-precipitation assay
RISC	RNA inducing silencing complex
ROS	Reactive oxygen species
rRNA	Ribosomal RNA
SDH	Succinate dehydrogenase
SDS	Sodium dodecyl sulfate
SDS-PAGE	Sodium Dodecyl Sulphate-Polyacrylamide Gel Electrophoresis
SMAC	Second mitochondria-derived activator of caspases
TBST	Tris-buffered saline Tween
TCA	Tricarboxylic acid
TEMED	Tetramethylethylenediamine
TME	Tumor microenvironment
TNF	Tumor necrosis factor
TP53 or p53	Tumor suppresser 53
TRAIL	TNF-related apoptosis-inducing ligand

TRAP1	Tumor necrosis factor (TNF) receptor associated protein 1
tRNA	Transfer RNA
FADH2	Flavin adenine dinucleotide
NADH	Nicotinamide adenine dinucleotide
VDAC	Voltage-dependent anion channel
VEGF	Vascular endothelial growth factor
VSMC	Vascular smooth muscle cell
WHO	World Health Organization

## **Chapter One: General introduction**

### **1.1 Cancer**

Cancer is considered to be a leading cause of death worldwide. According to a WHO report in 2015 cancer deaths are projected to increase from 8.2 million deaths in 2012 to more than 13million deaths per year in 2030. There are more than 100 types of cancer with different risk factors, which can originate from different cell types and organs. These cells can proliferate uncontrollably and migrate and invade normal surrounding tissue and metastasize to distant organs (Hanahan and Weinberg, 2000; Stratton et al., 2009).

Transformation of normal cells to cancerous cells is a multistep process which is started by mutations in genetic material that accumulate over time. This can lead to changes in gene expression and function, and this will reflect on the growth and behaviour of cells (Hanahan and Weinberg, 2000; Lopez-Saez et al., 1998). Unlimited capacity for cell division and the ability to migrate and colonise in distant parts of body makes cancer a dangerous disease that threatens life (Martin et al., 2013; Sudheer Shenoy P, 2014)

In general cancer cells acquire several biological capabilities that enable them to develop from normal cells. Hanahan and Weinberg (2000) described six Hallmarks of cancer cells which are self-sufficiency in growth signals, insensitivity to anti-growth signals, tissue invasion and metastasis, limitless replicative potential, sustained angiogenesis and evading apoptosis and these are illustrated in Figure 1.1. Then they address two new enabling characteristic of cancer which is genomic instability in cancer cells, and tumour-promoting inflammation, which promotes tumour progression via a variety of ways (Hanahan and Weinberg, 2011).

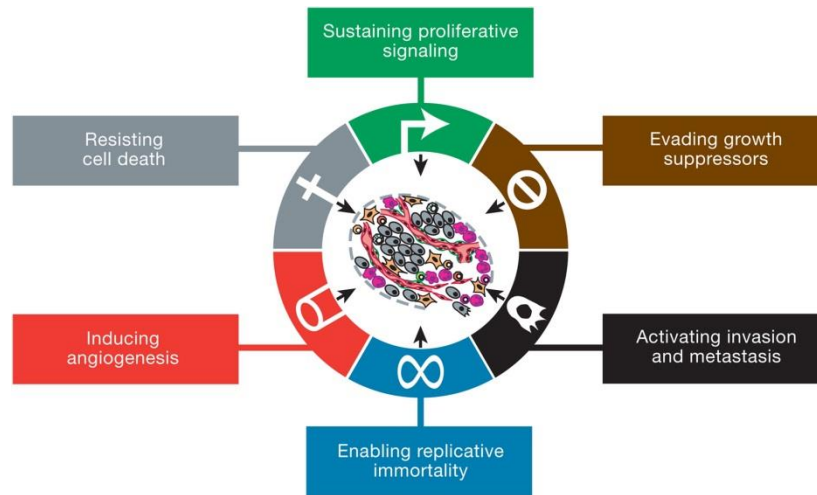


**Figure 1.1: The Hallmarks of cancer.** The characteristics are believed to govern the transformation of normal cells to a malignant cancer.

Cited from (Hanahan and Weinberg, 2011).

They also address other two additional emerging Hallmarks, which play an important role in the development of cancer cells. The first includes reprogramming of cellular energy metabolism and the second includes the ability of cancer cells to avoid the immune system. Figure 1.2 shows the new emerging hallmarks and enabling characteristics of cancer cells.

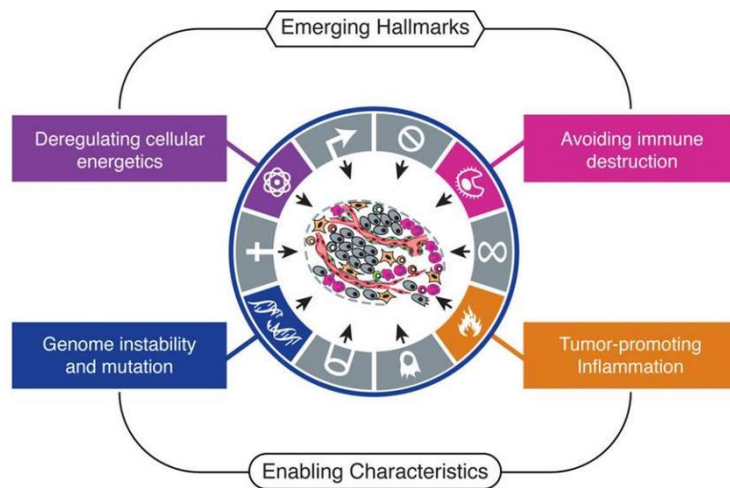


**Figure1.2: emerging hallmarks and enabling characteristics**

Cited from (Hanahan and Weinberg, 2011)

The Hallmarks of cancer cell can be summarized in the following points:

- I. Sustaining Proliferative Signaling: Proliferation of normal cells requires growth factors, which bind with receptors on cell surface and trigger cell division. Cancer cells have the ability to sustain proliferative signaling by several ways: they can

generate their own growth factors that ligand its receptors, thus resulting in autocrine proliferative stimulation. In some cases cancer cells increase their growth factor receptors. Cell surface receptors can also be deregulated as a result of mutation leading to hyper-responsive of growth factor ligand and constant cell division, permitting cancer cells to survive beyond its normal life span (Feitelson et al., 2015; Hanahan and Weinberg, 2011).

- II. Evading Growth Suppressors: There are several anti-growth signals that limit growth and proliferation in normal cells called tumour suppressor proteins such as suppressor protein RB (retinoblastoma-associated) and TP53 (tumor protein p53) that code for either inhibiting cell cycle or promoting apoptosis, and sometimes do both. Cancer cells evade these mechanisms as a consequence of mutations in tumour suppressor genes (Hanahan and Weinberg, 2000; Nahta et al., 2015).
- III. Evading apoptosis: Apoptosis is a normal process that removes abnormal cells when their DNA is damaged and cannot be repaired. Cancer cells can evade apoptosis through downregulating or inhibiting pro-apoptotic proteins and/or upregulating of anti-apoptotic proteins (Fernald and Kurokawa, 2013; Fulda, 2010; Hanahan and Weinberg, 2011).
- IV. Enabling Replicative Immortality: Cell growth and division in normal cells is limited by telomeres, which are terminal ends of chromosomes. During the cell cycle telomeres progressively shorten, until cells reach their senescence and die. It has been observed that normal cells have capacity for only 60-70 doublings. While, cancer cells are able to overcome this barrier through telomere maintenance through up-regulating expression of the telomerase enzyme that adds to the end of telomere DNA hexa-nucleotide repeats. As a result, the cancer cells can continue to proliferate without senescence and death (Hanahan and Weinberg, 2000; Yaswen et al., 2015).

- V. **Inducing Angiogenesis:** As cells divide and the number of them increases, there will be more requirements for oxygen and nutrients which are essential for cell growth. Cancer cells have the ability to encourage the formation of new blood vessels to supply developed tumour tissue with essential growth requirements and to ensure their survival and expansion. This is achieved by changes in the regulated balance between angiogenesis induction factors and inhibitors of it (Broertjes, 2015; Hanahan and Weinberg, 2011).
- VI. **Activating Invasion and Metastasis:** one of most important characteristics of cancer cells is their ability to migrate and spread from their origin location to other parts of the body, where they may succeed to form a secondary tumour. Cancer cells acquire this ability by modification in their membrane proteins, which reduces cell to cell adhesion, also they secrete extracellular proteolytic enzymes that digest surrounding barriers (Broertjes, 2015; Fouad and Aanei, 2017)
- VII. **Evading the immune system:** it is clear that the immune system is constantly monitoring cells and tissues and plays an essential role in the detection and eradication of any abnormal growth of incipient neoplasia. However, cancer cells can escape from immune-mediated detection and limit immunologic killing using several mechanisms especially in non-virus inducing cancer. One strategy to evade the immune system is by impairing antigen presentation that fails to activate an immune response (Hanahan and Weinberg, 2011; Igney and Krammer, 2002).
- VIII. **Genomic Instability:** One characteristic of most cancer cells is genomic instability. There are different forms of genomic instability. However, chromosomal instability (CIN) is considered a major form, which is characterized by high rate of changes in chromosome structure and number over time in cancer cells compared with normal cells. Microsatellite instability is another form of genomic instability. This is characterized by the expansion or contraction of the number of oligonucleotide

repeats present in microsatellite sequences (Microsatellites refer to 2-5 nucleotide repeats in DNA sequences) (Broertjes, 2015).

There are several components of the genomic maintenance machinery, tumor suppresser 53 (p53) is an essential protein that controls DNA damage either through inducing DNA repair or apoptosis if the damage is excessive, however, cancer cells through a breakdown in repairing machinery can increase the rates of mutation for tumor progression (Ferguson et al., 2015; Negrini et al., 2010).

IX. Tumour promoting inflammation: Inflammation is an immune response in a specific microenvironment that reflects an attempt of the immune system to eradicate infected cells, injured cells, or neoplasia. There are several evidences that indicate that in the earliest stages of neoplastic progression, inflammation has an important role in development of incipient neoplasia into cancer (de Visser et al., 2006; Qian and Pollard, 2010). Inflammatory cells through release of chemicals which include growth factors, survival factors, pro-angiogenic factors, extracellular matrix-modifying enzymes that facilitate angiogenesis, invasion, and cell migration, and inductive signals that lead to activation of epithelial-mesenchymal transition EMT and other characteristics that facilitating programs into the tumor microenvironment can contribute in accelerating the tumor growth (de Visser et al., 2006; Grivennikov et al., 2010).

X. Reprogramming energy metabolism: Usually normal cells obtain ATP energy through the oxidative phosphorylation process, in which cells metabolize glucose to pyruvate in the glycolysis process in cytoplasm, then pyruvate completely oxidizes in the citric acid cycle in mitochondria into  $\text{CO}_2$  and the reduced molecules of NADH and  $\text{FADH}_2$ . The electron transport system that includes a series of oxidation – reduction reactions, transfer the electrons from NADH and  $\text{FADH}_2$  to  $\text{O}_2$  leading to production of  $\text{H}_2\text{O}$  and generation of ATP. However, cancer cells reprogram the

pathway of energy production: they convert pyruvate to lactate in the cytosol. The ATP energy produced in glycolysis is only 2ATP which is less by 18 times the energy yield in oxidation phosphorylation. However the consumption of glucose and production of ATP in cancer cell is more than 100 times faster than non-cancer cells (Hanahan and Weinberg, 2000; Hanahan and Weinberg, 2011).

Although most developed anti-cancer drugs are designed to target the hallmarks of cancer, their effectiveness are still limited (Cree and Charlton, 2017). This issue may be due to that majority of anticancer therapy has specific molecular targets which have role in one hallmark, and such specificity with cancer cells maybe not effective since each hallmark can be regulated by more than one pathway. This allowing cancer cells to survive and adapted to applied therapy through mutation, reprogramming, epigenetic, and remodeling of the stromal microenvironment, which can give the capability to renew tumor growth and progress resistance (Cree and Charlton, 2017; Hanahan and Weinberg, 2011).

To overcome this issue, it will be more effective if targeting multiple signaling pathways that modulate the same hallmark or targeting more than one hallmark to get better results from cancer treatment. However, despite difficulty studying this strategy, the concept remains important to improve the efficacy of cancer treatment.

## **1.2 Cancer Metastasis**

Metastasis, which is the process of invasion and spreading of neoplastic cells from the original site of the tumor to other distant organs, is the biggest challenge for treatment and is responsible for the majority of cancer deaths (Khan and Mukhtar, 2010; Labelle and Hynes, 2012). In order to metastasize successfully, tumor cells must complete several sequential events, called the metastatic cascade (Gupta and Massagué, 2006; Martin et al., 2013). This process as shown in Figure 1.3 includes; detachment of cancer cells from the extracellular matrix in the original site, which is called the primary tumor (1), migration to invade surrounding stroma, which is called the process of invasion (2), successful

penetration into lumina of blood vessels or lymphatic channels, which is called intravasation (3), successful transport via vasculature (4), arrest and colonization in distant organ sites (5), extravasation into the surrounding parenchyma tissue (6), initiation of growth, colonization and survival the new microenvironment, this step is called metastatic colonization (Labelle and Hynes, 2012; Martin et al., 2013; Ray and Jablons, 2010; Valastyan and Weinberg, 2011).

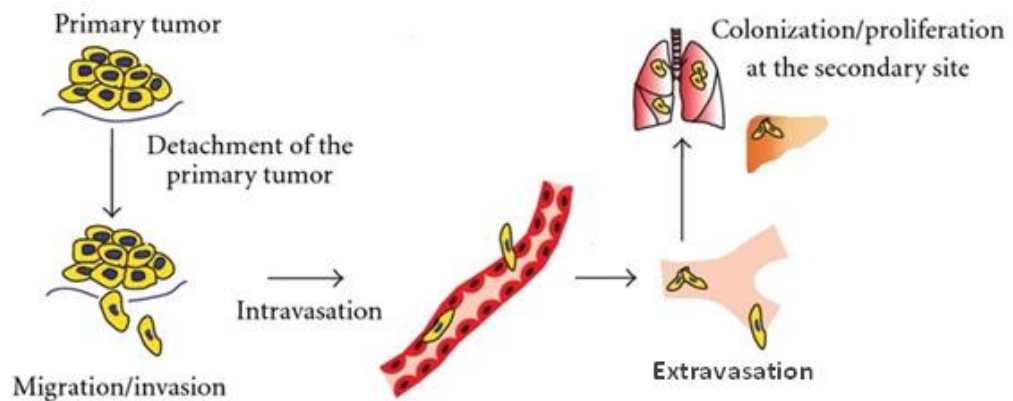


**Figure1.3: Sequential events of the metastatic cascade.**

Cited from (Alsarraj and Hunter, 2012)

### 1.3 Cell Migration

Cell migration plays a crucial role in several important processes in the multicellular organisms such as, formation, development and maintenance of new tissues, wound healing, and immune responses (Franz et al., 2002; Trepate et al., 2012; Weaver, 2017). However, changes in the signaling pathways can lead to many pathologic states such as mental disorders (Horwitz and Webb, 2003) and progression of cancer (Sever and Brugge, 2015). In fact, it is considered as one of the main factors that affect the cell invasion and metastatic character of cancer cells (Aguiar et al., 2014; Martin et al., 2013).

The process of cell migration involves changes in cell shape as a result of cytoskeletal modifications, changes in the cell-cell and cell-extracellular matrix (ECM) adhesion, and responses to stimulus (Chen et al., 2013). The migration of single cells is initiated by extending protrusions in the direction of movement, which is driven by polymerization of

actin and filament elongation at the leading edge, forming a lamellipodia and/or filopodia that attach to the specific ECM protein on the substrate. Since, attachment of the cells to the ECM at the leading edge is tighter than at the rear of the cell (trailing edge) and as a result of cell contraction, the cell body extends forward; this process is coupled with detachment of the trailing edge of the cell from substrate, as shown in Figure 1.4 (Chen et al., 2013; Lauffenburger and Horwitz, 1996; Martin et al., 2013; Schmidt et al., 1993).

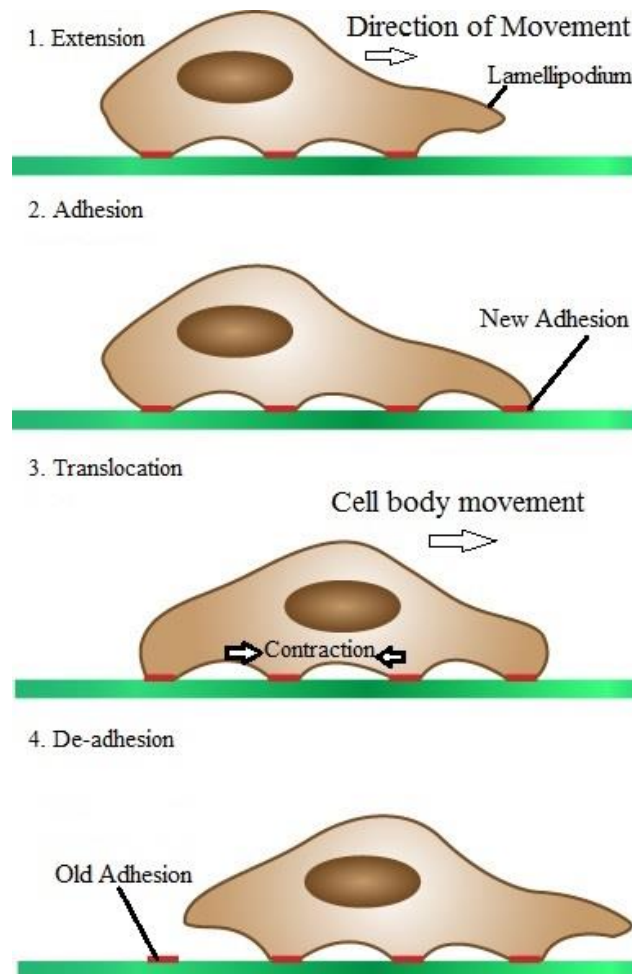


**Figure 1.4: Mechanism of cell migration.** Migrating cells extend a protrusion in the direction of motion by actin polymerization at the leading edge, then adhere its leading edge to the surface on which it is moving and detach at the trailing edge. Finally, it pulls the whole cell body forward by contractile forces generated at the cell body and rear of the cell. Cited from (Ananthakrishnan and Ehrlicher, 2007).

It has been documented that a migrating cell secretes protease enzymes such as matrix metalloproteinases (MMP), which degrade the extracellular matrix proteins at the trailing edge (Lu et al., 2011) leading to increased cell migration speed (DiMilla et al., 1993; Nabeshima et al., 2002).

Several molecules and pathways have been documented that can play an important role in the signaling processes that enhance or suppress cell migration (Martin et al., 2013). Metabolism reprogramming, which is known as the Warburg effect, and changes in mitochondrial morphology are two important factors that can control cell migration (Caino and Altieri, 2015; Campello and Scorrano, 2010; Han et al., 2013; Marelli-Berg and Jangani, 2018; Wang et al., 2015b).

#### **1.4 Mitochondria**

Mitochondria are important organelles in cells due to their essential role in regulating several processes and pathways. They are considered a powerhouse of the cell; since they supply the cells with more than 90% of required ATP energy (Marchi et al., 2012; Vyas et al., 2016). They also have a crucial role in apoptosis, production of reactive oxygen species (ROS), biosynthesis of required molecules for proliferation, calcium signaling, and aging (Bratic and Larsson, 2013; Jeong and Seol, 2008; Vandecasteele et al., 2001). Therefore, it is not surprising that mitochondria are implicated in range of disorders and diseases including progression of tumors (Hsu et al., 2016; McInnes, 2013; Ridge and Kauwe, 2018).

##### **1.4.1 Mitochondrial structure and morphology**

Mitochondria are unique organelles within the cells; they are surrounded by double membrane, which are the outer and inner mitochondrial membrane. In general, mitochondria are composed of four compartments and each of them has different functions. The outer membrane (OM) contains many porins, which are protein like channels that allow free diffusion of molecules into the intermembrane space. The intermembrane space (IMS) is a space located between the two membranes and contains proteins such cytochrome c that play a fundamental role in apoptosis. The inner membrane (IM) is inwardly folded forming several cristae expanding the inner surface area of the mitochondrial membrane and is also characterized by its impermeability for most ions and

molecules. However, it contains transporter proteins that allow crossing of selected molecules and ions, in addition to the electron transport chain enzymes and ATP synthase. And the last mitochondrial compartment is the matrix, which contain about 65% of the total mitochondrial proteins, including enzymes and proteins participating in tricarboxylic acid cycle (TCA cycle), as shown in Figure 1.5 (Kühlbrandt, 2015; Mannella, 2006; McCarron et al., 2013).

The number of mitochondria are varies widely by cell types, tissue types, and organism depending on metabolic demands. Some cells, such as immune cells have only few mitochondria, whilst, others such as hepatocytes contain hundreds to thousands (Zeviar et al., 2014). Their shape is typically range from spherical to tubular networks, with the size ranging from 1-10 $\mu\text{m}$  (McCarron et al., 2013). The number and shape of mitochondria in the cell can be changed as a response to different physiological, pathological, and environmental conditions (Knez et al., 2016; Verschoor et al., 2013).

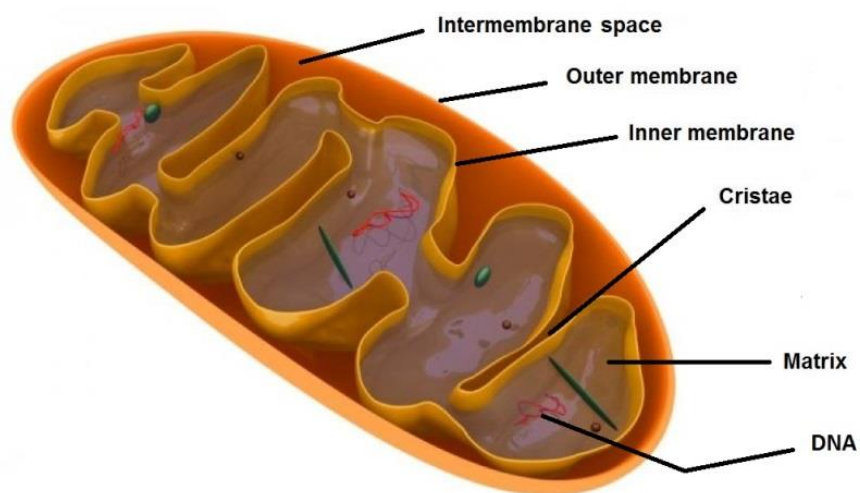


**Figure 1.5: Basic mitochondrial structure.** Typically mitochondria composed of four compartments; outer membrane, intermembrane space, inner membrane, and matrix

Mitochondria contain their own DNA (mtDNA). In humans this genome, which is inherited from the mother, consists of 16,569 base pairs and encodes 37 genes; 13 genes are for electron transport chain proteins, 22 genes are for transfer RNA (tRNA), and two genes for ribosomal RNA (rRNA). Typically, mtDNA content in each cell ranges between

$10^3$  and  $10^4$  copies and this number can vary by cell type. Replication of mtDNA is carried out by DNA polymerase  $\gamma$ , which is found only in the mitochondria, and is independent from nuclear DNA (Hu et al., 2016; Rooney et al., 2015).

Mutation in mtDNA is linked to many diseases including type 2 diabetes (Rolo and Palmeira, 2006) neurodegenerative diseases such as Parkinson and Alzheimer Disease (Coskun et al., 2012), and several cancers (Yu, 2011). This is may be due to the fact that mtDNA lack introns and histones that protect them from mutation induced by oxidative stress and other sources of genotoxic damage, as well as the fact that the DNA repair mechanisms are inefficient. Therefore, mtDNA mutations can lead to defects in oxidative phosphorylation (Gredilla, 2011). Recently, changes in mtDNA copy number have been used as a biomarker for studying many diseases related to mitochondria. These changes in mtDNA can be measured through quantitative real-time PCR (qPCR) method (Mei et al., 2015; Memon et al., 2017).

#### **1.4.2 Mitochondrial dynamics**

Mitochondria are highly dynamic organelles and continuously undergo morphological changes through mitochondrial fission, fusion, and movement of mitochondria in the cytosol (van der Bliek et al., 2013). The balance between fission and fusion is necessary for cell survival and several physiological functions including cell growth, cell death, and cell migration, and they are tightly related to metabolic function (Hu et al., 2017; Mishra and Chan, 2014; Simula et al., 2017; Zemirli et al., 2018). These processes require coordinated synthesis and import of more than 1000 proteins which are encoded by the nuclear genome and mitochondrial genome. In addition to that, mitochondrial fission requires an additional step, which is mitochondrial DNA replication (Mishra and Chan, 2014).

The balance between fission and fusion processes is regulated through specialized protein machinery. As summarized in Figure 1.6, the fission of mitochondria is induced by

dynamamin-related protein1 (Drp1) (Frank et al., 2001). This protein, which is a large GTPase and localized in the cytosol, translocates to the mitochondrial outer membrane (OMM) during mitochondria fission where it binds to OMM through several receptors such as mitochondrial fission 1 protein (Fis1), mitochondrial fission factor (Mff), and mitochondrial dynamics proteins of 48 and 51 kDa (MiD48/51), leading to polymerization and formation of a ring-like structure around the mitochondria (Gao et al., 2017; Trewin et al., 2018), which divides the mitochondria into two separate organelles upon hydrolysis of guanosine triphosphate (GTP) (Mishra et al., 2010).

In contrast to fission, the mitochondrial fusion process involves fusion of both outer and inner membrane. This process is regulated by three large GTPase proteins, which includes; Mitofusin 1 (Mfn1), Mitofusin 2 (Mfn2), and optic atrophy protein 1 (OPA1) (Ni et al., 2015). During mitochondria fusion, Mfn1/Mfn2 proteins dimerise at the OMM between two individual mitochondria, which are drawn to each other upon GTP hydrolysis. After fusion of the outer membrane of two adjacent mitochondria, OPA1 starts to fuse the IMM, depending on the GTPase activity and hydrolysis of GTP (Santel and Fuller, 2001; Trewin et al., 2018).

### **1.4.3 Mitochondrial morphology and function**

It has been documented that changes in mitochondrial morphology accompany changes in metabolic function (Shin et al., 2016). The relationship between mitochondrial size and metabolic activity has revealed that elongated, network-like mitochondria are characteristic metabolically active cells, whereas, small size mitochondria are common in inactive cells (Mitra et al., 2009; Westermann, 2012).

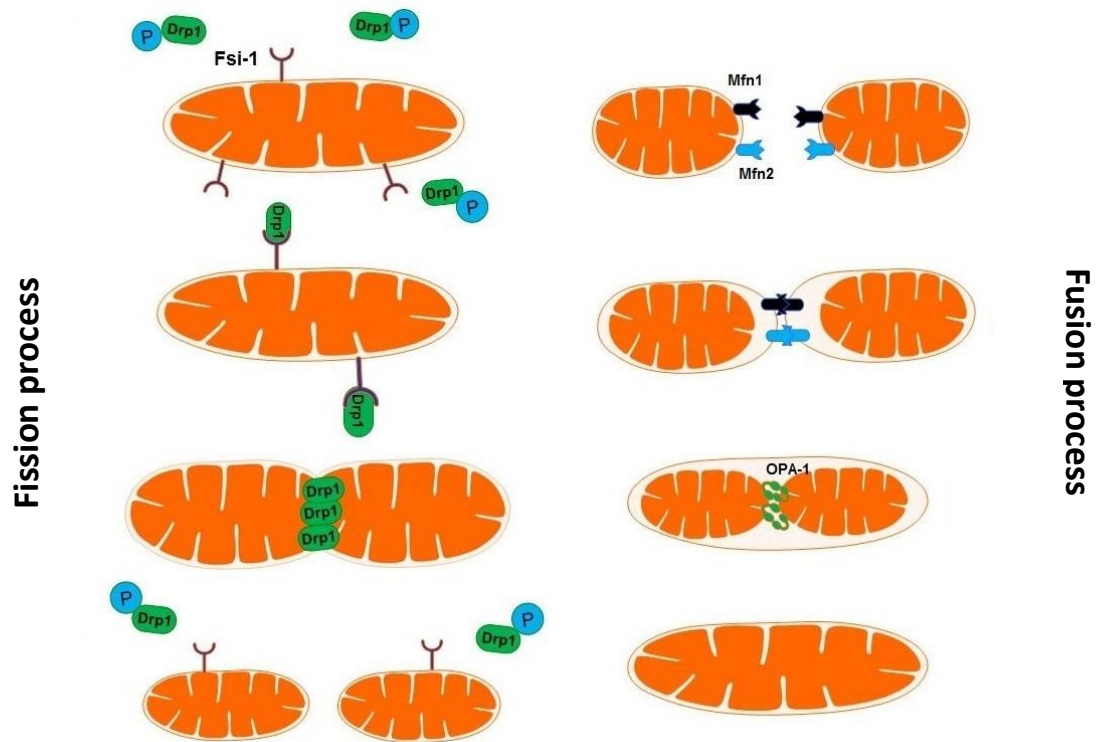


**Figure 1.6: Mitochondrial fission and fusion.** Mitochondria alter their morphology toward fusion or fission to maintain cellular homeostasis depending on physiological conditions. Mfn1, Mfn2, and OPA1 proteins are the major regulators of mitochondrial fusion. The mitochondrial fission process is mainly conducted by Drp1, and Fis1.

Mitochondrial morphology can be maintained via the balance between fission-fusion continuously, however, several factors that can cause a stress on the cells such as exercise, temperature, U.V., hyperglycaemia,  $H_2O_2$ , anti-cancer agents can disrupt this balance leading to hyperfragmentation of mitochondria (Aung et al., 2017; Van Beersel et al., 2013; Yu et al., 2011; Yu et al., 2006), which can lead to reduced capacity for ATP production via oxidative phosphorylation (Alecu et al., 2017); this is implicated in several pathological conditions including cardiovascular disease, neurodegenerative disease, diabetes mellitus, and cancer progression (Bordi et al., 2017; Rosdah et al., 2016; Suárez-Rivero et al., 2017). In contrast, it has been shown that conditions such as starvation, which can lead to elongation of mitochondria, enhance resistance to oxidative stress and apoptosis (Mai et al., 2010; Rambold et al., 2011), and stimulates the cell to shift their metabolism from glycolysis to oxidative phosphorylation (Li et al., 2017), as illustrated in

Figure 1.7. However, the mechanism responsible for the initiation and changes in mitochondrial morphology is still not entirely clear.

#### **1.4.4 Mitochondrial biogenesis**

Mitochondrial biogenesis is the mechanism through which the cell can adapt to increased energy demands through increasing their individual mitochondrial mass and increasing mitochondrial copy number (Fabian et al., 2014; Jornayvaz and Shulman, 2010). It can be stimulated by distinct signaling pathways in response to exercise, to development, and in several diseases (Hood, 2009; Sanchis-Gomar et al., 2014; Vaarmann et al., 2016).

It has been suggested that increasing mitochondrial biogenesis in cancer cells can impair carcinogenesis, and decrease growth rates since it boosts oxidative phosphorylation for ATP production and decreases dependence on aerobic glycolysis, which is essential for high proliferation in cancer cells. Moreover, it was found that mitochondrial biogenesis leads cancer cells to be less invasive due to reduction in lactate production (Wang and Moraes, 2011). Other studies have demonstrated that mitochondrial biogenesis can promote cancer tumor growth via increased energy production and protects cancer cells from autophagy as a result of increasing role of antioxidant which neutralized mitochondrial-released ROS (Salem et al., 2012). It was reported that increasing mitochondrial mass via mitochondrial biogenesis can enhance carcinogenesis of epithelial cells (Sotgia et al., 2013). Despite that, the role of mitochondrial biogenesis in cancer cell proliferation as well as in migration and metastasis of cancer cells remains controversial and requires more investigation.

#### **1.4.5 Mitochondrial mitophagy**

Human cells can selectively remove damaged or unnecessary mitochondria through mitochondrial autophagy, which is called mitophagy. This process is crucial in maintaining mitochondrial quality, as well as for maintaining cellular homeostasis. Damaged mitochondria can generate a high amount of stress signals which can lead to cellular

dysfunction and induction of apoptosis (Hamacher-Brady and Brady, 2016; Novak, 2012). Reducing this process can lead to several diseases such as metabolic disease, neurodegenerative diseases, and cancer (Song et al., 2015; Um and Yun, 2017).

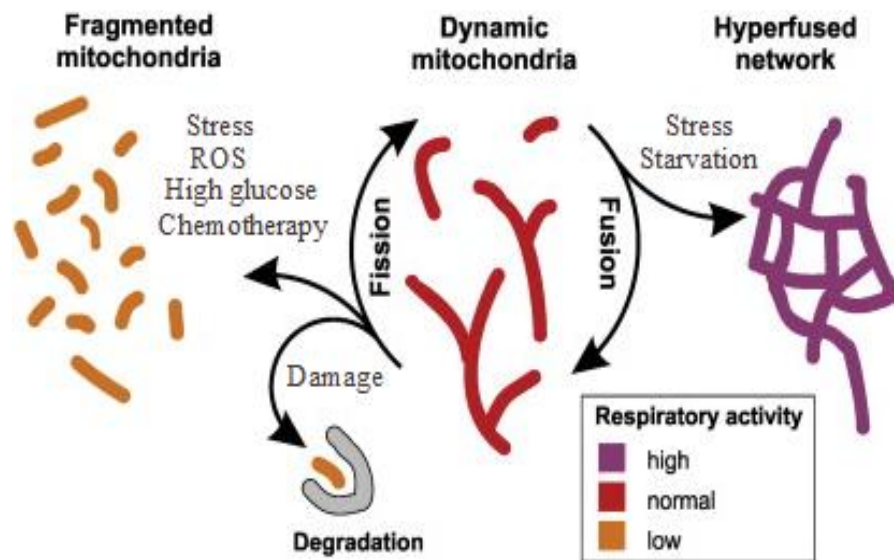


**Figure 1.7: Mitochondrial morphology and activity depending on the conditions.** Under normal condition mitochondria undergo frequent cycles of fusion and fission to allow spreading of metabolites and macromolecules throughout the entire compartment. When the bioenergetics state becomes critical, for example under nutrient deprivation, highly fused mitochondria are formed to optimize mitochondrial function. Mitochondrial fission is required for removal of damaged and inactive organelles by autophagy or for resistant abnormal condition. Fragmented mitochondria constitute the preferred morphological state when respiratory activity is low. Modified from (Westermann, 2012).

The process of mitophagy starts when factors such as ROS, aging, and lack of nutrients cause mitochondrial dysfunction, this leads to accumulation of high levels of ROS as a result, mitochondria become depolarized and damaged. Damaged mitochondria can then fuse with lysosomes forming autophagosome, which degrades damaged mitochondria completely, as shown in Figure 1.8 (Song et al., 2015). This process usually leads to decline in mitochondria mass(Gou et al., 2017).

### 1.4.6 Effect of glucose level on mitochondrial morphology

Mitochondrial morphology is highly dynamic; it can be shift between small, fragmented and large, elongated network-like shape. Several factors such as high glucose level (Trudeau et al., 2011) , anticancer agents (Cao et al., 2017), U.V. (Sanjuán Szklarz and Scorrano, 2012), and H<sub>2</sub>O<sub>2</sub> (Iqbal and Hood, 2014) can affect mitochondrial morphology.

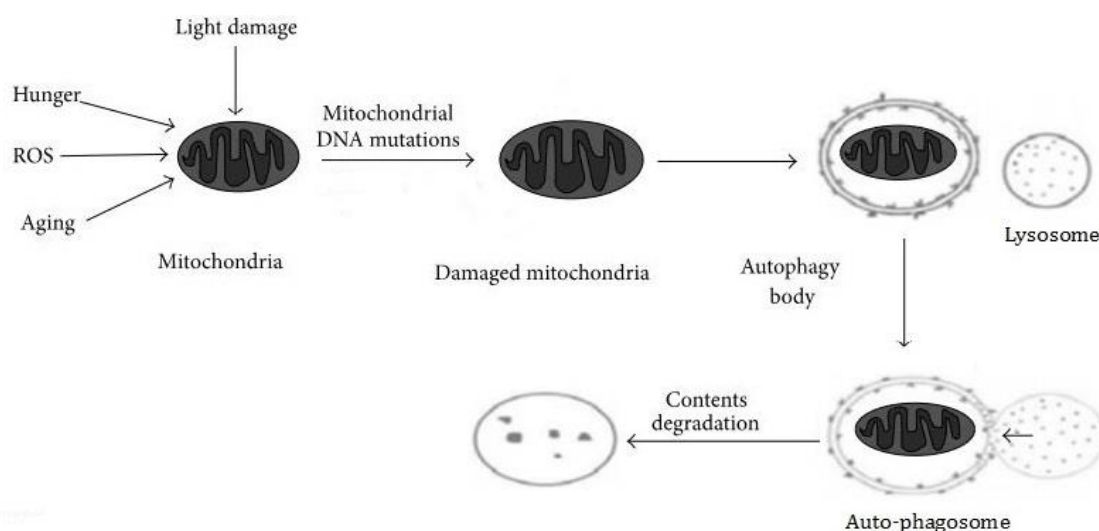


**Figure 1.8: Mitophagy process.** Defective mitochondria will damage themselves then fused with lysosomes forming autophagosome, which degraded mitochondria completely. Cited from(Song et al., 2015).

It has been demonstrated that high glucose level affects mitochondrial morphology and shifts them toward fragmentation (Trudeau et al., 2011) which may be due to activation of Drp1 protein (Filippi et al., 2017). There is evidence that hyperglycaemia, which is characterized by high glucose levels in the blood, is implicated in several diseases such as neurodegenerative diseases, cardiovascular disease, diabetes mellitus, and cancer (Knott et al., 2008; Ong and Hausenloy, 2010; Rolo and Palmeira, 2006; Ryu et al., 2014).

Elevated levels of glucose exerts oxidative stress on the cells, which can lead to mtDNA mutation and changes in ROS scavenger enzymes, leading to mitochondrial dysfunction and increasing ROS generation. This state can lead to fragmentation of mitochondria and induce apoptosis (Hou et al., 2015). However, despite the fact that it is well known that

high glucose is essential for maintaining high cancer cell proliferation and metastasis; it is still not clear how cancer cells avoid the apoptotic effect of high glucose.

In contrast, it has been reported that low glucose levels support an elongation shape of mitochondria due to inhibition of Drp1 protein (Rambold et al., 2011). However, it does not seem that this protein, which is essential in mitochondrial fission, plays any role in mitochondrial fusion and in mitochondrial biogenesis.

#### **1.4.7 Effect of H<sub>2</sub>O<sub>2</sub> on mitochondrial morphology**

While, generation of low concentrations of ROS is necessary for the regulation of several biological processes in the cell such as cellular proliferation and differentiation, high level of ROS exerts several damaged outcomes including accumulation of mtDNA mutation, mitochondrial dysfunction, growth inhibition and apoptosis (Chen et al., 2010; Cribbs and Strack, 2007)

It has been shown that exposure to exogenous hydrogen peroxide (H<sub>2</sub>O<sub>2</sub>) promotes several defense mechanisms by the cells including changes in mitochondrial morphology toward fragmentation through enhancing Drp1 activation (Fan et al., 2010). Despite that the exact mechanism is not clear as H<sub>2</sub>O<sub>2</sub> can interact with several proteins and pathways (Gough and Cotter, 2011; Lennicke et al., 2015).

Contrary to normal cells, cancer cells might exploit increases in H<sub>2</sub>O<sub>2</sub> for their reprogramming metabolism, proliferation, angiogenesis and metastasis (Lopez-Lazaro, 2007).

#### **1.4.8 Effect of PGC-1 $\alpha$ on mitochondrial morphology**

The peroxisome proliferator-activated receptor  $\gamma$  activator-1 alpha (PGC-1 $\alpha$ ) is a transcription factor that is involved in the regulation of mitochondrial biogenesis through stimulation of several transcription factors such as nuclear respiratory factors-1 (NRF-1) and NRF-2, which interact and promote the expression of mitochondrial transcription factor A (Tfam). This leads to activation of mitochondrial enzymes that induce

transcription and replication of mtDNA (Jornayvaz and Shulman, 2010). It can be activated in response to several factors including cold exposure, nutrient deprivation, exercise, chemotherapy, and oxidative stress (Tan et al., 2016).

PGC-1  $\alpha$  regulates oxidative metabolism through increasing metabolic enzymes required for glycolysis and oxidative phosphorylation, as well as through increasing mitochondrial mass and number in order to generate a greater amount of required ATP energy by the cell (LeBleu et al., 2014). Moreover, it can play a protective role against apoptotic effects of ROS generation via increasing ROS scavenger enzymes in mitochondria (Chen et al., 2011).

It was documented that exercise elevates expression of PGC-1 $\alpha$  in skeletal muscle, which partially switch to glycolysis. Upon expression, it reduces the expression of lactate dehydrogenase A (LDH A), which converts pyruvate and L-lactate, and enhances oxidative phosphorylation (Summermatter et al., 2013). It has been reported that PGC-1 $\alpha$  promotes metastasis and its silencing reduces invasive ability (LeBleu et al., 2014).

Recently, it has been shown that PGC-1 $\alpha$  plays an important role in mitochondrial fission-fusion processes through controlling expression of the mitochondrial fission protein, Drp1, and its overexpression can induce mitochondrial fragmentation and cell death (Dabrowska et al., 2015). The evidence suggests that excessive mitochondrial fragmentation in some diseases such as Parkinson's disease is due to overexpression of PGC-1 $\alpha$ , which is increased as a result of increasing ROS level, which in- turn can induce expression of Drp1 protein (Peng et al., 2017; Santos et al., 2015).

#### **1.4.9 Role of mitochondria in apoptosis**

Apoptosis or programmed cell death is a highly organized process in which cells signal to their self-destruction in order for proper homeostasis, embryonic development, or to prevent abnormal cell growth (Elmore, 2007). This process is characterized by certain morphological changes, which includes membrane blebbing, cell shrinkage, protein

cleavage, chromatin condensation, nuclear and DNA fragmentation, then the dying cells will be eliminated by phagocytic cells (Xiong et al., 2014).

Apoptosis is regulated via two pathways called death receptor (extrinsic) and mitochondrial (intrinsic) pathways (Jin and El-Deiry, 2005). The first pathway is activated by external signals, which are called death inducing ligands such as, Fas ligand, tumor necrosis factor (TNF) ligand, and TNF-related apoptosis-inducing ligand (TRAIL), which bind to death receptors such as Fas, TNFR1, and DR4/DR5. This pathway is mainly activated by other cells such as immune cells. Whereas, the second pathway is initiated by endogenous signals such as oxidative stress, DNA damage, chemical agents. An essential event in this pathway is mitochondrial outer membrane permeabilization (MOMP) and formation of the permeability transition pore complex (PTPC) (Jin and El-Deiry, 2005; Wang and Youle, 2009).

A set of caspase enzymes, which are widely expressed in the cell as an inactive proenzyme form, can be activated following initiation of external or internal pathway and then cleave proteins at aspartic acid residues. Once proenzyme caspase is activated, it can activate other procaspases, leading to initiation of a protease cascade. This leads to amplifying the apoptotic signaling pathway and promotes rapid cell death. There are 10 major identified caspases, which can be categorized into initiators includes (caspase 2, 8, 9, 10), effectors or executioners includes (caspase 3, 6, 7) and inflammatory caspases includes (caspase 1, 4, 5). There are four more inflammatory caspases (caspase 11, 12, 13, and 14), which are activated in apoptosis in specific cells or tissues, as shown in Table 1.1 (Bratton et al., 1997; Jin and El-Deiry, 2005).

**Table 1.1: The caspase family in human**

<b>Initiator caspases</b>	<b>Effector or Executioner caspases</b>	<b>Inflammatory caspases</b>
Caspase 2	Caspase 3	Caspase 1
Caspase 8	Caspase 6	Caspase 4
Caspase 9	Caspase 7	Caspase 5
Caspase 10		Caspase 11
		Caspase 12
		Caspase 13
		Caspase 14

In humans, oxidative stress, which can be induced by many factors including hyperglycaemia, has been implicated in several disorders and diseases including cancer, and diabetes mellitus. Exposure to strong or prolonged oxidative stress can induce mitochondrial induced apoptosis via elevation of intracellular ROS (Nita and Grzybowski, 2016).

Initiation of mitochondrial apoptosis is controlled by a family of proteins known as Bcl-2 family (Chipuk and Green, 2008). As summarized in Table 1.2, the Bcl-2 family consists of three groups; pro-apoptotic Bcl-2 proteins, which include Bax, Bak, and Bok, Anti-apoptotic Bcl-2 proteins includes Bcl-X<sub>L</sub>, Bcl-w, Mcl-1, A1, Bcl-Rambo, Bcl-L10, and Bcl-G, and heterogeneous group of proteins which known as BH3 only protein and includes Puma, Noxa, Bid, Bad, Bim, Bik, Hrk, and Bmf. Proteins of the third group hence act as proapoptotic proteins through suppression of anti-apoptotic Bcl-2 proteins and activation of pro-apoptotic Bax/Bak proteins (Shamas-Din et al., 2013).

**Table 1.2: Bcl-2 Family protein**

Anti-apoptotic protein	Pro-apoptotic protein	
	Multi-domain effectors	BH3-only activators
Bcl-2	Bax	Bid, Bad, Bik
Bcl-X <sub>L</sub>	Bak	Bim
Mcl-1	Bok	Hrk, Bmf
Bcl-w		Puma, Noxa
A1		
Bcl-Rambo		
Bcl-L10		

The apoptotic stimulus such as ROS can change the balance between pro-apoptotic and anti-apoptotic proteins of Bcl-2 family, and lead to activation of apoptotic effector Bax/Bak proteins. Bax is present in the cytosol as a monomer, upon activation, it will translocate to mitochondria where oligomers form, while, Bak present on the mitochondria constantly, after activation undergoes a series of conformational changes forming oligomers. This conformational change of Bax/Bak is essential for mitochondrial outer membrane permeabilization which allows release of intermembrane space proteins into the cytosol including; cytochrome c, SMAC/DIABLO, and Omi/Htra2, which induce caspase activation, as well as Apoptosis inducing factor (AIF), and endonuclease G, which act in a caspase-independent manner (Griffiths et al., 1999; Hata et al., 2015; Kuwana and Newmeyer, 2003).

In the cytosol, released cytochrome c binds with apoptotic protease activating factor-1 (Apaf-1) and pro-caspase-9 forms together a complex known as an apoptosome, as shown in Figure 1.9. The apoptosome cleaves the pro-caspase to active caspase 9, which in turn propagates the apoptotic signal through activating downstream effector caspases 3, 6, and 7 by proteolytic cleavage (Schafer and Kornbluth, 2006).

Bax/Bak can be activated via two models; the direct activation model through Bim/ Bid/ Puma or by other BH3-only proteins when they releasing Bim/Bid/Puma from association with anti-apoptotic Bcl-2 proteins, and indirect activation model when the anti-apoptotic Bcl-2 proteins are suppressed by BH3-only protein (Kim et al., 2006; Willis et al., 2007).

Another group of proteins known as inhibitor of apoptosis proteins (IAPs), which includes: XIAP, ILP-2, c-IAP1, c-IAP2, ML-IPA, NAIP, Survivin, and Apollon, also play an essential role in the regulation of apoptosis. IAPs inhibit apoptosis through binding with effector caspases. These proteins can be inhibited by SMAC/DIABLO proteins, which are released from mitochondria and prevent their association with caspases, as shown in Figure. 1.9 (Wang and Youle, 2009).

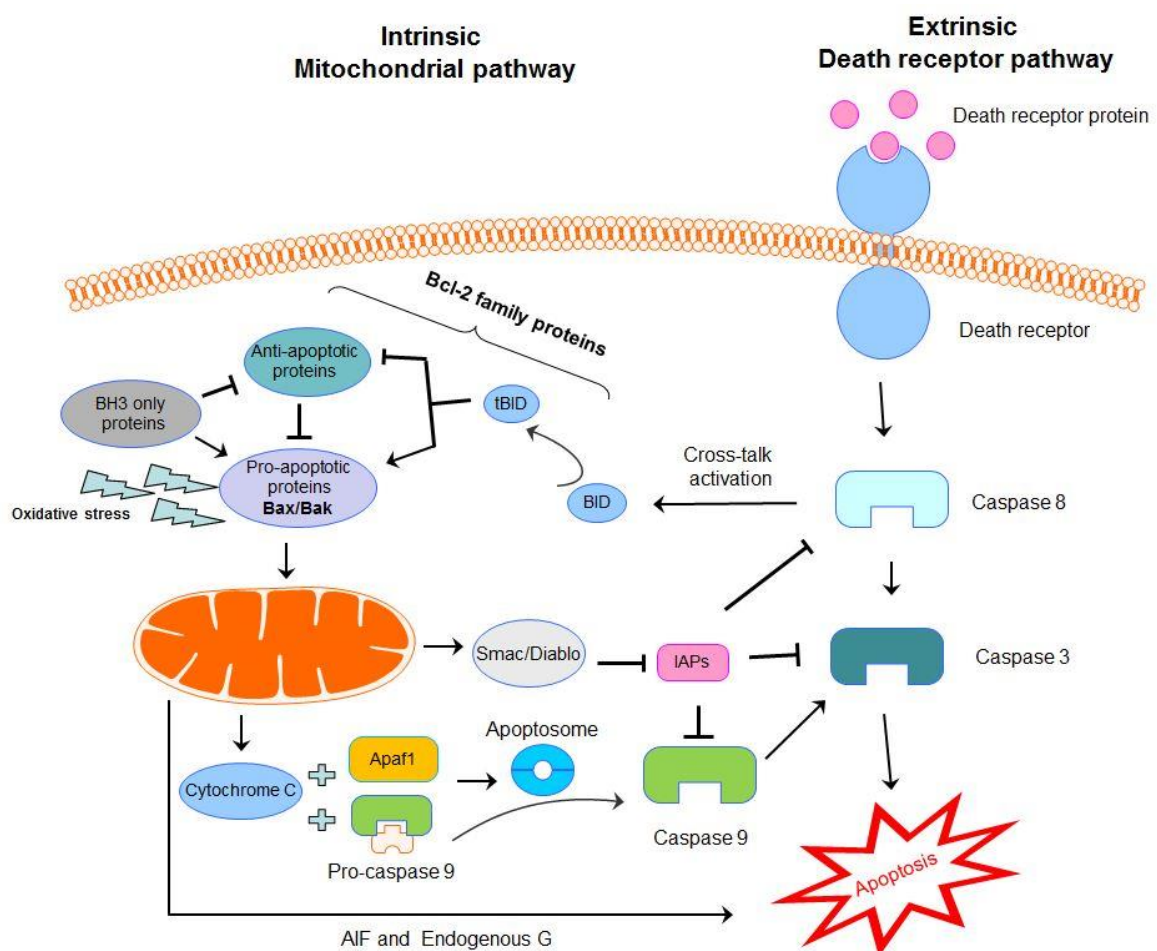


**Figure 1.9: Death receptor and mitochondrial pathways of apoptosis.**

External pathway activated by external ligand, whereas, internal pathway activated by internal stress, it also can be activate by external pathway through activation of Bid protein by caspase 8.

The mitochondrial apoptosis pathway can cross-talk with extrinsic pathways through activated caspase 8, which cleaves and activates BID to tBID; a pro-apoptotic member of Bcl-2 family proteins. Activated tBID protein can activate pro-apoptotic Bax/Bak protein through inhibition anti-apoptotic Bcl-2 proteins (Marquez et al., 2013).

One hallmark of cancer cells, is their ability to evade apoptosis (Hanahan and Weinberg, 2011). Inhibition of apoptosis is fundamental for cancer cell survival, progression and metastasis (Fernald and Kurokawa, 2013). Indeed, cancer cells have several mechanisms to circumvent apoptosis at multiple stages. Deviation of normal apoptotic pathways, caspases inhibition, and loss of tumour suppressor protein, p53, as well as changing the expression of Bcl-2 family proteins thereby preventing MOMP can be effective mechanisms for suppression of apoptosis (Koff et al., 2015; Lopez and Tait, 2015; Renault et al., 2015).

There is evidence that cancer cells reduce reliance on mitochondrial activity as a strategy for surviving apoptosis (Palorini et al., 2013), since mitochondria are a main regulator of apoptosis as well as being considered a main sources for ROS generation, which is a strong apoptosis stimulator (Giampazolias and Tait, 2016).

A link has been suggested between mitochondrial morphology and apoptosis (Suen et al., 2008). Several studies have postulated that mitochondrial fragmentation is related to apoptosis, and it enhances mitochondrial outer membrane permeabilization (MOMP) and release of cytochrome c (Landes and Martinou, 2011; Youle and Karbowski, 2005). By contrast, several studies found that MOMP can occur before mitochondrial fragmentation (Arnoult, 2007), and even apoptosis can occur independently from mitochondrial fragmentation (Parone et al., 2006; Sheridan and Martin, 2010).

Furthermore, research has shown that cancer cells can increase resistance to apoptosis through changes in mitochondrial morphology toward fragmentation, which leads to

reducing surface area required for activation of pro-apoptotic Bax protein and mitochondrial outer membrane permeabilization, as shown in Figure 1.10 (Renault et al., 2015). Whereas, another study has reported that elongation of mitochondria exhibits apoptosis resistance which may be due to inhibiting translocation of pro-apoptotic Bax protein to mitochondria, and prevention of release of cytochrome c from mitochondria (Jeong and Seol, 2008). However, the exact relationship between mitochondrial morphology and apoptosis is still not clear.

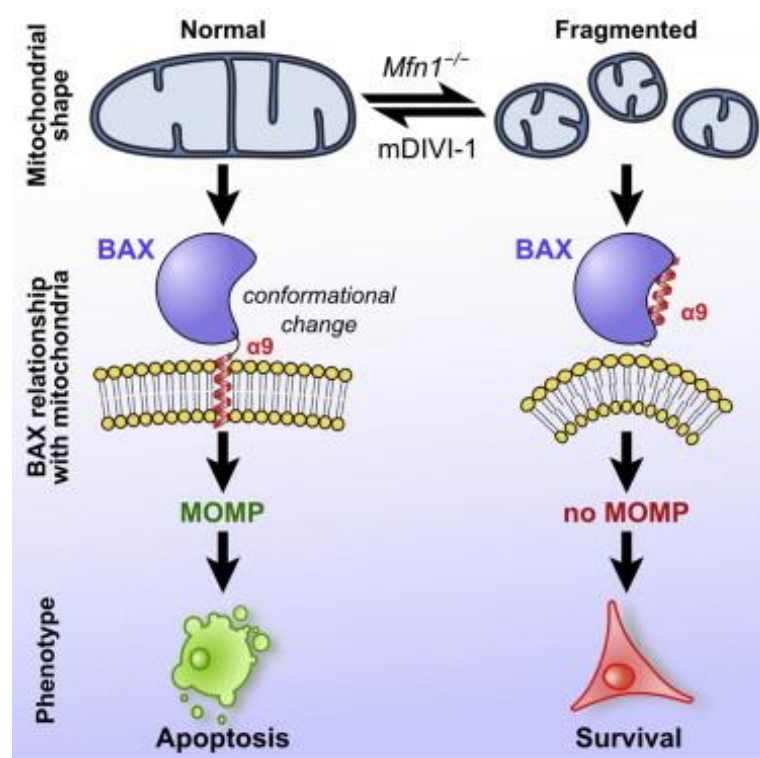


**Figure 1.10: Role of mitochondrial morphology in apoptosis.** In contrast to tubular-like shape mitochondria, small size mitochondria prevent MOMP, an essential initial step for mitochondrial apoptosis.

Cited from (Renault et al., 2015)

#### 1.4.10 Inhibition of mitochondrial fragmentation with mdivi-1

Mitochondrial fragmentation is the result of excessive mitochondrial fission, which is mediated by several proteins including Mff, MiD49/51, Fis1, and Drp1 (Rosdah et al., 2016). It has been reported that mitochondrial fragmentation leads to mitochondrial dysfunction (Jheng et al., 2012), and apoptosis (Young et al., 2010), and it is responsible

for several diseases related to mitochondria such as Parkinson's disease and Alzheimer's disease (Burte et al., 2015; Itoh et al., 2013; Wang et al., 2017b; Winklhofer and Haass, 2010).

Recently, several compounds including P110, and mdivi-1 have been designed for targeting Drp1 protein and preventing mitochondrial fragmentation (Rovira-Llopis et al., 2017). Mdivi-1 inhibitor, which is a small chemical molecule, can inhibit mitochondrial fission protein Drp1 selectively and reversibly through binding with it at allosteric site, suppressing its ability to hydrolyse GTP and assembly around mitochondria to form ring-like structures, as seen in Figure 1.11 (Cassidy-Stone et al., 2008; Rosdah et al., 2016).

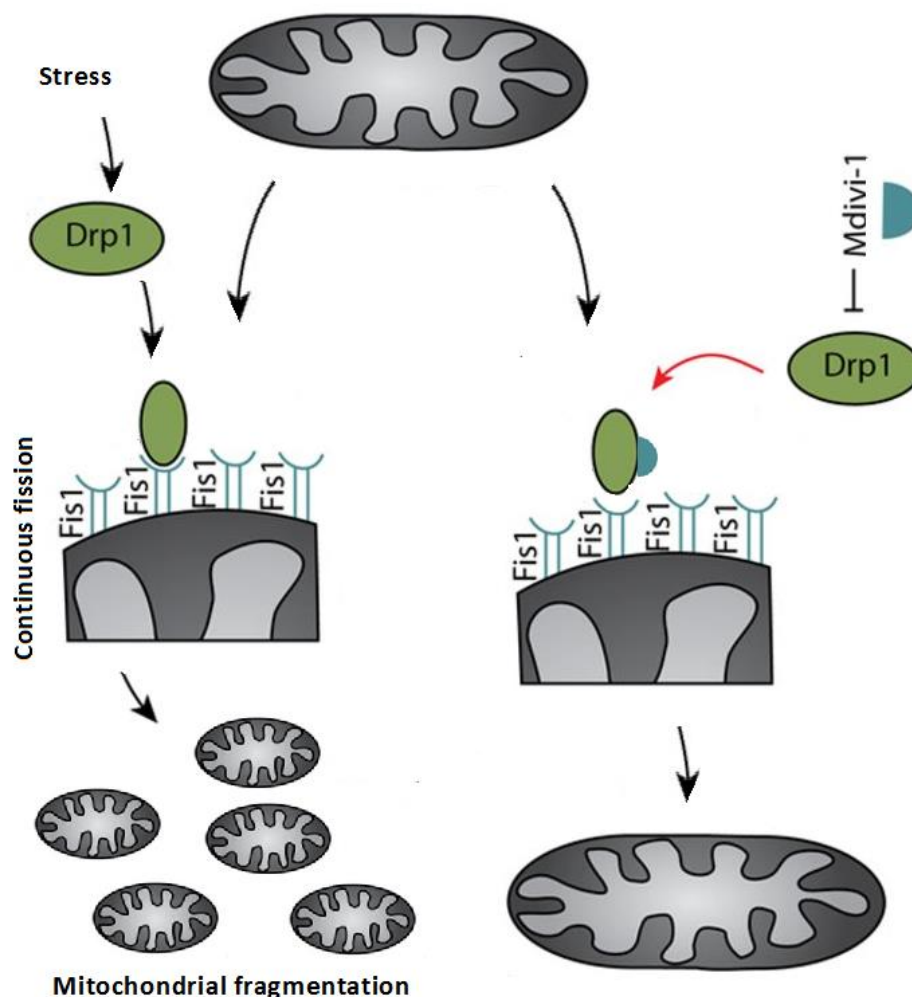


**Figure 1.11: Mechanism of mdivi-1 inhibitor effect.** Targeting of Drp1 protein with mdivi-1 inhibitor can prevent mitochondrial fragmentation through inhibition of fission process.

Modified from (Kornfeld et al., 2015).

Studies has shown that targeting mitochondrial fragmentation with mdivi-1 inhibitor could prevent apoptosis in different cell types, especially in nerve and cardiovascular cells through declining ROS production (Reddy, 2014), whereas, it has been revealed that targeting Drp1 with mdivi-1 inhibitor can affect cell proliferation via increasing apoptosis (Qian et al., 2013; Rosdah et al., 2016). However, its effect on mitochondrial metabolism and cell migration in cancer cells is still unknown.

### **1.5 Cancer cell metabolism**

Unlike normal cells, which depend on mitochondrial oxidative phosphorylation for generation ATP, most cancer cells have enhanced glycolysis and reduced oxidative phosphorylation even in the presence of oxygen. This metabolic shift was suggested first by Otto Warburg in 1924 and is known as the Warburg effect (Vander Heiden et al., 2009). It was believed for a long time that shifting to aerobic glycolysis in cancer cells is due to a permanent defect in mitochondrial oxidative phosphorylation (Zheng, 2012). However, several investigations have found that mitochondrial oxidative phosphorylation in many cancers is intact (Hsu and Sabatini, 2008; Scott et al., 2011).

Cancer cells can reprogram their metabolism to aerobic glycolysis as a result of different factors such as oncogenes such as *RAS*, *MYC*, mtDNA and genomic DNA mutation, loss of tumor suppressors such as p53, and hypoxic microenvironment (Hanahan and Weinberg, 2011; Zheng, 2012). Recently, changes in mitochondrial morphology have been identified as an inducer of metabolic reprogramming in some cancers (Guido et al., 2012; Mishra and Chan, 2016).

#### **1.5.1 Aerobic glycolysis**

Metabolic reprogramming from oxidative phosphorylation to glycolysis even in the presence of oxygen considered an important hallmark of cancers (Hanahan and Weinberg, 2011). The glycolysis process, which is carried out in cytosol and generates only 2ATPs, include a number of steps starting with uptake of glucose and end with pyruvate

production, as shown in Figure 1.12. In aerobic conditions, pyruvate transported into the mitochondria for complete oxidation via the Krebs cycle. Whilst, in the absence of oxygen, pyruvate reduced to lactate in cytosol by lactate dehydrogenase A (LDH-A), then exported through monocarboxylate transporters (MCTs) into extracellular space. Most cancer cells convert pyruvate to lactate even in oxygen availability, and this phenomenon is called aerobic glycolysis or the Warburg effect (Hanahan and Weinberg, 2011; Lopez-Lazaro, 2008).

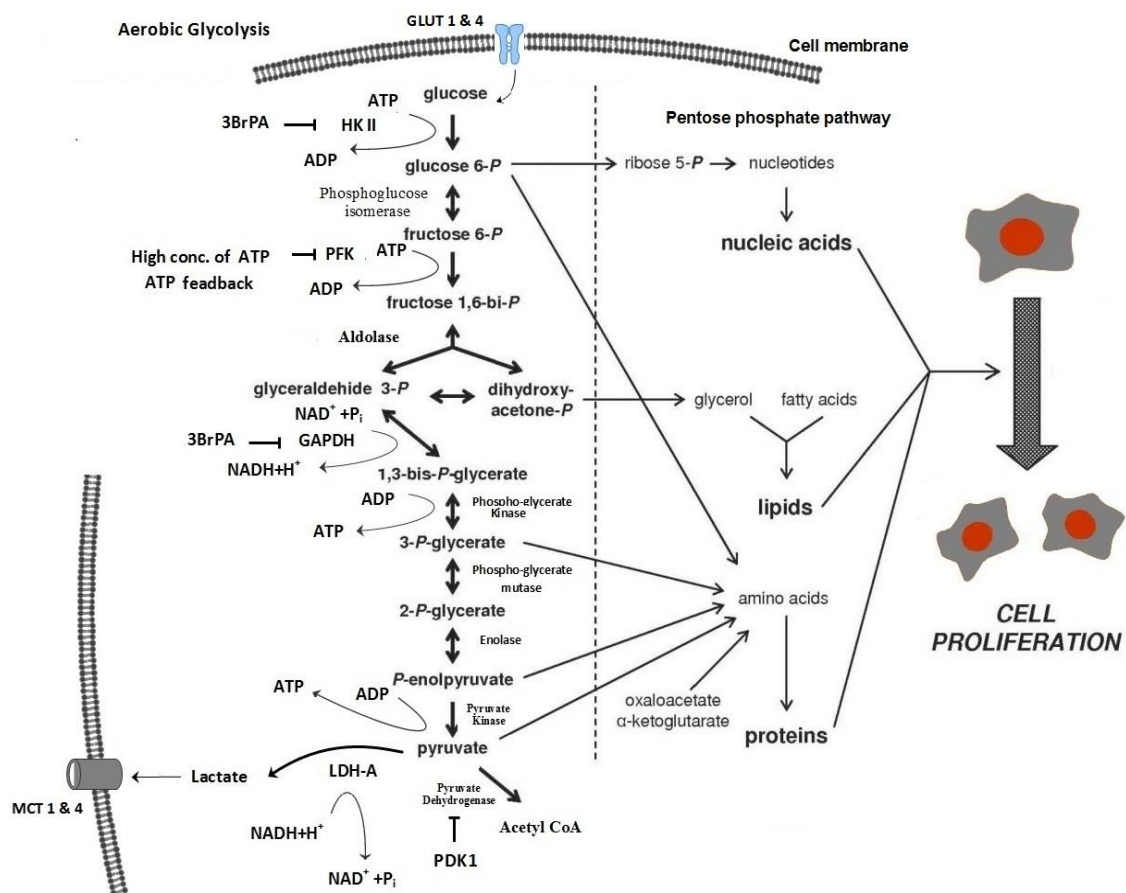


**Figure 1.12: Aerobic glycolysis.** Show glycolysis steps and intermediates for macromolecule synthesis in pentose phosphate pathway. HKII; hexokinase II, PKF; phosphofruktokinase, PDK1; pyruvate dehydrogenase kinase, LDH-A; lactate dehydrogenase kinase, GLUT; glucose transporter, MCT; monocarboxylate transporter

Cancer cells reprogram their metabolism from oxidative phosphorylation to aerobic glycolysis for several reasons. First, high proliferation rates of cancer cells require a high amount of energy, which can be obtained through aerobic glycolysis. Despite that generated energy in glycolysis is less by 18 times than oxidative phosphorylation, aerobic glycolysis can generate much more ATP than oxidative phosphorylation through

producing ATP faster by 10-100 times (Liberti and Locasale, 2016; Lunt and Vander Heiden, 2011). Second, mitochondrial oxidative phosphorylation is accompanied by reactive oxygen species (ROS) production, therefore, reducing oxidative phosphorylation by cancer cells decreases ROS levels, which has cytotoxic effect on the cells (Kang and Pervaiz, 2012; Nogueira et al., 2008). Third, several intermediates from glycolysis can be used for macromolecule biosynthesis such as ribose-5-phosphate for nucleotide, and glycerol for lipid, which are essential for cell division and cancer proliferation, as illustrated in Figure 1.12 (Kroemer and Pouyssegur, 2008; Lunt and Vander Heiden, 2011). Fourth, lactic acid, the end product of glycolysis that is secreted to the tumor microenvironment through monocarboxylate transporter (particularly MCT1 and MCT4) decreases the pH of the microenvironment, which is crucial for increasing cancer cell migration and metastasis (Doherty and Cleveland, 2013; Jiang, 2017). Finally, acidification of the tumor microenvironment can suppress an immune response. For example, acidic pH can weaken T-helper cells and cytokines, which activate effector T-cells; which are an essential for cancer immune response (Huber et al., 2017; Jiang, 2017).

### **1.5.2 Pentose phosphate pathway and its role in antioxidant response**

The pentose phosphate pathway (PPP), which branches out from glycolysis at first committed step of glucose metabolism (Sreedhar and Zhao, 2018), is an important pathway in order to synthesize precursors for nucleotides and amino acids which are required in large quantities for building new cells (Sreedhar and Zhao, 2018; Stincone et al., 2014), it is also an exclusive source of NADPH generation, which plays an essential role in detoxification of intracellular reactive oxygen species (ROS) (Jiang et al., 2014; Riganti et al., 2012).

In the cell, hexokinase (HK) enzyme catalyses phosphorylation of glucose to glucose-6-phosphate (G6P) which can be further metabolized through glycolysis or dehydrogenated by glucose-6-phosphate dehydrogenase (G6PD) in the PPP (Tsouko et al., 2014).

The PPP comprises of two branches: the oxidative branch and the non-oxidative branch. The oxidative branch includes series of irreversible reactions starting with G6P generating ribulose-5-phosphate that converts later to ribose-5-phosphate, and two molecules of NADPH. While, the non-oxidative branch includes a series of reversible reactions in which intermediates in glycolysis such as fructose-6-phosphate (F6P) and glyceraldehyde-3-phosphate (G3P) convert to ribose-5-phosphate and xylulose-5- Phosphate and vice versa, creating a reversible link between glycolysis and PPP (Jiang et al., 2014; Patra and Hay, 2014; Stincone et al., 2014) as shown in Figure 1.13.

Produced NADPH in PPP is crucial for glutathione reductase function as a cofactor to reduce oxidized glutathione. Oxidized glutathione consists of two molecules of disulfide linked together (GSSG). Upon reducing, disulfide breaks and two molecules of reduced GSH will form, as shown in Figure 1.14. Reduced GSH then will be used by glutathione peroxidase as an electron donor for reducing reactive oxygen species such as hydrogen peroxide ( $H_2O_2$ ) and lipo-peroxide (L-OOH) (Rivas-Arancibia et al., 2011).

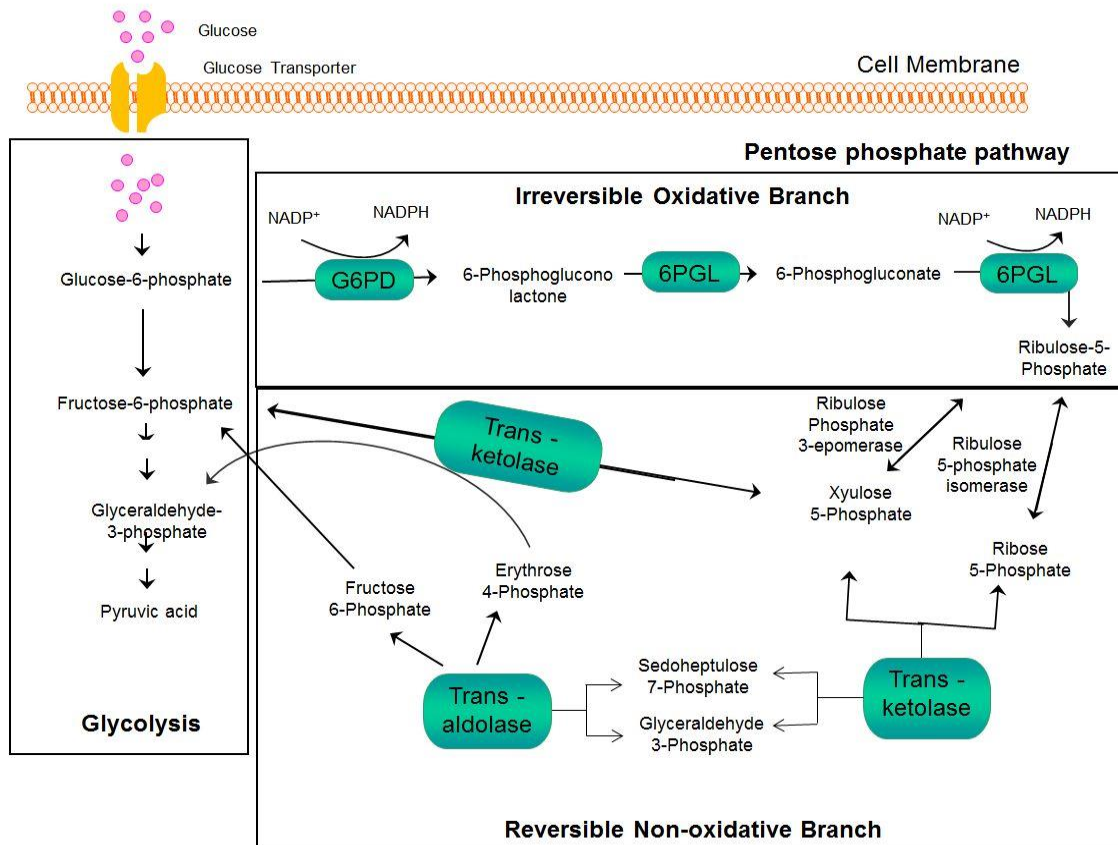


**Figure 1.13:** A schematic representation shows the pentose phosphate pathway and its crosslink with glycolysis. The oxidative branch of the PPP generates NADPH, whereas, the non-oxidative branch produces ribose-5-phosphate from oxidative branch as well as glycolytic intermediates. G6PD: glucose-6-phosphate dehydrogenase, 6PGD: 6-phosphogluconate dehydrogenase, 6PGL: 6-Phosphogluconolactonase.

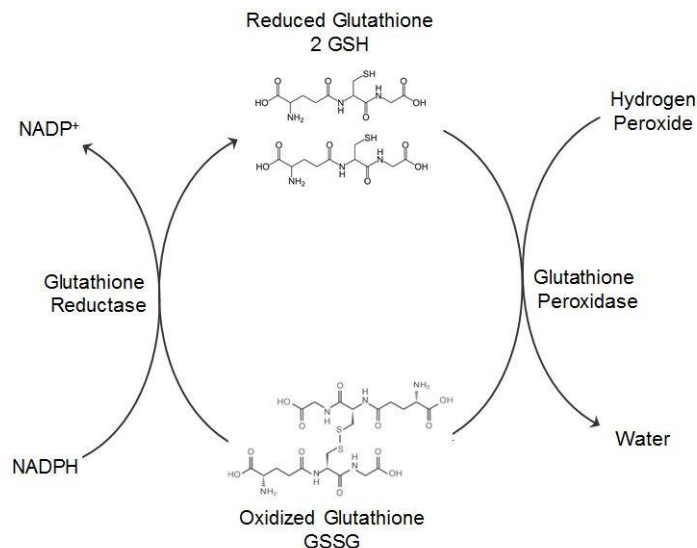


**Figure 1.14:** Scheme representation shows the role of NADPH in reducing of oxidized glutathione GSSG by glutathione reductase.

Although oxidative stress in cancer cells is higher than normal cells (Schumacker, 2006), cancer cells can tolerate these increases in oxidative stress through several

mechanisms(Thorpe et al., 2004). One of the effective ways is through increasing activity of the antioxidant systems including glutathione to keep generated reactive species that can induces apoptosis at non-toxic levels (Redza-Dutordoir and Averill-Bates, 2016).Therefore, the PPP plays a critical role in cancer progression since it provides cancer cells with large amount of macromolecules required for nucleotide biosynthesis, a building unit for repair and synthesis of DNA and RNA (Jiang et al., 2014; Tsouko et al., 2014), it has also been reported that cancer cells, which reprogram their metabolism, direct most of glucose flux into PPP (Jiang et al., 2014). Furthermore, PPP produces the reducing agent; NADPH that maintains the redox homeostasis in cancer cells through glutathione production, and serves as a cofactor in lipids and amino acids biosynthesis (Ayala et al., 2014; Lushchak, 2012; Sreedhar and Zhao, 2018), hence, this pathway could be effective strategy for treatment of cancer cells.

### **1.5.3 Targeting glycolysis with 3-Bromopyruvic acid**

Targeting glycolysis can provide a promising strategy for cancer therapy since glycolysis plays an important role in cell transformation, cancer cell proliferation, and metastasis (Finley and Thompson, 2015; Pascual et al., 2018). There is evidence that expression of several proteins and enzymes, which are related to glycolysis pathway, such as HKII, MCTs, GLUTs, LDH, and PFK-B, are raised significantly in most cancers (Ganapathy-Kanniappan and Geschwind, 2013; Li et al., 2014). Many chemicals and antimetabolites have been developed to be used as anticancer drugs through targeting glycolysis pathway, however, the majority of them are unsuccessful due to development of resistance, lack of specificity, low efficiency, or toxicity to normal cells (Ganapathy-Kanniappan, 2016; Scholar, 2007). 3-Bromopyruvic acid (3BrPA), can inhibit glycolysis through targeting HKII, GAPDH, and pyruvate, as shown in Figure 1.12 (Ganapathy-Kanniappan et al., 2010; Leni et al., 2013). Moreover, it was reported that 3BrPA can affect oxidative phosphorylation through inhibiting succinate dehydrogenase(Sanborn et al., 1971).

It was demonstrated that chemotherapy can induce oxidative stress, which can affect cancer cells. However, the mechanism by which these drugs promote ROS production as well as their effect is not clear yet (Molavian et al., 2016; Yokoyama et al., 2017). 3BrPA like other anticancer drugs can induce ROS production. In fact, it was reported that treating breast cancer cells; MDA-MB-435 and MDA-MB-231 cells, with 3-BrPA has induced autophagy through stimulating ROS production (Zhang et al., 2014). Despite that, the effect of 3BrPA on the mitochondrial shape and the cell migration remains unclear.

#### **1.5.4 Oxidative phosphorylation in cancer cells**

According to the Warburg hypothesis, cancer cells reprogram their metabolism due to defect in mitochondrial oxidative phosphorylation (Vander Heiden et al., 2009). However, it has been proved that oxidative phosphorylation in most cancer cells is intact (Moreno-Sanchez et al., 2007), despite the fact that cancer cells prefer to rely on glycolysis for ATP production (Jiang, 2017). The Warburg theory has been modulated by some authors who consider that metabolic reprogramming in cancer cells is due to suppression of mitochondrial oxidative phosphorylation by enhanced glycolysis rather than defect in oxidative phosphorylation, and it can be restored if glycolysis is inhibited (Fantin et al., 2006; Moreno-Sanchez et al., 2007; Smolkova et al., 2011).

A key of metabolic reprogramming in cancer cells is pyruvate dehydrogenase (PDH), which is converts pyruvate to acetyl CoA (Eyassu and Angione, 2017). This enzyme can be inhibited by pyruvate dehydrogenase kinase (PDK), which was found to be overexpressed in hypoxic conditions and in many cancers, leading to reprogram metabolism toward glycolysis (Sradhanjali and Reddy, 2018; Waters et al., 2014). Therefore, targeting PDK can enhances PDH activity and reverse metabolism from glycolysis to oxidative phosphorylation (Saunier et al., 2017).

Despite this metabolic reprogramming in cancer cells, evidence shows that oxidative phosphorylation contributes to total ATP by 30%. This ratio is varying depending on

cancer cell and microenvironment condition. For example, it was reported that oxidative phosphorylation contributes to ATP production by 79 and 91% in HeLa cells and MCF-7 cells, respectively. While, this ratio reduced to 29 and 36% respectively under hypoxic condition (Rodríguez-Enríquez et al., 2010; Zu and Guppy, 2004).

Mitochondrial structure and shape especially inner mitochondrial membrane can play an important role in mitochondrial function. It was reported that reducing inner mitochondrial membrane can affect ETC function, thereby ATP production (Mannella, 2006). which is essential in cancer progression (Maiuri and Kroemer, 2015), including cell migration (Hüttemann et al., 2007). In contrast, many studies linked mitochondrial dysfunction to cancer cell proliferation and cell migration (Antico Arciuch et al., 2012; Ma et al., 2013). Despite that the effect of mitochondrial metabolism on cancer cells remains controversial.

#### **1.5.5 Targeting oxidative phosphorylation with Antimycin A**

AMA is a secondary metabolite produced by *Streptomyces kitazawensis* (Ma et al., 2011), and is considered a potent inhibitor of cytochrome c oxidoreductase complex (complex III) of electron transport chain in mitochondria. It binds to the Qi site of complex III inhibiting the oxidation of ubiquinol, which blocks transfer of electron between cytochrome  $b_L$  and  $b_H$  in complex III, as shown in Figure 1.15 (Alexandre and Lehninger, 1984; Pham et al., 2000).

Targeting complex III inhibits transport of electrons between ETC proteins, which results in a collapse of the proton gradient across the inner membrane. This can lead to the loss of the mitochondrial membrane potential, which is essential for synthesis of ATP (Ma et al., 2011; Quinlan et al., 2011).

It was reported that treating cancer cells such as HeLa cells, which mainly depend on the mitochondrial oxidative phosphorylation (Rodríguez-Enríquez et al., 2010), can lead to significant decreases in ATP production (Maguire et al., 1992; Pham et al., 2000). However, its effect on glycolytic cancer cells is not known.

Increasing ROS level is considered one consequence of targeting complex III with AMA (Balaban et al., 2005; Panduri et al., 2004). It was found that treating FRTL, thyroid normal cell of rat, with 10  $\mu\text{M}$  AMA induced mitochondrial superoxide production without inducing apoptosis (Wang et al., 2015a).

Recent evidence suggests that treating plant roots of *Tritium aestivum* with AMA showed a change in mitochondrial morphology, it may be due to high level of ROS production (Rakhmatullina et al., 2016). However, no previous study has investigated the effect of AMA on mitochondrial morphology in mammalian cells.

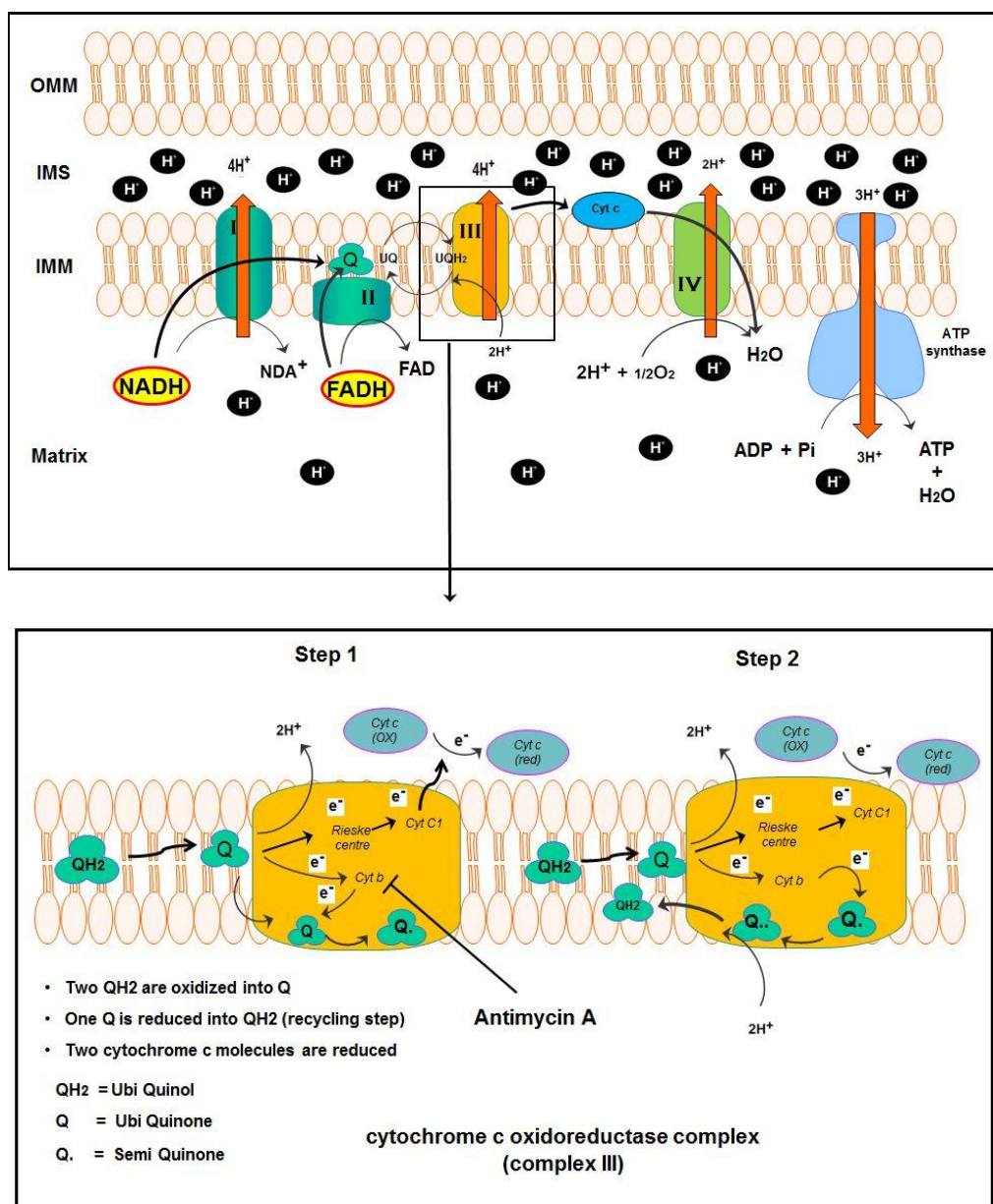


**Figure 1.15: Target site of Antimycin A in Electron Transport Chain.** AMA inhibit transport of electron from cytochrome b<sub>L</sub> to cytochrome b<sub>H</sub> thereby inhibition of mitochondrial oxidative phosphorylation.

## 1.6 Pro-apoptotic protein p66shc

P66shc protein is 66kDa isoform of adaptor protein shc 1 (or shc A) (Src homology 2 domain containing transforming protein 1). In mammals shc protein is encoded by three shc genes: shc A, shc B, and shc C (Ravichandran, 2001). Whereas shc B and shc C expression are limited to the neuronal cells, shc A has ubiquitous expression and has 3 isoforms p46shc, p52shc, and p66shc with molecular weight 46, 52, 66 kDa, respectively. They share a Src-homology 2 domain (SH2), a collagen homology region (CH1), and phosphotyrosine-binding domain (PTB). p66shc contains an additional CH-like domain termed (CH2) that contains a serine phosphorylation site (Ser36), which is critical for its pro-oxidant properties (Galimov, 2010; Sakai et al., 2000), as shown in Figure 1.16.

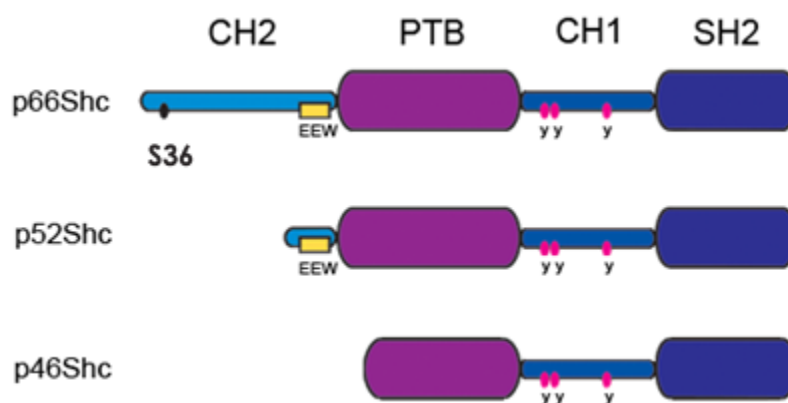


Figure1.16: Organization of Shc A isoforms.

Cited from <http://www.atlasgeneticsoncology.org>

The shc proteins function as phosphotyrosine adaptor molecules in different receptor mediated signalling cascades. Whereas both protein p46shc and p52shc participate in the transmission of mitogenic signals from cell surface receptor tyrosine kinases to RAS proteins that lead to rising cell proliferation, the protein p66shc functions as a critical redox enzyme involved in mitochondrial reactive oxygen species (ROS) generation and inducer of apoptosis (Ravichandran, 2001; Trinei et al., 2002).

In normal cells, ROS production is maintained at a low level by various enzyme systems and this small ratio has an essential role in cell signalling and homeostasis. However, a number of external and internal factors can raise the level of ROS production and disturb this balance that leads to the state known as oxidative stress, which is responsible for damage of DNA, proteins, and lipids (Bhattacharyya et al., 2014; Stanczyk et al., 2005).

It is well established that in response to DNA damage induced by oxidative stress, protein 53 will activate and induce arrest in the cell cycle until DNA damage repairs, in case repair is impossible, it will induce apoptosis through activation of several pro-apoptotic proteins (Amundson et al., 1998). Trinei and co-workers (2002) suggested that p66shc, which is a downstream target of the p53, is essential for stress-activated p53 that induces the elevation of intracellular oxidants, releases of cytochrome c, and apoptosis. It has also been shown by Tomita and co-workers (2012) that p53 deficiency suppresses the enhanced p66Shc signaling which causes apoptosis during oxidative stress. However, others believe that p66shc also can induce apoptosis independently from p53 (Orsini et al., 2004; Tiberi et al., 2006; Xiong et al., 2013).

Giorgio and co-workers (2005) have suggested a mechanism that describes the role of p66shc in mitochondria-dependent apoptosis. According to this mechanism in normal conditions protein p66shc is inactive and 44% of total p66shc is localized to the mitochondria, while 32% and 24% are localized in the cytoplasm and the endoplasmic reticulum, respectively. Oxidative stress enhances translocation of protein p66shc into mitochondria.

According to Pinton and co-workers (2007), p66shc translocates into the mitochondria through a signal pathway. Upon exposure to oxidative stress, PKC $\beta$  is activated, and this leads to p66Shc phosphorylation at Ser36. This phosphorylation allows it to transfer from the cytoplasm into mitochondrial intermembrane space. Giorgio and co-workers (2005) found that p66shc can translocate through the TIM-TOM import system. In the

mitochondria, the protein p66shc is inactive and binds with TIM-TOM complex through mtHsp70. Pro-apoptotic stimuli can dissociate it from the complex, the monomeric form of p66shc is active and can oxidize cytochrome c and catalyze production of  $H_2O_2$  through reduction of  $O_2$ , this leads to permeability-transition pore formation that allow entering of ions, solutes, and water into mitochondria and release the cytochrome c into the cytosol, which is the initiator of apoptosome assembly, and caspase activation that lead to apoptosis, as shown in Figure 1.17.

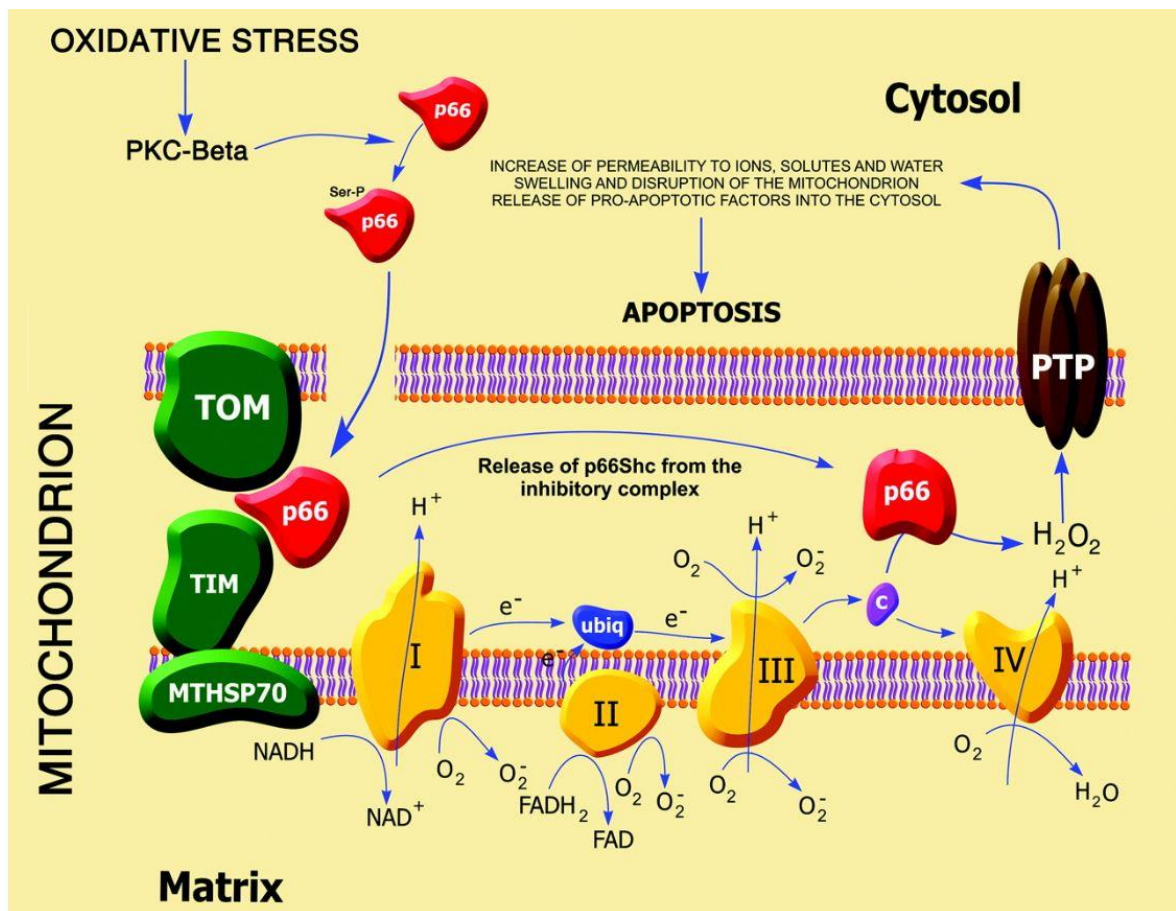


**Figure 1.17: Mechanism of p66shc activation and translocation to mitochondria.** Phosphorylation of p66Shc at Ser36 is essential for its translocation from cytosol to mitochondria via TIM-TOM complex. In mitochondria, activated p66Shc can oxidizes cytochrome c and catalyzes the reduction of  $O_2$  to  $H_2O_2$ , which can induce opening of the mitochondrial permeability transition pore (PTP), as a result mitochondrial membrane permeability to ions, solutes and water will increase and this lead to swelling and disruption of mitochondrial outer membrane, which allow to release of cytochrome c into cytosol that induce apoptosis. Cited from (Cosentino et al., 2008).

### **1.7 Role of p66shc in cancer cell metabolism and cell migration**

It has been demonstrated that p66shc plays important roles in many biological processes and it is implicated in various pathological processes including cancer development, progression, and metastasis, and mostly related to the cellular responses to oxidative stress (De Marchi et al., 2013).

In normal cells, oxidative stress induced by external factors can cause cellular damage and trigger cancer progression. Pro-apoptotic p66shc can play a protective role through removing of damaged cells via ROS induced apoptosis (Lebiedzinska-Arciszewska et al., 2015). However, cancer cells can avoid apoptosis, which is considered one of cancer hallmarks (Hanahan and Weinberg, 2011). Moreover, cancer cells can exploit normal cellular mechanisms and proteins including p66shc for their proliferation and progression (Rajendran et al., 2010).

Oxidation of cytochrome c, which is an essential enzyme that transfers electrons from reduced Cytc to molecular oxygen in electron transport system, can lead to defects mitochondrial ATP production (Tsukihara et al., 1996). Moreover, increased ROS levels, which can be induced by several factors including high glucose levels, can induce mutation of mtDNA and inhibition of several mitochondrial enzymes. This leads to significant depletion of ATP levels, which can affect most cellular processes (Wallace, 2012). To compensate these decreases in ATP level, cancer cells enhance reprogramming metabolism to glycolysis, which can leads to increasing cell migration due to raising lactic acid production, the end product of glycolysis (Zheng, 2012). In fact, previous research has established that ROS induced by hyperglycaemia, which is an important characteristic of several diseases including diabetes and obesity, can increase p66shc expression (Berniakovich et al., 2008; De Marchi et al., 2013; Xi et al., 2010).

It has been found that p66shc levels increased in several cancer cell lines especially highly metastatic variants, suggesting a possible role of p66shc in cancer cell migration and

metastasis (Jackson et al., 2000). Despite that, there remains a paucity of evidence on its role in cell migration and metastasis.

Apoptosis induced by mitochondrial ROS, which can be increased as a result of overexpressed p66shc, remains a major challenge for cancer cells (Bhat et al., 2015). Increased ROS levels in cancer cells can induce several changes within the cell including mitochondrial morphologic changes (Wu et al., 2011) and increasing the expression of protein TRAP1 (Kadye et al., 2014), which can play an important role in apoptotic resistance. Despite the well characterized role of p66shc in inducing ROS generation, its relationship to TRAP1, which can be induced under oxidative stress condition (Basit et al., 2017; Yoshida et al., 2013), has not been investigated.

### **1.8 Role of cytoprotective TRAP1 protein in cancer cells**

Tumor necrosis factor (TNF) receptor associated protein 1 (TRAP1) is a mitochondrial chaperone protein that belongs to the heat shock protein 90 (HSP90) family. This protein has ATPase activity and interacts with TNF1. It plays an important role in regulation of several biological processes specifically, in regulation of mitochondrial integrity, protection from DNA damage and cell death induced by oxidative stresses (Kang, 2012; Matassa et al., 2012; Ou et al., 2014). It has been found that the majority of cancers exploit TRAP1 protein for their survival and metastasis, therefore, its expression is upregulated dramatically in cancer cells compared to the normal cells (Gao et al., 2012; Guzzo et al., 2014).

Previous research has demonstrated that the antioxidant activity of TRAP1 protects cancer cells from apoptosis through avoiding lethal opening of the mitochondrial permeability transition pore (mPTP) (Guzzo et al., 2014). The mechanism of opening this channel has been described by Tsujimoto and co-workers (2006). They suggested that this channel consists of the voltage-dependent anion channel (VDAC), located at mitochondrial outer membrane, the adenine nucleotide translocator (ANT), which is located at the inner

membrane of mitochondrial, and Cyclophilin D (Cyp D) that is located in the mitochondrial matrix.

Cyp D, which is show peptidyl-prolyl cis-trans isomerase activity and able to catalyse protein folding, can be activated under oxidative stress induced by several pathological conditions such diabetes and obesity (Karamanlidis et al., 2013; Yan et al., 2016). Upon activation, it can interacts with the PTP complex forming non-selective pore in the mitochondrial inner membrane that allow free movement of molecules smaller than 1500 Daltons, leading to mitochondrial swelling and cell death (Elustondo et al., 2016; Marzo et al., 1998). However, cancer cells can prevent activation of Cyp D thereby inhibiting apoptosis through increasing the expression of TRAP1, which binds and inhibits the Cyp-D function (Kang, 2012), as illustrated in Figure 1.18.

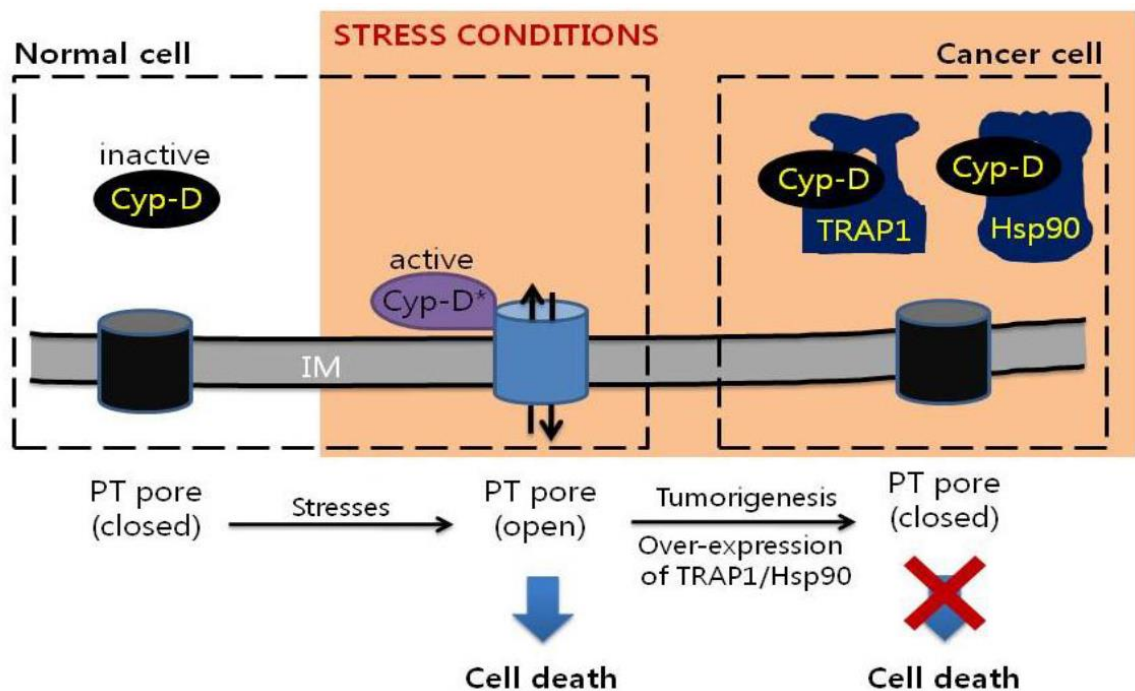


**Figure 1.18: CypD control mitochondrial permeability transition pore opening.** Under normal conditions, the CypD in a mitochondrial matrix is inactive and the PTP is closed. Under stress conditions, the Cyp D is activated and interacts with the PTP, which triggers opening of the pore and results in the increase permeability, leading to swelling of the mitochondria and rupturing of the mitochondrial outer membrane, this lead to release of cytochrome c and thus induction of cell death. Cancer cells, under same conditions overexpressed TRAP1 which inhibits the function of the Cyp-D and prevent formation of PTP. Cited from (Guzzo et al., 2014).

### **1.9 Role of TRAP1 in cancer cells metabolism and cell migration**

In addition to cytoprotective role of mitochondrial chaperone TRAP1, it has been demonstrated that TRAP1 also play an important role in the growth and spreading of cancer cells through binding to and inhibiting SDH, which induces reprogramming of mitochondrial metabolism to aerobic glycolysis (Amoroso et al., 2014; Briere et al., 2005; Sciacovelli et al., 2013), and it is well known that aerobic glycolysis promote cell migration (Jiang, 2017).

It was reported that silencing TRAP1 can suppress cancer cell migration and invasion significantly without any effect on cell proliferation (Caino et al., 2013). In contrast, others found that TRAP1 knockdown can inhibit proliferation and induce apoptosis (Tain et al., 2014). Similarly, Zhang and co-workers (2015) found that TRAP1 knockdown can inhibit cell growth in MDA-MB-231 and MCF-7 breast cancer cells. They suggested that TRAP1 can play an important role in the regulation of mitochondrial morphology. They also had suggested that low expression of TRAP1 gene is related to the small and rod-shape mitochondria in metastatic cancer cells, whereas, high levels of TRAP1 expression are related to elongated shape mitochondria in non-metastatic cancer cells. Moreover, they found that overexpression of TRAP1 can induce elongation of mitochondria and suppress cell migration and invasion ability. This finding may be contradictory with the role of TRAP1 in cancer cells, since TRAP1 can be overexpressed when the cells encountered oxidative stress such as being induced by hyperglycaemia, diabetes, and obesity (De Marchi et al., 2013; Hall and Martinus, 2013; Montesano Gesualdi et al., 2007; Pridgeon et al., 2007), and this leads to inhibiting SDH that defects oxidative phosphorylation and enhances cancer cells to reprogram their metabolism to glycolysis (Guzzo et al., 2014; Sciacovelli et al., 2013), which in turn enhances cell migration. Despite that, the role of TRAP1 in cancer cell migration and metabolism requires more investigations.

### **1.10 Link between p66shc and TRAP1**

Many studies have demonstrated that oxidative stress can induce expression of both p66shc and TRAP1 (Kadye et al., 2014; Lebedzinska-Arciszewska et al., 2015); however, they show different effects on the cells. While, activation of p66shc can induce apoptosis and enhance metabolic reprogramming due to inhibition of mitochondrial oxidative phosphorylation as a result of cytochrome c oxidation (Ott et al., 2007), increasing TRAP1 expression can inhibit apoptosis induced by ROS and inhibit mitochondrial oxidative phosphorylation (Yoshida et al., 2013). Despite the high expression of both p66shc and TRAP1 proteins in cancer cells, the link between them has not been investigated.

### **1.11 Effect of microenvironment on the mitochondrial morphology**

The tumor microenvironment (TME), which in addition to cancer cells includes stromal cells, signaling molecules, immune cells, nerve cells, extracellular matrix (ECM), and blood vessels, has an important role in the initiation, progression, and migration of cancer cells (Weber and Kuo, 2012; Kamińska et al., 2015).

The interaction between cancer cells and microenvironment is a very complex process, in which several tumor microenvironment components play critical roles in cancer cell survival, proliferation, and successful metastasis (Jayappa et al., 2016). In turn, cancer cells can affect the microenvironment through secreting many enzymes and factors that remodel surrounding ECM making it more suitable for their growth, progression, migration and colonization at distant organs (Lu et al., 2012; Xiong and Xu, 2016). Moreover, cancer cells through secretion of H<sub>2</sub>O<sub>2</sub> into microenvironment can promote neighbouring stromal cells to reprogram their metabolism to glycolysis and efflux by-products to the microenvironment, which can be used by cancer cells for generation of energy and/or affect microenvironment acidity (Kato et al., 2013; Rofstad et al., 2006; Sotgia et al., 2012;

Xing et al., 2015). These interactions between cancer cells and their microenvironment pose a challenge in cancer cell investigation in the artificial micro-environments.

Two-dimensional (2D) cell culture technique have been used for long time as an essential tool in studying cancer cells and molecular biology (Lee et al., 2008, Edmondson et al., 2014, Antoni et al., 2015). However, it differs from true microenvironment that is present in vivo, where cell-cell and cell-extracellular matrix (ECM) interaction occur (Aljitawi et al., 2014, Edmondson et al., 2014). Three dimensional (3D) cell culture model, which is also known as scaffolds, has been developed to allow the cells to grow and interact with surrounding artificial microenvironment that resembles to some extent to human tissues and tumor microenvironments (Lee et al., 2008; Vinci et al., 2012). However, there are limitations, since artificial 3D cell culture lacks the vascular system which is essential to support tissues with oxygen, nutrients, and to remove waste as in vivo (Yamada and Cukierman, 2007).

Recently, several models have been designed to be used as 3D cell culture more resembling to tumor microenvironments such as Alvetex scaffolds and decellularised tissue. Indeed, using decellularised tissue, in which biomedical engineering is used to isolate the ECM of specific tissues such as lung, and liver tissues from their cells, leaving only an ECM scaffold, to be used as 3D cell culture, has taken important consideration since it overcomes the limitations of uses of 3D cell cultures in-vitro (Aljitawi et al., 2014; MacDonald et al., 2014; Mazza et al., 2015; Mishra et al., 2012; Mokhtari-Jafari et al., 2015). Therefore, it will be of a great value to investigate the impact of mitochondrial morphologic changes on metabolism and cell migration in 3D environments such as collagen matrices, Alvetex scaffolds and Decellularised lung tissue which have characteristics more resemble to their microenvironment.

### **1.12 Aim of the study**

As described above, mitochondrial morphology is highly dynamic and it can be shifted easily between small, fragmented and large, elongated network-like shape as a response to oxidative stress that can be induced by many factors such as high glucose level, anticancer agents, and ROS. However, the effect of mitochondrial morphological changes on the metabolism and the cell migration, which is critical for metastasis, is not clear. In this study, we hypothesized that mitochondrial fragmentation induced by factors including high glucose level, H<sub>2</sub>O<sub>2</sub>, PGC1 $\alpha$  coactivator, and anticancer drugs targeting metabolism, can induce metabolic reprogramming from oxidative phosphorylation to aerobic glycolysis that play essential role in accelerating cancer cell migration.

To achieve this goal we treated MDA-MB-231 breast cancer cells with different glucose concentrations (1, 5.5, and 25mM), Hydrogen peroxide, ZLN005 activator (PGC-1 $\alpha$  coactivator), and anti-metabolic anticancer drugs including Antimycin A (Sigma) and 3-Bromopyruvic acid (Sigma) to study changes in mitochondrial morphology, mitochondrial metabolism, and cell migration.

Over the past decade investigation added valuable information concerning role of p66shc and TRAP1 in cancer cells. However, to date, no evidence has been found associating p66shc with TRAP1 and their effect on cancer cell migration. We hypothesized that expression and activation of cytoprotective protein TRAP1 are strongly affected by activation of pro-apoptotic protein p66shc since the function of both are related to mitochondria and both activated under oxidative stress that can be induced by several factors such as hyperglycaemic condition.

To fill this gap in information and for a better understanding, we investigated the relationship between p66shc and TRAP1 through silencing the expression of their genes, as well as their effect on the metabolism and cell migration were investigated. Using three

cell lines: breast cancer cell line MDA-MB-231, fibrosarcoma cell line HT1080, and cervical cancer HeLa cells, for this study.

Finally, in this study, we aimed to uncover the impact of mitochondria in 3D environments, which mimic tissue culture in vivo, on cell migration in MDA-MB-231 cells, to determine whether growing these cells in 3D culture nullified different mitochondrial morphology, compared with 2D culture and to explain the effect on cell migration.

## **Chapter two: Material and Methods**

### **2.1 Materials**

#### **2.1.1 Reagent and Kits**

All chemicals and reagents used in the study were of analytical grade.

Reagents used in cell culture including; Dulbecco's modified Eagle medium (DMEM; Catalog no. 11880-028 and A14430-01), Eagle's Minimum Essential Medium (EMEM; Catalog no.51200-046), Fetal bovine serum (FBS; Catalog no.10500-064), Penicillin-Streptomycin (Catalog no. 15140-122), L-Glutamine (Catalog no. 25030-081), 0.05% Trypsin-EDTA (Catalog no. 25300-054) , D-glucose (Catalog no.A13275-04), Phosphate buffer saline (PBS) (Catalog no.10010-023), Hank's Balanced Salt Solution ( Catalog no.14175-095), were purchased from Fisher Scientific, UK.

Reagents used for total protein harvesting including; RIPA buffer, 1X (Catalog no.10230544), and the Protease Inhibitor Cocktail (Catalog no. 539131) were purchased from Fisher Scientific, UK, and Merck Millipore, UK respectively. The protein quantification was performed using the Pierce Bradford assay kit (Catalog no. 23246), it was purchased from Fisher Scientific, UK.

Reagents used for western blot; Precision plus Protein™ Dual Color Standards (Catalog no.161-0374) and Clarity™ Western ECL Blotting Substrate (Catalog no. 17050-61) were purchased from Bio-Rad Laboratories, Inc., UK. ReBlot Plus Mild Antibody Stripping Solution, 10X (Catalog no. 2502) was purchased from Merck Millipore. All primary antibodies used are listed in Table 2.1, as well as their respective Catalog number and brand.

Chemicals used for hand cast SDS-PAGE gel: Sodium dodecyl sulfate (SDS) (99%) (Catalog no. 10593335), Ammonium persulfate (Catalog no. 17874), Proto Gel 30% Solution (Catalog no. 12381469), Tris-Base (Catalog no. BP 152-500), NaCl, KCl, Glycine, and Gelatine were purchased from Fisher Scientific, UK. N, N, N', N'-

Tetramethylethylenediamine (Catalog no. T9281-25ML) and methanol were purchased from Sigma-Aldrich, UK.

4-20% Mini-Protein® TGX™ Precast Protein Gels (Catalog no. 4561094) and Trans-Blot® Turbo™ Mini PVDF Transfer Packs (Catalog no. 1704156) were purchased from Bio-Rad Laboratories, Inc., UK.

Reagents used for studying mitochondrial dynamics including; Hydrogen peroxide solution (H<sub>2</sub>O<sub>2</sub>) 30% (Catalog no. 7722-84-1), ZLN005 (Catalog no. 49671-76-3), Mdivi-1 inhibitor (Catalog no. M0199), Antimycin A (Catalog no. A8674), and 3-bromopyruvic acid (Catalog no. 16490) were purchased from Sigma-Aldrich, UK.

All primers used were purchased from Sigma-Aldrich and are listed in Table 2.2. Total DNA was isolated using DNeasy Blood & Tissue Kit (Catalog no. 69504) which was purchased from Qiagen, UK. QuantiTect SYBR Green PCR Kit (SYBR Green PCR master mix) (Catalog no. 204141) was also purchased from Qiagen, UK.

To confirm primer specificity, agarose gel electrophoresis was performed using Agarose I (17850), Blue Juice Gel loading buffer (Catalog no. 10816-015), TAE Buffer (Tris-acetate-EDTA) (50X) (Catalog no. B49), and a 1000bp plus GeneRuler DNA Ladder (Catalog no. SM0321) which were all purchased from Fisher Scientific, UK.

Metabolism Assay Kits used in metabolic studying include; ATP Assay Kit (Catalog no. ab83355) was purchased from Abcam LTD, UK. Glycolysis Cell-Based Assay Kit (Catalog no. CAY600450-1 ea) and OxiSelect™ ROS Assay Kit (Catalog no. STA-342) were purchased from Cambridge bioscience LTD, UK.

Reagent and siRNA used in transfection: DharmaFECT 1 Transfection Reagent and DharmaFECT 4 Transfection reagent were purchased from Thermo Scientific, UK. ON-TARGET plus Non-targeting control siRNA and ON-TARGET plus SMART pool TRAP1 siRNA were purchased from Dharmacon GE Company. Designed SMART pool P66shc siRNA was purchased from Sigma-Aldrich, UK.

MitoTracker Orange (M7510) and Alexa Fluor 488 Phalloidin were purchased from Invitrogen-Thermo Fisher Scientific, UK. Vectashield-Mounting Medium with DAPI was obtained from Vector laboratories, UK.

Collagen Type 1 (Catalog no 2561888) was purchased from Millipore. Goat serum was purchased from Life Technologies. UK. Triton X-100, DMSO and TWEEN<sup>®</sup> 20 were purchased from Sigma-Aldrich. Paraformaldehyde was purchased from Agar Scientific.

Six and twelve well plates, 25cm<sup>2</sup>, 75cm<sup>2</sup> cell culture flasks, and Nunc<sup>™</sup> Micro Well<sup>™</sup> 96-Well Optical-Bottom Plates with Polymer Base (Catalog no. 12-566-70) were purchased from Fisher Scientific, UK. Alvetex Scaffold 12-well plate (Catalog no. AMS.AVP002-10) was purchased from AMS Biotechnology (Europe) Limited.

Table 2.1: list of antibodies used in western blot protein analysis and in immunocytochemistry assay

Code	Dilution	Host species	MWt (kDa)	Catalog no.	Manufacturer
P66shc	1:1000	Rabbit	66	2432	Cell signaling
TRAP1	1:200	Mouse	80	Sc-13134	Santa Cruz
Drp1	1:1000	Mouse	82	ab56788	abcam
PGC-1 $\alpha$	1:1000	Mouse	92	ab54484	abcam
$\beta$ -actin	1:2500	Mouse	45	3700	Cell signaling
$\beta$ -actin	1:2500	Rabbit	45	4970S	Cell signaling

Table 2.2: list of primers used in real-time qPCR

Gene	Forward primer 5`-3`	Reverse primer 5`-3`	Fragment size (bp)
tRNA	CACCCAAGAACAGGGTTTGT	TGGCCATGGGTATGTTGTTA	107
$\beta$ -actin	GATGCCTCTCTTGCTCTGGG	GTGCTCAGGGCTTCTTGTC	101

### **2.1.2 Preparation of stock solutions:**

1mM (w/v) of Mito-Tracker® Orange CM-H2TMRos stock solution was prepared by dissolving the contents of one vial (50µg) in 127µl of Dimethyl sulfoxide (DMSO). 10 mM (w/v) of Antimycin A stock solution from Antimycin A (90%) was prepared by dissolving it in Ethanol (100%). 20 mM (w/v) of 3- Bromopyruvate stock solution from 3- Bromopyruvate (98%) was prepared by dissolving it in sterilized ultra-pure water. 20 mM (w/v) of ZLN005 stock solution from ZLN005 (95%) and 20 mM (w/v) of mdivi-1 inhibitor stock solution from mdivi-1 inhibitor (98%) were prepared by dissolving them in DMSO. Working solutions for the above mentioned chemicals were prepared by diluting stock solutions in DMEM just before using them in experiments.

## **2.2 Methods**

### **2.2.1 Cell culture**

In the present study, three cell lines from American Type Culture Collection (ATCC) were used.

MDA-MB-231            human breast cancer cell line

HT1080                human fibrosarcoma cell line

HeLa cell              cervical carcinoma cell line

Depending on ATCC guidelines, MDA-MB-231 cells were grown in Dulbecco's modified Eagle medium (DMEM) (Gibco, UK), whereas, HT1080, and HeLa cells were grown in Eagle's Minimum Essential Medium (EMEM) (Gibco, UK), in humidified atmosphere supplemented with 5% CO<sub>2</sub> at 37°C. The media were supplemented with

- Fetal bovine serum (FBS)    (Gibco, UK)            (10% V/V)
- Penicillin                        (Gibco, UK)            (100 IU/mL)
- Streptomycin                  (Gibco, UK)            (100 µg/mL)
- L-Glutamine                    (Gibco, UK)            (2mM)

The glucose concentration in the medium was modified to (1, 5.5 and 25mM) using D-glucose (Gibco) and cells were continuously cultured in medium with relevant glucose levels.

### **2.2.2 Counting cells**

It is important to seed equal numbers of the cells in all experimental units in order to obtain optimum results from experimental replicates. Cells were counted using a haemocytometer slide. A clean coverslip was put over the haemocytometer slide and a small amount of cell suspension (about 10  $\mu$ L) was placed in the space between the haemocytometer slide and the cover slip, later cells were counted with an inverted light microscope (Leitz Labovert) using 10x objective lens. Depending on the following equation the number of cells/ml was calculated:

$$\text{No. of cells / mL} = (\text{No. of Cells counted} / \text{No. of Square counted}) \times 10^4 \times \text{dilution factor}$$

Cell suspensions were made directly from fresh flasks with 70-80% cell confluence after being washed twice with sterilized PBS and de-attached by using Trypsin-EDTA (0.05%). During all experiments cells were seeded 24-48 hours earlier and were washed with sterilized PBS before exposing them to any sort of treatments.

### **2.2.3 Preparing cell lysates**

At the end of the experiments cells that were grown in T-25 culture flasks (25 cm<sup>2</sup>) or T-75 culture flasks (75 cm<sup>2</sup>) were collected and lysates were extracted. The growth media were removed and cells were washed once using chilled PBS. Immediately cells were scraped into PBS and moved into 15 ml tubes then centrifuged in 4° C at 2000 rpm (Eppendorf centrifuge 5804 R) for 15 minutes. Supernatant was discarded and 400  $\mu$ L of protein inhibitor cocktail; A cocktail containing six protease inhibitors: which are AEBSF (Amino-ethyl benzene-sulfonyl fluoride hydrochloride), Aprotinin, E-64, Leupeptin, Pepstatin A and Bestatin hydrochloride, to inhibit a broad range of proteases, and Radio-immunoprecipitation assay (RIPA) buffer (25mM Tris-HCl pH 7.6, 150mM NaCl, 1% NP-40, 1%

sodium deoxy cholate, 0.1% SDS) mixture (1:100), was added to the pellets and mixed well. Lysates were then passed through 21 gauge needles several times to shear the DNA. The suspension was incubated in 4°C for 30 minutes then transferred into 1.5ml Eppendorf tubes and centrifuged in 4°C at 13000 rpm for 15 minutes. Supernatants were collected and stored in freezer (-20° C).

#### **2.2.4 Bradford Protein Assay**

A Bradford protein assay was used to measure the quantity of protein in the samples. The principle of this assay depends on the reaction of protein with the Bradford reagent, which contains Coomassie Brilliant Blue G-250, forming a stable blue solution that has a maximum absorbency at 595nm, the intensity of this blue solution increases with increasing protein concentration and vice versa (Bradford, 1976). This assay was carried out in 96 well plates. Three replicates from each lysate were tested. In the first column of the plate, 195 µL of blank Bradford reagent was applied. While, in columns two and three 5 µL of ascending concentrations of bovine serum albumin standards (25-2000 µg/ml) and 195 µL of Bradford reagent were applied. Columns two and three were used to produce a standard curve to reveal protein concentration in each of the lysates. Finally 5 µL of lysates with 195 µL of Bradford reagent were added to the remaining wells. Details were recorded in a data sheet as shown in Figure 2.1

A plate reader, E max Molecular Device, was used to read the absorbance at 600 nm. From the data provided by the plate reader the concentration of protein in each well and average protein concentration for each sample was displayed in µg/ml.

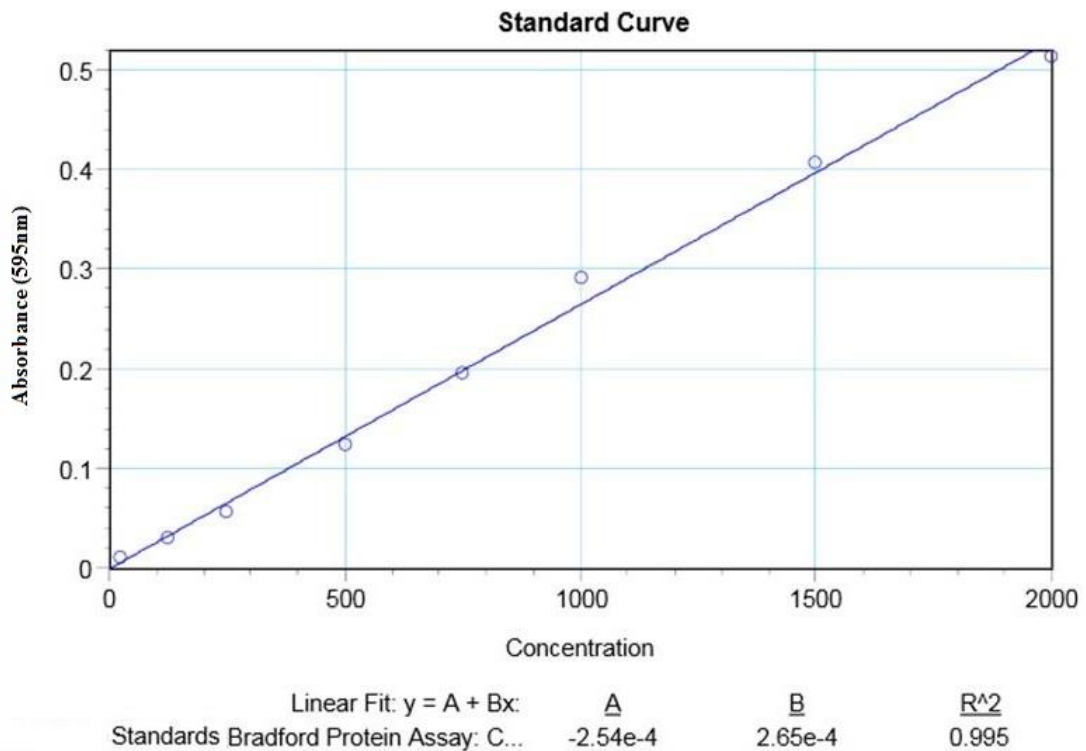
A linear regression equation was then obtained by plotting absorbance versus protein amount. An unknown amount of protein was then estimated by measuring the absorbance and using the linear regression equation that was obtained from the standard, as shown in Figure 2.2.

Type of cell	Date	Experiment No.	R <sup>2</sup>

	Blank	Standard protein		Samples								
	1	2	3	4	5	6	7	8	9	10	11	12
A	195µL Bradford Reagent	5µL BSA (25µg/ml) + 195µL BR										
B	195µL Bradford Reagent	5µL BSA (125µg/ml) + 195µL BR										
C	195µL Bradford Reagent	5µL BSA (250µg/ml) + 195µL BR										
D	195µL Bradford Reagent	5µL BSA (500µg/ml) + 195µL BR										
E	195µL Bradford Reagent	5µL BSA (750µg/ml) + 195µL BR										
F	195µL Bradford Reagent	5µL BSA (1000µg/ml) + 195µL BR										
G	195µL Bradford Reagent	5µL BSA (1500µg/ml) + 195µL BR										
H	195µL Bradford Reagent	5µL BSA (2000µg/ml) + 195µL BR										

**Figure 2.1:** Data sheet shows a standard 96 well plate. Used for loading standard protein and sample with unknown concentration of protein to be measure by a plate reader at 595nm.



**Figure 2.2:** Standard curve for protein with known concentrations and absorbance. For measuring unknown protein concentration using the linear regression equation

## **2.2.5 Sodium Dodecyl Sulphate-Polyacrylamide Gel Electrophoresis (SDS-PAGE)/ Western Blot Analysis**

### **2.2.5.1 Protein Running**

After performing Bradford protein assay, 25  $\mu\text{L}$  of 5X (v/v) loading buffer was added to 100  $\mu\text{L}$  of sample lysate, to ensure the loading lysate protein ran consistently. Later this mixture was boiled for 3-5 minutes at 95  $^{\circ}\text{C}$ . The mixture could be stored at  $-20^{\circ}\text{C}$  until the next step.

After processing lysates with loading buffer, samples were run on a pre-casted SDS-PAGE, 4-20% Mini-PROTEAN<sup>®</sup> TGX<sup>™</sup> gel or 12% hand cast SDS-PAGE gel, in order to dissociate the proteins into their individual polypeptide subunits, depending on their size and molecular weight. Running buffer was added to the gel tank, and then a molecular weight marker and samples between 50-75 $\mu\text{g}$  were loaded in stacking gel wells (after been filled with running buffer). Electrical current was applied to the running tank, 100mA with a constant voltage (250V) during running through the stacking gel and at 50mA through the resolving gel for one hour. After separation of the proteins, the gel was removed from the running tank and transferred to transfer buffer and left to equilibrate in western blot transfer buffer for 15-20 minutes. The gel was transferred to Trans-Blot<sup>®</sup> Turbo<sup>™</sup> Mini PVDF Transfer Packs, which have 0.2 mm pore size, the transfer pack was a pre-processed ready to use product with a PVDF membrane in-between two stacks of filtered papers. The stacks were pre-treated with transfer buffer by the manufacturer. The gel was put on top of the PVDF membrane and the sandwich was packed and transferred into the Trans Blot Turbo Transfer System Bio-Rad cassette. A roller was used to remove bubbles and the cassette was assembled. Electric current; 2.5A and Voltage 25V, was applied for 7 minutes. After transfer was complete the PVDF membrane was blocked with 5% (w/v) of bovine serum albumin (BSA) or low fat milk solution dissolved in Tris-buffered saline Tween (TBST), for 1 hour at room temperature with agitation. After that the membrane was washed three times with TBST, 10 minutes for each with agitation. Primary antibody

was added to the membrane after dilution 1:1000 in 5% (w/v) BSA or 5% low fat milk powder (dissolved in TBST) and incubated overnight at 4°C with slow agitation on plate shaker. The membrane was then washed in TBST three times. Secondary antibody, after dilution 1:4000 in 1% (w/v) low fat milk powder (dissolved in TBST), was applied to the membrane for one hour at room temperature with agitation.

Three washings were applied to the membrane each for 10 minutes with agitation, and then covered with Clarity™ Western ECL Blotting Substrate (reagents were mixed 5 minutes before use) and protein bands were detected by using Image-Quant LAS 4000 mini - GE Healthcare machine. All protein bands were quantified by using Image-Quant TL 8.1 software.

#### **2.2.5.2 Preparation of SDS-PAGE**

SDS gels were cast using two glass plates which were separated by 1.5mm spacers. The gels consisted of a stacking gel of 5% and resolving gel of 12%. The concentration of the resolving gel depended on the protein being investigated ensuring sufficient separation of proteins. For preparing a gel 25ml of 12% resolving gel and 5ml of 5% stacking gel were required to fill the gel cassette, as illustrated below:

Preparing 25ml of 12% Resolving gel	10ml of 30% acrylamide 6.3ml 1.5M Tris base pH 8.8 8.2ml distilled H <sub>2</sub> O 0.25ml of 10% SDS 0.25ml of 10% ammonium persulfate (APS) 0.01ml of TEMED
Preparing 5ml of 5% Stocking gel	0.83ml of 30% acrylamide 0.63ml 1M Tris base pH 6.8 3.4ml distilled H <sub>2</sub> O 0.05 of 10% SDS 0.05ml of 10% ammonium persulfate (APS) 0.005ml of TEMED

After assembling the cassette, the resolving gel was added and left to polymerize for 20 minutes, then the stacking gel was added above resolving gel and left for 10-15minutes. A comb of 2.5cm depth with 10 wells was inserted into the stacking solution to make wells before the gel solution polymerized.

### **2.2.5.3 SDS-PAGE buffers and reagents**

1L 5X Running buffer

15.1 g Tris base

72.1 g glycine

50ml of 10% SDS

Making up 1L by ddH<sub>2</sub>O

For preparation 1X running buffer take 200ml of 5X running buffer and volume complete to 1L with ddH<sub>2</sub>O

1L 1 X Transfer Buffer

2.8g Tris base

2.9g Glycine

200ml Methanol

Making up 1L by ddH<sub>2</sub>O

1L 10X Tris Buffer Saline

30g Tris base

80g of NaCl

2g KCl

Add 800ml of ddH<sub>2</sub>O

Adjust to the pH to 7.4 using concentrated HCl

Complete to 1 liter by ddH<sub>2</sub>O

1L 1X Tris Buffer Saline Tween (TBST)

100ml of 10X Tris Buffer Saline

900ml of ddH<sub>2</sub>O

1ml of Tween 20

### **2.2.6 Preparing collagen coated surfaces**

2mg/ml (v/v) of collagen type 1 was prepared according to a protocol provided by the supplier (Millipore, UK). 0.75ml of 2mg/ml of collagen solution was added to each well of a six well plate. The plates placed in an incubator for 20-30minutes for polymerization of the collagen. Later cells were seeded onto the collagen gel and left for 24hrs.

### **2.2.7 Mitochondrial Staining**

Clean cover slips were transferred into six well plates, submerged within methanol for 30 minutes. The methanol was removed and coverslips /plates were left to air dry. Later they were covered with sterilized gelatin solution (0.1 % w/v) for 30 minutes and then the gelatine was removed from the wells and plates were left to air dry. Depending on the experiments, cells were seeded on these coverslips at  $10^4$  cells/well density. After 24 hours the cells were treated and incubated for a further 24-48 hrs. At the end of the experiment, the medium was replaced with 2 mL of pre-warmed serum and antibiotic free growth medium containing reduced mitochondrial- selective fluorescent probe (MitoTracker® Orange CMTMRos, Invitrogen Cat. no. M7510) with a final concentration 300-400 nM, then plates incubated for 15-30 minutes. The probe was designed to enter actively respiring cells and to be sequestered permanently in the mitochondria, reacting with thiols groups on proteins and peptides to form an aldehyde-fixable conjugate. The cells were washed twice using pre-warmed PBS. Cells were fixed with 4.0 % (w/v) paraformaldehyde - PBS for 20 minutes. The fixative was aspirated and cells were washed twice with PBS, one minute each, and covered with 0.1% (v/v) Triton X100 - PBS for 10 minutes (to permeabilize the cells) then washed twice, for one minute each time with PBS. Cover slips were mounted on glass slides using VECTASHIELD mounting medium with DAPI and the edges of the cover slips were sealed with nail polish. Z-stack images were captured at 100x oil immersion lens using Nikon AIR confocal microscope running NIS Elements AR imaging

software, then Images were processed and analysed using NIS elements AR (Nikon) and ImageJ (Fiji, 64bit) software.

### **2.2.8 Immunostaining**

This technique depends on an antibody to detect a specific protein in a sample, in which cells were seeded on coated cover slips with sterilized gelatin, as described in the mitochondrial staining section above. Cells were seeded at density  $2.5 \times 10^4$  cells/well in six well plates and incubated overnight, and then cells were treated with different treatments depending on the experiment. At the end of each experiment, cells were washed with PBS and fixed with 4.0 % (w/v) paraformaldehyde for 20 minutes. After fixing the cells, the fixative was aspirated and cells were washed twice with PBS, for one minute each time. Then cells were covered with 0.1% v/v Triton X100 - PBS for 10 minutes and washed twice with PBS, one minute each time. After that cells were covered with blocking solution (10% v/v goat serum – PBS) and washed twice with PBS. Primary antibody solution (1:100 v/v diluted in 1% goat serum – PBS) was applied for one hour. Later primary antibody solution was removed and followed by 3-5 washings, one minute each, with PBS. Secondary fluorescent antibody solution (1:500 v/v in 1% goat serum – PBS) was applied in dark for one hour and later it was aspirated and cells were washed with PBS three times (five minutes each). Then, cover slips were recovered from six the well plates and mounted on glass slides using VECTASHIELD Mounting Medium with DAPI and the edges of the cover slips were sealed with nail polish. Slides were either stored in the refrigerator at 4°C or examined immediately by confocal microscopy. Later Image J software was used in quantification the changes in treated cells compared to control cells.

### **2.2.9 Gene Knockdown with siRNA**

After overnight seeding, cells were transfected with 25nM of either Non-target siRNA, TRAP1 siRNA, or p66shc siRNA. Dharma-FECT 1 or Dharma-FECT 4 Transfection reagent and siRNA were added to serum and antibiotic-free media in separate sterile tubes, then both solutions were incubated at room temperature for 5 minutes, after that, they were mixed well and incubated at room temperature for 20 minutes. The final volume of working solution was achieved by adding antibiotic-free media. For each of normal and high glucose controls, only Dharma-FECT 1 or Dharma-FECT 4 Transfection was added to serum and antibiotic free media. Concentrations and volumes of reagents were determined by the manufacturer's protocol (DharmaFECT Transfection protocol), depending on the cell type and the surface area of the wells.

For western blot analysis, cells were seeded in 75 cm<sup>2</sup> flask with a density of 10<sup>6</sup> cells / flask; at the end of the experiments (48 hrs after transfection) cells were collected. For time-lapse microscopy, cells were seeded in 12-well plates at a density of 10<sup>4</sup> cells/ well, while, for measuring ROS, ATP, and glycolysis, cells were seeded in 96-well plates at a density 2.5x 10<sup>4</sup> cells/ well. After 24 hrs of silencing a gene, medium containing siRNA + transfection reagent was replaced with fresh medium without antibiotics.

### **2.2.10 Quantitative Real- Time PCR (qRT-PCR)**

Quantitative real-time polymerase chain reaction (qRT-PCR) was used to investigate the changes of mitochondrial DNA (mtDNA) copy number in treatment cells compared to non-treated control cells. Total DNA including mtDNA was isolated from cultured cells and purified using DNeasy Blood & Tissue kit (Qiagen) according to manufacturer's instructions. The DNA concentration of samples was measured using a Nano-drop Spectrophotometer then from each sample an equal amount of DNA (10 ng) was used. qPCR primers for the t-RNA gene (a mitochondrial gene) and the  $\beta$ -actin gene locus (for nuclear) were designed using the NCBI website tool called Primer-Blast, each one

designed to be 18-22bp (details of qPCR primers are in Table 2.2). The primer efficiencies were tested prior to the experiments by running them on an agarose gel electrophoresis using DNA Ladder to verify the size and singularity of amplified segments as shown in Figure 2.3.

All qPCR experiments were conducted in 96-well plates and the reaction for each well was set up as follows:

- 0.3  $\mu$ L primers mix (5 $\mu$ M)
- 7 $\mu$ L 2X quantiTect SYBR Green Master Mix (Qiagen) and
- 6.7 $\mu$ L of the diluted DNA

The plate was sealed then centrifuged briefly. The reactions were incubated in an AB StepOne Plus real time PCR machine (Applied Biosystems) at 50°C for 2 min and 95°C for 15 min (initial cycle), followed by 40 cycles of 95°C for 15 sec, 60°C for 1 min and 72°C for 1 min. PCR products were visualized using gel electrophoresis in a 1% agarose gel and stained with ethidium bromide (1 $\mu$ g/ml) for visualisation.

The threshold cycle (Ct) is defined as the fractional cycle number at which fluorescence pass the threshold. The expression of each gene was defined from the threshold cycle (Ct).

The copy number of mtDNA was calculated using the delta Ct ( $\Delta$ Ct) which is equal to average Ct of t-RNA gene subtracted from average Ct value of  $\beta$ -actin, depending on the following formula

$$\Delta\text{CT} = (\beta\text{-actin DNA Ct}) - (\text{t-RNA DNA Ct})$$

$$\text{mtDNA copy number} = 2 \times 2^{\Delta\text{CT}}$$

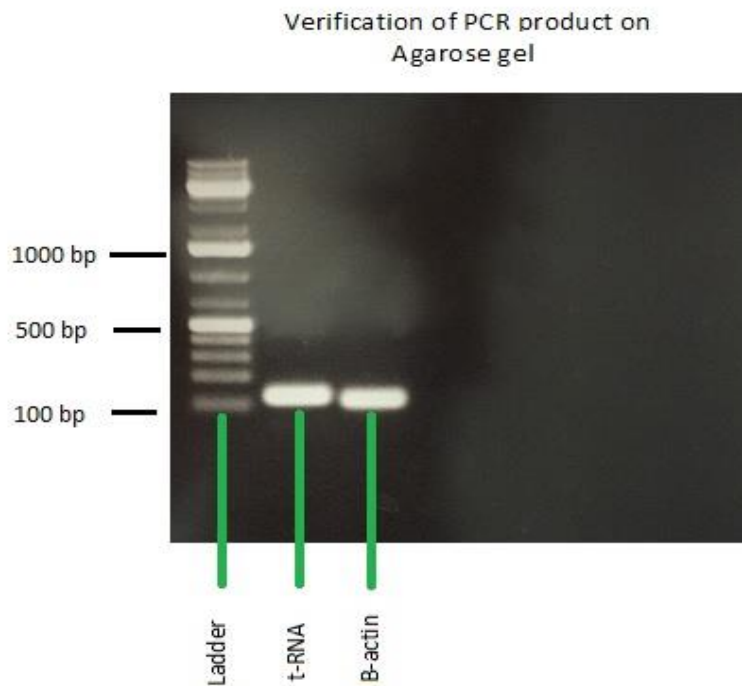


**Figure 2.3: Agarose gel electrophoresis.** Shows nuclear DNA gene;  $\beta$ -actin with size 101 bp, and mitochondrial DNA gene; t-RNA with size 107 bp. Samples taken from results of glucose level effect on mtDNA copy number in MDA-MB-231 cells for verification of the qPCR results.

### 2.2.11 Cell viability assay (MTT assay)

We used an MTT (3-(4, 5-dimethylthiazol-2-yl)-2, 5-diphenyltetrazolium bromide) assay to measure cell viability.  $5 \times 10^3$ - $10^4$  cells/well were seeded in 96-well microtiter plates and incubated for 24 hours in a humidified atmosphere at 37°C and 5% CO<sub>2</sub>. Cells were then treated depending on the experiment with either an inhibitor, an activator, or with chemotherapy drugs and plates incubated for further 24 - 48hrs depending on the experiment. Next, the MTT reagent was added directly to the culture medium. Viable cells with active metabolism can reduce MTT tetrazolium, which has yellow colour, into formazan, which has a purple colour, by Nicotinamide adenine dinucleotide; NADH, as seen in Figure 2.4. The quantity of formazan (assumed to be directly proportional to the number of viable cells) is measured by recording changes in absorbance at 570nm using a plate reading spectrophotometer. The viable cells are quantified depending on the

following equation and a histogram of cell viability plotted on Y axis and treatments on the X axis

$$\text{Cell viability} = (\text{OD of treated sample} - \text{OD of blank}) / (\text{OD of control} - \text{OD of blank}) \times 100\%$$

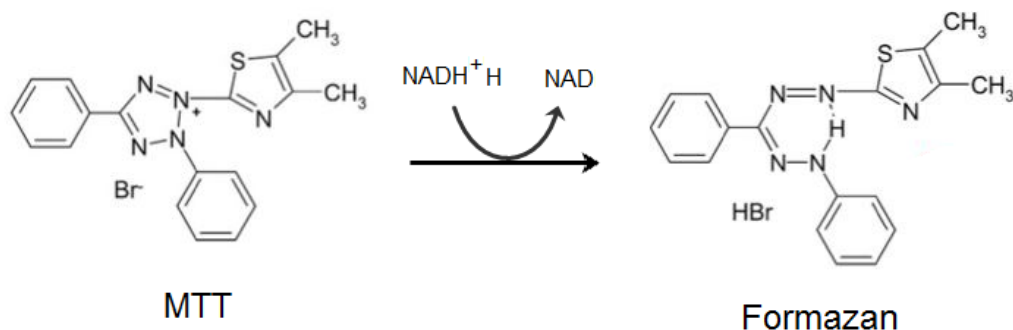


**Figure 2.4: Yellow colour MTT tetrazolium changed to purple colour formazan in metabolic active cells.**

### 2.2.12 Quantification of Reactive Oxygen Species (ROS)

OxiSelect™ Intracellular ROS Assay Kit (Green Fluorescence) (Cell Biolabs, STA-342) was used to measure intracellular ROS level according to the manufacturer's instructions. In brief,  $2.5 \times 10^4$  cells/well were cultured in black 96-well cell culture plate and incubated overnight, and then the medium was replaced with 2', 7'-dichloro dihydro fluorescein diacetate (DCFH-DA) (100 $\mu$ L) and incubated for 60 min at 37°C. After washing with Hank's buffered salt solution (HBSS), cells were treated depending on the experiment. Intracellular generated ROS can oxidize non-fluorescent DCFH into highly fluorescent 2', 7'-Dichlorodihydrofluorescein (DCF), as shown in Figure 2.5, which can be read with fluorescent microplate reader at 485 nm (excitation) and 535 nm (emission). Results were presented as relative fluorescence unit (RFU).

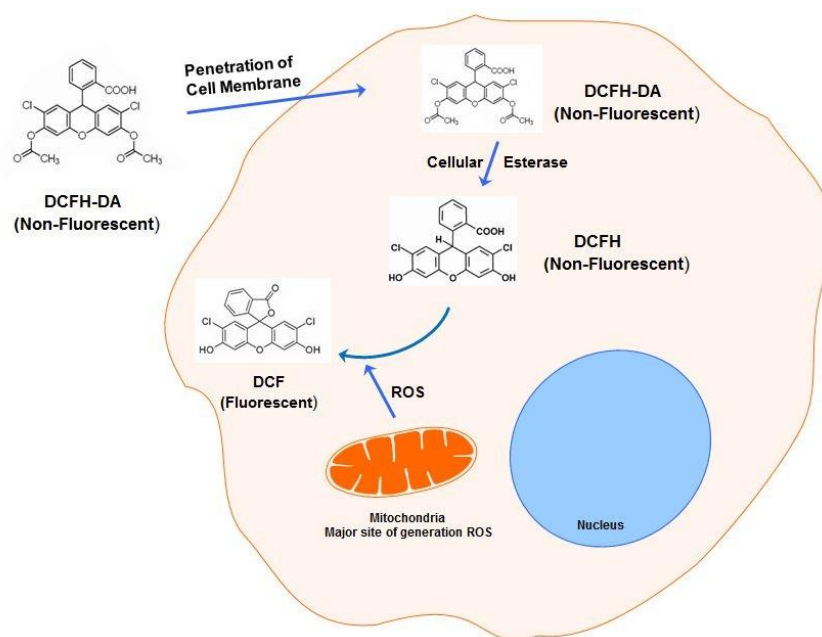


**Figure 2.5: Mechanism of quantification of intracellular ROS.**

Generated ROS within the cell can oxidize non-fluorescent DCFH into fluorescent DCF

### 2.2.13 Quantification of L-Lactate production (Glycolysis)

The concentration of lactate in culture media, which represents glycolytic activity of the cells, was measured by colorimetric-based method using a Glycolysis Cell-Based Assay Kit (Cayman Chemical Company) according to the manufacturer's instructions.

In the assay, lactate dehydrogenase catalyzes the oxidation of lactate to pyruvate, in which the formed NADH reduces a tetrazolium substrate (INT) to a highly-coloured formazan which absorbs strongly at 490-520 nm. The amount of formazan produced is proportional to the amount of lactate released into the culture medium and could be used as an indicator of cellular glycolytic rate, as shown in Figure 2.6.

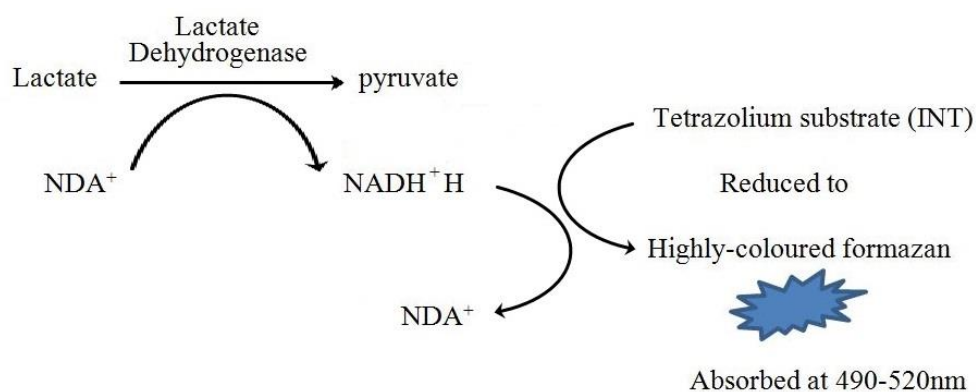


**Figure 2.6: Mechanism of L-Lactate quantification.** The colorimetric assay for measuring L-Lactate, the end product, formazan is proportional to the amount of lactate released into the culture medium.

In brief,  $2.5 \times 10^4$  cells / well were cultured in 96-well cell culture plate overnight in 5% CO<sub>2</sub> at 37°C, and then the cells were treated depending on the experiment and incubated for a further 24-48 hrs depending on the experiment. At the end of the experiment, the plate was centrifuged at 1000 rpm for 5 minutes, and then 10µL of supernatant from each sample was added to 90µL of assay buffer in a new 96-well plate, and 100µL of reaction solution added. The plate was then incubated for 30 minutes after shaking, and the absorbance was read at 490 nm. The amount of generated lactate was calculated using standard curve equation, based on the obtained absorbance value for each sample.

#### 2.2.14 Quantification of ATP production

An ATP Assay Kit (abcam, ab83355) was used to determine the total generated ATP, according to manufacturer's instructions. The assay is based on the phosphorylation of glycerol to generate a product that can be measured by colorimetric methods at 570 nm. Briefly,  $5 \times 10^5$  cells / well were seeded in 6-well plates and allowed to attach overnight. The cells were treated depending on the experiment. Later  $1 \times 10^6$  cells from each sample were harvested and suspended in 100µL of ATP buffer. After homogenization and centrifugation at 1000 rpm for 2 minutes, 50µL of supernatant from each sample was mixed with 50µL of reaction mix in 96-well plate. A SpectraMax microplate reader was used to

read the optical density at 570 nm. A standard curve equation was used to determine the concentration of each treatment based on the optical density.

### **2.2.15 Time-lapse microscopy analysis**

Cells were seeded in six or twelve well plates with density  $5 \times 10^4$  and  $1 \times 10^4$  cells /well respectively in a humidified atmosphere at 37°C and 5% CO<sub>2</sub> overnight. After treating cells with different treatments depending on the experiment, the plates were put on a Nikon Eclipse TiE Time-lapse microscope with automated stage and environmental chamber running NIS Elements software and Plan 10x / 0.25 ph1 DL lens was selected to monitor cellular response to treatments. Three locations from each well were selected randomly and the microscope software was programmed in a way that a series of photos was taken every 15 minutes (for single cell tracking and monitoring apoptosis) or every 1 hour (for wound healing assay) for 24 hours. Images were analysed using Image J Software. The MtrackJ plugin was used to track and measure the speed of cell migration, and the cell counter plugin was used to measure apoptosis. Whereas, Measure Analyze plugin was used for wound healing analysis. Data was then analysed using Microsoft excel and Graph pad Prism.

### **2.2.16 Confocal microscopy analysis**

Nikon A1R confocal microscope was used to obtain series of high quality 3D images of mitochondria with 1024 X 1024 pixel format at 400 Hz speed in xyz plane. To obtain 3D images, a z-stack was taken from the top to the bottom and 3 colours (Laser) were used: Alexa 405, 488, and 561nm for the blue, green and orange respectively. Images were analyzed using ImageJ Software to measure the number, size, and volume of mitochondria in both control and treatments. The following steps were done with ImageJ to analyse images

### **Opening image**

**Image** → **colour** → **split channels**

**Image** → **Adjust** → **brightness/contrast**

**Set contrast of image under maximum slider to middle**

**Image** → **Lookup Tables** → **Grays**

**Plugin** → **3D Object Counter** → **3D object counter**

**Set threshold slider in such a way that only  
mitochondrial appear with stain**

**(Without over saturation of mitochondria with stain)**

### **Under size filter space**

**Write 0.1 in Min. and 200 in Max**

**Click Enter**

**Wait 2-5 minutes**

**Select display results and copy- paste into an Excel spreadsheet**

**Of the results we only use the number, size ( $\mu\text{M}^2$ ), and  
volume size ( $\mu\text{M}^3$ ) of mitochondria for calculation.**

## **2.2.17 Measuring cancer cell migration**

Two techniques were used for measuring cancer cell migration: a wound healing assay and single cell tracking. For wound healing assays, cells were seeded in twelve well plates at a density  $2.5 \times 10^5$  cells / well and incubated in a humidified atmosphere at  $37^\circ\text{C}$  and 5%  $\text{CO}_2$  and left to grow until the confluence of the cells reached 90-95%. Then the cell monolayer cells were scratched in a straight line using a sterilized pipette tip. After washing wounded monolayer with PBS or medium to remove non-adherent and scratched cells, fresh medium with a treatment agent was added. Plates were placed on the stage of the phase contrast time-lapse microscope and a series of photos was taken every 1 hour for 24 hours, as seen in Figure 2.7, and from each well three locations were selected randomly. ImageJ software (Polygon selections / Analyze measure) was used to measure the wound area at beginning

of experiment and at the end of experiment and the following equation was used to calculate wound closure area, which is represent cell migration.

$$\% \text{ Wound closure area} = \{ \text{Wounded area at 0h} - \text{Wounded area at 24h} / \text{Wounded area at 0h} \} \times 100$$

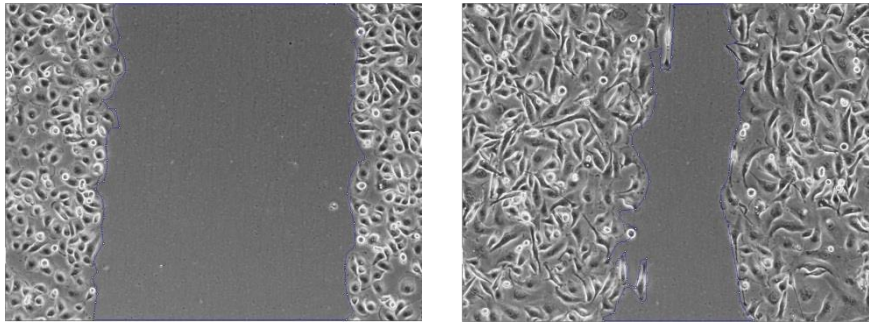


**Figure 2.7: Micrographs showing wound healing in MDA-MB-231 cells**

Wound area at 0 hour

Wound area at 24hrs

For measuring cancer cell migration through tracking single cell migration, cells were seeded either in six or twelve well plates at density  $3 \times 10^4$  and  $1 \times 10^4$  cells / well respectively, and incubated overnight. Cell migration was monitored, after treating the cells with different treatments depending on the experiment, with time-lapse microscopy for 24 hrs. ImageJ software (MtrackJ plugin) was used to track cells and to measure the speed and distance of migrating cells; at least twenty cells were tracked randomly for each location

### **2.2.18 Measuring apoptosis**

For measuring apoptosis, cells were seeded in six or twelve-well plates with a density of  $5 \times 10^4$  and  $1 \times 10^4$  cells / well respectively in a humidified atmosphere at  $37^\circ\text{C}$  and  $5\% \text{ CO}_2$  overnight. Cells were treated with different treatments depending on the experiment. Nikon TiE Time-lapse microscope running NIS Elements software and Plan 10x / 0.25 ph1 DL lens was used to monitor cells death tacking a series of images every 15 minutes for 24hrs. From each well three locations were selected randomly and all cells/location were tracked (Al-Gubory, 2005; Huh et al., 2012; Röttgermann et al., 2016). ImageJ software (counter plugin) was used to analyse data and following steps were done with ImageJ

Open ImageJ file

- Plugin → Analyze → cell counter
- In new window press initialize then choose type 1 under counters
- During run of video image point on apoptotic cells for measuring dead cells, then count total cells.

The rate of cell death during the 24hrs was calculated using the following equation.

$$\% \text{ cell death} = (\text{number of dead cells per location} / \text{total number of cells per location}) \times 100$$

Apoptotic cells can be distinguished from live cells and other forms of cell death in time-lapse video microscopy by observing shrinkage of cell that is followed by blebbing, fragmentation and cell rupture, as seen in Figure 2.8.



**Figure 2.8: Morphological changes of apoptotic cells enable differentiating them from other cells.**

### 2.2.19 Quantifying p66shc

Activated p66shc was measured using confocal microscopy. First, cells were seeded in a six or twelve well plated at a density of  $5 \times 10^3$  and  $1.5 \times 10^3$  cells / well respectively in a humidified atmosphere at  $37^\circ\text{C}$  and 5%  $\text{CO}_2$  overnight. Cells were then transfected with p66shc siRNA and /or TRAP1 siRNA for 48hrs, next, cells were subjected to staining with a mitochondrial probe, and the immunofluorescence with anti-p66shc antibody as detailed above in 2.2.7 and 2.2.8 respectively. A series of z-stack images was taken using confocal microscope and ImageJ software was used to measure activated p66shc (Steps described in below) in treated cells compared to scrambled siRNA.

### **Opening image**

**Image** → **Adjust** → **brightness/contrast**

**Set contrast of image under maximum slider to middle**

**Use polygon selections to determine edge of each cell**

**Process** → **Find Edges**

**Analyze** → **Measure**

**From obtained results select Mean and copy-paste them  
into an Excel spreadsheet**

### **2.2.20 Statistical analysis**

Data were expressed as mean  $\pm$  standard error of mean ( $M \pm SE$ ) and statistical analysis was carried out using Microsoft Excel and Graph Pad Prism version 5.01 software. One-way analysis of variance (ANOVA) followed by Tukey (to compare between the mean of treatments) or Dunnett (to compare between the mean of treatments with control mean) multiple comparison test, and significance level was expressed as following:

(\*) represent P values  $< 0.05$  statistically significant

(\*\*) represent P values  $< 0.01$  statistically highly significant

(\*\*\*) represent P values  $< 0.001$  statistically very high significant

## **Chapter Three: Investigating the impact of glucose levels on mitochondrial dynamics, metabolism, and cell migration in MDA-MB-231 cells**

### **3.1 Introduction**

Mitochondria mediate several essential functions in the cell and are highly dynamic organelles (Rambold et al., 2011). Through fission and fusion process, they continuously regulate their morphology and structure between a fragmented, small size and tubular, network-like shapes. The balance between these two processes is essential for exchange of the damaged mitochondrial DNA, lipid, and protein with healthy mitochondria to maintain the normal function and structure of mitochondria (Scott and Youle, 2010, Otera et al., 2013, van der Bliek et al., 2013, Guitart-Mampel et al., 2017).

Many factors such as hyperglycaemia, hypoxemia, heat, U.V., and chemotherapy which cause oxidative stress through increase in ROS levels can shift mitochondrial dynamics toward the fission process resulting in hyper-fragmented mitochondria (Yu et al., 2006, Yu et al., 2011, Van Beersel et al., 2013, Aung et al., 2017). There are several published studies (Yu et al., 2006, Yu et al., 2008, Jheng et al., 2012, Kumari et al., 2012, Li et al., 2017) that reported the responsibility of hyperglycaemia on mitochondrial fragmentation and cell death in patients with diabetes mellitus (DM) and cardiovascular disease.

In contrast to the normal cells, cancer cells can tolerate high level of ROS. Indeed, cancer cells are able to exploit high levels of ROS to enhance their function, processes and pathways; it can induce overexpression, secretion, or inhibition of several enzymes that participate in cell motility, cell metabolism, and cell death (Fiaschi and Chiarugi, 2012). One of the enzymes that is overexpressed and activated at high ROS levels is Dynamin-related protein 1 (Drp1), which is translocated from cytosol to mitochondrial surface where it interacts with fission 1 (Fis1) protein forming a ring around mitochondria that leads to mitochondrial fission (Qi et al., 2013), as explained in Figure 3.1

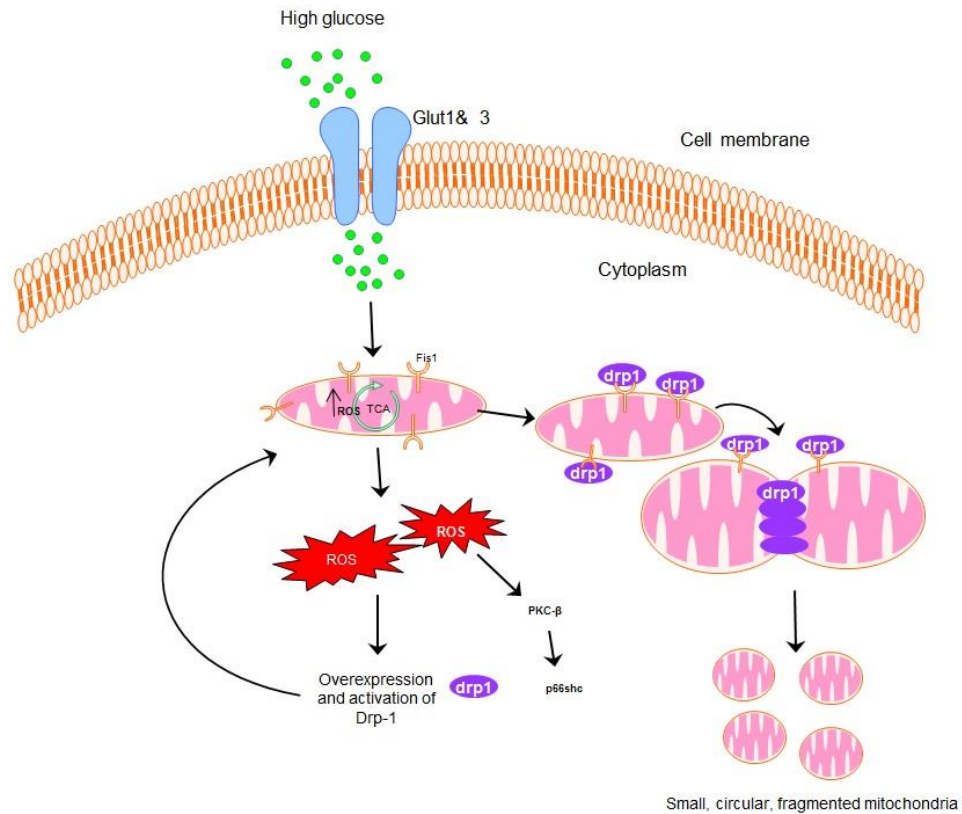


**Figure 3.1: Mechanism of inducing mitochondrial fragmentation in high glucose level.** High glucose generates cellular ROS mainly through mitochondrial metabolism, elevated ROS activate dynamin-related protein 1 (Drp1) which bind with Fis1 on the surface of mitochondria. Assembling of Drp1 around mitochondria drives the fission process. Graph made using Motifolio - Scientific illustration Toolkits.

It has been reported that during early steps of apoptosis, mitochondria encounters fragmentation through participation of the mitochondrial fission machinery, which can induce mitochondrial outer membrane permeabilization (MOMP) and cell death. Therefore, it is postulated that mitochondrial fragmentation is related to apoptosis (Youle and Karbowski, 2005, Perfettini et al., 2005). However, several studies suggest that apoptosis can occur independently from mitochondrial fragmentation or activation of MOMP (Tondera et al., 2004, Parone et al., 2006, Arnoult, 2007, Sheridan and Martin, 2010). Incontrast , it has been reported that fragmentation of mitochondria can increase resistance to apoptosis. Renault and co-workers (2015) investigated the relationship between mitochondrial shape and BCL<sub>2</sub>-associated X protein (BAX) induced MOMP for

apoptosis. They concluded that small mitochondrial size can restrict BAX from inducing MOMP and apoptosis (Renault et al., 2015).

Many studies have suggested that the morphology of mitochondria plays important roles in the normal function of mitochondria (Jeong and Seol, 2008, Picard et al., 2013). In an investigation by Jheng and co-workers (2012), they found an association between mitochondrial fragmentation and mitochondrial dysfunction. They induced mitochondrial fragmentation by using palmitate (PA) in C2CL mouse myoblast cell line and it led to mitochondrial depolarization and loss of ATP production which is characteristic of mitochondrial dysfunction. They also found that prevention of mitochondrial fragmentation can inhibit mitochondrial dysfunction (Jheng et al., 2012). It appears that fragmentation of mitochondria can reduce the surface area of the inner mitochondrial membrane which plays an important role in oxidative phosphorylation (Mannella, 2006).

Unlike normal cells, cancer cells prefer to rely on aerobic glycolysis to enhance rapid proliferation and metastasis which is also known as the Warburg Effect (Cantor and Sabatini, 2012, Li et al., 2016). There are studies that have found that growth of A549 lung cancer cells can be inhibited using Antimycin A; an inhibitor of mitochondrial electron transport chain (Han et al., 2008), this means that cancer cells may not be depending on glycolysis completely to obtain required energy.

It should be remembered that measuring metabolic changes including O<sub>2</sub> consumption, ATP and lactate production directly in live cells using Seahorse XF Analyzer can show better understand of changes in glycolysis as well as changes in oxidative phosphorylation rate. However, due to unavailability of Seahorse XF Analyzer during studying time had limited this investigation.

Upon exposure of cancer cells to extrinsic oxidative stress, levels of ROS increase and this can cause mitochondrial oxidative damage and cell death. To avoid apoptosis and the effect of excess ROS, cancer cells switch metabolism from oxidative phosphorylation to glycolysis. This reprogramming of metabolism leads to acidification of the microenvironment which can enhance cell migration (Pani et al., 2010, Fiaschi and Chiarugi, 2012).

Previous studies have found that mitochondrial dynamics are linked to cell migration, it was found that up-regulation of Dynamin-related Protein (Drp1) and fission of mitochondria increase migration and invasion of metastatic breast cancer cells (Zhao et al., 2013a). Also in the study by Takatani and co-workers (2014), they found that hyperglycaemia can promote motility of MCF-7 breast cancer through increasing uptake of zinc (Takatani-Nakase et al., 2014). In contrast, another study reported that vascular smooth muscle cell (VSMC) migration can be limited by controlling mitochondrial fission (Wang et al., 2015b). Despite that, the effect of changes in mitochondrial morphology on cancer cell migration remains unclear.

We hypothesize that morphological changes of mitochondria can affect glucose metabolism in cancer cells, which in turn affect cell migration and cancer metastasis.

In this chapter we used different concentrations of glucose; low glucose (1mM), normal glucose (5.5mM), and high glucose (25mM), to investigate the link between mitochondrial dynamics; through measuring mitochondrial number, size, volume and total mitochondrial mass, and mitochondrial metabolism through measuring generated ATP and lactate; end product of glycolysis, and cell migration through tracking single cell movements and wound healing assay.

In order to understand the effect of generated ROS on the mitochondrial dynamics changes, we investigated the effect of exogenous hydrogen peroxide ( $H_2O_2$ ), which causes oxidative stress, on the mitochondrial dynamics, metabolism, and the cell migration.

Inhibition of mitochondrial fission using mitochondrial division-1 (mdivi-1) inhibitor, will be another point that focusing on it in this investigation as a confirmation of the link between mitochondrial dynamics, metabolism, and cell migration in MDA-MB-231 cells.

## **3.2 Material and methods:**

### **3.2.1 Cell culture**

MDA-MB-231 breast cancer cells were continuously cultured in Dulbecco's Modified Eagles Media (DMEM) with relevant glucose levels (1, 5.5, and 25mM) and supplemented with 10% FBS, 1% L-glutamine, 100 Unit/ml of penicillin and 100 µg/ml of streptomycin (Gibco), at 37°C in a humidified atmosphere containing 5% CO<sub>2</sub>.

For preparation medium with different glucose concentrations, D-glucose was added to glucose free medium to final (1, 5.5 and 25mM) concentrations.

In H<sub>2</sub>O<sub>2</sub> study, the cells were treated in normal glucose DMEM medium with different concentrations of H<sub>2</sub>O<sub>2</sub> (50, 100, 250, and 500µM) for 24hrs after overnight seeding.

In the mdivi-1 inhibitor study, the cells were seeded overnight in high glucose DMEM medium then treated with different concentrations of mdivi-1 inhibitor (10, 30, 50µM) for 24hrs.

### **3.2.2 Mitochondrial staining**

A selective fluorescent probe (MitoTracker® Orange) was used to stain mitochondria. At the end of the experiments, the cells were incubated for 15 minutes with probe in serum free DMEM medium. The probe enters an actively respiring cell and sequestered permanently in the mitochondria. Then the cells washed twice using pre-warmed PBS. Later cells were fixed by using 4.0 % w/v paraformaldehyde for 20 minutes. After fixing the cells, fixative was aspirated and cells were washed twice, one minute each, and covered with 0.1% v/v Triton X100 - PBS for 10 minutes (to permeabilize the cells) and washed twice, for one minute each time with PBS. Then coverslips were mounted on glass slides using VECTASHIELD Mounting Medium with DAPI and the edges of the cover slips were sealed with nail polish. Z-stack images were captured at 100x objective lens using Nikon AIR confocal microscope running NIS Elements AR imaging software, then Images

were processed and analysed using NIS elements AR (Nikon) and ImageJ (Fiji, 64bit) software.

### 3.2.3 Confocal microscopy images analysis

The mitochondrial z-stack images were acquired by a Nikon A1R confocal microscopy using 100 X Oil immersion objectives with a format of 1024x1024 at 0.25 $\mu$ m intervals, which provides steady state 3D information about mitochondrial morphology. Then obtained 3D z-stack video images were analyzed using Image J (Fiji) Software to measure the number, size, and volume of mitochondria in control and treatments. The steps for analyse images were as follow

Opening image

Image Colour  $\longrightarrow$  split channels

Image  $\longrightarrow$  Adjust  $\longrightarrow$  brightness/contrast

Set contrast of image under maximum slider to middle

Image  $\longrightarrow$  Lookup Tables  $\longrightarrow$  Grays

Process  $\longrightarrow$  Find edges

Analyze  $\longrightarrow$  3D Object Counter  $\longrightarrow$  3D object counter

Set threshold slider in such a way that only mitochondrial appear with fully stain if needed  
(Without over saturation of mitochondria with stain)

Under size filter space

Write 0.1 in Min. and 200 in Max

It takes 2-5 minutes to analyse images

Copy displayed results and paste it into an Excel spreadsheet

In the results we used only the number, size ( $\mu\text{m}^2$ ), and volume size ( $\mu\text{m}^3$ ), whereas total mitochondrial mass calculated by multiplying the number of mitochondria to the volume of mitochondria.

### **3.2.4 Quantitative Real- Time PCR (qRT-PCR)**

The Quantitative real time polymerase chain reaction (qRT-PCR) used for investigation the changes of mitochondrial DNA (mtDNA) copy number in MDA-MB-231 cells treated with different glucose levels, H<sub>2</sub>O<sub>2</sub>, or Mdivi-1 inhibitor. The total DNA including mtDNA was isolated and purified using DNeasy Blood & Tissue kit (Qiagen) according to manufacturer's instructions, and concentration of DNA samples were measured using Nano-drop Spectrophotometer, then from each sample an equal amount of DNA (10 ng) was used. As described in section 2.2.10, mtDNA copy number was calculated through measuring t-RNA gene which represent mitochondrial gene and housekeeping gene  $\beta$ -actin which represent nucleus gene as control using AB StepOne Plus real time PCR machine (Applied Biosystems). Then PCR products were run through 1% agarose gel electrophoresis to visualized purity and singularity of amplified segments.

### **3.2.5 Western blot analysis**

Immunoblotting was performed as described in section 2.2.8, to measure quantitative changes in expression of Drp1 and PGC-1 $\alpha$  proteins, which normalized to housekeeper protein  $\beta$ -actin, between different treatments or between treatments compare to control. In brief, Cellular extracted proteins were fractionated using SDS-page gels (4-20% Mini-PROTEAN® TGX™ Precast Protein Gels, Bio-Rad) and transferred to polyvinylidene difluoride (PVDF) membranes (Bio-Rad). Immunoblot analysis was visualized using the secondary antibody conjugated with horseradish peroxidase followed by the ECL Western blotting detection system (Amersham Biosciences), through Image-Quant LAS 4000 mini - GE Healthcare machine .The protein bands were quantified using Image-Quant TL 8.1 software.

### **3.2.6 Measurement of glycolysis activity**

Glycolytic activity in MDA-MB-231 breast cancer cells was determined by colorimetric-based method for measuring lactate levels using Glycolysis Cell-Based Assay Kit (Cayman

Chemical Company) according to manufacturer's instructions. In the assay, lactate dehydrogenase catalyzes the oxidation of lactate to pyruvate, in which the formed NADH reduces a tetrazolium substrate (INT) to a highly-coloured formazan which absorbs strongly at 490-520 nm. The amount of formazan produced is proportional to the amount of lactate released into the culture medium and could be used as an indicator of cellular glycolytic rate as shown in Figure 3.2. In brief,  $2.5 \times 10^4$  cells/well were cultured in 96-well cell culture plate overnight in 5% CO<sub>2</sub> at 37°C, then depending on experiment the cells were treated and incubated either with glucose level, H<sub>2</sub>O<sub>2</sub> or mdivi-1 inhibitor.

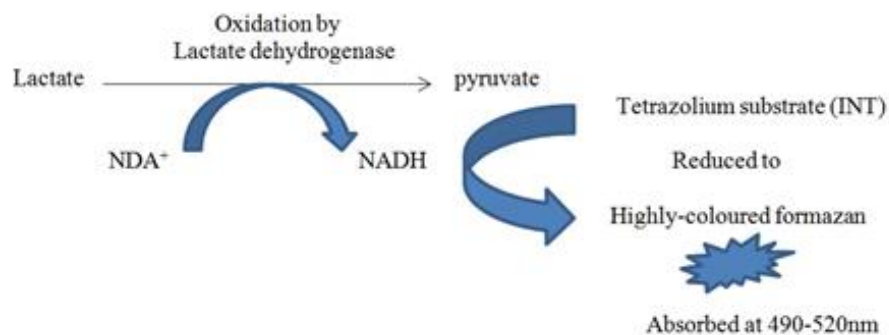


**Figure3.2: The illustration shows principle of glycolysis assay kit.** The colorimetric assay for assessing of L-Lactate, it based on glycolysis activity. The end product, formazan is proportional to the amount of lactate released into the culture medium.

Then 10µL of supernatant from each sample, after centrifugation of cell cultured plate at 1,000 rpm for five minutes, transferred to 90µL of assay buffer in new 96-well plate, and added to them 100µL of reaction solution. The plate was incubated for 30minutes after shaking. The absorbance was read at 490nm, and amount of generated lactate was calculated through standard curve equation using obtained absorbance value.

### 3.2.7 Measurement of ATP

ATP levels were determined using ATP Assay Kit (abcam, ab83355) according to the manufacturer's instructions. The assay is based on the phosphorylation of glycerol to generate a product that can be measured by colorimetric methods at 570 nm. Briefly,  $5 \times 10^5$  cells / well were plated in 6-well plates and allowed for attachment overnight. Then the cells treated depending on the experiments. Later  $1 \times 10^6$  cells from each sample were

harvested and suspended in 100 $\mu$ L ATP buffer. After homogenization and centrifugation at 1000 rpm for 2 minutes, 50 $\mu$ L of supernatant from each sample were mixed with 50 $\mu$ L of reaction mix in 96-well plate. Microplate read used to read optical density at 570nm. Through standard curve equation, concentration of each treatment was calculated using an obtained OD.

### **3.2.8 Measurement of intracellular ROS**

Intracellular ROS generation was assessed using OxiSelect™ Intracellular ROS Assay Kit (Cell Biolabs, STA-342) according to manufacturer's instructions. In brief,  $2.5 \times 10^4$  cells/well were cultured in black 96-well cell culture plate and incubated with 2', 7'-Dichloro dihydro fluorescein diacetate (DCFH-DA) (100 $\mu$ L) for 60 min at 37°C. After washing with Hank's buffered salt solution (HBSS), cells were incubated with different glucose level, or treated either with H<sub>2</sub>O<sub>2</sub> or mdivi-1 inhibitor. Generated ROS by cells can oxidize non-fluorescent DCFH-DA into highly fluorescent 2',7'-Dichlorodihydrofluorescein (DCF), which can be read with fluorescent microplate reader at 485 nm (excitation) and 535 nm (emission). Results are presented as relative fluorescence unit (RFU).

### **3.2.9 Wound Healing Assay**

$1.5 \times 10^5$  cells were added to each well of 12 well plates and cultured overnight at 37°C in 5% CO<sub>2</sub>. Then cells were treated and incubated with different glucose levels, H<sub>2</sub>O<sub>2</sub>, or mdivi-1 inhibitor for 24hrs. Next cell monolayer scratched with a standard 200 ml pipette tip to create a narrow wound-like gap (confluency should be reach to more than 80% before scratching). Wounded monolayers were washed twice to remove non-adherent cells and images were captured at 0 h, 24 hrs using a Nikon TiE Time Lapse microscopy.

### **3.2.10 Cell migration**

MDA-MB-231 cells were seeded in 12 wells plates at density  $5 \times 10^3$  cells/well in humidified atmosphere with 37°C and 5% CO<sub>2</sub>. After 24 hrs the cells were treated with different concentrations of glucose, H<sub>2</sub>O<sub>2</sub>, or mdivi-1 inhibitor and cell migration was monitored by time-lapse microscopy for 24hrs with images taken at 15 minute intervals. ImageJ (Fiji) software (MtrackJ plugin) was used to track and measure the speed of cell movement and from each microscopic field 20 cells were tracked.

### 3.3 Results:

#### 3.3.1 Effect of glucose level on the mitochondrial dynamics, metabolism, and cell migration:

To evaluate the effect of mitochondrial dynamics on metabolism and cell migration, MDA-MB-231 cells were cultured in different glucose concentrations; low glucose; 1mM, normal glucose; 5.5mM, and high glucose; 25mM for 48hrs then subjected to mitochondrial staining with MitoTracker to show changes in mitochondrial morphology, as shown in Figure 3.4, through measuring mitochondrial number, size, volume, and total mass per cell using confocal fluorescence microscopy. Results showed that the number of mitochondria was increased significantly to  $197.4 \pm 7.4$  in high glucose level compared to  $103.5 \pm 8.9$  in normal glucose level ( $p < 0.01$ ), and  $76.4 \pm 10.6$  in low glucose level ( $p < 0.001$ ), while, no significant changes in the mitochondrial number was observed between normal glucose and low glucose levels, as seen in Figure 3.3 A.

The size and volume of the mitochondria were also affected by the changes in glucose levels. Results in Figure 3.3B shows a clear trend of decreasing of the mitochondrial size from  $6.49 \pm 0.28 \mu\text{m}^2$  in low glucose to  $3.56 \pm 0.15 \mu\text{m}^2$  in normal glucose and  $1.57 \pm 0.11 \mu\text{m}^2$  in high glucose levels ( $p < 0.001$ ). The changes in the mitochondrial size between cells cultured in normal glucose and cells cultured in high glucose was also significant ( $p < 0.001$ ).

Similarly, the volume of mitochondria was decreased with the increases in the glucose levels. The results of the volume analysis shown in Figure 3.3 C revealed that mean of the mitochondrial volume has been decreased from  $0.52 \pm 0.035 \mu\text{m}^3$  in low glucose to  $0.29 \pm 0.025 \mu\text{m}^3$  in normal glucose ( $p < 0.01$ ) and into  $0.09 \pm 0.003 \mu\text{m}^3$  in high glucose ( $p < 0.001$ ). The decreases in the mitochondrial volume in high glucose compared to normal glucose was also significant ( $p < 0.01$ ).

We calculated total mass of mitochondria by multiplying obtained data of the mitochondrial volume to the number of the mitochondria. Results presented in Figure 3.3D, revealed that the total mass of mitochondria decreased significantly from  $38.2 \pm 2.61 \mu\text{m}^3$  in low glucose to  $14.8 \pm 0.86 \mu\text{m}^3$  in high glucose medium ( $p < 0.001$ ). No significant changes were detected between low glucose and normal glucose or between normal glucose and high glucose.

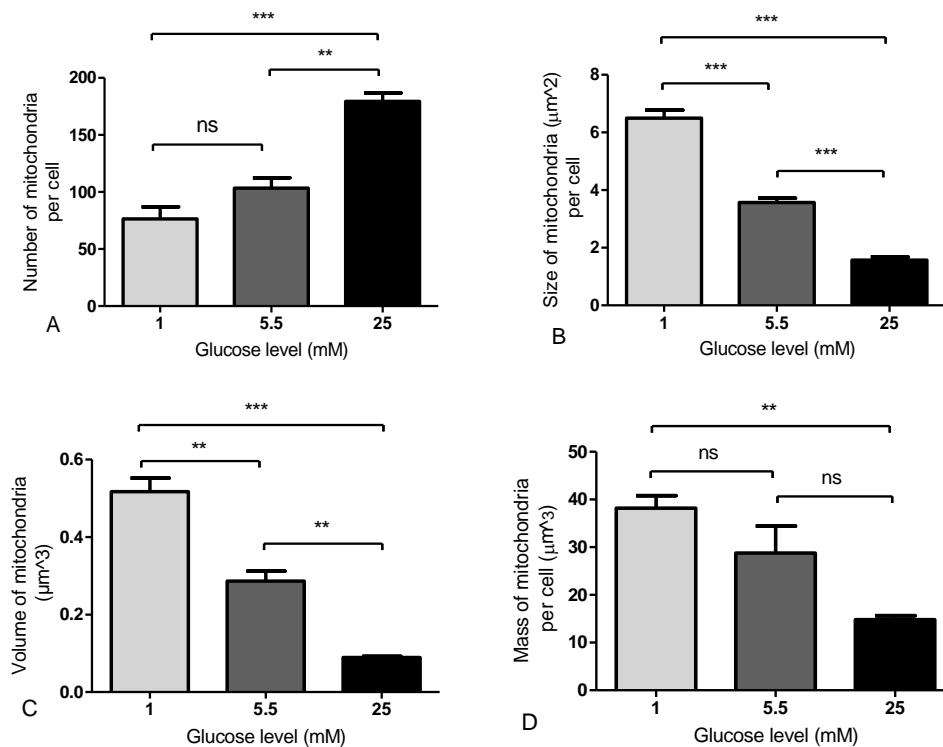


**Figure 3.3: Effect of glucose level on mitochondrial fragmentation in MDA-MB-231 cells.** Cells were grown in different glucose levels (1, 5.5, and 25mM) for 48hrs then stained with MitoTracker probe and confocal microscopy was used to take mitochondrial images. (A) Quantification analysis of number of mitochondria, (B) Size of mitochondria, (C) Volume of mitochondria, and (D) represent quantification analysis of total mitochondria mass per cell. Data represent the mean  $\pm$  standard error of three independent experiments performed in triplicate; each experiment contained at least 30 cells. One-way ANOVA and Tukey's Multiple Comparison test used to compare between the mean of treatments (\*, \*\*, and \*\*\*represent  $P < 0.05$ ,  $0.01$ , and  $0.001$  respectively).

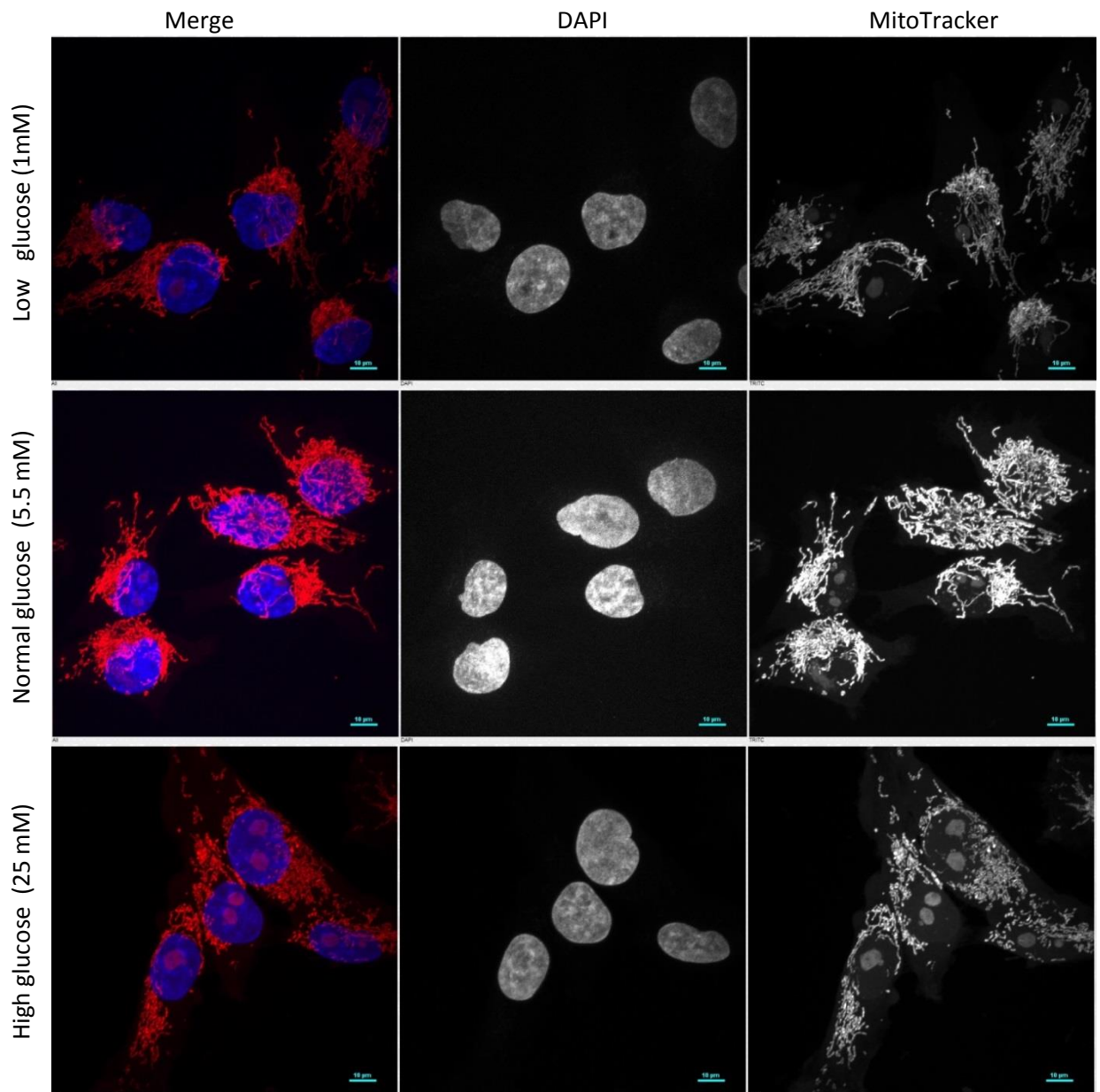


**Figure 3.4: Micrographs showing the mitochondrial morphology.** Mitochondria were stained with MitoTracker orange CMTMRos probe (red colour) and nucleus stained with DAPI (blue colour), for MDA-MB-231 breast cancer cells grown in different glucose levels in DMEM medium; low glucose (1mM), normal glucose (5.5mM), and high glucose (25mM). Image analysis was performed by confocal microscopy. Scale bar = 10  $\mu$ m.

To confirm our results obtained by confocal microscopy we measured mtDNA copy number through measuring t-RNA gene of mtDNA normalized to  $\beta$ -actin gene as housekeeping gene. Results shown in Figure 3.5A revealed that the changes in mtDNA copy number due to increases in glucose concentrations statistically were not significant. However, linear regression analysis of data shows a relationship between increases in glucose concentration and increases in mtDNA copy number, as seen in Figure 3.5B. Then to verify the qPCR results and purity of amplified segments we ran qPCR products on 1% agarose gel electrophoresis as shown in Figure 3.5D.

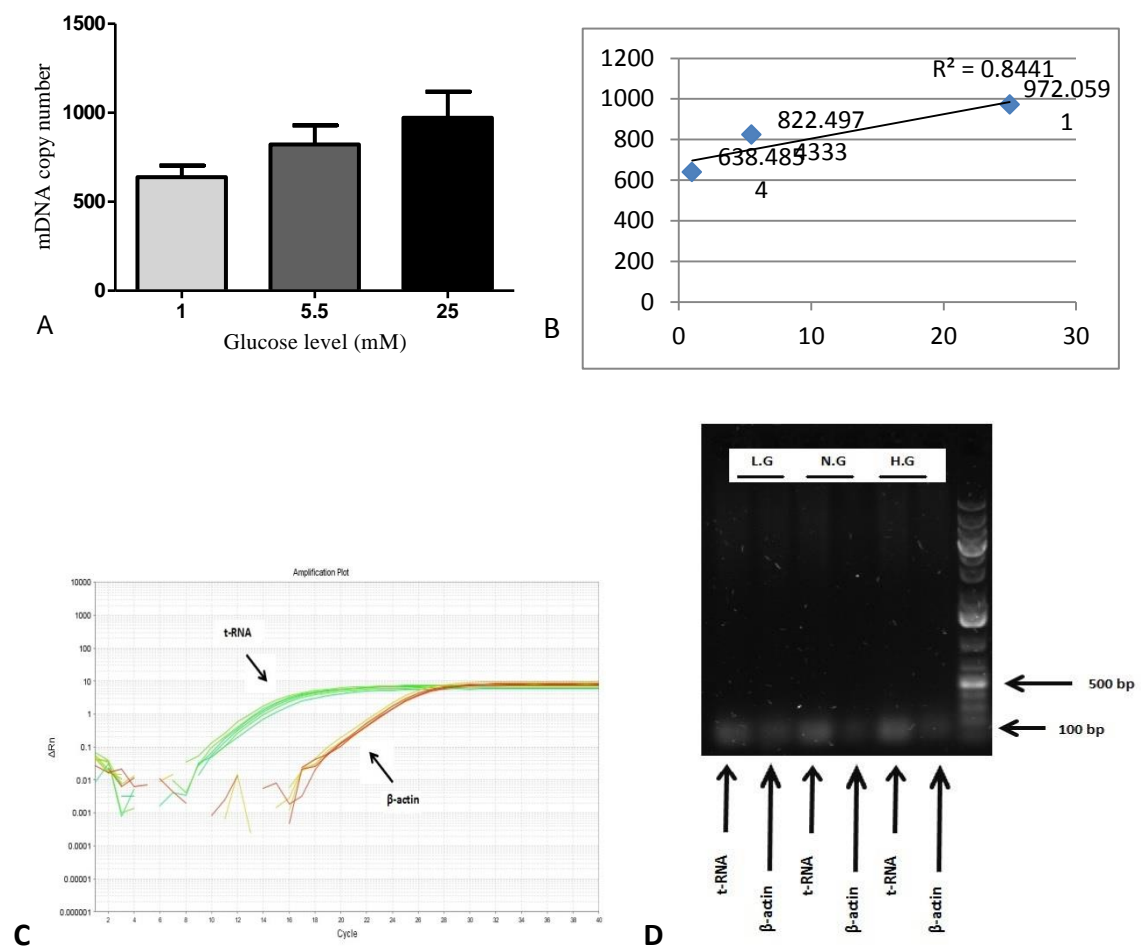


**Figure 3.5: Quantification of mtDNA copy number in MDA-MB-231 cells grown in different glucose levels.** Total DNA extracts used to measure mtDNA by qPCR (A) Represent quantification analysis of mtDNA copy number, (B) linear regression analysis of data, (C) amplification plot and Ct values of  $\beta$ -actin and t-RNA genes, and (D) represent Agarose gel electrophoresis of  $\beta$ -actin (101 bp) and t-RNA gene (107 bp). Data represent the mean  $\pm$  standard error of three independent experiments performed in triplicate. One-way ANOVA followed by Tukey's Multiple Comparison Test to compare mean of treatments.

To uncover the effect of glucose level on the expression of dynamin-related protein (Drp1), a key protein of mitochondrial fission, we measured its expression in MDA-MB-231 cells grown under different concentrations of glucose for 48hrs.

The results revealed that increases in the glucose level increased the expression of Drp1 as shown in Figure 3.6. The expression of protein was increased significantly from  $13.7 \pm 2.11$  in low glucose to  $30 \pm 1.66$  in normal glucose ( $p < 0.05$ ), and into  $39.6 \pm 3.77$  in high glucose ( $p < 0.01$ ); which means the expression of protein Drp1 was increased by 118.6%, in normal glucose and by 188.5% in high glucose compared to low glucose. While, no significant changes in the expression of the Drp1 protein between normal glucose and high glucose were recorded.

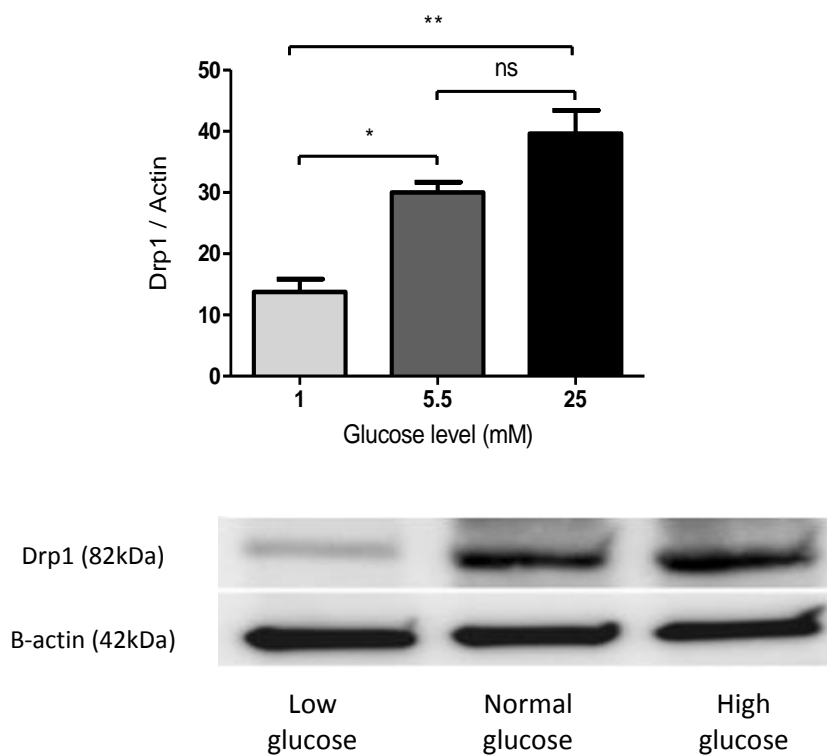


**Figure 3.6: Western blot showing the effect of glucose levels on the Drp1 protein expression in MDA-MB-231 cells after 48hrs.** Data represent the mean  $\pm$  standard error of three independent experiments performed in triplicate. One-way ANOVA followed by Tukey's Multiple Comparison Test to compare mean of treatments. (\*, and \*\*represent  $P < 0.05$  and  $0.01$  respectively).

To uncover the role of glucose level on metabolism, MDA-MB-231 cells were cultured for 48hrs in medium with different concentrations of glucose and production of ATP and lactate were measured.

The results of quantification ATP in Figure 3.7; show that the production of ATP by cells increased significantly with increasing glucose concentration in the medium. ATP production increased significantly from  $0.75 \pm 0.013$  mM in low glucose to  $1.11 \pm 0.016$  mM in normal glucose ( $p < 0.01$ ) and to  $2.05 \pm 0.086$  mM in high glucose ( $p < 0.001$ ). Data also showed significant increases of ATP production in high glucose compared to normal glucose ( $p < 0.001$ ).

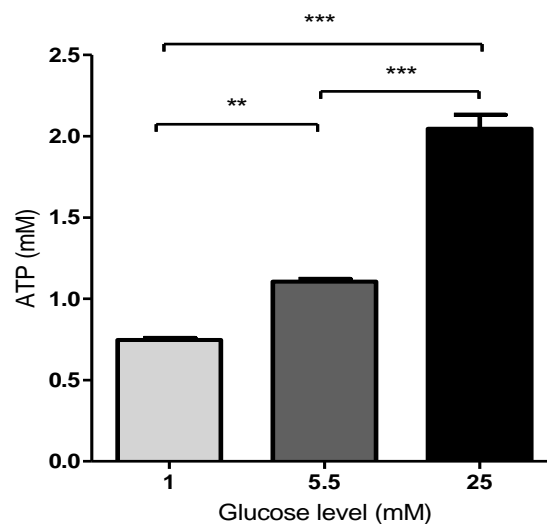


**Figure 3.7: Quantitation of ATP in MDA-MB-231 cells grown in different glucose levels.** Lysate of  $1 \times 10^6$  cells were used for measuring ATP level by colorimetric ATP assay kit. Data represent the mean  $\pm$  standard error of three independent experiments performed in triplicate. One-way ANOVA followed by Tukey's Multiple Comparison Test to compare mean of treatments. (\*\*, and \*\*\*represent  $P < 0.01$  and  $0.001$  respectively)

Similarly, our results as seen in Figure 3.8 revealed that increasing glucose concentration increased the generation of lactate in MDA-MB-231 cells. Lactate production was increased significantly from  $5.52\pm 0.14\text{mM}$  in low glucose to  $14.43\pm 0.42\text{mM}$  in normal glucose and to  $17.98\pm 0.69\text{mM}$  in high glucose ( $p < 0.001$ ). The increases in production of lactate in high glucose was also significant compared to normal glucose ( $p < 0.01$ ).

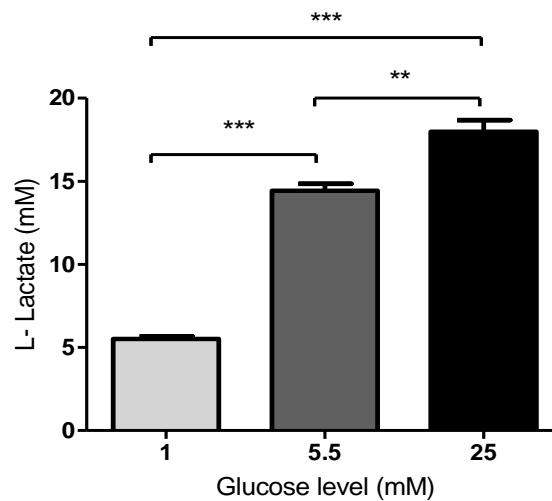


**Figure 3.8: Lactate generation in MDA-MB-231 cells grown in different glucose levels.** Cells were seeded in a 96-well plate at a density of 25,000 cells/well in DMEM supplemented with 10% FBS and different concentrations of glucose. After 48 hrs of incubation, the supernatants were assayed to determine generated L-Lactate level. Data represent the mean  $\pm$  standard error of four independent experiments performed in triplicate. One-way ANOVA followed by Tukey's Multiple Comparison Test to compare mean of treatments. (\*\*, and \*\*\*represent  $P < 0.01$  and  $0.001$  respectively).

Afterwards wound healing assay was performed to investigate the impact of glucose at different concentrations on the cell migration in MDA-MB-231 cells. Results showed that cell migration markedly increased with increasing glucose concentrations. As shown in Figure 3.9 and Figure 3.10, migrated cells covered  $36.5 \pm 2.84\%$  of scratched area in low glucose level. This ratio was increased significantly in normal glucose to  $64.2 \pm 5.46\%$  ( $p < 0.01$ ), and to  $90.9 \pm 0.49\%$  ( $p < 0.001$ ) in high glucose. We also found that the increased ratio of covered wounded area in the high glucose level was significant compared to the normal glucose level ( $p < 0.01$ ).

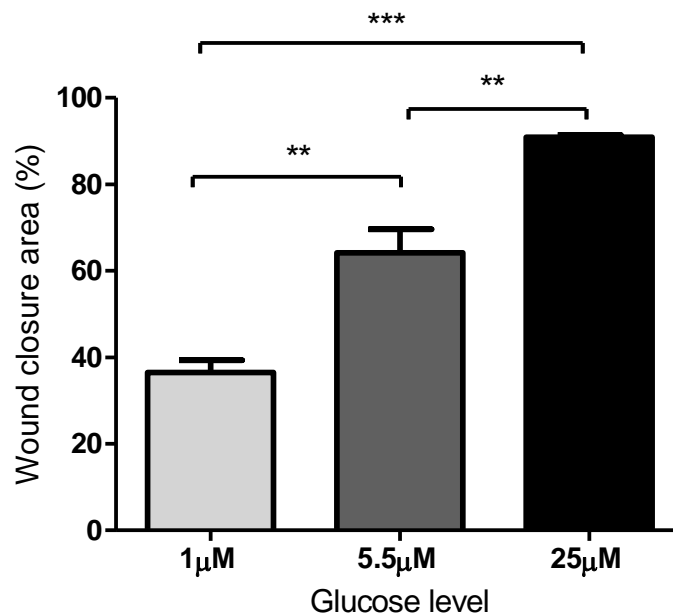


**Figure 3.9: Wound healing assay to evaluate MDA-MB-231 cell migration in different glucose levels.** Cell cultured in different glucose concentrations for 24hrs then monolayer cells were scratched. Time-lapse microscopy was used to taken images every hour for 24 hrs. The wound area was quantified using ImageJ Software. Data represent the mean  $\pm$  standard error of three independent experiments performed in triplicate. One-way ANOVA followed by the Tukey's Multiple Comparison test to compare between mean of treatments (\*\* and \*\*\* represent  $P < 0.01$  and  $0.001$  respectively).

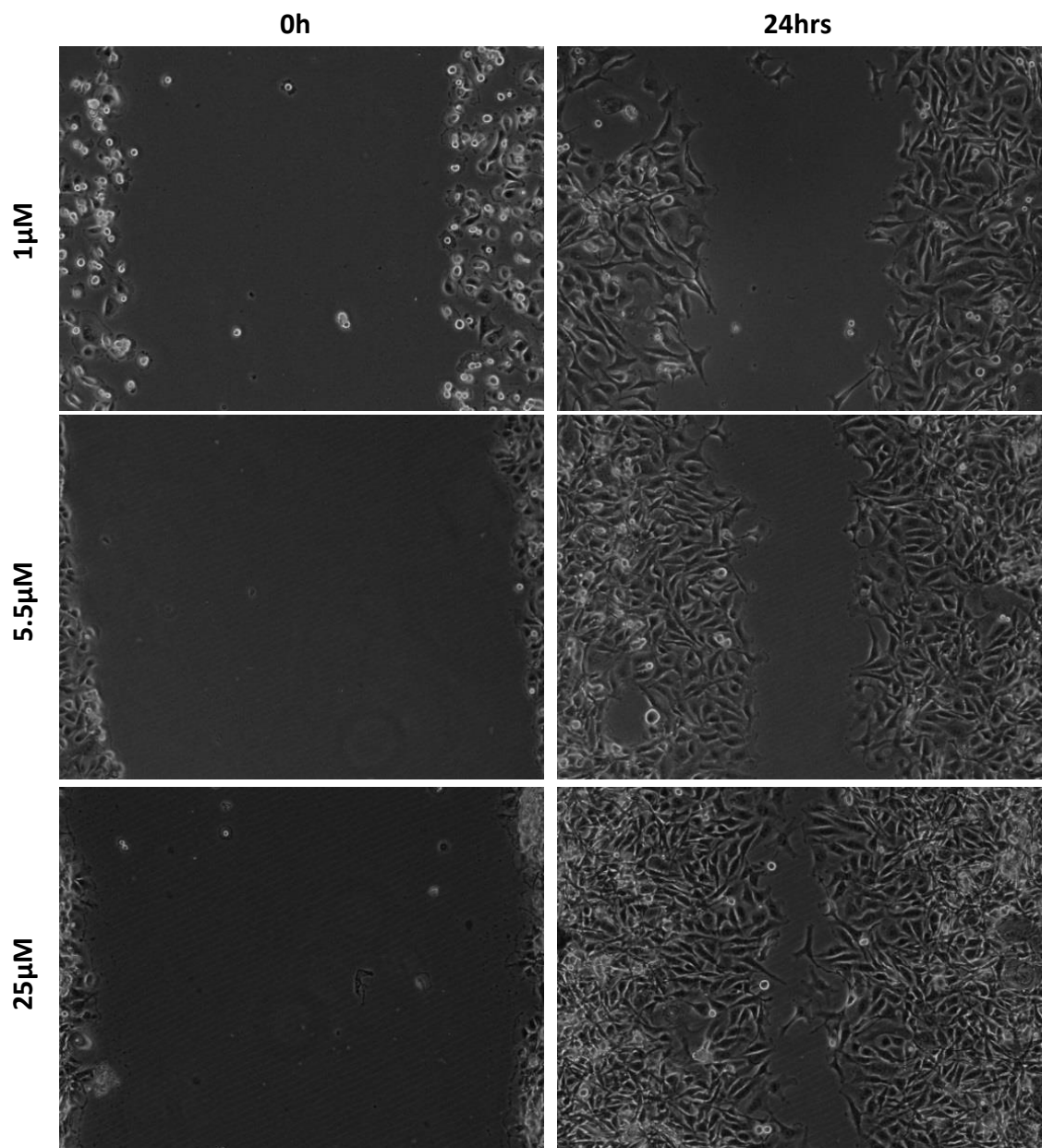


**Figure 3.10: Wound healing assay Micrographs showing the MDA-MB-231 cells under the effect of different glucose levels in DMEM medium.** Time-lapse microscopy used to take images at 0, and 24hrs of cells grown in the different glucose concentrations; low glucose 1mM, normal glucose 5.5mM, and high glucose 25mM.

To confirm the previous result of wound healing assay, cell tracking was performed to investigate the effect of glucose in different concentration on cell migration in MDA-MB-231 cells. The results revealed that cell migration increased with increasing glucose concentrations. As shown in Figure 3.11 cell migration was increased to  $18.1 \pm 0.54 \mu\text{m}/\text{hour}$  in high glucose level compared to  $15.9 \pm 0.21 \mu\text{m}/\text{hour}$  in normal glucose ( $p < 0.05$ ), and  $13.96 \pm 0.66 \mu\text{m}/\text{hour}$  in low glucose ( $p < 0.001$ ). While, no significant differences in the cell migration was detected between the cells cultured in the normal glucose and the cells cultured in low glucose.

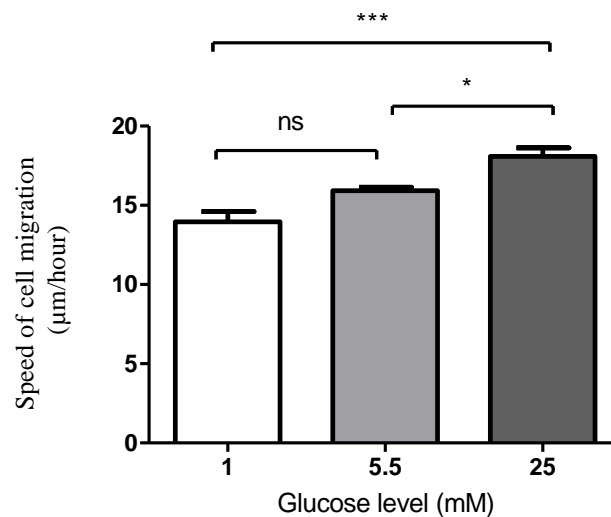


**Figure 3.11: Impact of different glucose levels on cell migration in MDA-MB-231 cells.** The cell migration was monitored by the time-lapse imaging microscopy. Images were taken every 15 minutes over 24 hours, and ImageJ software was used for measuring single cell movement. Data represent the mean  $\pm$  standard error of four independent experiments performed in triplicate. One-way ANOVA followed by Tukey's test to compare mean of treatments (\*and \*\*\* represent  $P < 0.05$  and  $0.001$  respectively).

To confirm whether production of reactive oxygen species (ROS) was increased with increasing concentration of glucose in MDA-MB-231 cells, we measured intracellular ROS using a commercial assay kit. Our results revealed that production of ROS in high glucose was significantly increased to  $20717 \pm 2029$  Unit compared to  $12361 \pm 403.8$  Unit in low glucose level ( $p < 0.01$ ). While, no significant differences was found in the production ROS between high glucose and normal glucose or between normal glucose and low glucose, as seen in Figure 3.12.

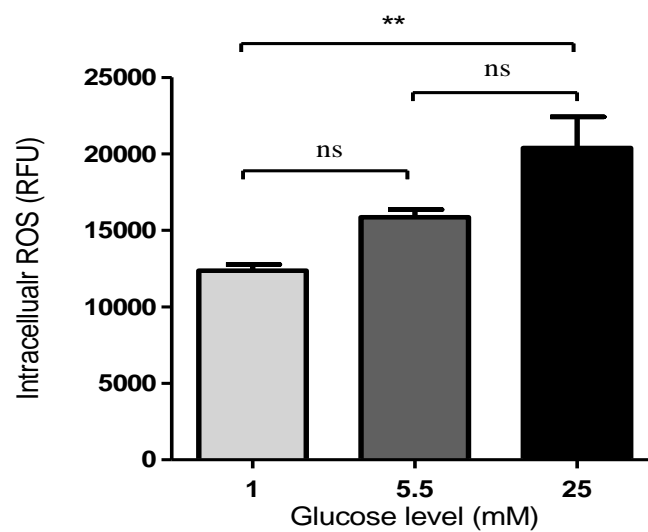


**Figure 3.12: Reactive oxygen species (ROS) in MDA-MB-231 cells in different glucose levels.** Cells were treated with 0.2mM DCFH-DA for 60 minutes, and then incubated in different concentrations of glucose for 24 hrs. The intensity of fluorescence was read with a fluorometric plate reader at 485 nm/535 nm. Data represent the mean  $\pm$  standard error of the mean of three independent experiments performed in triplicate (\*\* represent  $P < 0.01$ ). (RFU mean relative fluorescence unit).

### 3.3.2 Effect of H<sub>2</sub>O<sub>2</sub> on mitochondrial dynamics, metabolism, and cell migration:

When we studied the effect of glucose on mitochondrial dynamic, we postulated that increased ROS will be responsible for fragmentation of the mitochondria as illustrated in Figure 3.1. To test this postulate we investigated the effect of exogenous hydrogen peroxide (H<sub>2</sub>O<sub>2</sub>) on mitochondria, as well as its effect on the metabolism and the cell migration. Therefore we treated MDA-MB-231 cells with different concentrations of H<sub>2</sub>O<sub>2</sub> (50, 100, 250, and 500 $\mu$ M) for 24hrs in our studies.

To confirm that H<sub>2</sub>O<sub>2</sub> with the concentrations that we used does not affect cell viability, we carried out MTT assay to MDA-MB-231 cells treated with different concentrations of H<sub>2</sub>O<sub>2</sub> for 24hrs. The results shown in Figure 3.13, which are analysed using One-way ANOVA followed by Tukey post-test, revealed that H<sub>2</sub>O<sub>2</sub> in all used concentrations has no significant effects on the cell viability compared to control as well as statistically there were no significant differences between treatments.

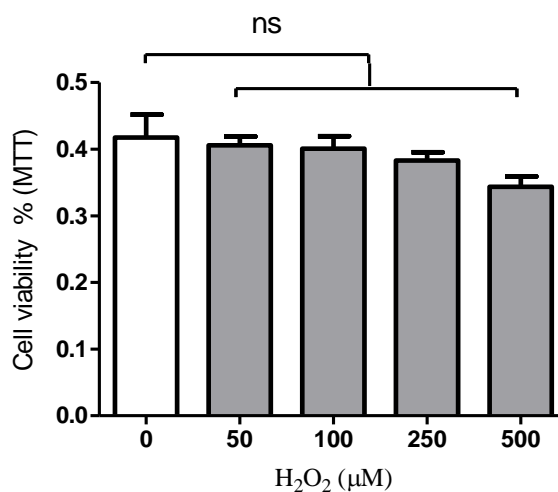


**Figure 3.13: MTT assays showing the effect of H<sub>2</sub>O<sub>2</sub> on the cell viability in MDA-MB-231cells.** Cells were seeded in a 96-well plate at a density of 10,000 cells/well in DMEM containing 10% FBS and incubated overnight then treated with different concentrations of H<sub>2</sub>O<sub>2</sub> for 24hrs. After adding MTT reagent incubated for 4hrs at same conditions, cell viability was determined by reading plates at 570 nm with plate reader. Data represent the mean  $\pm$  standard error of three independent experiments performed in triplicate.

We investigated the effect of H<sub>2</sub>O<sub>2</sub> on the mitochondrial morphology in MDA-MB-231. The results in Figure 3.14A show that no significant differences in the mitochondrial number were found between the cells treated with H<sub>2</sub>O<sub>2</sub> at concentrations 50, 100, and 250µM with the control cells, except at concentration 500µM where mitochondrial number was increased significantly to 254.5±7.61 compared to 122.6±49.34 in the control cells ( $p<0.05$ ). The impact of H<sub>2</sub>O<sub>2</sub> on the size and the volume of the mitochondria were also studied, and results shown in Figure 3.14B revealed that H<sub>2</sub>O<sub>2</sub> at concentrations 50, and 100µM does not affect the mitochondrial size, while at the concentrations 250µM and 500µM, mitochondrial size reduced to 1.72±0.078 and 1.34±0.064 µm<sup>2</sup> ( $p<0.01$  and  $p<0.001$ ) respectively compared to mitochondrial size 4.39±0.76 µm<sup>2</sup> in the control cells.

The volume of the mitochondria was also affected by H<sub>2</sub>O<sub>2</sub> as it was decreased with ascending concentrations of H<sub>2</sub>O<sub>2</sub>. In Figure 3.14 C, the results of the mitochondrial volume analysis show that mitochondrial volume was decreased significantly from 0.41±0.079 in the control cells to 0.24±0.024µm<sup>3</sup> in the cells treated with 100µM of H<sub>2</sub>O<sub>2</sub> ( $p<0.05$ ), and into 0.11±0.002 and 0.069±0.007µm<sup>3</sup> at concentrations 250, and 500µM of H<sub>2</sub>O<sub>2</sub> respectively ( $p<0.001$ ). Whereas, no significant differences were observed between cells treated with 50µM of H<sub>2</sub>O<sub>2</sub> and control cells.

The total mass of mitochondria was obtained by multiplying data of the mitochondrial volume to the number of the mitochondria, and results shown in Figure 3.14D, revealed that the total mass of mitochondria decreased significantly from 48.8±6.54µm<sup>3</sup> in the control to 31.7±1.26µm<sup>3</sup> at concentration 100µM ( $p<0.05$ ), and into 17.8±2.44, and 15.6±3.46µm<sup>3</sup> at concentrations 250, and 500µM respectively ( $p<0.001$ ). While, no significant changes in the total mass of mitochondria was detected at concentration 50µM compared to control.

Figure 3.15 shows the morphological changes in the mitochondria in MDA-MB-231 cells after treating them with different concentrations of H<sub>2</sub>O<sub>2</sub> for 24hrs.

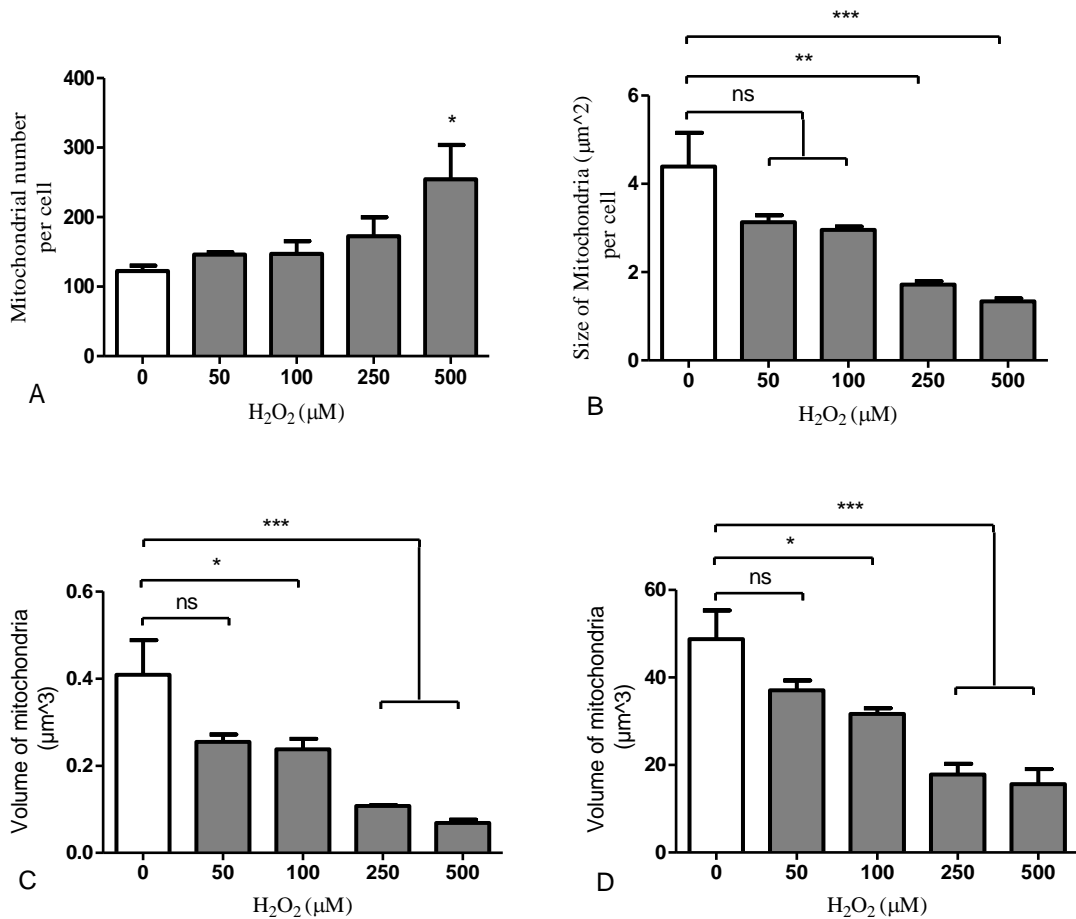


**Figure 3.14: Effect of hydrogen peroxide (H<sub>2</sub>O<sub>2</sub>) on mitochondrial fragmentation in MDA-MB-231 cells.** Cells exposed to different concentrations of H<sub>2</sub>O<sub>2</sub> (50, 100, 250, and 500 μM) for 24hrs then stained with MitoTracker probe and confocal microscopy used to take mitochondrial images. (A) represent quantification analysis of number of mitochondria, (B) Size of mitochondria, (C) Volume of mitochondria, and (D) which represent quantification analysis of total mitochondria mass per cell. Data represent the mean ± standard error of three independent experiments performed in triplicate; each experiment contained at least 30 cells. One-way ANOVA and Dunnett's Multiple Comparison test was used to compare between the mean of treatments with control mean (\*, \*\*, and \*\*\* represent P < 0.05, 0.01, and 0.001 respectively).

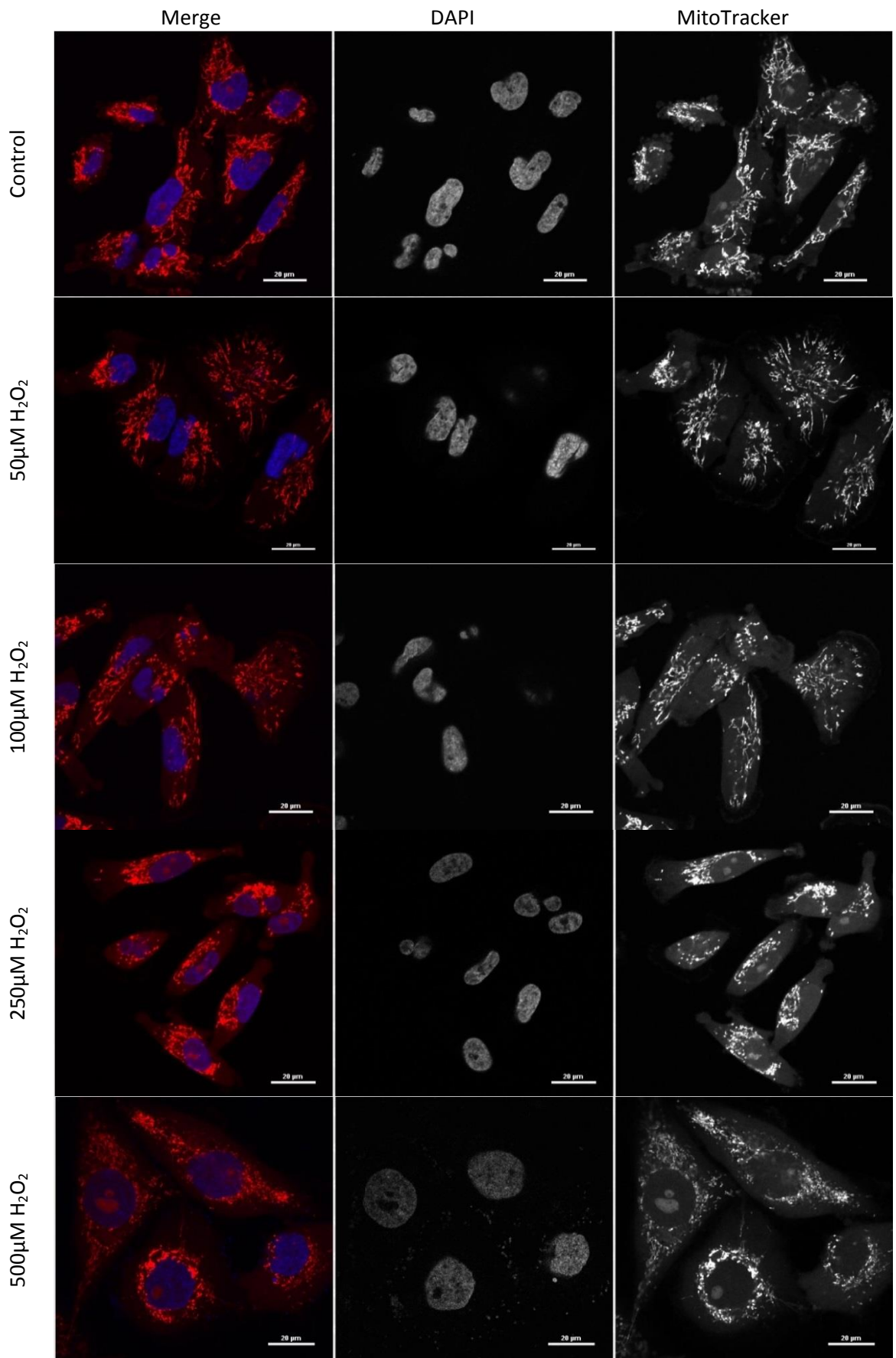


**Figure 3.15: Micrographs showing the mitochondrial shape in MDA-MB-231 cells.** Mitochondria were stained with MitoTracker orange probe (red) and nucleus stained with DAPI (blue), for the cells treated with different concentrations of H<sub>2</sub>O<sub>2</sub>. Scale bars on all images = 20μm

To confirm our results obtained through confocal microscopy, we measured mtDNA copy number after exposing the cells to different concentrations of H<sub>2</sub>O<sub>2</sub> for 24hrs. Results shown in Figure 3.16 revealed no changes in the mtDNA copy number at concentrations 50, and 100μM of H<sub>2</sub>O<sub>2</sub> compared to the control. While at concentrations 250, and 500μM of H<sub>2</sub>O<sub>2</sub>, mtDNA copy number was increased significantly to 1535.84±128.2 ( $p<0.001$ ) and to 1293.45±50.83 ( $p<0.05$ ) respectively compared to 822.497±106.4 in the control.

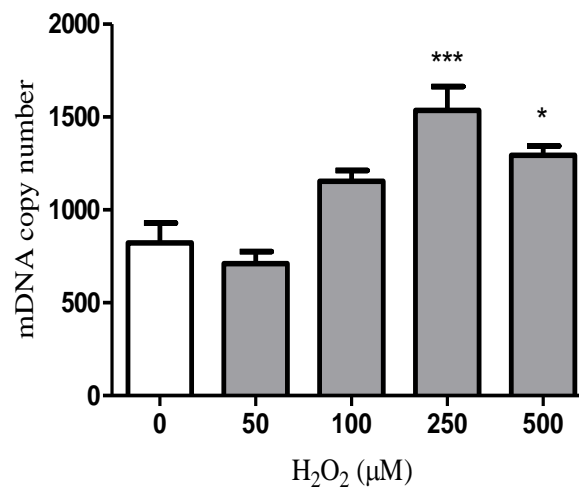


**Figure 3.16: Quantification of mtDNA copy number in MDA-MB-231 cells treated with different concentrations of H<sub>2</sub>O<sub>2</sub>.** Total DNA were extracted and used to determine mtDNA by quantitative real-time PCR. Data represent the mean ± standard error of three independent experiments performed in triplicate. One-way ANOVA followed by Dunnett's Multiple Comparison Test to compare mean of treatments with mean of the control (\*, and \*\*\*represent  $P<0.05$ , and  $0.001$  respectively).

Later we studied the effect of H<sub>2</sub>O<sub>2</sub> on the metabolism in MDA-MB-231 cells. The results in Figure 3.17 show that ATP production was significantly increased in the cells treated with 100 and 250µM of H<sub>2</sub>O<sub>2</sub> to 1.23±0.02mM ( $p<0.01$ ) and to 1.3±0.05mM ( $p<0.001$ ) respectively compared to 1.05±0.04mM in the control cells. While, no significant changes was observed between the cells treated with 50, and 500µM of H<sub>2</sub>O<sub>2</sub> with control cells.

Also we measured the amount of the lactate produced by MDA-MB-231 cells after 24hrs of treating with different concentrations of H<sub>2</sub>O<sub>2</sub>. Our results in Figure 3.18 showed increases in lactate production in the cells treated with H<sub>2</sub>O<sub>2</sub> at concentrations 100, and 250µM to 16.6±0.54 and 16.96±0.34mM respectively ( $p<0.05$ ) compared to 14.42±0.42mM in control cells. Whilst, no significant differences were detected between cells exposed to H<sub>2</sub>O<sub>2</sub> at concentrations 50, and 500µM and control cells.

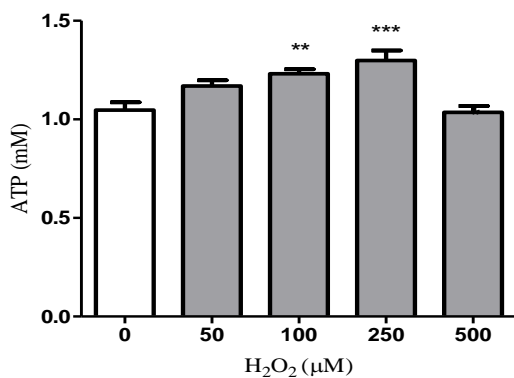


**Figure 3.17: Effect of H<sub>2</sub>O<sub>2</sub> on ATP generation in MDA-MB-231 cells.** Lysate of 1x10<sup>6</sup> cells were used for measuring ATP level by colorimetric ATP assay kit. Data represent the mean ± standard error of four independent experiments performed in triplicate. One-way ANOVA followed by Dunnett's Multiple Comparison Test to compare mean of treatments with control mean (\*\*, and \*\*\* represent P < 0.01, and 0.001 respectively).

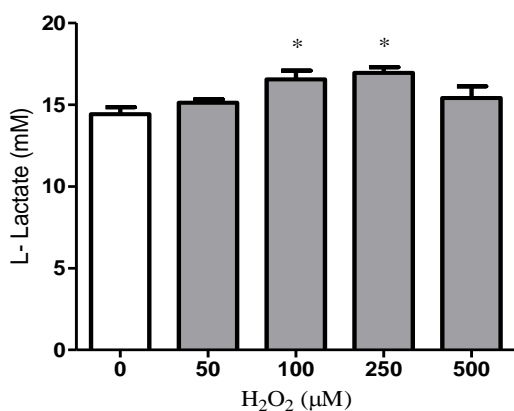


**Figure 3.18: Effect of H<sub>2</sub>O<sub>2</sub> on lactate production in MDA-MB-231 cells.** Cells were treated with different concentrations of H<sub>2</sub>O<sub>2</sub> for 24 hrs, and then supernatants were assayed to determine the L-Lactate concentrations. Data represent the mean ± standard error of three independent experiments performed in triplicate. One-way ANOVA followed by Dunnett's Multiple Comparison Test to compare mean of treatments with control mean (\*represent P < 0.05).

We have carried out the experiment to uncover the effect of H<sub>2</sub>O<sub>2</sub> on cell migration in MDA-MB-231 cells. The results obtained from wound healing assay revealed that increasing concentrations of H<sub>2</sub>O<sub>2</sub> have positive effect on the cell migration. As appears in Figure 3.19, covered wounded area by migrated cells was increased significantly from 53.98±2.3% in the control to 81.9±4.48%, and 78.6±9.24% in cells treated with H<sub>2</sub>O<sub>2</sub> at concentrations 250 and 500µM respectively ( $p<0.05$ ). Whereas, no significant differences in the cell migration was observed in the cells treated with 50 and 100µM of H<sub>2</sub>O<sub>2</sub> compared to the control.

Figure 3.20 shows the time-lapse microscope captured images at zero time and after 24hrs. The scratched area was covered by migrated cells treated with different concentrations of H<sub>2</sub>O<sub>2</sub>.

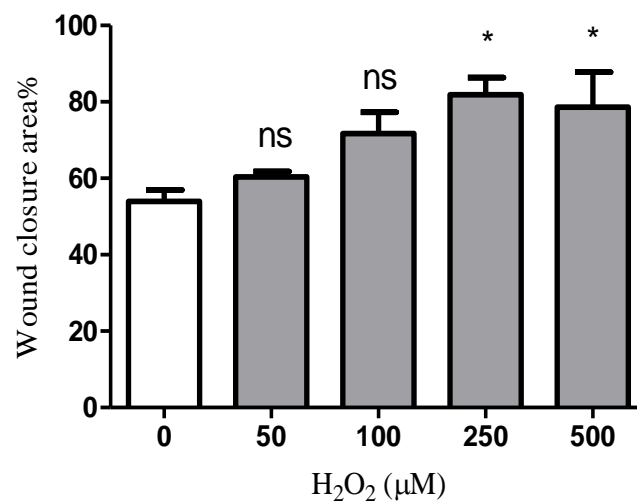


**Figure 3.19: Wound healing assay of MDA-MB-231 cells treated with hydrogen peroxide (H<sub>2</sub>O<sub>2</sub>).** The wounded monolayer was incubated with different concentrations of H<sub>2</sub>O<sub>2</sub>, and images were captured every hour for 24 hrs using Time-lapse microscopy. ImageJ Software was used to measure closure area. Data represent the mean ± standard error of three independent experiments performed in triplicate. One-way ANOVA followed by the Dunnett's Multiple Comparison test to compare mean of treatments with mean of control (\* represent  $P < 0.05$ ).

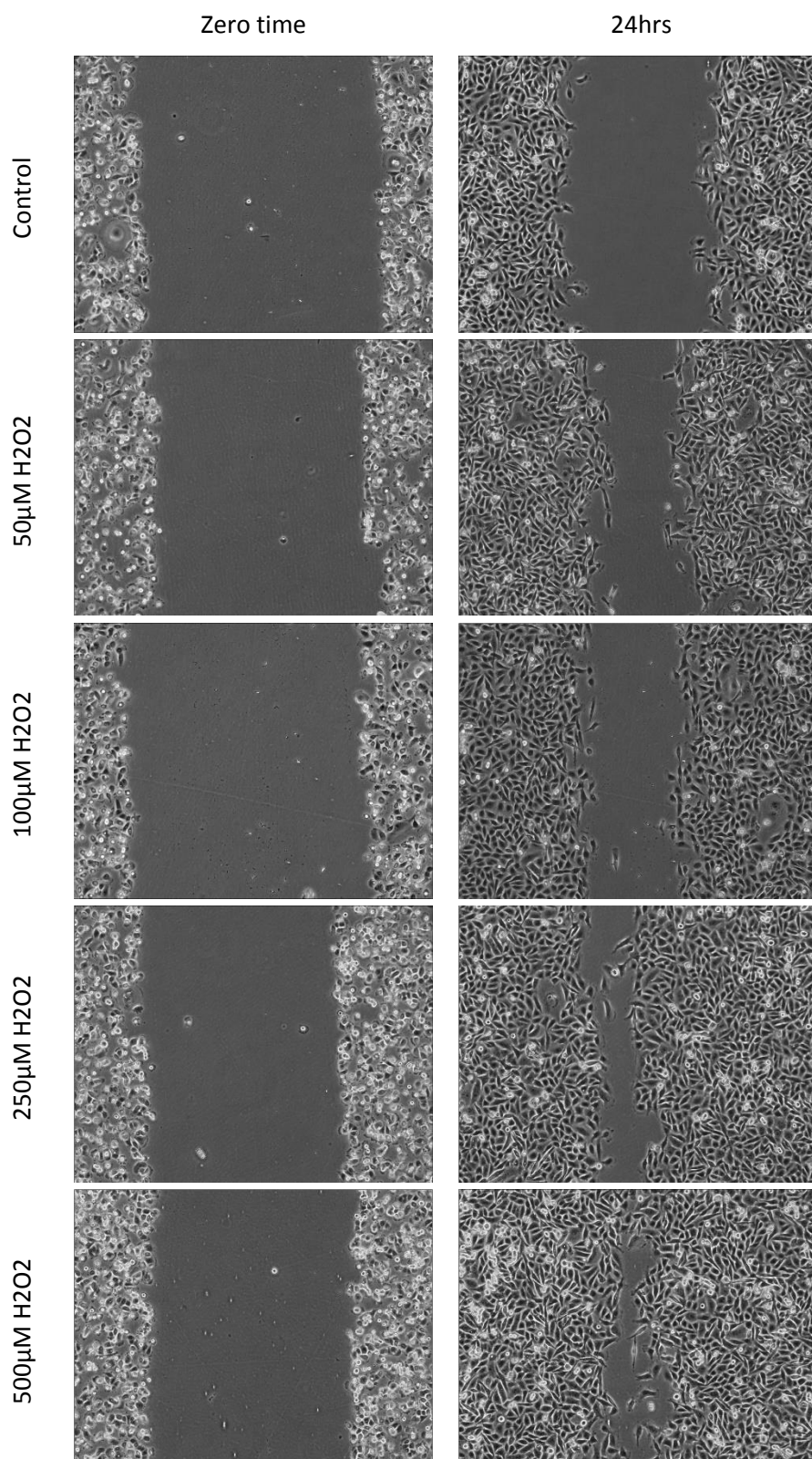


**Figure 3.20: Wound healing assay micrographs showing the MDA-MB-231 cells treated with hydrogen peroxide (H<sub>2</sub>O<sub>2</sub>).** Time-lapse microscopy used to take images at 0, and 24hrs of cells treated with different concentrations of H<sub>2</sub>O<sub>2</sub>.

We also tracked cell movement using time-lapse microscopy to investigate the effect of  $H_2O_2$  on the cell migration. Results in Figure 3.21 showed that the cell migration was increased significantly at concentrations 100, and 250 $\mu$ M to  $18.71\pm 0.37$ , and  $18.96\pm 0.49\mu$ m/hour respectively ( $p < 0.01$ ) compared to  $14.95\pm 0.37\mu$ m/hour in control. While, no significant changes was detected at concentrations 50, and 500 $\mu$ M compared to control.

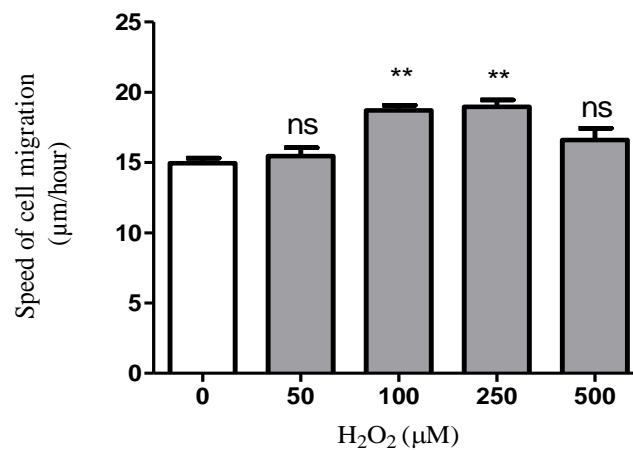


**Figure 3.21: Effect of hydrogen peroxide ( $H_2O_2$ ) on the cell migration in MDA-MB-231 cells.** Time-lapse microscopy used to track single cell movement; images were taken every 15 minutes during 24hrs. ImageJ Software used to measure cell movement. Data represent the mean  $\pm$  standard error of three independent experiments performed in triplicate. One-way ANOVA followed by the Dunnett's Multiple Comparison test to compare mean of treatments with control mean (\*\*represent  $P < 0.01$ ).

To find out if exposing cells to exogenous  $H_2O_2$  affected intracellular levels of reactive oxygen species (ROS), we treated MDA-MB-231 cells with different concentrations of  $H_2O_2$  for 24hrs. The result shown in Figure 3.22 revealed that production of ROS was increased significantly to  $22356.7 \pm 2067$ , and  $21635 \pm 1317$  Unit at concentrations 250 and  $500 \mu M$  respectively ( $p < 0.05$ ) compared to  $15855 \pm 509.8$  Unit in the control. While, no changes in ROS production were observed at lower  $H_2O_2$  concentrations.

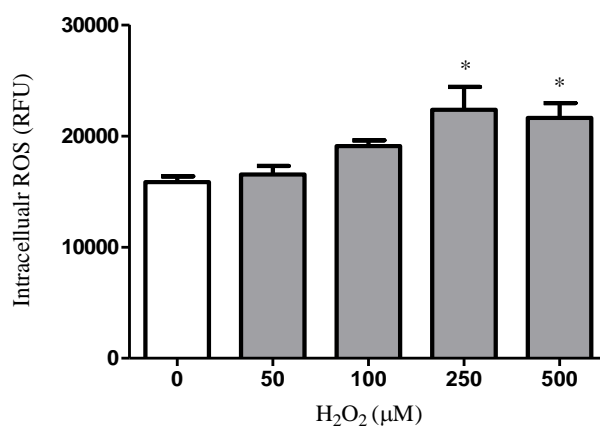


**Figure 3.22: Effect of  $H_2O_2$  on generation of reactive oxygen species (ROS) in MDA-MB-231 cells.** Cells were treated with  $0.2 \text{ mM}$  DCFH-DA for 60 minutes then treated with different concentrations of  $H_2O_2$  for 24 hours. The intensity of fluorescence was read with a fluorometric plate reader at  $485 \text{ nm}/535 \text{ nm}$ . Data represent the mean  $\pm$  standard error of three independent experiments performed in triplicate (\* represent  $P < 0.05$ ).

### 3.3.3 Effect of inhibition mitochondrial fragmentation on mitochondrial metabolism, and cell migration:

We studied the effect of the glucose levels on mitochondrial dynamics and we found that high glucose has induced the mitochondrial fragmentation; which in turn affected the metabolism, and cell migration. In this section, we investigated the effect of inhibition of mitochondrial fission induced by high glucose level in MDA-MB-231 cells on the metabolism, and the cell migration.

For this purpose we used mitochondrial division inhibitor (mdivi-1); a selective chemical inhibitor of mitochondrial fission protein Drp1. It can inhibit mitochondrial fission through inhibiting Drp1 enzyme activity and blocking Drp1/Fis1 interaction, consequently inhibiting assembly of Drp1 protein around mitochondria which is essential for its function (Yeon et al., 2015) as presented in Figure 3.23.

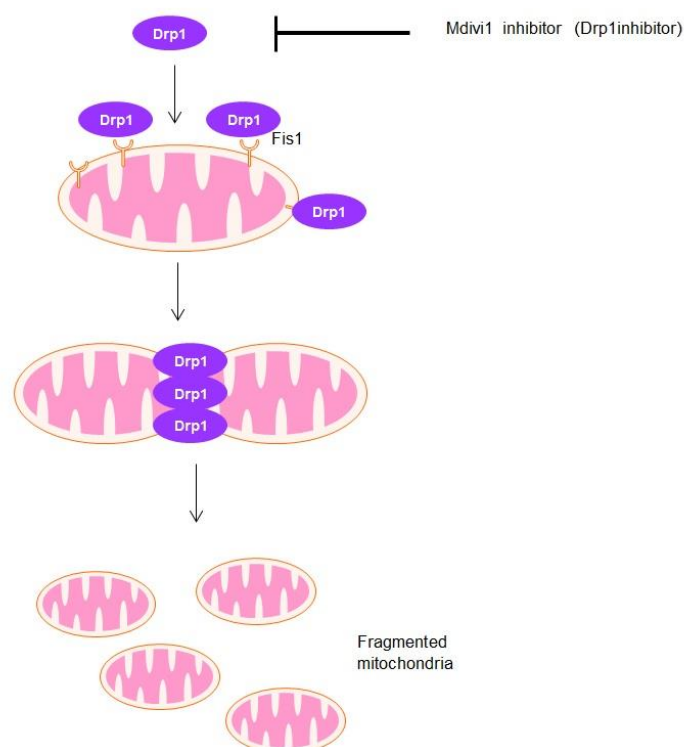


**Figure 3.23: Mechanism of mitochondrial fragmentation inhibition by Mdivi-1 inhibitor.** Graph made using Motifolio - Scientific illustration Toolkits.

To uncover the effect of mdivi-1 inhibitor on the mitochondrial dynamics, we treated MDA-MB-231 cells with different concentrations 10, 30, and 50 $\mu$ M of mdivi-1 inhibitor for 24hrs in high glucose; 25mM, medium. Results in Figure 3.24A showed that no significant differences in the mitochondrial number have occurred in the cells treated with mdivi-1 inhibitor compared to control cells.

The size of the mitochondria were measured in the treated cells with mdivi-1 inhibitor and the results as presented in Figure 3.24B revealed that size of the mitochondria was increased significantly from  $1.79\pm 0.15\mu\text{m}^2$  in non-treated cells to  $2.98\pm 0.25$ , and  $3.18\pm 0.087\mu\text{m}^2$  in treated cells with 30, and 50 $\mu$ M of mdivi-1 inhibitor respectively ( $p<0.01$ ). Whereas, no changes were observed at concentration 10 $\mu$ M compared to non-treated control cells.

Similar results were obtained when we measured the volume of mitochondria. Figure 3.24C shows that mitochondrial volume was increased significantly from  $0.14\pm 0.005\mu\text{m}^3$  in the control cells to  $0.21\pm 0.009\mu\text{m}^3$  in the treated cells with 10 $\mu$ M of mdivi-1 inhibitor ( $p<0.05$ ), and into  $0.27\pm 0.015$ , and  $0.31\pm 0.017\mu\text{m}^3$  in the treated cells with 30, and 50 $\mu$ M of mdivi-1 inhibitor respectively ( $p<0.001$ ).

Results for measuring total mass of the mitochondria shown in Figure 3.24D, revealed significant changes in the cells treated with 50 $\mu$ M of mdivi-1 inhibitor; in which total mitochondrial mass was increased significantly to  $31.7\pm 5.78\mu\text{m}^3$  ( $p<0.05$ ) compared to  $17.6\pm 0.22\mu\text{m}^3$  in the control cells. While, no changes were observed between cells treated with mdivi-1 inhibitor at concentrations (10, and 30 $\mu$ M) and control cells.

Figure 3.25 shows the micrograph of mitochondrial morphology in MDA-MB-231 cells after 24hrs of treating cells with different concentrations of mdivi-1 inhibitor.

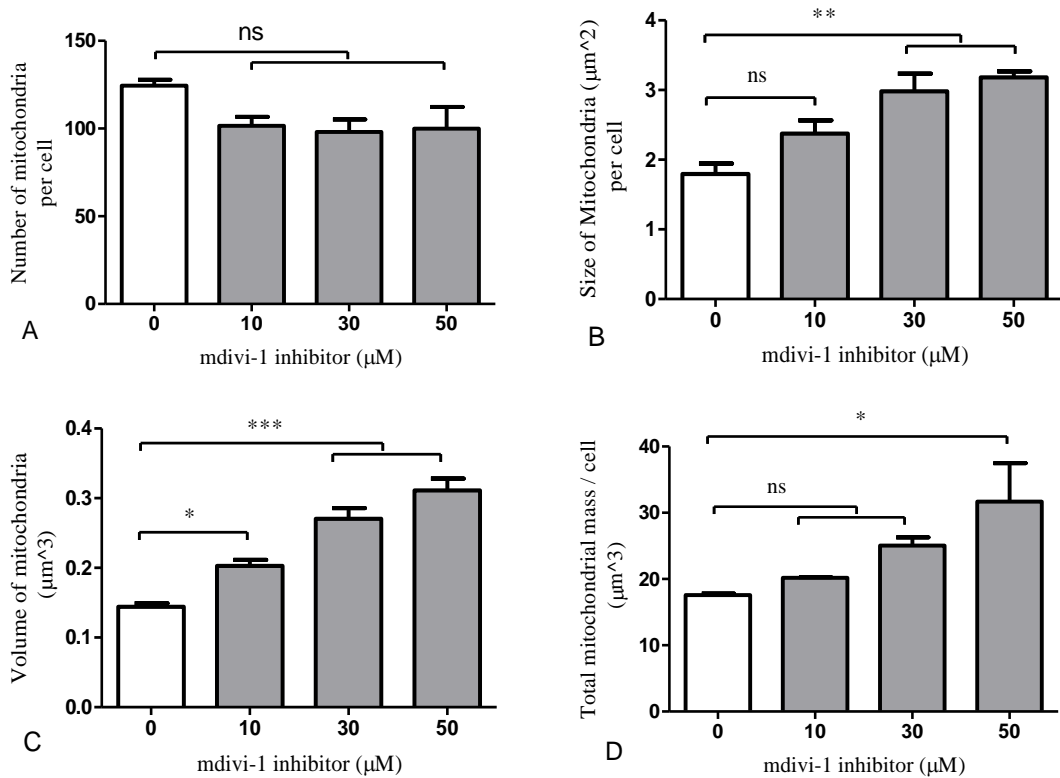


**Figure 3.24: Effect of mdivi-1 inhibitor on the mitochondrial morphology in MDA-MB-231 cells.** Cells cultured in high glucose medium were treated with different concentrations (10, 30, and 50µM) of mdivi-1 inhibitor for 24hrs. MitoTracker probe used for staining mitochondria and confocal microscopy was used to take images. (A) Represent quantification analysis of mitochondrial number, (B) Size of the mitochondria, (C) Volume of the mitochondria, and (D) Total mass of the mitochondria per cells. Data represent the mean  $\pm$  standard error of three independent experiments performed in triplicate; each experiments with more than 30 cells. One-way ANOVA followed by Dunnett's Multiple Comparison test to compare between the mean of treatments with mean of the control (\*, \*\*, and \*\*\*represent P < 0.05, 0.01, and 0.001respectively).

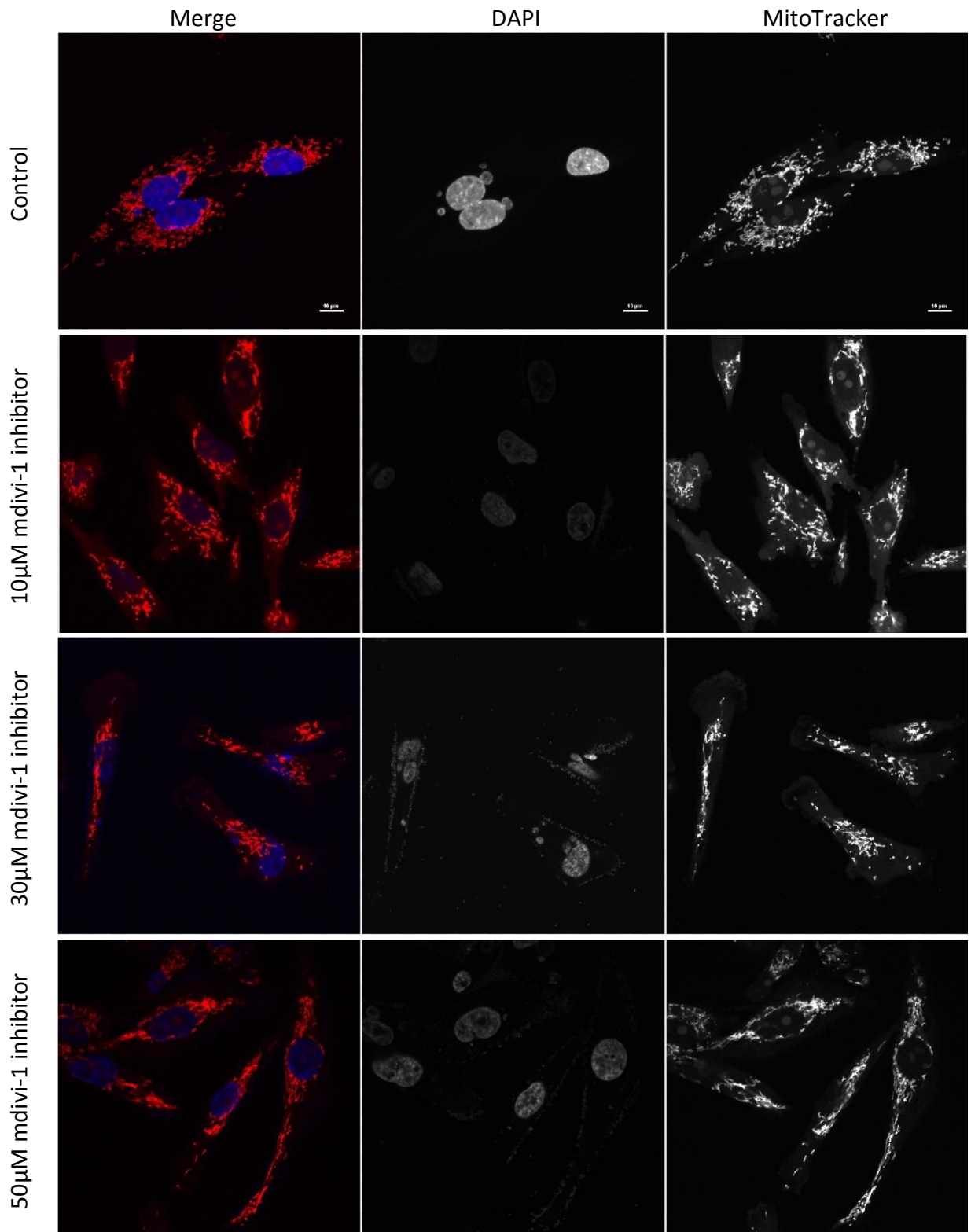


**Figure 3.25: Micrographs showing the effect of mdivi-1 inhibitor on the mitochondrial morphology in MDA-MB-231 cells.** Cells treated with different concentrations Mdivi-1 inhibitor in high glucose medium. Mitochondria were stained with MitoTracker probe (red) and nucleus stained with DAPI (blue). Scale bars for all images = 10µm.

To confirm obtained results by confocal microscopy for mitochondrial morphology in MDA-MB-231 cells treated with mdivi-1 inhibitor, we measured mtDNA copy by qPCR . Results in Figure 3.26 show that no significant differences were observed in the copy number of mtDNA between cells treated with mdivi-1 inhibitor compared to non-treated control cells.

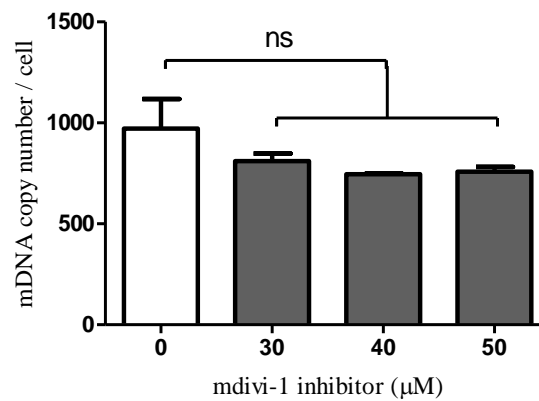


**Figure 3.26: Quantification of mtDNA copy number in MDA-MB-231 cells treated with mdivi-1 inhibitor.** Cells were treated with different concentrations of mdivi-1 inhibitor for 24hrs in high glucose (25mM) medium, and then DNA extracted and used to determine mtDNA content using quantitative real-time PCR. Data represent the mean  $\pm$  standard error of three independent experiments performed in triplicate. One-way ANOVA followed by Dunnett's Multiple Comparison Test to compare mean of treatments with mean of the control at p value 0.05.

Afterward we investigated the effect of mdivi-1 inhibitor on the metabolism through measuring the level of ATP production and lactate production. Results of quantification ATP production in Figure 3.27 revealed that mdivi-1 inhibitor at the concentrations 30, and 50 $\mu$ M caused significant reduction in the ATP production to  $1.39\pm 0.03$ , and  $1.11\pm 0.02$ mM compared to  $2.05\pm 0.09$ mM in the control ( $p<0.001$ ). Whereas, no significant differences were detected at concentration 10 $\mu$ M compared to the control.

The levels of lactate production were also measured and results as seen in Figure 3.28 showed significant decreases in lactate production in the cells treated with mdivi-1 inhibitor at all used concentrations. Compared to the non-treated control cells; in which lactate production was  $17.98\pm 0.7$ mM, it has been decreased to  $13.87\pm 0.16$ ,  $12.59\pm 0.32$ , and  $11.2\pm 0.17$ mM in treated cells with mdivi-1 inhibitor at concentrations 10, 30, and 50 $\mu$ M respectively ( $p<0.001$ ).

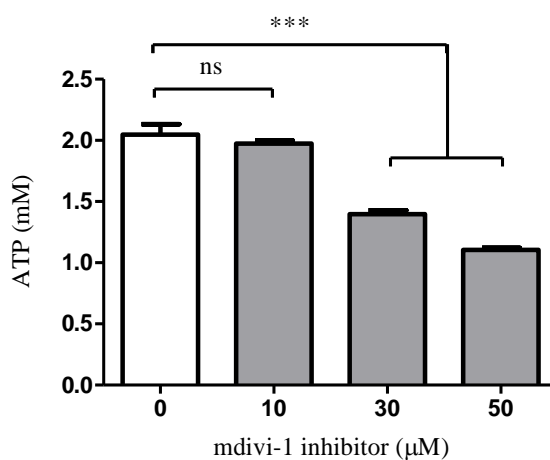


**Figure 3.27: Effect of mdivi-1 inhibitor on ATP production in MDA-MB-231 cell.** ATP levels were measured using colorimetric ATP assay kit at 570nm, after treating cells with different concentrations of mdivi-1 inhibitor in high glucose medium for 24hrs. Data represent the mean  $\pm$  standard error of the mean of four independent experiments performed in triplicate. One-way ANOVA followed by Dunnett's Multiple Comparison Test to compare mean of treatments with the mean of control (\*\*\*) represent  $P < 0.001$ ).

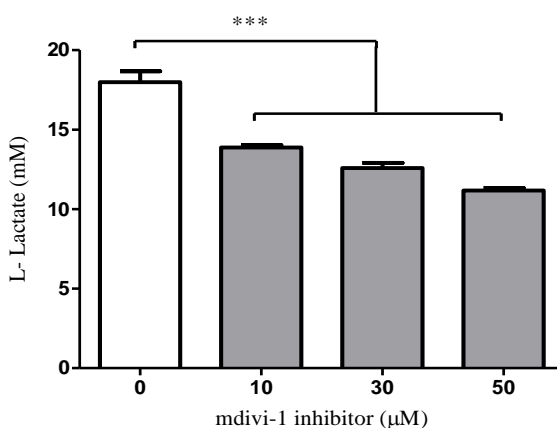


**Figure 3.28: Effect of mdivi-1 inhibitor on lactate production in MDA-MB-231 cell.** After 24hrs treating cells with different concentrations of mdivi-1 inhibitor in high glucose medium; supernatants were assayed using colorimetric glycolysis assay kit at 490nm to determine the L-Lactate concentrations. Data represent the mean  $\pm$  standard error of three independent experiments performed in triplicate. One-way ANOVA followed by Dunnett's Multiple Comparison Test to compare mean of treatments with control mean (\*\*\*) represent  $P < 0.001$ ).

Later we assessed the production level of ROS in the MDA-MB-231 cells treated with mdivi-1 inhibitor using commercial ROS assay kit. Results in Figure 3.29 showed that the production of ROS was decreased significantly from  $20383.7 \pm 2029$  Unit in the control to  $13394.3 \pm 1350$  Unit in the treated cells with  $50 \mu\text{M}$  of mdivi-1 inhibitor ( $p < 0.05$ ). Whereas, no significant differences in ROS production was recorded between treated cells with  $10$  and  $30 \mu\text{M}$  of mdivi-1 inhibitor with non-treated control cells.

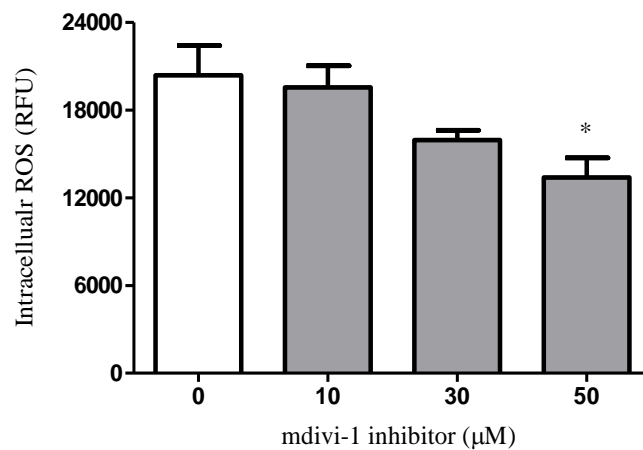


**Figure 3.29: Effect of mdivi-1 inhibitor on the ROS production in MDA-MB-231 cells.** Cells were treated with  $0.2 \text{mM}$  DCFH-DA for 60 minutes then treated with different concentrations of mdivi-1 inhibitor in high glucose medium for 24hrs. The intensity of fluorescence was read with a fluorometric plate reader at  $485 \text{ nm}/535 \text{ nm}$ . Data represent the mean  $\pm$  standard error three independent experiments performed in triplicate (\* represent  $P < 0.05$ ).

The impact of mdivi-1 inhibitor on cell migration was investigated using time-lapse microscopy in tracking cell movement. Figure 3.30 shows that the cell migration was decreased significantly from  $26.64 \pm 1.23 \mu\text{m}/\text{hour}$  in the control to  $19.22 \pm 0.79 \mu\text{m}/\text{hour}$  in the treated cells with  $30 \mu\text{M}$  of mdivi-1 inhibitor ( $p < 0.01$ ), and into  $15.95 \pm 1.12 \mu\text{m}/\text{hour}$  in the treated cells with  $50 \mu\text{M}$  of mdivi-1 inhibitor ( $p < 0.001$ ). While, no significant changes in cell migration was observed between cells treated with  $10 \mu\text{M}$  of mdivi-1 inhibitor and the control cells.

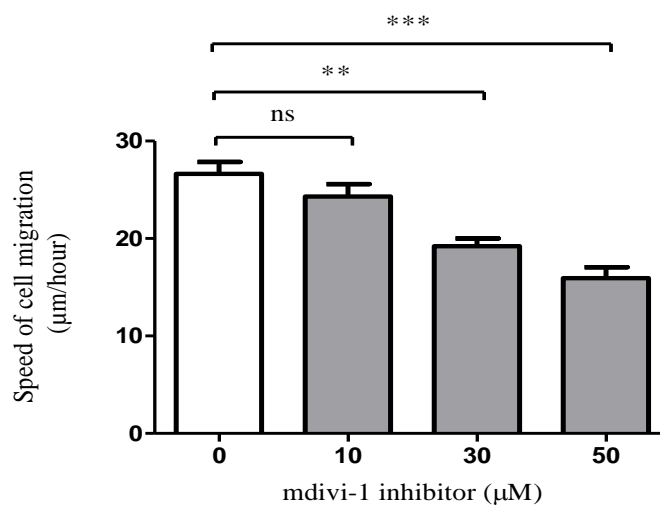


**Figure 3.30: Impact of mdivi-1 inhibitor on the cell migration in MDA-MB-231.** Cell migration was monitored by the time-lapse microscopy, and images were taken every 15 minutes over 24 hours. ImageJ software was used for measuring cell movement. Data represent the mean  $\pm$  standard error of three independent experiments performed in triplicate. One-way ANOVA followed by Dunnett's test used to compare mean of treatments with control mean (\*\*, and \*\*\* represent  $P < 0.01$ , and  $0.001$  respectively).

### **3.4 Discussion**

#### **3.4.1 Glucose levels affect mitochondrial morphology, metabolism, and cell migration.**

It was believed that reprogramming of glucose metabolism from mitochondrial oxidative phosphorylation to glycolysis in cancer cells, which is known as the Warburg effect, is due to permanent changes in mitochondria, however, there are investigations which find that most cancer cells depend on mitochondrial oxidative phosphorylation for generation of ATP and production of metabolic intermediate precursors for the synthesis of macromolecules such as lipids, proteins, and nucleic acids (Brault and Schulze, 2016). Moreover, there is evidence that cancer cells can restore mitochondrial oxidative phosphorylation, this means that mitochondria are intact and oxidative phosphorylation is inhibited rather than being permanently altered (Zheng, 2012).

One outcome of reprogramming glucose metabolism by cancer cells, which may be induced by the change in the mitochondrial dynamics, is production of lactate; the end product of glycolysis, which can change the pH of the tumour microenvironment towards acidity which may affect the motility of cells (Beckert et al., 2006, Zheng, 2012, Jiang, 2017).

Despite the importance of cancer cells regulating their mitochondrial morphology on the basis of their requirements for ATP and their need to enhance growth, proliferation and migration, and in response to environmental and pathologic factors including glucose concentration (Bordi et al., 2017), there is a gap in knowledge linking mitochondrial morphology, and their metabolism to cell migration.

This chapter investigates the effect of glucose level, using three concentrations; normal concentration (5.5mM), low glucose (1mM), and high glucose (25mM), on mitochondrial dynamics and their metabolism on cell migration in MDA-MB-231 breast cancer cells. This study has identified that glucose concentration can affect mitochondrial morphology

strongly, which in turn induces changes in the mitochondrial metabolism as well as in cell migration. In low glucose concentration (1mM), which mimics severe hypoglycaemia in humans, mitochondria appeared as elongated, network-like shapes. While in high glucose concentration (25mM), which mimics hyperglycaemic condition in humans, mitochondria were fragmented to small, circular shapes. In normal glucose (5.5mM), which represents normal glucose level in human blood, elongated shape mitochondria were shown (Figure 3.4). We evaluated these changes in mitochondrial dynamics induced by glucose concentrations more accurately through measuring the number, size, volume, and total mass of mitochondria via confocal microscopy using a mitochondrial specific stain (MitoTracker probe). Although the mitochondria are highly dynamic organelles and the processes of fission and fusion can take place easily during the course of experiments, these challenges were solved through fixation of cells. The results confirmed our expectations, increasing glucose level led to increases in the number of mitochondria, while, mitochondrial size and volume became smaller as well as the total mass of mitochondria (Figure 3.3).

Mitochondrial overlapping was one of difficulties in mitochondrial counting. Despite that the confocal microscopy provides high quality 3D images of mitochondria, the large number of mitochondria within cells can impede mitochondrial counting especially in high glucose level where mitochondria were fragmented and can appear overlapped or aggregated.

To confirm the results obtained by confocal microscopy, mitochondrial DNA (mtDNA) copy number was measured using quantitative polymerase chain reaction (qPCR). Even though the results suggested that increases in glucose concentrations affected mtDNA copy number, statistically the difference was non-significant (Figure 3.5). One explanation may be that the lysate buffer which used to disrupt cell membrane during isolation of DNA has affected the tubular network-like shape mitochondria.

In mammalian cells, dynamin-related protein 1 (Drp1); key mediators of mitochondrial fission, can be activated in response to several factors including stress induced by high glucose (Wang et al., 2012, Rovira-Llopis et al., 2017) and trigger mitochondrial fragmentation through interaction with mitochondrial fission 1 protein which is localized on the outer surface of mitochondrial membrane (Otera and Mihara, 2011). Our results from western blots confirm that increases in glucose concentrations led to increases in the expression of Drp1 protein (Figure 3.6).

There are several studies suggesting that reactive oxygen species (ROS), which is mostly generated during mitochondrial oxidative phosphorylation (Gao et al., 2008), is responsible for mitochondrial fragmentation (Yu et al., 2006, Wang et al., 2012), and there are reports that linked high glucose level with overproduction of ROS (Trudeau et al., 2011, Yu et al., 2011). However, studies have found that blocking ROS generation in high glucose concentration did not prevent mitochondrial fragmentation (Yu et al., 2006). Furthermore, it was reported that mitochondrial fragmentation induced by ROS leads to mitochondrial dysfunction (Russell et al., 2002, Georgieva et al., 2017). Which means that mitochondrial oxidative phosphorylation is inactivated, and this raises the question of whether the increased ROS is from other sources rather than mitochondria and how defective mitochondria can induce ROS production. In the present study, our results confirm that increases in the glucose concentration increased production of ROS; however, only in high glucose was this increase significant compared to low glucose (Figure 3.12). Despite these results, there will be need to further study to confirm that source of ROS is mitochondrial oxidative phosphorylation. There are studies that suggest the non-mitochondrial sources also have a role in enhancing ROS after high glucose flux into the cells (Barazzoni, 2012). Yu and co-workers (2006) studied the effect of hyperglycaemic conditions on cell lines Clone 9 and H9c2 of rat and they reported that mitochondrial fragmentation induced under hyperglycaemic condition contribute to overproduction of ROS and they suggest

prevention of mitochondrial fragmentation as a target to control ROS production, which means that ROS is a result of mitochondrial fragmentation not a cause to it. Other studies found that blocking Drp1 which triggers mitochondrial fission increases oxidative phosphorylation and leads to suppression of ROS production (Gan et al., 2015). Röth and co-workers (2014) found reduced ROS production in T cells after inhibition of Drp1.

Many studies have documented mitochondrial dysfunction in cancer cells, this makes cells rely on glycolysis for generation of ATP (Phan et al., 2014), and it has been suggested that mitochondrial function can be correlated strongly with changes in mitochondrial morphology (Wai and Langer, 2016). In the present study, ATP production as well as lactate production was measured to determine the effect of mitochondrial morphology affected by glucose concentration on the function of mitochondria and the cells. The data confirm a strong correlation between mitochondrial shape and function. Mitochondrial fragmentation induced by high glucose led to increases in ATP production (Figure 3.7), which has been accompanied by an increase in glycolysis (Figure 3.8). In contrast, in low glucose, where mitochondria have elongated network-like shapes, cells rely less on glycolysis and as a result generation of ATP was lower (Figure 3.8 and 3.7 respectively). This study supports evidence from previous observations (Aravamudan et al., 2014); they found that stress due to exposure to cigarette smoke induces changes in the mitochondrial morphology and in turn lead to mitochondrial dysfunction. Also Palorini and co-workers (2013) found that depletion of glucose induced cancer cells to switch from glycolysis to mitochondrial oxidative phosphorylation. However, they did not study its effect on mitochondrial morphology.

This is might be due to reduction in the inner mitochondrial surface area in fragmented mitochondria which can alter the normal function of mitochondria for generating ATP (Mannella, 2006), while, in low glucose, where mitochondria have elongated shapes the

inner surface area is enough to support electron transport chain enzymes to work properly, glycolysis is decreased compared to normal glucose.

The increases in generated ROS may also cause damage to mitochondrial proteins and enzymes that participate in oxidative phosphorylation, and this makes the cells reprogram their metabolism to glycolysis (Guo et al., 2013).

Previous studies showed that cancer cells reprogram metabolism to glycolysis to support their rapid growth and proliferation, and as a result lactate; an end product of glycolysis will increase in the cells (Lunt and Vander Heiden, 2011, Liberti and Locasale, 2016).

It is exported via monocarboxylate transporters (MCTs) into the tumor microenvironment, causing an extracellular acidification (Kato et al., 2013). This acidic condition activates protease enzymes that degrade extracellular matrix (ECM) accompanied by detachment of the cells, thus facilitating cell migration (Han et al., 2013, Jiang, 2017). Due to the effect of mitochondrial morphology on metabolism, it is expected that mitochondrial fragmentation increases cell migration and elongation of mitochondria decreases cell migration. Our data from wound healing assays (Figure 3.9) and single cell tracking by time-lapse microscopy (Figure 3.11) for MDA-MB-231 cells confirm our expectation. In high glucose where mitochondria are fragmented cell migration is significantly increased compared to normal glucose where mitochondrial shape is elongated. In low glucose in which cells has network-like shaped mitochondria, cell migration was lower compared to normal glucose. Our results can be supported by findings of Wang and co-workers (2015b) where they found that inhibition of mitochondrial fission induced by platelet-derived growth factor (PDGF) in vascular smooth muscle decreases cell migration through changing mitochondrial function.

The results suggest that mitochondrial function and morphology are strongly correlated to each other. Fragmentation of mitochondria due to high glucose leads to reduction in mitochondrial metabolism and this enhances cells to depend more on glycolysis which in

turn leads to increases in the cell migration. In contrast, shifting mitochondria to become more elongated and forming network-like shape, enhances cells to rely more on mitochondrial oxidative phosphorylation to obtain high amount of ATP as possible from low concentration of glucose (Palorini et al., 2013), and this leads to reduction in glycolysis and subsequently decreases in cell migration.

### **3.4.2 Hydrogen peroxide induces mitochondria fragmentation, changes metabolism, and increases cell migration**

We found that high glucose induces mitochondrial fragmentation, possibly through increased intracellular ROS production. To investigate whether changes in mitochondrial morphology was due to elevated ROS, MDA-MB-231 cells were treated with hydrogen peroxide ( $H_2O_2$ ) as an exogenous ROS for 24hrs to study its impact on the mitochondrial dynamics as well as cellular metabolism and cell migration. It has been suggested that  $H_2O_2$  plays an important role in cancer development; however, in high levels it can induce apoptosis (Lopez-Lazaro, 2007, Pan et al., 2011, Xiang et al., 2016)

Mitochondria, which are high dynamic and flexible, could adjust their morphology as a response to the stress induced by microenvironmental changes (Ferree and Shirihai, 2012). The present study showed that MDA-MB-231 cells treated with  $H_2O_2$  led to changes in mitochondria morphology. The number of mitochondria increased, and this increase was significant at concentration of  $500\mu M$  (Figure 3.14A). We confirmed this result with quantitative PCR; where data showed that mtDNA copy number was increased significantly after treating cells with  $H_2O_2$  at concentrations 250 and  $500\mu M$  (Figure 3.16). Treating cells with  $H_2O_2$  led to reduction in the size, volume, and total mass of mitochondria (Figure 3.4 and 3.15). These data confirm that stress induced by elevated ROS is likely to be responsible for fragmentation of mitochondria. This can be supported

by findings of Fan and co-workers (2010), who found that  $H_2O_2$  can contribute to the changes in the mitochondrial morphology in  $C_2C_{12}$  mouse myoblasts.

The extracellular pH in normal tissues is relatively basic, while, in cancer cells it is lower due to generation of ROS which is accompanying mitochondrial oxidative phosphorylation for ATP production (Gerweck and Seetharaman, 1996). Previous studies have documented that  $H_2O_2$  can lead to increases in the ROS level and inhibition of oxidative phosphorylation in HeLa cells (Hall and Martinus, 2013). In our study, analysis of data has shown that treating cells with  $H_2O_2$  at low concentrations (100 and 250 $\mu$ M) led to increases in ATP generation (Figure 3.17) and lactate production (Figure 3.18). These results suggest that  $H_2O_2$  shifts metabolism toward glycolysis which is faster in ATP generation. Surprisingly, at higher concentration (500 $\mu$ M of  $H_2O_2$ ) the ATP generation has decreased which was also accompanied by decreases in the lactate production. Although it is difficult to explain the reason, there maybe other pathways that are affected by high concentration of  $H_2O_2$  led to decline of glycolysis and in turn decreases in ATP production. Similar results were found by Molavian and co-workers (2016), who found that treating cells with  $H_2O_2$  increases glucose uptake and leads to raising generated ROS, this in turn activates pentose phosphate pathway (PPP) and aerobic glycolysis for ATP production.

The above observation opens up an expectation that treating cells with  $H_2O_2$  can increase cell migration, and we also found previously that excessive ROS due to high glucose flux can increase cell migration. We found that  $H_2O_2$  enhances wound closure in cultured MDA-MB-231 cells at concentrations of 250 and 500 $\mu$ M (Figure 3.19 and 3.20). Time lapse microscopy for tracking single cells also showed  $H_2O_2$  enhanced cell migration at concentrations of 100 and 250 $\mu$ M (Figure 3.21), suggesting that cell migration can be increased with exogenous  $H_2O_2$ . This result is in agreement with previous reports by Pan and co-workers (2011), who found that treating corneal epithelial cells with exogenous  $H_2O_2$  enhances their cell migration.

Although  $H_2O_2$  is one species of ROS, exogenous  $H_2O_2$  can induce greater production of intracellular ROS through a self-amplifying mechanism (ROS-induced ROS production) (Park, 2016). Our data showed that intracellular ROS increased with increasing  $H_2O_2$  concentration, and it was significant at concentrations of 250 and 500 $\mu$ M (Figure 3.22). This result is in agreement with the findings of Park (2016), who found treating human pulmonary artery smooth muscle cells (HPASMCs) with exogenous  $H_2O_2$  leads to increases in intracellular ROS. He postulated that exogenous  $H_2O_2$  can lead to increases in ROS through generation of mitochondrial superoxide anion ( $O_2^{\bullet}$ ) and depletion of glutathione (GSH) levels which protects cellular components from damage by ROS.

### **3.4.3 Mitochondrial division-1 inhibitor decreases mitochondrial fragmentation, glycolysis, and cell migration.**

It has been documented that mitochondrial division-1 (mdivi-1) inhibitor, a specific inhibitor for dynamin related protein1 (Drp1), can prevent mitochondrial fission through inhibiting assembly of Drp1 around mitochondria (Cassidy-Stone et al., 2008). Recently, it was reported by Kim and colleagues (2017) that an mdivi-1 inhibitor attenuated cell death induced by increased intracellular and mitochondrial ROS through inhibition of translocation and assembly of Drp1 around the mitochondria in rat hippocampal neural stem cells (NSCs). In the present study, we inhibited mitochondrial fragmentation induced by high glucose using an mdivi-1 inhibitor to investigate its effect on cellular metabolism and cell migration. Our results showed that mitochondrial shape changed to become more elongated (Figure 3.25), and analysis of data appeared to show that size and volume of mitochondria increased (Figure 3.24 B and C) especially in the cells treated with mdivi-1 at concentrations of 30 and 40 $\mu$ M. Treating with the inhibitor did not affect the number of mitochondria. One explanation of this result is that maybe the inhibitor prevents fragmentation, however, because the cells are still under the effect of stress induced by

high glucose, the fusion process cannot be activated and mitochondria just grew and increased their mass (Figure 3.24 D) and became elongated in the shape without fusion of mitochondria which may lead to decrease in their numbers.

We confirmed the confocal microscopy results for measuring mitochondrial number with qPCR for measuring mtDNA copy number, and our results showed no significant changes in mitochondrial number following treatment with mdivi-1 inhibitor compared with non-treated control cells. This result is in agreement with results found by Akita and co-workers (2014) who found that mdivi-1 inhibitor led to elongation of mitochondria and made them more sensitized to apoptosis induced by tumor necrosis factor-related apoptosis-inducing ligand (TRAIL). They also found that silencing of Drp1 gives the same results, confirming that the mdivi-1 inhibitor affects mitochondria through inhibition of Drp1 protein. Similarly, Parker (2017) found that mdivi-1 inhibitor reduces mitochondrial fragmentation and increases apoptosis due to increases in sensitivity to radiation in A549 lung cancer cells.

Previously our data showed that mitochondrial fragmentation induced by high glucose led to reprogramming of metabolism to glycolysis. In the present study we inhibited mitochondrial fragmentation using mdivi-1 inhibitor to study its effect on the cellular and mitochondrial metabolism. Our results showed significant decreases in glycolysis (Figure 3.28) accompanied by decreases in ATP production (Figure 3.27). This result confirms our previous finding which suggests correlation between mitochondrial morphology and function, and it is in agreement with the finding of Peiris-Pagès and co-workers (2018), where they found that mdivi-1 inhibitor reduces glycolysis and ATP generation in MCF7 cells. Elongated, tubular mitochondria provide longer and wider cristae; an inner mitochondrial membrane, shape which will be efficient for mitochondrial oxidative phosphorylation (Mannella, 2006, Cogliati et al., 2013, Cogliati et al., 2016) to generate

ATP energy, therefore reliance on aerobic glycolysis for ATP production by the cells will decrease. Theoretically, in high glucose levels, metabolism reversing from aerobic glycolysis to oxidative phosphorylation should lead to increases in ROS generation, and this can induce apoptosis. Cai and co-workers (2002) have reported that high levels of glucose induced apoptotic cell death in cultured cardiac myoblast; they also revealed apoptotic cell death in myocardium tissue in diabetic mice, which is characterized by hyperglycaemia. However, in cancer cells, high glucose not only does not induce cell death, but, instead promotes proliferation, migration and invasion (Lin et al., 2015, Hou et al., 2017).

We next sought to determine whether inhibition of mitochondrial fragmentation using the mdivi-1 inhibitor affects cell migration and ROS production in high glucose. Therefore, we studied measured intracellular ROS after 24hrs of treatment with inhibitor. Data showed decreases in ROS production at 50 $\mu$ M of the mdivi-1(Figure 3.29). This unexpected finding is quite interesting as inhibition of mitochondrial fragmentation decreased ROS generation. A possible explanation is that mitochondrial fragmentation may damage the mitochondrial antioxidant system and the mdivi-1 inhibitor removes this effect on the antioxidant system in mitochondria, leading to reduced ROS generation in mitochondria. It has been suggested to use antioxidants as therapy in neurodegenerative disease such as Parkinson's disease, which are characterized with mitochondrial dysfunction, oxidative stress, and mitochondrial fragmentation (Jin et al., 2014, Santos et al., 2015), and it was reported that exercise can increase mitochondrial mass and upregulate cellular antioxidant defense system (Trewin et al., 2018). This opens a possibility that the mitochondrial antioxidant system activity can be affected with changes in the mitochondrial morphology, and it would be interesting in the future to investigate the impact of mitochondrial fragmentation on the mitochondrial antioxidant system.

Previously we found that high glucose (which induces mitochondrial fragmentation, a switch to glycolysis and increased ROS) promotes cell migration. Therefore, it is expected that inhibition of mitochondrial fragmentation through using the mdivi-1 inhibitor would negatively affect cell migration, and as we expected, results showed decreases in cell migration (Figure 3.30). This result is in agreement with findings by Peiris-Pagès and co-workers (2018), who found that the mdivi-1 inhibitor inhibit cell migration in MCF7 breast cancer cells.

We have concluded that mitochondrial morphology and metabolism are strongly correlated with ROS generation which can be elevated in high glucose or via exogenous hydrogen peroxide, and that alteration of oxidative phosphorylation metabolism to glycolysis induces cancer cell migration. However, there is a need for more study to know correlation between mitochondrial morphology and cellular metabolism which we will discuss in the next Chapters.

## **Chapter Four: Investigating the impact of PGC-1 $\alpha$ on mitochondrial dynamics, cellular metabolism, and cell migration**

### **4.1 Introduction**

The peroxisome proliferator-activated receptor  $\gamma$  activator-1 alpha (PGC-1 $\alpha$ ) is a powerful transcription factor involved in the regulation of mitochondrial biogenesis, oxidative metabolism, and other processes in the cells (Austin and St-Pierre, 2012). It can be activated in response to several factors including cold exposure, nutrient deprivation, exercise, chemotherapy, and oxidative stress (Tan et al., 2016).

Cancer cells, which are characterized by high proliferation rate, require high energy production (Boroughs and DeBerardinis, 2015). It was reported that high demands for energy may activate PGC-1 $\alpha$ . Once activated, PGC-1 $\alpha$  signals for expression of several transcription factors that lead to upregulation of proteins required for increasing the number and mass of the mitochondria in order to increase the production of ATP to meet the required energy demands (Dabrowska et al., 2015).

Mitochondrial biogenesis which involves increases in mitochondrial mass through growth and division of pre-existing mitochondria is regulated by PGC-1 $\alpha$  (Bhatti et al., 2017), and Dabrowska and co-workers (2015) discovered that PGC-1 $\alpha$  can regulate mitochondrial dynamics, which include coordinated cycles of fission and fusion of mitochondria, through controlling Drp1 expression. This means that PGC-1 $\alpha$  can regulate both mitochondrial biogenesis and mitochondrial dynamics through Drp1 expression.

Balance between fission/fusion in mitochondrial dynamics can be changed in several pathologic disorders. There are reports mention that excessive mitochondrial fragmentation in some diseases such as Parkinson's disease is associated with overexpression of PGC-1 $\alpha$  through increasing production of ROS; which in- turn regulates expression and phosphorylation of Drp1 protein (Santos et al., 2015, Peng et al., 2017).

It was also reported that long term expression of PGC1 $\alpha$  in nerve cells exposed to neurotoxic lead induces neurodegeneration through changes in the mitochondrial morphology and alteration in the cellular metabolism(Dabrowska et al., 2015). Recently, studies have reported that PGC1 $\alpha$  expression is strongly associated with the cancer progression through inducing alteration in mitochondrial mass and function (Jones et al., 2012, Girnun, 2012). However, its effect on mitochondrial metabolism as well as cell migration, which is correlated with metabolism, is not clear.

PGC1 $\alpha$  also considered a powerful regulator of ROS through increasing expression of several ROS-detoxifying enzymes (Austin and St-Pierre, 2012). Despite that, its role remains unclear in cancer cells which is characterized by elevated rates of ROS due to high utilization of glucose (Liou and Storz, 2010).

We hypothesize that inducing overexpression of PGC-1 $\alpha$  coactivator (by using ZLN005 activator) can increase mitochondrial fragmentation away from effect of ROS, which is detoxified by PGC-1 $\alpha$ , and this changes metabolic pathway toward glycolysis which in turn affect cell migration and cancer metastasis.

Thus this study aims the better understanding of the link between mitochondrial morphology, mitochondrial metabolism, and cell migration through inducing mitochondrial fragmentation using PGC-1 $\alpha$  coactivator. Another aim is to know the impact of glucose levels and in combination with PGC-1 $\alpha$  overexpression on mitochondrial morphology, mitochondrial metabolism, and cell migration.

The specific objectives in this study include:

- Determination the effect of ZLN005 activator on the expression of PGC-1 $\alpha$  and Drp-1 proteins in different glucose concentrations; low (1mM), normal (5.5mM), and high (25mM) glucose concentrations
- Determination the effect of ZLN005 activator on the mitochondrial morphology in different glucose concentrations

- Determination the effect of ZLN005 activator on the ATP, lactate, and ROS production in different glucose concentrations
- Determination the effect of ZLN005 activator on the cancer cell migration in different glucose concentrations

## **4.2 Material and Methods**

### **4.2.1 Cell culture**

We used MDA-MB-231 cells in our experiments and cells were continuously cultured in Dulbecco's Modified Eagles Media (DMEM) with relevant glucose levels (1, 5.5, and 25mM). ZLN005 (Sigma-Aldrich) is a potent PGC-1 $\alpha$  transcriptional activator used to increase expression of PGC-1 $\alpha$ . To prepare a stock solution of 20mM, we dissolved 10mg of ZLN005 in 1.997ml of DMSO. In our experiments we treated cells with three concentrations (10, 20, and 30 $\mu$ M) of ZLN005 for 24hrs in DMEM medium with different glucose levels as mentioned above.

### **4.2.2 Mitochondrial staining and analysis**

Cells were treated with different concentrations of ZLN005 in different glucose media for 24hrs, then mitochondria were stained with MitoTracker probe (Invitrogen, M7510), and DAPI was used to stain nucleus as described in section 2.2.7 Images were taken using confocal microscopy and analysed by ImageJ software as explained in section 2.2.16

### **4.2.3 Quantitative Real- Time PCR (qRT-PCR)**

The Quantitative real time polymerase chain reaction (qRT-PCR) was used in measuring mtDNA copy number (as described in section 2.2.10) using extracted DNA in MDA-MB-231 cells after treating with different concentrations of ZLN005 in different glucose levels for 24hrs.

#### **4.2.4 Analysis of metabolism and ROS**

MDA-MB-231 cells treated with different concentrations of ZLN005 in different glucose levels for 24hrs, and then generated ATP was measured as described in section 2.2.14, lactate production was measured as described in section 2.2.13, and level of generated ROS was measured as described in section 2.2.12

#### **4.2.5 Western blot analysis**

Expression of Drp1 and PGC-1 $\alpha$  proteins were measured by western blot in MDA-MB-231 cells treated with different concentrations of ZLN005 in different glucose levels for 24hrs as described in section 2.2.5

#### **4.2.6 Cell migration**

cell migration in MDA-MB-231 cells treated with different concentrations of ZLN005 in different glucose levels was monitored by time-lapse microscopy for 24hrs ImageJ (Fiji) software (MtrackJ plugin) was used to track and measure the speed of cell movement as described in section 2.2.17

### 4.3 Results:

We investigated the effect of ZLN005 (PGC-1 $\alpha$  activator) in different concentrations 10, 20, and 30 $\mu$ M on the mitochondrial dynamics in MDA-MB-231 cells. Results in Figure 4.1A showed significant increases in the mitochondrial number in the cells treated with 20 $\mu$ M of ZLN005; in which mitochondrial number was increased to  $166.7 \pm 11.41$  compared to  $93.1 \pm 4.1$  in non-treated control cells ( $p < 0.05$ ). While, the changes were non-significant at concentrations 10, 30 $\mu$ M of ZLN005 compared to the control cells.

The effect of ZLN005 on the mitochondrial size shown in Figure 4.1B revealed a significant decrease in the mitochondrial size from  $4.2 \pm 0.45 \mu\text{m}^2$  in the control cells to  $2.65 \pm 0.12 \mu\text{m}^2$  in the treated cells with 10 $\mu$ M of ZLN005 ( $p < 0.01$ ), and into  $1.7 \pm 0.22$ , and  $1.1 \pm 0.05 \mu\text{m}^2$  at concentration 20, and 30 $\mu$ M of ZLN005 respectively ( $p < 0.001$ ).

Similar changes in the mitochondrial volume were observed when the cells treated with ZLN005. Results in Figure 4.1C showed that mitochondrial volume was reduced from  $0.34 \pm 0.017 \mu\text{m}^3$  in non-treated control cells into  $0.21 \pm 0.018$ ,  $0.13 \pm 0.002$ , and  $0.06 \pm 0.003 \mu\text{m}^3$  in the treated cells with 10, 20, and 30 $\mu$ M of ZLN005 respectively ( $p < 0.001$ ).

Total mass of the mitochondria was also measured. Results in Figure 4.1D revealed significant decreases of total mitochondrial mass from  $31.17 \pm 2.96 \mu\text{m}^3$  in non-treated control cells to  $8.19 \pm 1.31 \mu\text{m}^3$  in treated cells with 30 $\mu$ M of ZLN005 ( $p < 0.01$ ). Whilst, no significant changes were detected statistically at concentrations 10, and 20 $\mu$ M of ZLN005 compared to control.

The Figure 4.2 shows the hyper-fragmentation of the mitochondria in MDA-MB-231 cells after treating with different concentrations of ZNL0005 for 24hrs.

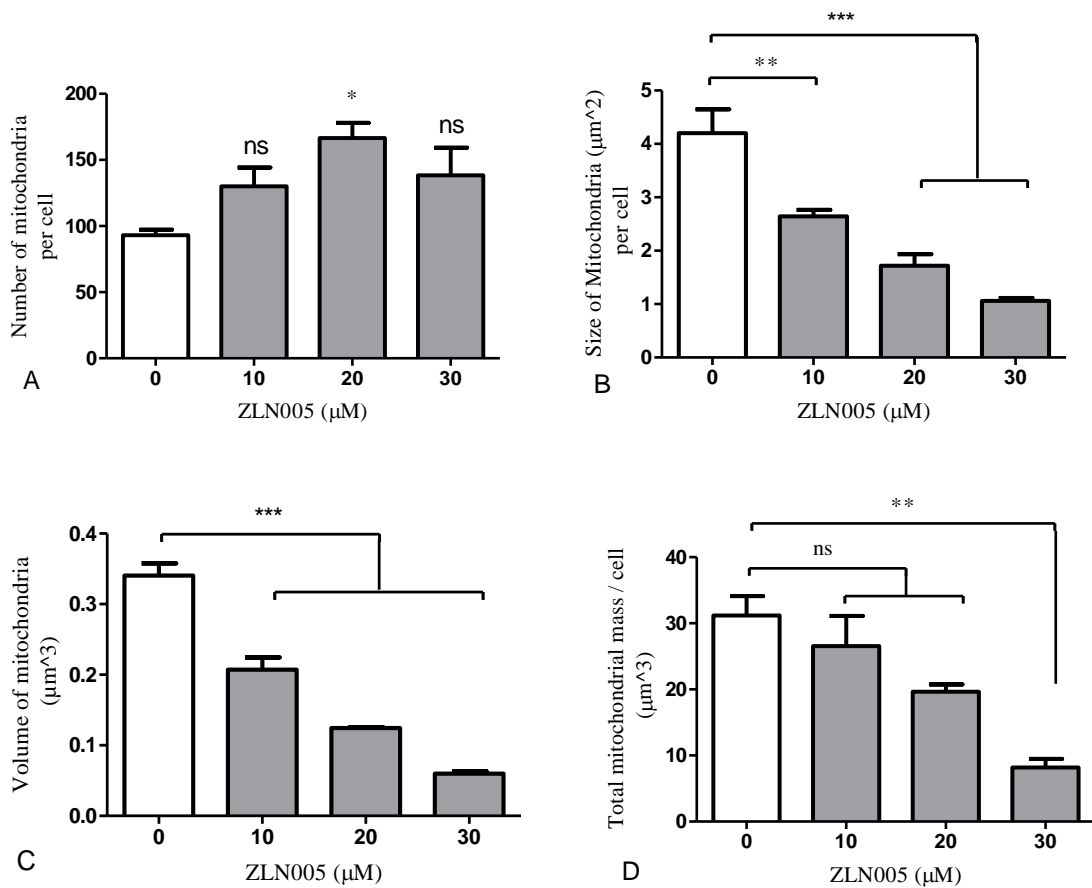


**Figure 4.1: Effect of ZLN005 on the mitochondrial dynamics in MDA-MB-231 cells.** Cells treated with different concentrations of ZLN005 (10, 20, and 20mM) for 24hrs in normal glucose (5.5mM) medium, then mitochondria were stained with MitoTracker probe and confocal microscopy used to take mitochondrial images. (A) represent quantification analysis of number of mitochondria, (B) Size of mitochondria, (C) Volume of mitochondria, and (D) which represent quantification analysis of total mitochondria mass per cell. Data represent the mean  $\pm$  standard error of three independent experiments performed in triplicate; each experiments with more than 30 cells.. One-way ANOVA and Dunnett's Multiple Comparison test was used to compare between the mean of treatments with control mean (\*, \*\*, and \*\*\*represent  $P < 0.05$ ,  $0.01$ , and  $0.001$  respectively).

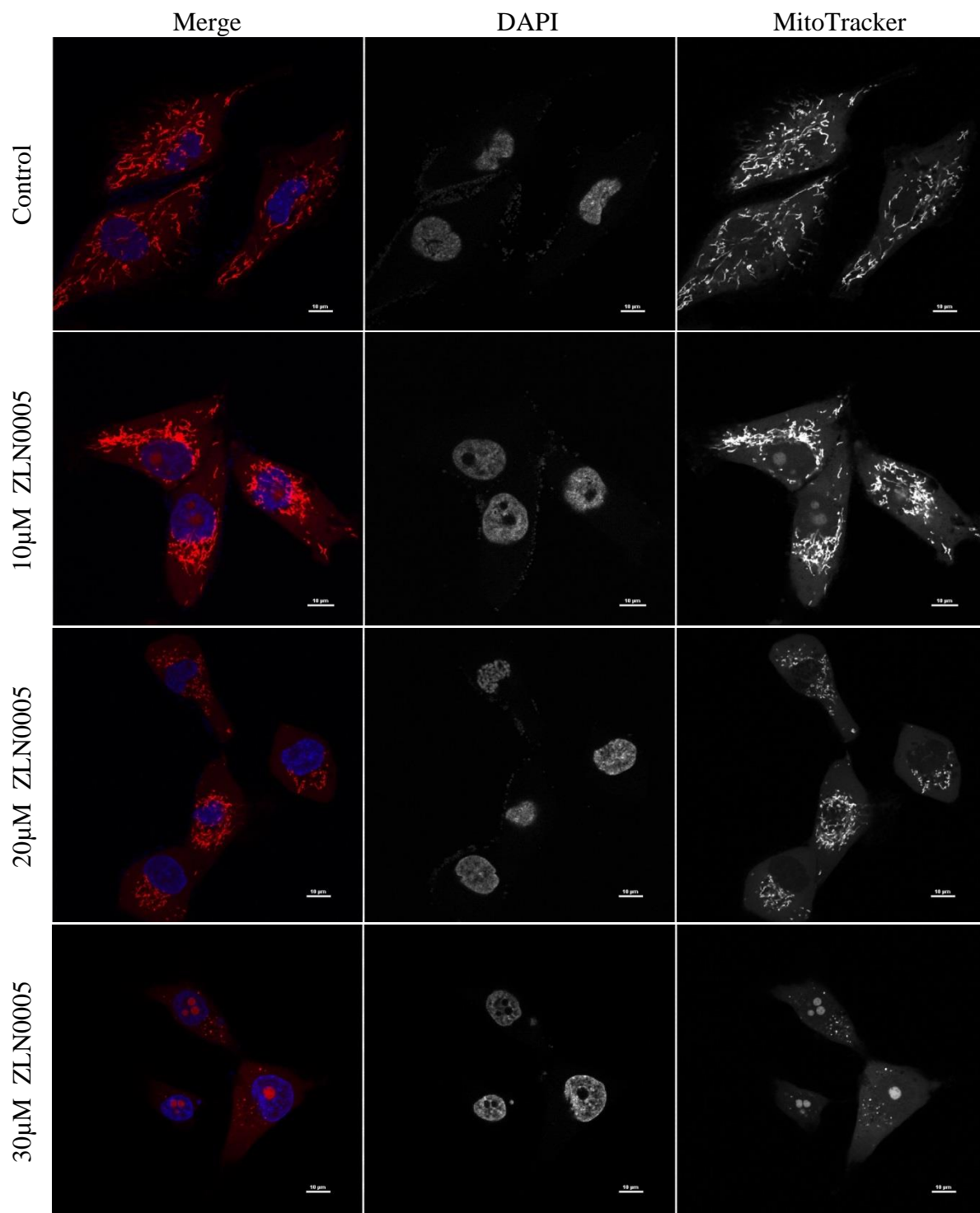


**Figure 4.2:** Micrographs shows the changes in the mitochondrial morphology in MDA-MB-231 cells. After 24hrs of treating cells with different concentrations of ZLN005, mitochondria were stained with MitoTracker probe (Red) and nucleus was stained with Dapi (blue). Scale bar=10µm

Then we investigated the effect of ZLN005 in low glucose medium on mitochondrial morphology. Therefore, we cultured MDA-MB-231 cells in 1mM of glucose in DMEM medium overnight, and then the cells were treated with ZLN005 in different concentrations 10, 20 and 30 $\mu$ M for 24hrs. Results in Figure 4.3A showed that treating with ZLN005 led to increases the number of mitochondria in the cells. This increase was significant at concentrations 10, and 20 $\mu$ M of ZLN005; in which numbers of the mitochondria was increased to 113.1 $\pm$ 8.9 ( $p$ <0.05), and 146.6 $\pm$ 7.01 ( $p$ <0.001) respectively compared to 79.8 $\pm$ 3.95 in non-treated control cells. While, no changes were detected between cells treated with 30 $\mu$ M of ZLN005 and to control cells.

Treating cells with ZLN005 also affected the size and the volume of the mitochondria. Figure 4.3B shows that mitochondrial size was decreased significantly from 5.92 $\pm$ 1.19  $\mu$ m<sup>2</sup> in the control cells to 2.42 $\pm$ 0.21 $\mu$ m<sup>2</sup> in the treated cells with 10 $\mu$ M of ZLN005 ( $p$ <0.05), and into 1.57 $\pm$ 0.24, and 0.89 $\pm$ 0.156 $\mu$ m<sup>2</sup> at concentrations 20, and 30 $\mu$ M of ZLN005 respectively ( $p$ <0.01).

The same changes in the mitochondrial volume were observed when the cells were treated with ZLN005 for 24hrs in low glucose medium. Results in Figure 4.3C showed that mitochondrial volume was reduced from 0.59 $\pm$ 0.14  $\mu$ m<sup>3</sup> in non-treated control cells to 0.22 $\pm$ 0.006 $\mu$ m<sup>3</sup> in the treated cells with 10 $\mu$ M ZLN005 ( $p$ <0.05), and into 0.11 $\pm$ 0.005, and 0.063 $\pm$ 0.015  $\mu$ m<sup>3</sup> at concentrations 20, and 30 $\mu$ M of ZLN005 respectively ( $p$ <0.01).

Results in Figure 4.3D revealed that total mass of the mitochondria was decreased significantly from 46.6 $\pm$ 8.8 $\mu$ m<sup>3</sup> in the control cells to 25.41 $\pm$ 2.78 $\mu$ m<sup>3</sup> in the cells treated with 10 $\mu$ M of ZLN005 ( $p$ <0.05), and into 16.1 $\pm$ 0.94 $\mu$ m<sup>3</sup> at concentration 20 $\mu$ M ( $p$ <0.01). As well as in the cells treated with 30 $\mu$ M of ZLN005, the total mitochondrial mass was reduced to 6.31 $\pm$ 1.67 $\mu$ m<sup>3</sup> ( $p$ <0.001).

The Figure 4.4 shows the morphological changes in the mitochondrial dynamics in MDA-MB-231 cells after 24hrs of treating with different concentrations of ZLN005 in low glucose medium.

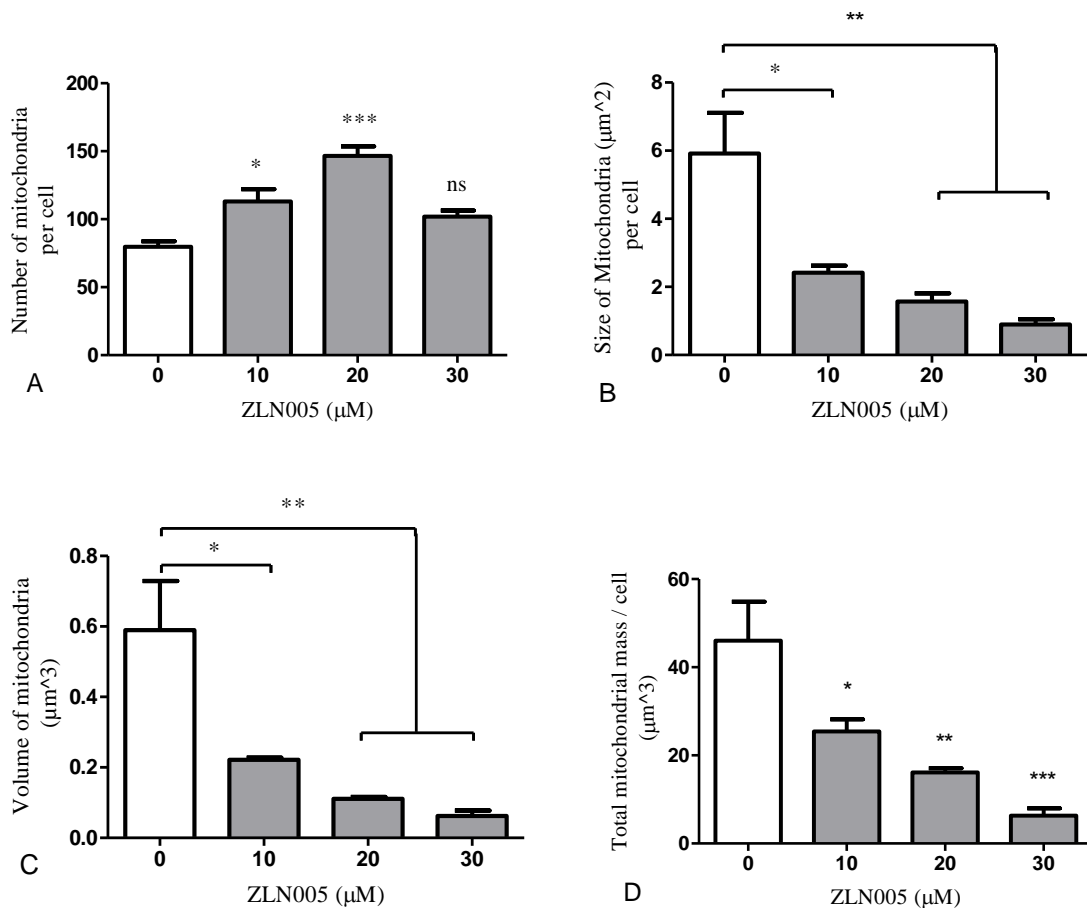


**Figure 4.3: Effect of ZLN005 on the mitochondrial morphology in MDA-MB-231 cells grown in low glucose medium.** After treating the cells with different concentrations of ZLN005 in (1mM) DMEM medium, the mitochondria were stained with MitoTracker probe and DAPI was used to stain nucleus then z-stack mages were taken using confocal microscopy. (A) represent quantification analysis of number of mitochondria, (B) Size of mitochondria, (C) Volume of mitochondria, and (D) which represent quantification analysis of total mitochondria mass per cell. Data represent the mean  $\pm$  standard error of three independent experiments performed in triplicate; in each experiment more than 30cells were taken. One-way ANOVA followed by Dunnett's Multiple Comparison test was used to compare between the mean of treatments with control mean (\*, \*\*, and \*\*\*represent  $P < 0.05$ ,  $0.01$ , and  $0.001$  respectively).

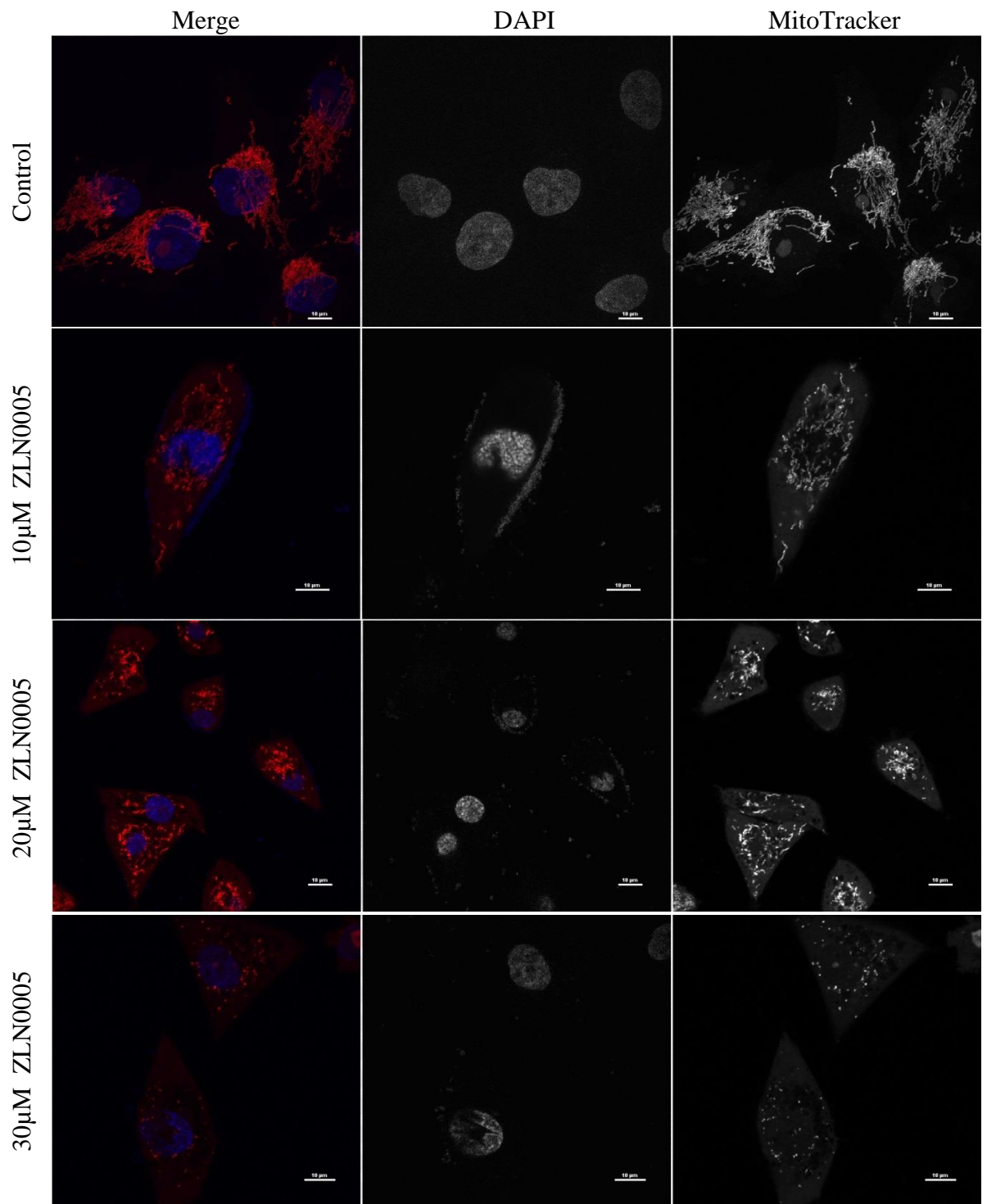


**Figure 4.4: Micrographs showing mitochondrial hyper-fragmentation in MDA-MB-231 cells.** After 24hrs of treating cells with different concentrations of ZLN005 in low glucose (1mM) DMEM medium, mitochondria were stained with MitoTracker probe and nucleus stained, Dapi. Scale bare =10µm.

Afterward we investigated the effect of ZLN005 on the mitochondrial dynamics in high glucose medium. Therefore, MDA-MB-231 cells were cultured in high glucose; 25mM, medium overnight, then treated with ZLN005 in different concentrations 10, 20 and 30 $\mu$ M for 24hrs. Results in Figure 4.5A showed significant increases in the mitochondrial number in the cells treated with 20 $\mu$ M of ZLN005; in which mitochondrial number was increased to  $168.6 \pm 10.3$  compared to  $129.8 \pm 9.7$  in non-treated control cells ( $p < 0.05$ ). While, no changes was detected at concentrations 10, and 30 $\mu$ M of ZLN005 compared to the control cells.

Treating cells with ZLN005 also affected the size of the mitochondria. Figure 4.5B shows that mitochondrial size was decreased significantly from  $1.59 \pm 0.05 \mu\text{m}^2$  in the control cells to  $1.24 \pm 0.06 \mu\text{m}^2$  in the treated cell with 20 $\mu$ M of ZLN005 ( $p < 0.01$ ), and into  $1.12 \pm 0.06 \mu\text{m}^2$  at concentration 30 $\mu$ M of ZLN005 ( $p < 0.001$ ). While, no changes was observed between the cells treated with 10 $\mu$ M of ZLN005 and to control cells.

Similar results of the mitochondrial volume were obtained when the cells treated with ZLN005 for 24hrs in high glucose medium. Results in Figure 4.5C showed that mitochondrial volume were reduced from  $0.14 \pm 0.008 \mu\text{m}^3$  in non-treated control cells to  $0.09 \pm 0.009 \mu\text{m}^3$  in the treated cells with 20 $\mu$ M ZLN005 ( $p < 0.01$ ), and into  $0.064 \pm 0.004 \mu\text{m}^3$  at concentration 30 $\mu$ M of ZLN005 ( $p < 0.001$ ). Whilst, no changes in the mitochondrial volume were recorded at concentration 10 $\mu$ M of ZLN005 compared to control.

Results in Figure 4.5D revealed significant decreases in total mitochondrial mass to  $17.64 \pm 0.72 \mu\text{m}^3$  in the treated cells with 30 $\mu$ M of ZLN005 compared to  $8.47 \pm 0.75 \mu\text{m}^3$  in the control cells ( $p < 0.001$ ). Whereas, no significant differences was detected between cells treated with ZLN005 at concentrations 10, and 20 $\mu$ M and non-treated control cells.

The Figure 4.6 shows the morphological changes in the mitochondrial dynamics in MDA-MB-231 cells after 24hrs of treating with different concentrations of ZLN0005 in high glucose medium.

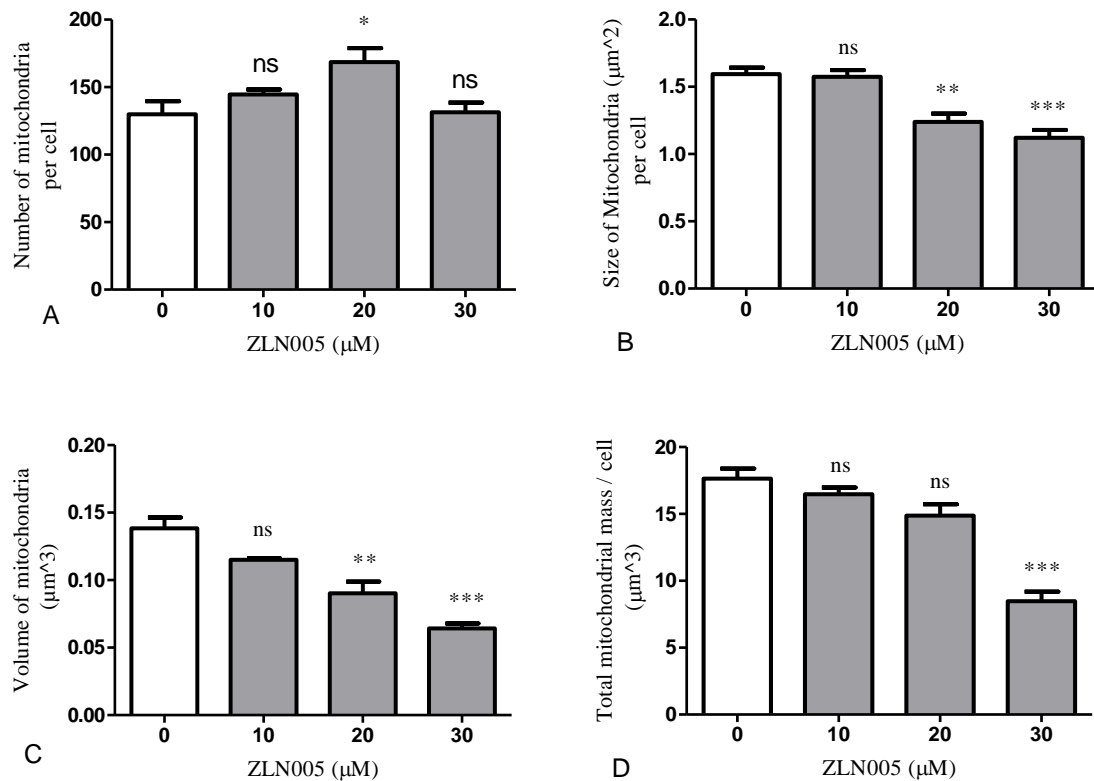


**Figure 4.5: Effect of ZLN005 on mitochondrial dynamics in MDA-MB-231 cell grown in high glucose level.** Cells treated with different concentrations of ZLN005 (10, 20, and 20mM) in high glucose (25mM)DMEME medium for 24hrs then MitoTracker probe used to stain mitochondria and z-stack images were taken by confocal microscopy. (A) represent quantification analysis of number of mitochondria, (B) Size of mitochondria, (C) Volume of mitochondria, and (D) which represent quantification analysis of total mitochondria mass per cell. Data represent the mean  $\pm$  standard error of three independent experiments performed in triplicate; in each experiment more than 30cells were taken. One-way ANOVA and Dunnett's Multiple Comparison test was used to compare between the mean of treatments with mean of control (\*, \*\*, and \*\*\*represent  $P < 0.05$ ,  $0.01$ , and  $0.001$  respectively).

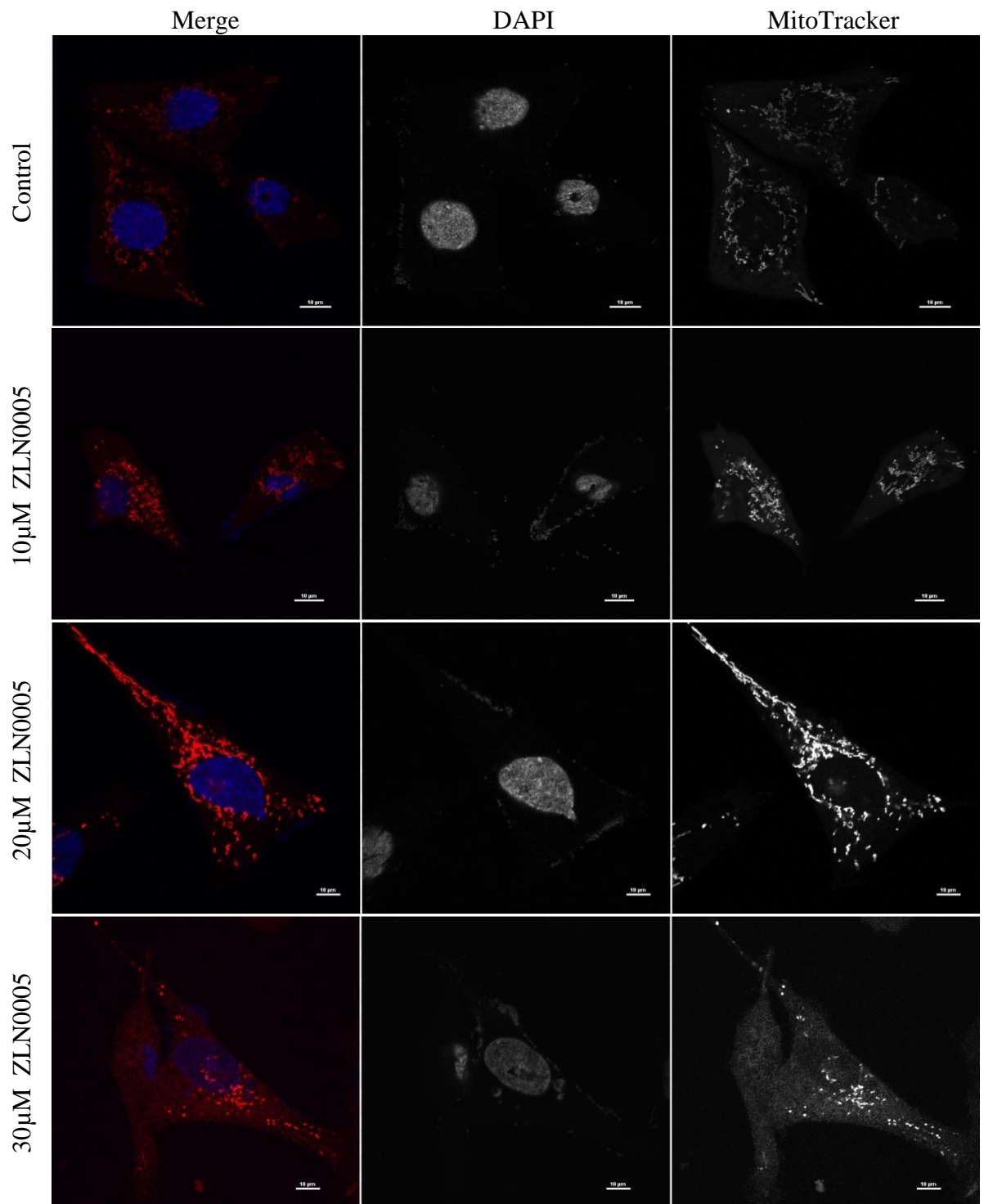


**Figure 4.6: Micrographs showing mitochondrial hyper-fragmentation in MDA-MB-231 cells.** After 24hrs of treating cells with different concentrations of ZLN005 in high glucose (25mM) DMEM medium, mitochondria were stained with MitoTracker probe and nucleus stained, Dapi. Scale bare =10μm.

We measured mtDNA copy number in MDA-MB-231 cells treated with different concentrations of ZLN005 in different glucose levels for 24hrs using real-time qPCR to confirm our results obtained by confocal microscopy for measuring the effect of ZLN005 on mitochondrial dynamics. Results in Figure 4.7 A showed that copy number of mtDNA was increased significantly from  $867.95 \pm 35.7$  in non-treated control cells to  $2353 \pm 143.5$  in treated cells with  $10 \mu\text{M}$  of ZLN005 ( $p < 0.001$ ), and into  $2038.3 \pm 320.2$  at concentration  $20 \mu\text{M}$  ( $p < 0.01$ ). Whilst, no changes were detected between cells treated with ZLN005 at concentration  $30 \mu\text{M}$  and control cells.

Then we measured mtDNA copy number in MDA-MB-231 cells treated with ZLN005 in low glucose and high glucose medium. Results as seen in Figure 4.7B revealed that no significant differences in mtDNA copy number were found between the cells cultured in low glucose medium and treated with ZLN005 compared to non-treated control cells. While, in high glucose medium results as presented in Figure 4.7C revealed that mtDNA copy number was increased significantly from  $1281.4 \pm 206.1$  in non-treated control cells to  $2613.1 \pm 16.7$  in treated cells with  $10 \mu\text{M}$  of ZLN005 ( $p < 0.05$ ), and into  $6691.2 \pm 510$  in treated cells with  $20 \mu\text{M}$  of ZLN005 ( $p < 0.001$ ) respectively. Whereas, no significant changes were observed at concentration  $30 \mu\text{M}$  compared to control.

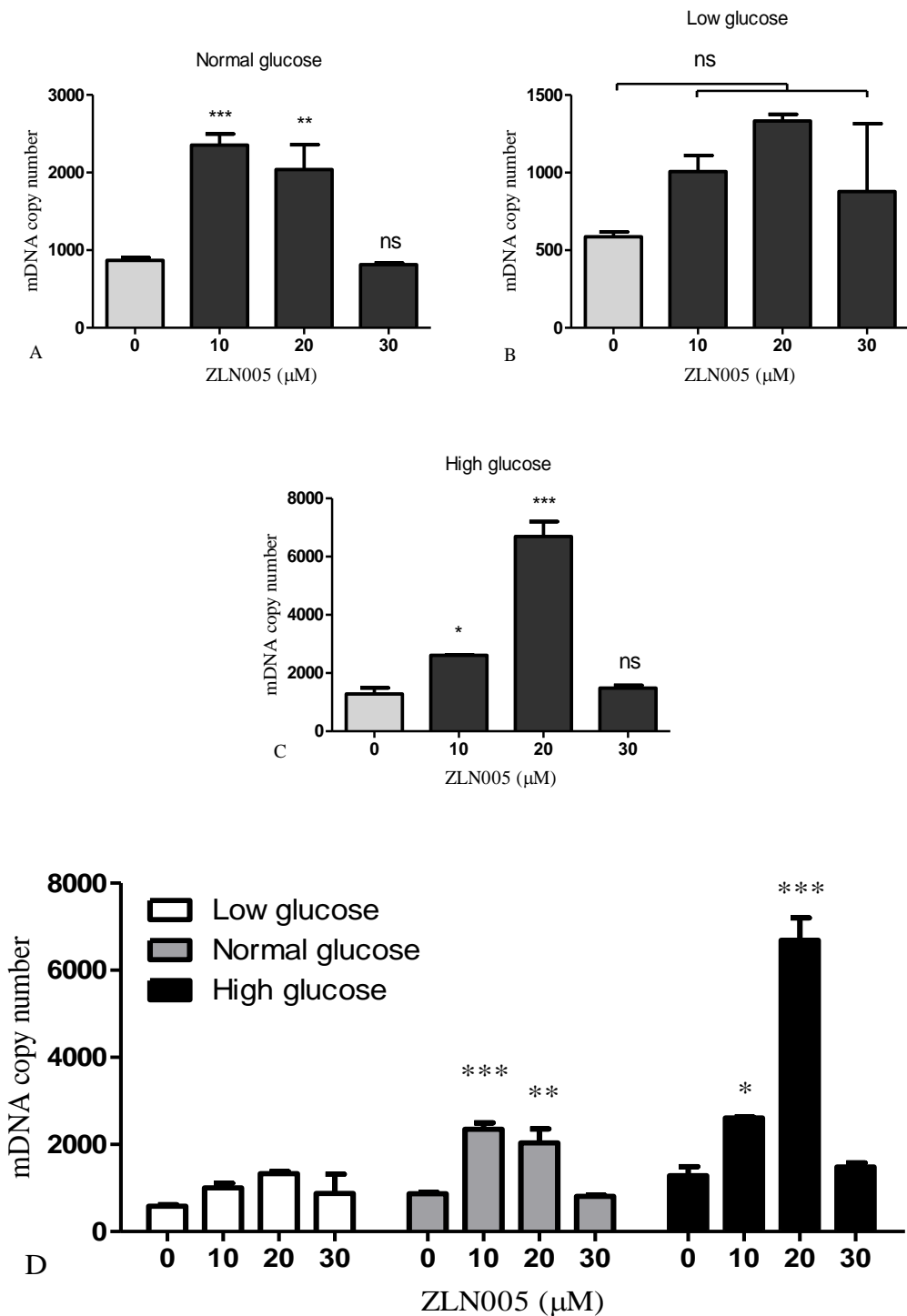


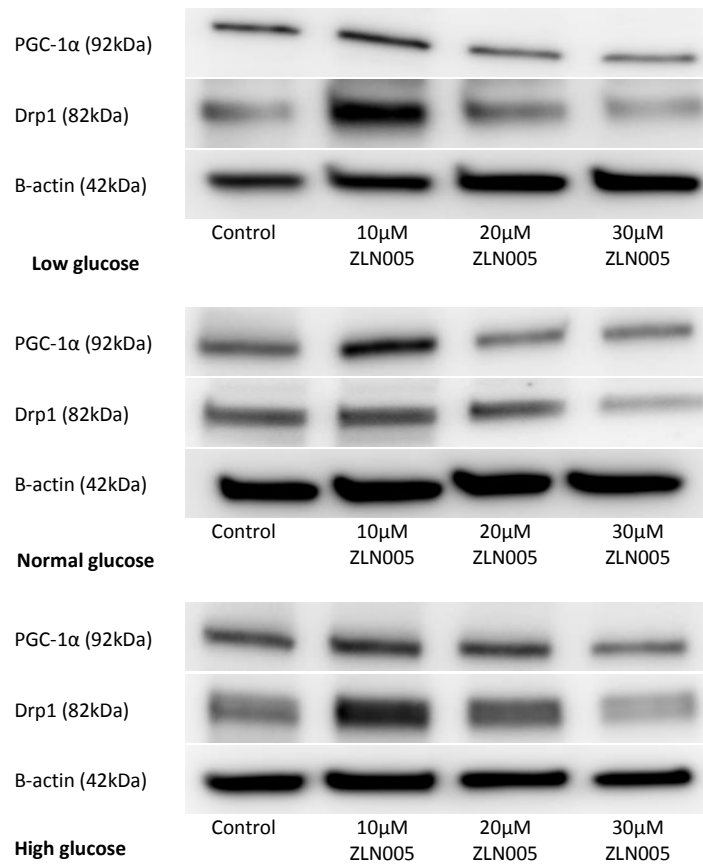
**Figure 4.7: Quantification of mtDNA copy number in MDA-MB-231 cells treated ZLN005.** Cells were treated with different concentrations of ZLN005 in different glucose levels for 24hrs. Extracted DNA was used to determine mtDNA using quantitative real-time PCR. (A) Represent quantification analysis of mtDNA copy number in the cells treated with different concentrations of ZLN005 in normal glucose, (B) in low glucose, (C) in high glucose, and (D) to compare between them. Data represent the mean  $\pm$  standard error of three independent experiments performed in triplicate. One-way ANOVA followed by Dunnett's Multiple Comparison Test to compare mean of treatments with control mean (\*, \*\*, and \*\*\*represent  $P < 0.05$ ,  $0.01$  and  $0.001$  respectively).

Later we investigated the effect of ZLN005 on the expression of PGC-1 $\alpha$  and Drp1 proteins in MDA-MB-231 cells. Therefore we treated the cells with three concentrations of ZLN005 10, 20, and 30 $\mu$ M for 24hrs in DMEM medium with different levels of glucose then the proteins were extracted and the expression of proteins were measured through western blot using  $\beta$ -actin as an internal loading control as shown in Figure 4.8A. In low glucose, results revealed that treating cells with ZLN005 statistically did not cause significant changes in the expression of the protein PGC-1 $\alpha$ . In the normal glucose, analyses data showed that expression of PGC-1 $\alpha$  protein was increased significantly from 20.09 $\pm$ 2.4 in the control cells to 40.42 $\pm$ 5.4 in the cells treated with 10 $\mu$ M of ZLN005 ( $p < 0.05$ ); which means that the expression of protein PGC-1 $\alpha$  was increased by 101.2% compared to the control. Whereas, no changes were detected between cells treated with 20, and 30 $\mu$ M of ZLN005 and the control cells. The results in high glucose revealed that PGC-1 $\alpha$  protein expression was increased significantly to 31.79 $\pm$  1.9, and 33.45 $\pm$ 1.74 in the cells treated with 10, and 20 $\mu$ M of ZLN005 respectively compared to 23.93 $\pm$ 1.7 in non-treated control cells ( $p < 0.05$ ); these mean that expression of protein PGC-1 $\alpha$  was increased by 32.85%, and 39.76% in treated cells with 10, and 20 $\mu$ M of ZLN005 respectively compared to the control. While, statistically no significant changes was observed at 30 $\mu$ M compared to control, as seen in Figure 4.8B.

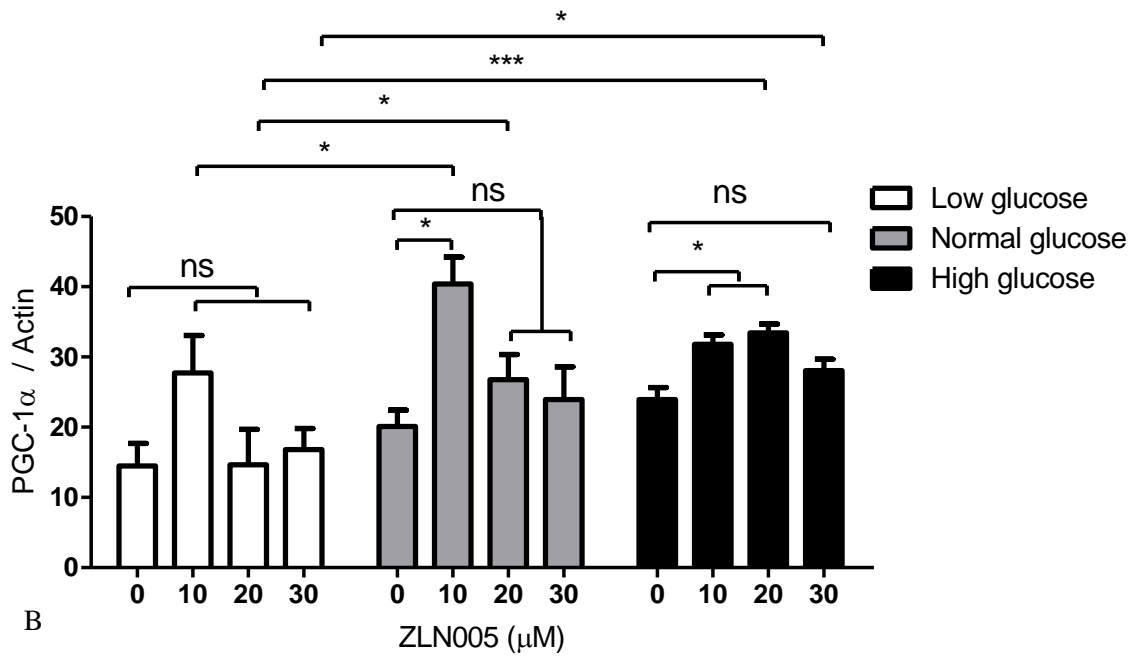
Analyses of data also show that changes in the glucose concentration affect expression of protein PGC-1 $\alpha$ . The expression of protein PGC-1 $\alpha$  was increased significantly, when cells treated with 10 $\mu$ M of ZLN005, from 27.7 $\pm$ 5.3 in low glucose to 40.42 $\pm$ 3.8 in normal glucose ( $p < 0.05$ ). In the cells treated with 20 $\mu$ M of ZLN005, expression of protein PGC-1 $\alpha$  was increased from 14.63 $\pm$ 5.06 in low glucose to 26.76 $\pm$ 3.6 in normal glucose ( $p < 0.05$ ) and into 33.45 $\pm$ 1.23 in high glucose ( $p < 0.001$ ). Also it was increased from 16.8 $\pm$ 3 in low glucose to 28.06 $\pm$ 1.63 in high glucose ( $P < 0.05$ ) when cells treated with 30 $\mu$ M of ZLN005, as seen in Figure 4.8B.

The results for measuring the expression of protein Drp1 was shown in Figure 4.8C. In low glucose, results showed that treating the cells with 10 $\mu$ M of ZLN005 led to significant increases in the expression of the protein Drp1, it was increased to 39.53 $\pm$ 8.39 compared to 13.73 $\pm$ 2.11 in control cells ( $p < 0.05$ ); which is mean the expression of protein Drp1 was increased by 187.94% compared to the control, whereas, no significant changes were observed between other treatments and control. Similar results were obtained when the cells treated with ZLN005 in normal glucose level, in which the expression of Drp1 protein was increased significantly from 30.01 $\pm$ 1.66 in the control cells to 50.57 $\pm$ 8.89 in the cells treated with 10 $\mu$ M of ZLN005 ( $p < 0.05$ ); which is mean that it has been increased by 68.53% compared to the control, whilst, no changes were observed between other treatments with control. In the high glucose level, treating the cells with ZLN005 statistically did not cause significant changes in the expression of the protein Drp1.

Changes in the glucose concentration in combination with ZLN005 also have affected expression of protein Drp1, as seen in Figure 4.8C. The expression of protein Drp1 was increased markedly from 13.73 $\pm$ 2.1 in low glucose to 39.6 $\pm$ 3.77 in high glucose ( $p < 0.01$ ), and from 26.33 $\pm$ 4 in low glucose and 32.76 $\pm$ 1.4 in normal glucose to 58.67 $\pm$ 3.43 in high glucose when the cells treated with 20 $\mu$ M of ZLN005 ( $p < 0.01$ ).



A



B

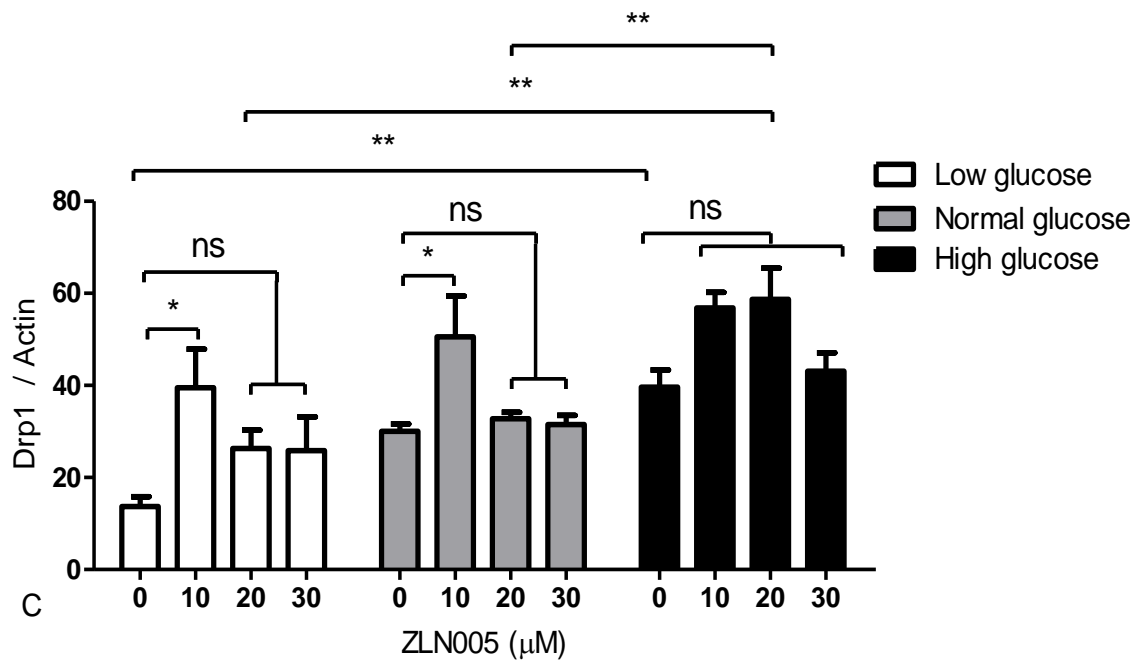


**Figure 4.8: Western blot showing the effect of ZLN005 on the PGC-1 $\alpha$  and Drp1 proteins expression.** MDA-MB-231 cells treated with different concentrations of ZLN005 for 24hrs in different glucose levels. (A) Shows PGC-1 $\alpha$  and Drp1 bands, (B) Represent quantification analysis of protein PGC-1 $\alpha$  expression, and (C) Represent quantification analysis of protein Drp1 expression. Data represent the mean  $\pm$  standard error of three independent experiments performed in triplicate. Two-way ANOVA followed by Bonferroni post hoc test to compare between the mean of treatments (\*, \*\* and \*\*\*represent P < 0.05, 0.01, and 0.001 respectively).

We investigated the impact of the ZLN005 on the cellular metabolism through measuring ATP production and lactate production in MDA-MB-231 cells. Therefore we treated the cells with different concentrations of ZLN005 for 24hrs in DMEM medium with different levels of glucose, then generated ATP and lactate were measured using specific commercial kits.

Results of ATP production shown in Figure 4.9A revealed that treating cells with ZLN005 led to significant increases in ATP production. It was increased from  $1.11 \pm 0.016$  mM in the control cells to  $1.4 \pm 0.03$ ,  $1.97 \pm 0.026$ , and  $1.31 \pm 0.014$  mM in treated cells with 10, 20, and 30  $\mu$ M of ZLN005 respectively ( $p < 0.001$ ); these mean that ATP production was increased by 26.37%, 78.42%, and 18.2% in treatments 10, 20, and 30  $\mu$ M of ZLN005 respectively compared to control.

In the low glucose results show that production of ATP was increased from  $0.75 \pm 0.013$  mM in control to  $0.93 \pm 0.034$  mM in treated cells with 10  $\mu$ M of ZLN005 ( $p < 0.01$ ), and no changes were recorded at concentration 20  $\mu$ M of ZLN005. While, in the cells which treated with 30  $\mu$ M of ZLN005, we found that ATP production was decreased significantly to  $0.52 \pm 0.024$  mM ( $p < 0.001$ ) compared to control. This means that ATP production in the cells treated with 10  $\mu$ M of ZLN005 was increased by 25.1% compared to control cells, while, when the cells treated with 30  $\mu$ M of ZLN005, ATP production was decreased by 31.01% compared to control cells.

In high glucose level, ATP production was increased markedly when cells treated with 10 and 20  $\mu$ M of ZLN005, it was increased to  $3.01 \pm 0.37$ , and  $3.74 \pm 0.43$  mM respectively compared to  $2.05 \pm 0.09$  mM in control ( $p < 0.001$ ), whereas, at 30  $\mu$ M of ZLN005, generation of ATP was declined to  $1.82 \pm 0.02$  mM compared to control ( $p < 0.05$ ). This means that ATP production was increased by 47.3% and 82.9% in treated cells with 10  $\mu$ M and 20  $\mu$ M of ZLN005 respectively compared to control, while, it was decreased by 11.3% in cells treated with 30  $\mu$ M of ZLN005 compared to control.

Changes in the glucose concentration in combination with ZLN005 also have affected significantly the ATP production, as seen in Figure 4.9D. The production of ATP was increased markedly from  $0.75 \pm 0.013$  in low glucose to  $1.11 \pm 0.02$  in normal glucose and into  $2.05 \pm 0.09$  in high glucose ( $p < 0.001$ ), the difference between normal glucose and high glucose was also significant ( $p < 0.001$ ).

Similarly, the production of ATP in the cells treated with 10, 20, and 30  $\mu\text{M}$  of ZLN005, was increased significantly in high glucose compared to normal and low glucose as well as in normal compared to low glucose ( $p < 0.001$ ). In 10  $\mu\text{M}$  of ZLN005, ATP production increased from  $0.94 \pm 0.03$  in low glucose to  $1.4 \pm 0.03$  in normal glucose and into  $3.01 \pm 0.04$  in high glucose ( $p < 0.001$ ). In 20  $\mu\text{M}$  of ZLN005, ATP production was increased from  $0.73 \pm 0.05$  in low glucose to  $1.97 \pm 0.03$  in normal glucose and into  $3.74 \pm 0.043$  in high glucose ( $p < 0.001$ ), and in 30  $\mu\text{M}$  of ZLN005, ATP production increased from  $0.51 \pm 0.02$  in low glucose to  $1.3 \pm 0.01$  in normal glucose and into  $1.82 \pm 0.02$  in high glucose ( $p < 0.001$ ).

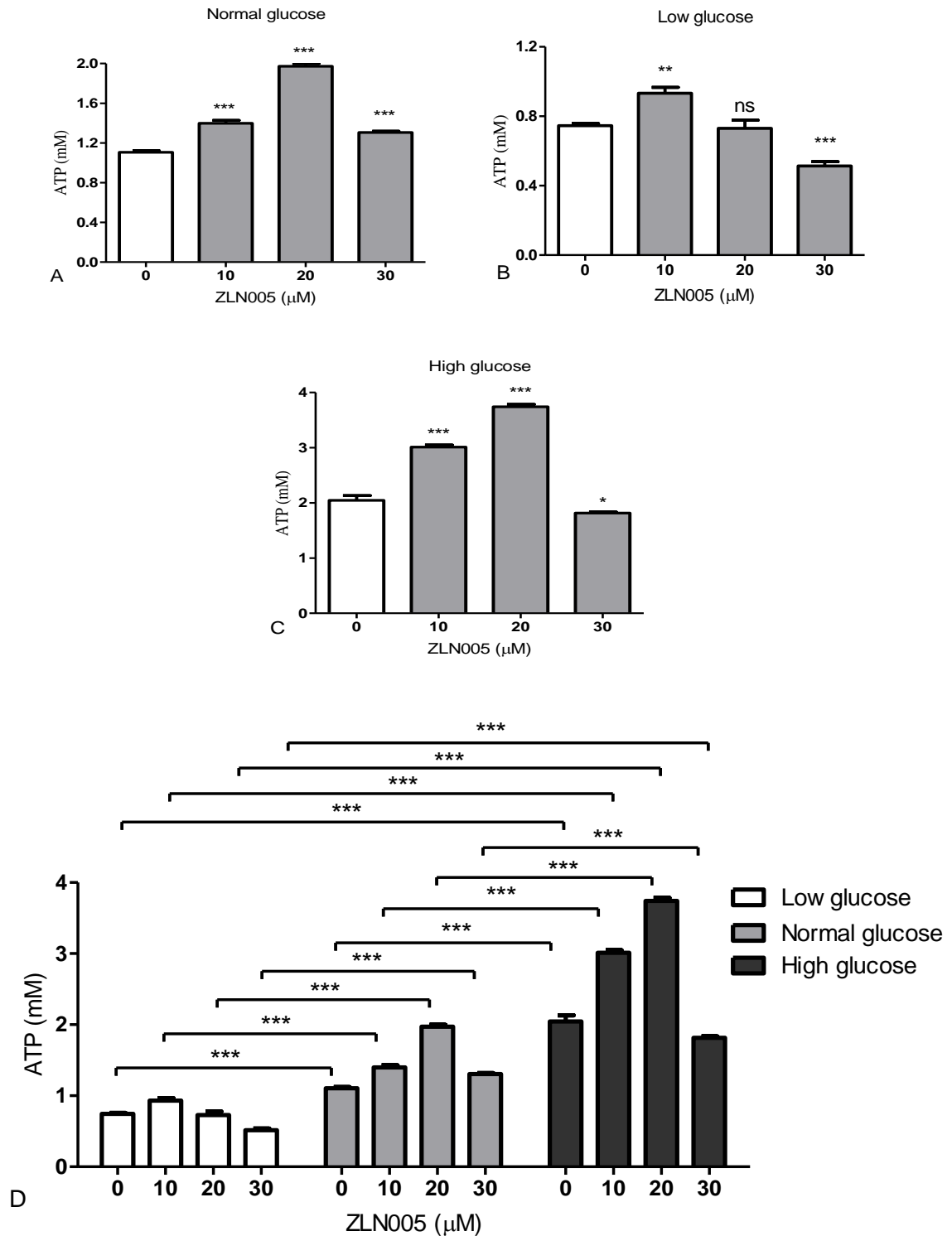


**Figure 4.9: Effect of ZLN005 on ATP production in MDA-MB-231 cells.** Lysate of  $1 \times 10^6$  cells were used for measuring ATP level by colorimetric ATP assay kit. Cells were grown in DMEM medium with different glucose levels A: in normal glucose (5.5mM). B: in low glucose (1mM).C: in high glucose (25mM), and D: graph to compare previous data. Data represent the mean  $\pm$  standard error of four independent experiments performed in triplicate. One-way ANOVA followed by Dunnett's post hoc test to compare mean of treatments with mean of control within each glucose level in A, B, and C. While, Two-way ANOVA followed by Bonferroni post hoc test to compare the mean of same treatments between different glucose level in graph D (\*, \*\* and \*\*\*represent  $P < 0.05$ ,  $0.01$ , and  $0.001$  respectively).

The results of measuring lactate production in MDA-MB-231 cells treated with ZLN005 in normal glucose presented in Figure 4.10A show that lactate production was significantly increased from  $14.43 \pm 0.42$  mM in the control cells to  $18.25 \pm 0.32$ , and  $18.7 \pm 0.41$  mM in the cells treated with 10, and 20 mM of ZLN005 respectively ( $p < 0.001$ ), and into  $17.44 \pm 0.32$  mM at concentration  $30 \mu\text{M}$  of ZLN005 ( $p < 0.01$ ). This means that lactate production was increased by 26.5%, 29.4%, and 20.9% in cells treated with 10, 20, and 30 mM of ZLN005 respectively compared to control.

While, no significant changes in the lactate production were observed in the cells treated with ZLN005 in low glucose as shown in Figure 4.10B, in high glucose level, treating cells with ZLN005 has increased lactate production significantly from  $17.98 \pm 0.69$  mM in the control cells to  $20.81 \pm 0.43$  mM in treated cells with 20 mM of ZLN005 ( $p < 0.01$ ), and into  $20.29 \pm 0.22$  mM at concentration  $30 \mu\text{M}$  of ZLN005 ( $p < 0.05$ ); which is mean that lactate production was increased by 15.7%, and 12.85% in treated cells with 20, and  $30 \mu\text{M}$  of ZLN005 respectively compared to control, whereas, no changes were observed at concentration 10 mM compared to control, as shown in Figure 4.10C.

The changes in the glucose concentration in combination with ZLN005 have affected lactate production. Data analysis show significant increases in lactate production in all treatments (Control, 10, 20, and 30 mM of ZLN005) in high glucose level compared to same treatments in the low glucose and normal glucose levels ( $p < 0.001$ ), except in the cells treated with 10 mM of ZLN005 in normal glucose in which the difference was non-significant. The increases in lactate production in all treatments in normal glucose was also significant compared to same treatments in low glucose ( $p < 0.001$ ), as seen in Figure 4.10D.

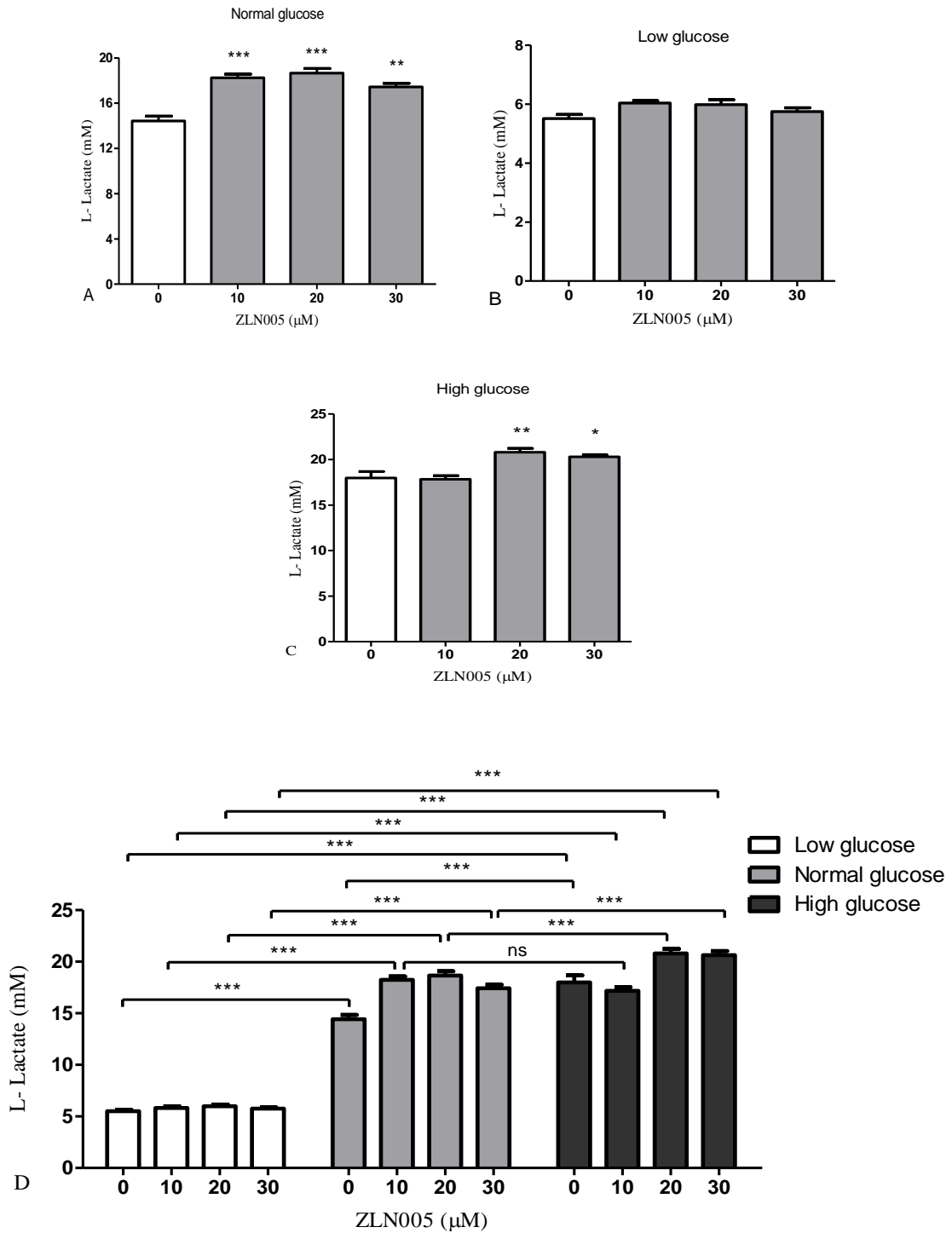


**Figure 4.10: Effect of ZLN005 on lactate production in MDA-MB-231 cells.** Cells were seeded in a 96-well plate at a density of 25,000 cells/well in DMEM supplemented with 10% FBS with different glucose level, then cells treated with different concentrations of ZLN005 for 24hrs. The supernatants were used to determine the generated L-Lactate. A: represent data analysis in normal glucose, B: in low glucose, C: in high glucose, and D: a graph to compare data between different glucose levels. Data represent the mean  $\pm$  standard error of three independent experiments performed in triplicate. One-way ANOVA followed by Dunnett's Multiple Comparison Test to compare mean of treatments with mean of control within each glucose level in A, B, and C. While, Two-way ANOVA followed by Bonferroni post hoc test to compare the mean of same treatments between different glucose level in graph D (\*, \*\* and \*\*\*represent  $P < 0.05$ ,  $0.01$ , and  $0.001$  respectively).

We investigated the impact of ZLN0005 on the level of ROS production in MDA-MB-231 cells. We treated cells with different concentrations of ZLN005 in different glucose levels for 24hrs, and then by using specific commercial kit the level of intracellular ROS were measured. Figure 4.11A that shows the result of generated ROS in the cells treated with ZLN005 in the normal glucose, revealed that ROS production was increased significantly from  $15855 \pm 509.8$  Unit in control cells to  $29796.7 \pm 5191$  Unit in treated cells with  $30 \mu\text{M}$  of ZLN005 ( $p < 0.05$ ); which is mean it was increased by 87.93% compared to the control cells, while, statistically no significant changes were detected between the cells treated with 10, and  $20 \mu\text{M}$  of ZLN005 and control cells.

In low glucose, no significant changes in the production of ROS were observed between the cells treated with ZLN005 and control cells, as shown in Figure 4.11B. In high glucose, significant increases in ROS production was detected only in the cells were treated with  $30 \mu\text{M}$  of ZLN005. It was increased from  $20383.7 \pm 2029$  Unit in non-treated control cells to  $39453.3 \pm 5080$  Unit in cells treated with  $30 \mu\text{M}$  ZLN005 ( $p < 0.05$ ); which is mean it was increased by 93.55% compared to the control cells; whilst, no significant changes were recorded in other treatments, as seen in Figure 4.11C.

Combination effects of glucose concentration and ZLN005 on the production of ROS in MDA-MB-231 also analysed, and results revealed ROS production was increased in the cells treated with  $20 \mu\text{M}$  of ZLN005 in low glucose from  $15091.3 \pm 1164.2$  Unit into  $27649 \pm 4855.8$  Unit in high glucose ( $p < 0.05$ ). Its production also increased significantly in the cells treated with  $30 \mu\text{M}$  of ZLN005 in low glucose from  $18319.3 \pm 2747.4$  Unit to  $29796.7 \pm 5190$  Unit in normal glucose ( $p < 0.05$ ), and into  $39453.3 \pm 5080$  Unit in high glucose ( $p < 0.001$ ), as seen in Figure 4.11D.

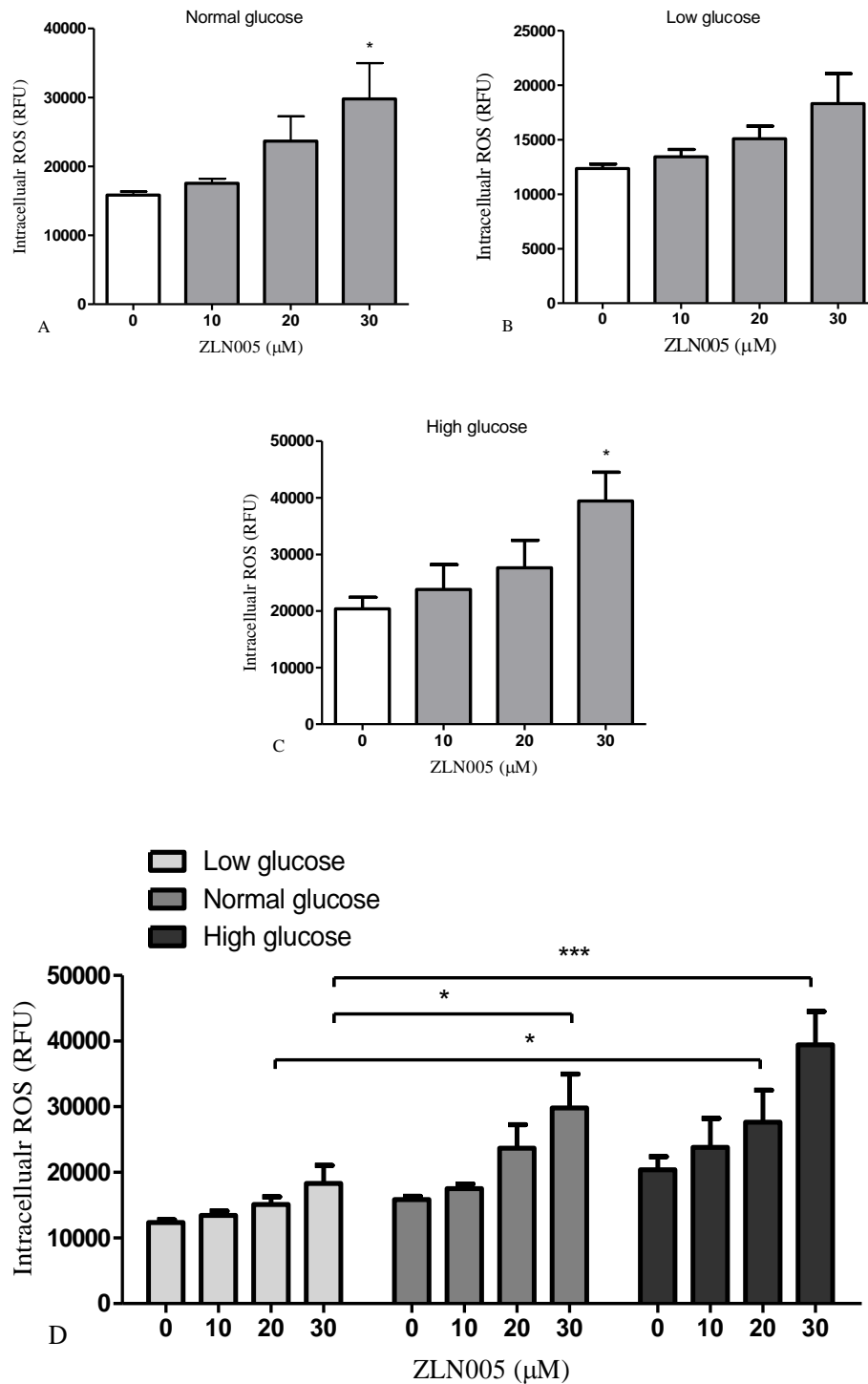


**Figure 4.11: Effect of ZLN005 on the ROS production in MDA-MB-231 cells.** Cells were treated with different concentrations of ZLN005 in different glucose level for 24hrs then level of intracellular ROS was measured using specific commercial kit. A: represent data analysis in normal glucose (5.5 mM), B: in low glucose (1mM), and C: in high glucose (25mM), and D: represent the graph to compare previous data. Data represent the mean  $\pm$  standard error of three independent experiments performed in triplicate. One-way ANOVA followed by Dunnett's post hoc test to compare mean of treatments with mean of control within each glucose level in A, B, and C. While, Two-way ANOVA followed by Bonferroni post hoc test to compare the mean of same treatments between different glucose level in graph D (\* and \*\*\*represent  $P < 0.05$ , and  $0.001$  respectively).

To assess whether PGC-1 $\alpha$  overexpression affects cell migration, and if glucose level have a role on the expression effect on cell migration, we treated MDA-MB-231 cells with different concentrations of ZLN005 (that induce overexpression of PGC-1 $\alpha$ ) in different glucose levels.

Results in Figure 4.12A revealed that treating cells with ZLN005 led to significant increases in the cell migration. It was increased from  $18.14 \pm 1.16 \mu\text{m}/\text{hour}$  in non-treated control cells to  $26.29 \pm 0.84 \mu\text{m}/\text{hour}$  in treated cells with  $10 \mu\text{M}$  of ZLN005 ( $p < 0.01$ ), and into  $23.01 \pm 0.77 \mu\text{m}/\text{hour}$  in treated cells with  $20 \mu\text{M}$  of ZLN005 ( $p < 0.05$ ). While, in the cells treated with  $30 \mu\text{M}$  of ZLN005 no significant changes in the cell migration was recorded.

Similar results were obtained when the cells treated with ZLN005 in low glucose as shown in Figure 4.12B. Cell migration was increased significantly into  $23.43 \pm 0.77 \mu\text{m}/\text{hour}$  in treated cells with  $10 \mu\text{M}$  of ZLN005 ( $p < 0.01$ ), and into  $20.67 \pm 1.23 \mu\text{m}/\text{hour}$  in treated cells with  $20 \mu\text{M}$  of ZLN005 ( $p < 0.05$ ) compared to  $15.92 \pm 0.77 \mu\text{m}/\text{hour}$  in non-treated control cells. And at concentration  $30 \mu\text{M}$  of ZLN005 no changes were observed compared to control.

In high glucose, we have shown a significant increase in the cell migration when the cells treated with  $10 \mu\text{M}$  of ZLN005, it was increased to  $31.4 \pm 1.54 \mu\text{m}/\text{hour}$  compared to  $25.5 \pm 0.94 \mu\text{m}/\text{hour}$  in non-treated control cells ( $p < 0.05$ ). In contrast, cells treated with  $30 \mu\text{M}$  of ZLN005 showed marked decline in the cell migration. It was decreased to  $18.02 \pm 1.03 \mu\text{m}/\text{hour}$  compared to control ( $p < 0.05$ ), whereas, in treatment with  $20 \mu\text{M}$  of ZLN005, no changes were detected compared to control cells.

Combination effects of glucose concentration and ZLN005 on the cell migration in MDA-MB-231 also analysed, and results revealed that increasing glucose concentration led to significant increases in cell migration into  $25.5 \pm 0.94 \mu\text{m}/\text{hour}$  in high glucose level compared to  $18.2 \pm 1.1694 \mu\text{m}/\text{hour}$  in normal glucose level and  $15.9 \pm 0.77$  in low glucose level ( $p < 0.001$ ). In the cells treated with  $10 \mu\text{M}$  of ZLN005, cell migration was increased significantly into  $31.4 \pm 1.5 \mu\text{m}/\text{hour}$  in high glucose level compared to  $26.3 \pm 0.85 \mu\text{m}/\text{hour}$  in normal glucose level ( $p < 0.05$ ), and compared to  $23.4 \pm 0.76$  in low glucose ( $p < 0.001$ ).

While, no significant differences in the cell migration were observed between treatments in normal glucose and treatments in low glucose, as shown in Figure 4.12D.

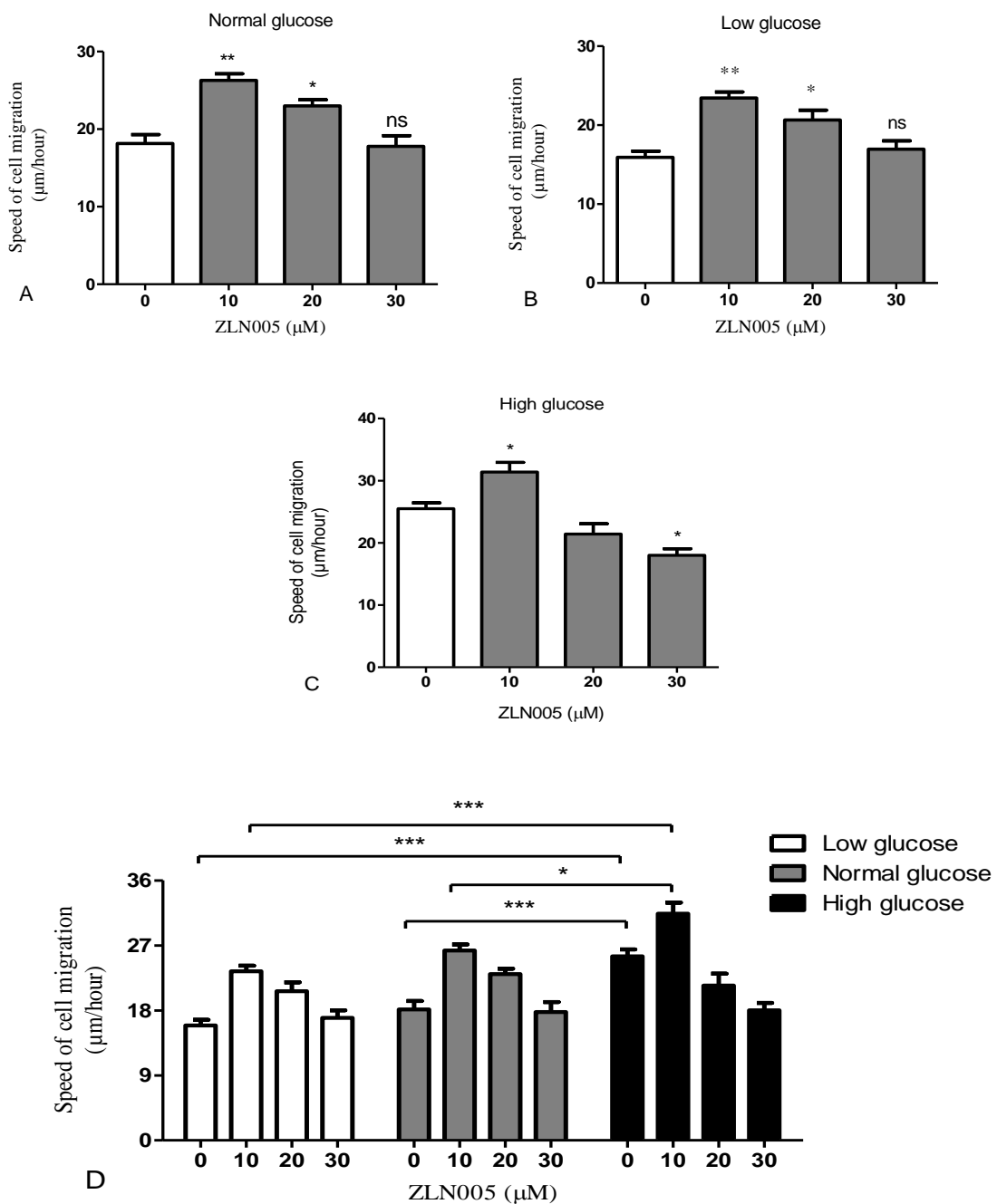


**Figure 4.12: Effect of ZLN005 on the cell migration in MDA-MB-231 cells.** Cells were cultured in A: low glucose level, B: normal glucose, and C: high glucose. Then cells were treated with different concentrations of ZLN005. The motility of cells was monitored by the time-lapse microscopy every 15 minutes for 24 hours. The cell migration measured via tracking single cell using Image J Software. Data represent the mean  $\pm$  standard error of three independent experiments performed in triplicate. One-way ANOVA followed by Dunnett's post hoc test to compare mean of treatments with mean of control within each glucose level in A, B, and C. While, Two-way ANOVA followed by Bonferroni post hoc test to compare the mean of same treatments between different glucose level in graph D (\*\*\*) and (\*\*\*) represent  $P < 0.05$ ,  $0.01$ , and  $0.001$  respectively).

#### 4.4 Discussion

PGC-1 $\alpha$ , is a key regulator of energy metabolism through stimulation of mitochondrial biogenesis, and it promotes cells to be more oxidative rather than glycolytic (Liang and Ward, 2006). Peng and co-workers (2017) suggested that PGC-1 $\alpha$  can regulate mitochondrial fission/fusion process through regulation of mfn2 and Drp1 protein expression. They also mentioned that PGC-1 $\alpha$  can regulate the expression of Drp1 protein directly through binding to its promoter (Dabrowska et al., 2015). Evidences showed that stresses, such as prolonged fasting and exercise training, oxidative damage, and chemotherapy treatment can activate PGC-1 $\alpha$  protein (Tan et al., 2016). There are reports that PGC-1 $\alpha$  has been overexpressed in some neurodegenerative diseases such as Parkinson's disease and Alzheimer's diseases, which are characterized by mitochondrial hyperfragmentation due to increasing production of ROS (Santos et al., 2015, Peng et al., 2017). It has also been found that in diabetes mellitus, which is characterized by hyperglycaemia, the expression of PGC-1 $\alpha$  is increased (Lin et al., 2003). Depending on these reports it can be predicted that there is a link between overexpression of PGC-1 $\alpha$  and mitochondrial hyperfragmentation.

Recently, it has been demonstrated that ZLN0005, a selective transcriptional regulator of the PGC-1 $\alpha$  gene, can elevate selectively the expression of PGC-1 $\alpha$  protein, and can increase glucose uptake, fatty acid oxidation, and induce mitochondrial oxidative phosphorylation (Zhang et al., 2013). We have previously found that high glucose and exogenous H<sub>2</sub>O<sub>2</sub> induce mitochondrial fragmentation and affect metabolism and cell migration through increasing intracellular ROS. To resolve the mystery about the source of ROS, we treated MDA-MB-231 breast cancer cells with ZLN005, which can increase expression of PGC-1 $\alpha$  protein and its downstream mitochondrial fission protein Drp1, to show a link between mitochondrial morphology and metabolism, and their effect on the cell migration. We expected that ZLN005 will induce overexpression of PGC-1 $\alpha$ , which in

turn it can increase mitochondrial fragmentation and elevate expression of Drp1 protein. In addition, PGC-1 $\alpha$  can regulate and minimize the effect of mitochondrial ROS accompanied to oxidative phosphorylation through increasing expression of several ROS-detoxifying enzymes (Austin and St-Pierre, 2012). Therefore, it can induce mitochondrial fission away from the impact of mitochondrial ROS. Moreover, different glucose concentrations were used to study their effect on the expression of PGC-1 $\alpha$  as it was suggested that changes in glucose concentration can induce a stress and induce PGC-1 $\alpha$  activation (Herzig et al., 2001, Finck and Kelly, 2006).

Results showed that mitochondrial morphology is markedly affected by ZLN005. In normal glucose ZLN005 treatment, increased the number of mitochondria, reduced their size and volume, indicating that mitochondria have fragmented (Figure 4.1 and 4.2). Similar results were found after cells were treated with ZLN005 in low and high glucose. However, the effect was stronger in low glucose compared to normal and high glucose as the total mass of mitochondria significantly decreased in all treatments, whereas, in other glucose levels only at 30 $\mu$ M ZLN005 affected the total mass of mitochondria. This might be because in low glucose, mitochondria have elongated and network-like shape and can be affected easily compared to shorter and smaller mitochondria in normal and high glucose.

Interestingly, data from confocal microscopy show that mitochondrial number were decreased at 30 $\mu$ M ZLN005 after it has been increased in lower concentrations of the activator and this was consistent in all three glucose concentrations (Figure 4.1A, 4.3A, and 4.5A). Data obtained from qPCR shows the same results (Figure 4.7). This may be due to mitochondrial mitophagy; a process of removing impaired or damaged mitochondria by autophagy, since at this ZLN005 concentration (30 $\mu$ M) the cells are under strong stress of ROS. It has been reported by Benischke and co-workers (2017) that mitochondrial mitophagy lead to reduction of mitochondrial mass, production of ATP, and mtDNA copy

number after increased mitochondrial fragmentation in human corneal endothelial cells (HCEncs).

The results in this investigation differ from those observed by Guo and co-workers (2015), who suggested that down regulation of PGC-1 $\alpha$  in hyperglycaemic condition leads to increases in mitochondrial fragmentation through increasing the expression of Drp1. In contrast, Dabrowska co-workers (2015) reported that PGC-1 $\alpha$  induction decreases the expression of Drp1 in rat mesencephalon-derived cell line 1RB<sub>3</sub>AN<sub>27</sub>, which can lead to increases in the level of Mfn2 transcripts, and this means that mitochondrial dynamics shift towards hyper fusion. However, no prior report has examined the effect of overexpression of PGC1 $\alpha$  on mitochondrial morphology and fusion/fission dynamics in cancer cells.

Western blot analysis of the effect of ZLN005 on expression of PGC-1 $\alpha$  protein and its downstream protein Drp1 showed that efficiency of ZLN005 on expression of these proteins is limited. In low glucose it has no significant impact on PGC-1 $\alpha$  protein expression; however, it significantly induced expression of PGC-1 $\alpha$  protein at 10 $\mu$ M in normal glucose and at 10 and 20 $\mu$ M in high glucose (Figure4.1A). Similar results were observed when downstream protein Drp1 was measured. It induced expression of Drp1 only at 10 $\mu$ M in both low and normal glucose (Figure4.1B). This unexpected finding is quite interesting as fragmentation of mitochondria was confirmed at all concentrations of ZLN005 used and in all glucose levels (Figure 4.2, 4.4, and 4.6).

Although ZLN005 is considered a potent activator of PGC-1 $\alpha$ , it has been observed to produce different results in different cells. For instance, in L6 myotubes it led to increasing expression of PGC-1 $\alpha$ , while, in rat primary hepatocytes, it did not cause any change in the expression of PGC-1 $\alpha$  (Zhang et al., 2013). Therefore, it is possible that ZLN005 induced fragmentation of mitochondria in low concentration (10 $\mu$ M) through increasing PGC-1 $\alpha$  expression, while, in higher concentrations, it affect mitochondrial morphology through inducing expression of other unknown genes rather than PGC-1 $\alpha$ .

Mitochondrial fission protein, Drp1 with mitochondrial fission 1 protein (Fis1) play an essential role in mitochondrial fission, therefore, it was expected that western blot analysis would show an increase in the expression of Drp1 protein, even if it was not affected by upstream protein regulator; PGC-1 $\alpha$ , especially at 20 and 30 $\mu$ M ZLN005 where mitochondria had been fragmented markedly. However, results showed no significant increases of Drp1 protein at these concentrations (Figure 4.8C). This novel finding demonstrates that the traditional view and notion of mitochondrial fission being mediated by Drp1 protein may not always be the case, as other proteins also can induce mitochondrial fission or prevent mitochondrial fusion. Recently, mitochondrial fragmentation has been linked to the expression of  $\alpha$ -synuclein, and it was suggested that mitochondrial fragmentation does not require Drp1 protein (Nakamura et al., 2011, Zhu et al., 2012, Guardia-Laguarta et al., 2014). This protein, which is localized in the mitochondria-associated endoplasmic reticulum (ER) membranes (MAM), is linked to neurodegenerative disorders and excessive accumulation of it can lead to decline a mitochondrial oxidative phosphorylation, changes in the mitochondrial morphology, and cell death (Nakamura et al., 2011, Xie and Chung, 2012, Guardia-Laguarta et al., 2014), and its high expression has been reported in several cancer cells (Matsuo and Kamitani, 2010, Ye et al., 2010, Ge and Xu, 2016). It has been suggested that under conditions of oxidative stress, nuclear alpha-synuclein can affect mitochondrial function partially through reducing PGC-1 $\alpha$  (Siddiqui et al., 2012, Ciron et al., 2015).

Since mitochondrial fusion-fission process is highly dynamic process and mitochondrial fragmentation is reversible process, treating cells with high concentrations of ZLN005 may induce mitochondrial fragmentation in a short time, then protein PGC-1 $\alpha$  and Drp1 will degrad. Therefore, effects at longer time points will be missed. It was reported by Din and co-workers (2013) that half life time of Drp1 is 16hrs. Therefore, future study on

mitochondria fragmentation using PGC-1 $\alpha$  should be conducted over different periods of time.

There are many studies that suggest that PGC-1 $\alpha$  protein plays a regulatory role in mitochondrial oxidative phosphorylation and protect cells against oxidative stress via induction of several ROS detoxifying enzymes including superoxide dismutase and glutathione in cancer cells (Sano and Fukuda, 2008, Dabrowska et al., 2015). In the study by Liang and Ward (2006) they found that PGC-1 $\alpha$  enhanced mitochondrial oxidative phosphorylation in skeletal muscle through remodeling skeletal muscle fibers type IIb, which exhibit relatively fewer mitochondrial numbers and is more glycolytic, to the more oxidative type I and type IIa fibres. In another study by LeBleu and co-workers (2014) they reported that PGC-1 $\alpha$  suppression in cancer cells leads to downregulation of mitochondrial oxidative phosphorylation, while, overexpression of it leads to mixed metabolic response. However, the effect of overexpression of PGC-1 $\alpha$ , which led to mitochondrial hyperfragmentation, on mitochondrial metabolism remains unclear.

Production of ATP and lactate were measured in MDA-MB-231 cells after treating these cells with ZLN005, to understand the link between mitochondrial fragmentation induced by ZLN005 and cell metabolism. In normal glucose, our data revealed that treating cells with ZLN005 led to a significant increase in the generation of ATP (Figure 4.9A) and this increase was due to the increase in the lactate production which represents glycolysis (Figure 4.10A). This result was expected as fragmented mitochondria drive the cells to reprogram their metabolism and rely more on glycolysis rather than oxidative phosphorylation due to reducing mitochondrial inner surface where electron transport chain enzymes located (Mannella, 2006, Cogliati et al., 2013). However, we cannot confirm that increasing ATP generation is restricted to glycolysis, because, increased PGC-1 $\alpha$  expression (Figure 4.8B) can elevate mitochondrial metabolism through control of generated ROS (Figure 4.12A) through increasing detoxification enzymes; therefore, it is

possible that mitochondrial metabolism has been also increased and contributed to increased ATP. This finding was also reported by LeBleu and co-workers (2014) that overexpression of PGC-1 $\alpha$  can enhance mixed metabolism. Also it has been demonstrated by Chen and co-workers (2014) that increasing expression of PGC-1 $\alpha$  can prevent cell death induced by P53 through maintaining a balance between oxidative phosphorylation and glycolysis. Our data also show that despite generated ATP being increased significantly at 30 $\mu$ M ZLN005 treatment compared to control in low glucose, it was decreased by 20 $\mu$ M treatment. This suggests that fragmented mitochondria are intact in the cells treated with low concentrations of ZLN005 and participate partially in ATP production through oxidative phosphorylation, while, in higher ZLN005 concentration (30 $\mu$ M), where mitochondria are defective and a number of them were removed via mitophagy, ATP energy is generated mainly through aerobic glycolysis.

In low glucose, where no differences in glycolysis were observed (Figure 4.10B), increasing ATP production in the cells treated with 10 $\mu$ M of ZLN005 (Figure 4.9B) suggests that mitochondrial metabolism is enhanced by excessive expression of ZLN005. While, at higher concentrations ATP production declined for the same reason mentioned for normal glucose above.

In high glucose, increasing ATP production (Figure 4.9 C) without changes in glycolysis in 10 $\mu$ M treatment (Figure 4.10 C) indicates increases in mitochondrial metabolism enhanced by excessive expression of ZLN005 (Figure 4.8B). While, at 20 $\mu$ M, where production of ATP and lactate were significantly increased, results suggest that aerobic glycolysis partially contributed to ATP production. In similar manner to low and normal glucose, at 30 $\mu$ M where ATP production was decreased despite increases in the aerobic glycolysis suggests defect in the mitochondrial oxidative phosphorylation. High fragmentation of mitochondria by ZLN005 at 30 $\mu$ M leads to reduction of mitochondria inner surface (Mannella, 2006), which is essential in ATP generation via oxidative phosphorylation,

causing defect of oxidative phosphorylation. This result suggests that mitochondrial oxidative phosphorylation contributes to total ATP production and increasing glycolysis is not enough for supply cancer cells with required ATP.

In regards to the impact of ZLN005 on cellular and mitochondrial metabolism, Iacovelli and co-workers (2016), revealed that overexpression of PGC-1  $\alpha$  in human Retinal Pigmented Epithelial cell lines leads to increases in the expression of mitochondrial oxidative phosphorylation and fatty-acid  $\beta$ -oxidation genes, they also found it induces a number of antioxidants to reduce ROS. Whereas, Chen and co-workers (2014) reported that suppression of PGC-1 $\alpha$  leads to defects in the mitochondrial oxidative phosphorylation in the receptor-interacting protein 1 (RIP1) gene knockdown.

Mitochondrial fragmentation has been linked with elevated ROS production in several cell lines (Picard et al., 2013, Martin-Guerrero et al., 2017, Ježek et al., 2018). Therefore, it is expected that production of ROS has been increased with increasing concentration of ZLN005 as it promotes mitochondrial fragmentation as mentioned above. However, it is well documented that PGC-1 $\alpha$  plays an important role in removing and detoxifying ROS (Austin and St-Pierre, 2012). To find out the effect of overexpression of PGC-1 $\alpha$  induced by ZLN005 on the ROS production in MDA-MB-231 cells; we measured total intracellular ROS in these cells after 24hrs of treating with different concentrations of ZLN005. Our data show that in low glucose level, no significant differences in the generation of ROS were observed between cells treated with ZLN005 compared to non-treated control cells (Figure 4.11B). This result was expected as increasing PGC-1 $\alpha$  expression can increase the expression of antioxidant enzymes which remove the excessive generated ROS. Similarly, in normal and high glucose levels, the cells were treated with 10 and 20 $\mu$ M of ZLN005 (Figure 4.11A and C) did not show significant changes in the production of ROS compared to non-treated control cells, and this suggests that despite the fragmentation, mitochondria are active and participate in the detoxification of generated ROS through enzymes such as

Manganese superoxide dismutase (MnSOD) which is located in the mitochondrial matrix (Li and Zhou, 2011, Miriyala et al., 2012). The production of ROS was significantly increased at 30 $\mu$ M, despite defects of mitochondrial oxidative phosphorylation; a main source of generated ROS. One explanation of this result might be defects of detoxifying enzymes system of which is located in mitochondria due to mitochondrial fragmentation. However, chronic mitochondrial fission may be another potential cause of increasing ROS level (Knott et al., 2008).

In regards to the PGC-1 $\alpha$  effect on ROS level, Baldelli and co-workers (2014) reported that downregulation of PGC-1 $\alpha$  leads to increases of ROS levels due to decreases in the antioxidant enzymes in the murine skeletal muscle cell line C<sub>2</sub>C<sub>12</sub>. Similar result was reported by Iacovelli and co-workers (2016) who found that expression of several antioxidant genes induced by PGC-1 $\alpha$  overexpression can limit the increase of ROS due to increased mitochondrial oxidative phosphorylation.

These findings suggest that ROS generation accompanying a mitochondrial oxidative phosphorylation have no role in inducing mitochondrial fragmentation. When mitochondria are active in ATP generation via mitochondria oxidative phosphorylation, detoxifying enzymes will also be active in removing generated ROS, while, in hyperfragmented mitochondria, where antioxidant enzymes are defective, mitochondria oxidative phosphorylation is also impaired and does not contribute in ROS production.

The present study also attempts to investigate the effect of ZLN005, which induces mitochondrial fragmentation, on cancer cell migration. Upon detailed analysis of cell migration monitored by time-lapse microscopy of MDA-MB-231 cells treated with ZLN005 during 24hrs revealed that cell migration was increased in low concentration of ZLN005 (10 $\mu$ M) in all glucose levels (Figure 4.12). Then in higher concentration (20 $\mu$ M); cell migration was decreased. However, it was still significant compared to control in low and normal glucose levels, whereas, at 30 $\mu$ M it was decreased more and in high glucose

level this decrease in the cell migration was significant compared to the control. This novel finding is quite interesting since cell migration decreased when the cells were treated with high concentration of ZLN005 despite increasing mitochondrial fragmentation and increasing aerobic glycolysis. These results suggest that cell migration is related to mitochondrial oxidative phosphorylation more than glycolysis, because, it was postulated that cell migration being increased at 30 $\mu$ M in all glucose levels due to significant mitochondrial fragmentation which has led to decreases in the mitochondrial oxidative phosphorylation and increases in the glycolysis, whilst, in contrast to the expectation, cell migration has been decreased. Moreover, at 20 $\mu$ M in normal and high glucose levels where production of ATP was increased significantly due to increases in glycolysis, cell migration also was decreased. This is the first time that ZLN005 used in studying cancer cell migration.

PGC-1 $\alpha$  regulates several genes involved in energy metabolism and mitochondrial biogenesis (Jornayvaz and Shulman, 2010) , and it was predicted that ZLN005 induce overexpression of PGC-1 $\alpha$  leading to hyperfragmentation of mitochondria. However, non-significant effect of ZLN005 on PGC-1 $\alpha$  gene expression as well as Drp1 gene expression despite fragmentation of mitochondria when used at high concentrations (20 and 30 $\mu$ M) suggests that the ZLN005 effect is not related to PGC-1 $\alpha$ . It may be ZLN005 induce changes through expression of unknown proteins and pathways, as it has several nuclear receptors and can regulate several metabolic processes(Lin et al., 2005). Moreover, increasing ATP and lactate production in the cells treated with ZLN005 activator especially at 20 $\mu$ M may be related to mitochondrial morphologic changes more than the effect of PGC-1 $\alpha$  which did not show significant changes at this ZLN005 concentration.

Our result in agreement to results obtained by Zhu and co-workers (2009) reported that overexpression of PGC-1 $\alpha$  induced either by stimulation with palmitic acid or infection with adenovirus can lead to reduces in the vascular smooth muscle cell proliferation and

migration induced by high glucose level. Whereas, LeBleu and co-workers (2014) suggested that silencing of PGC-1 $\alpha$  in cancer cells leads to reduction in cell migration and invasion of cells.

Taken together, these findings provide that PGC-1 $\alpha$  plays an important role in inducing cell migration through enhancing mitochondrial metabolism, while, overexpression of PGC-1 $\alpha$  leads to mitochondria hyperfragmentation and defects a mitochondrial metabolism and this can reduce cell migration. These effects are magnified with increases in glucose concentration.

Data presented in this chapter have demonstrated that treating MDA-MB-231 cells with ZLN005 induced mitochondrial fragmentation and promoted metabolic reprogramming to glycolysis. However, the novel finding here is despite these changes, cancer cell migration was decreased. In order to increase cell migration, increases in both mitochondrial oxidative phosphorylation and aerobic glycolysis are required by cancer cells (Jose et al., 2011). Mitochondria ROS have no role in inducing and activation of mitochondrial fission protein Drp1 and fragmentation of mitochondria.

Despite that ZLN005 activator is a selective transcriptional regulator of the PGC-1 $\alpha$  gene, It should be remembered that it may have, like many drugs, a direct or indirect effects on other factors which can involve in mitochondrial fragmentation and cellular metabolism, therefore, it is possible that its effect is not due to direct effect of expression of PGC-1 $\alpha$  or Drp-1 protein on the mitochondrial morphology or cellular metabolism.

## **Chapter Five: Investigating the effect of metabolism on mitochondrial dynamics and cell migration**

### **5.1 Introduction**

Since the discovery of metabolic reprogramming hallmark of cancer, many studies have been performed to targeting metabolism for cancer treatments (Podo et al., 2017, Luengo et al., 2017). At present, several inhibitors and drugs that target metabolic enzymes and pathways have been developed (Zhao et al., 2013b, Sborov et al., 2015). However, undesirable toxicity and side effects remain a big challenge in developing drugs, because all cells relay on oxidative phosphorylation and/or glycolysis in generation of ATP (Zhang et al., 2015). Moreover, there is evidence that targeting cell metabolism will induce significant increase in oxidative stress, which can lead to mitochondrial fragmentation and cell death (Le et al., 2010, Cao et al., 2017).

In the previous chapter the result showed that changes in the mitochondrial dynamic will affect cellular metabolism and cell migration. However, it is not clear if changes in cellular metabolism also affect the mitochondrial dynamics as well as cell migration. To understand the links between them, in this chapter we investigated the impact of the cellular metabolism, through targeting oxidative phosphorylation with Antimycin A, and glycolysis and 3-bromopyruvic acid, on the mitochondrial dynamics and cell migration in MDA-MB-231 cells.

#### **5.1.1 Targeting glycolysis with 3-bromopyruvate**

3-Bromopyruvate (3BrPA), a potent alkylating agent, can induce cell death through alkylating agents and through inhibition of aerobic glycolysis and oxidative phosphorylation (Jardim-Messeder and Moreira-Pacheco, 2016). It was reported that 3BrPA targets hexokinase II (HKII), which catalyses the first step of glycolysis (Zhang et al., 2014, Lis et al., 2016, Ho et al., 2016). Further studies show that 3BrPA causes cancer cell death via pyruvylation of glyceraldehyde-3-phosphate dehydrogenase (GAPDH). The

pyruvylation triggers loss of enzymatic activity of GAPDH resulting in the anti-glycolytic effects (Ganapathy-Kanniappan et al., 2009). It has been observed that 3BrPA treatment induces cell death through increasing level of ROS and total cellular stress (Kim et al., 2008), and it is well known that ROS can induce mitochondrial fragmentation. However, it is not clear if targeting cellular metabolism with 3BrPA affects mitochondrial dynamics and cell migration or not. To understand this relation, we targeted MDA-MB-231 cell metabolism with different concentrations of 3BrPA for 24hrs to study its effect on the mitochondria morphology, and cell migration.

### **5.1.2 Targeting oxidative phosphorylation with Antimycin A**

Antimycin A (AMA), is a specific inhibitor which targets cytochrome c oxidoreductase complex (complex III) of electron transport chain (ETC) in mitochondria, it can generate ROS and induce apoptosis (Wang et al., 2015a). In the study published by Rakhmatullina and co-workers (2016), they concluded that treating *Tritium aestivum* roots with AMA, which led to increase in the production of ROS, changed mitochondrial morphology (Rakhmatullina et al., 2016), and other studies suggested that AMA can inhibit growth of HeLa cells and A549 cells through increasing ROS levels (Park et al., 2007, Han et al., 2008). However, no attempt was made to study the effect of oxidative phosphorylation inhibited by AMA on mitochondrial morphology, as well as cell migration in the cancer cells. For this purpose, we targeted MDA-MB-231 cells with AMA in different concentrations for 24hrs.

## **5.2 Material and methods**

### **5.2.1 Cell culture**

MDA-MB-231 cells were used in our experiments. They were continuously cultured in Dulbecco's Modified Eagles Media (DMEM) supplemented with 10% FBS, 1% L-glutamine, 100 Unit/ml of penicillin and 100 µg/ml of streptomycin (Gibco), at 37°C in a

humidified atmosphere containing 5% CO<sub>2</sub>. However, antibiotic free medium was used when the cells treated with AMA (Sigma) or 3BrPA (Sigma) during experiments.

### **5.2.2 Mitochondrial staining and analysis**

Cells were treated with different concentrations of AMA (12.5, 25, 50, and 100µM) or 3BrPA (25, 50, 100, 250µM) for 24hrs, then mitochondria were stained with MitoTracker probe (Invitrogen, M7510), and nucleus stained with DAPI as described in section 2.2.7. Images were taken using confocal microscopy and analysed by ImageJ software as explained in section 2.2.16.

### **5.2.3 Quantitative Real- Time PCR (qRT-PCR)**

The Quantitative real time polymerase chain reaction (qRT-PCR) was used in measuring mtDNA copy number, as described in section 2.2.10, using extracted DNA in MDA-MB-231 cells after 24hrs treating with either AMA or 3BrPA.

### **5.2.4 Analysis of metabolism and ROS**

MDA-MB-231 cells treated with different concentrations of either AMA or 3BrPA for 24hrs, then generated ATP was measured as described in section 2.2.14, lactate production was measured as described in section 2.2.13, and level of generated ROS was measured as described in section 2.2.12.

### **5.2.5 Cell migration**

Cell migration in MDA-MB-231 cells treated with different concentrations of AMA or 3BrPA was monitored by time-lapse microscopy for 24hrs. ImageJ (Fiji) software (MtrackJ plugin) was used to track and measuring the speed of cell movement as described in section 2.2.17.

### 5.3 Results:

We investigated the effect of 3-bromopyruvic acid (3BrPA); which targets glycolysis, and Antimycin A (AMA); which targets oxidative phosphorylation, on the cellular metabolism, mitochondrial dynamics, and cell migration. Therefore, we treated MDA-MB-231 cells with 3BrPA in different concentrations 25, 50, 100, 250 $\mu$ M and different concentrations of AMA; 12.5, 25, 50, 100 $\mu$ M for 24hrs.

To determine whether treating cells with 3BrPA and AMA could affect cell viability, we performed MTT assay. The results shown in Figure 5.1A revealed that 3BrPA does not affect cell viability after 24hrs of treatment. Whereas, when we treated the cells with AMA, we found that AMA at concentration (200 $\mu$ M) strongly affected cell viability compared to non- treated control cells ( $p < 0.001$ ), while, at lower concentrations no significant differences were observed with control, as seen in Figure 5.1B.

Depending on these results we treated cells in our next experiments with 3BrPA in concentrations 25, 50, 100, 250 $\mu$ M, and with AMA in concentrations 12.5, 25, 50, 100 $\mu$ M.

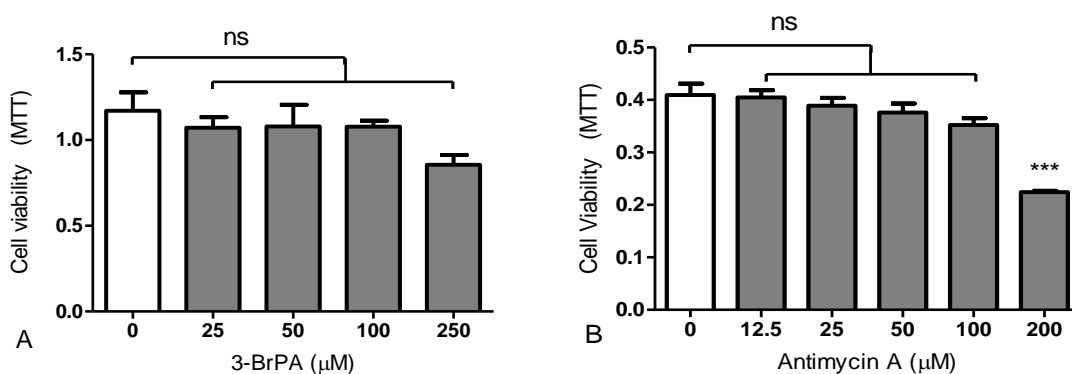


**Figure 5.1:** MTT assays showing the cell viability after 24hrs treating cells with 3BrPA or AMA. MDA-MB-231 cells were treated with different concentrations of (A) 3BrPA or (B) AMA, for 24hrs. Cell viability determined by reading plates at 570 nm with plate reader. Data represent the mean  $\pm$  standard error of three independent experiments performed in triplicate (\*\*\*) represent  $p < 0.001$ ).

To uncover the impact of treating MDA-MB-231 cells with 3BrPA and AMA on the generation of the intracellular ROS; we incubated cells with 0.2mM DCFH-DA for 60 minutes before treating them with different concentrations (25, 50, 100, 250 $\mu$ M) of 3BrPA and different concentrations (12.5, 25, 50,100 $\mu$ M) of AMA. After 24hrs of treating cells, the fluorescence intensity of DCF which was oxidized by ROS was read with a fluorometric plate reader at 485nm/535nm, the fluorescence intensity is proportional to the intracellular ROS levels generated by the cells. Results of 3BrPA treatments in Figure 5.2A showed that intracellular ROS level was increased markedly from 18578 $\pm$ 1823Unit in non-treated cells to 27315 $\pm$ 2442Unit in the treated cells with 25 $\mu$ M of 3BrPA ( $p<0.05$ ), and into 32546.5 $\pm$ 2566, 38436 $\pm$ 1571, and 45514.3 $\pm$ 1843Unit in the treated cells with 50, 100, and 250 $\mu$ M of 3BrPA respectively ( $p<0.001$ ); these mean that ROS production was increased by 47.03%, 75.19%, 106.89%, and 144.99% in the cells treated with 25, 50, 100, 250 $\mu$ M of 3BrPA respectively compared to control cells. Similar results were obtained when cells treated with AMA. As shown in Figure 5.2B, level of ROS was increased significantly from 16143.3 $\pm$ 306Unit in non-treated cells to 17355.7 $\pm$ 287Unit in the treated cells with 12.5 $\mu$ M of AMA ( $p<0.05$ ), and into 19208 $\pm$ 180.8, 28368.3 $\pm$ 192.9, and 24953.3 $\pm$ 360.9Unit in the treated cells with 25, 500, and 100 $\mu$ M of AMA respectively ( $p<0.001$ ); these mean that treating with AMA induced increases in the ROS production by 7.51%, 18.98%, 75.73%, and 54.57% at concentrations 12.5, 25, 50,100 $\mu$ M of AMA compared to control.

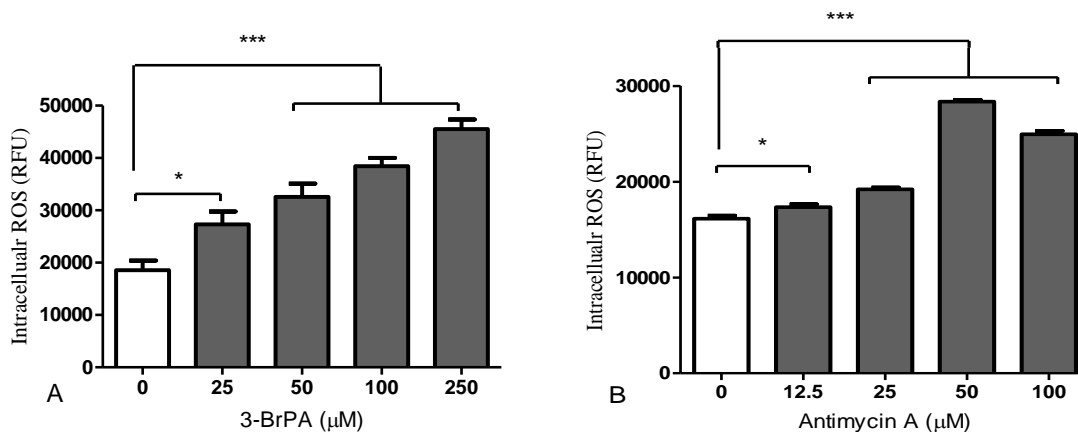


**Figure 5.2: Effect of 3-BrPA and AMA on the ROS production in MDA-MB-231cells.** Cells were incubated with 0.2mM DCFH-DA for 60 minutes treated either with (A): different concentrations of 3-BrPA or with (B): different concentrations of AMA for 24 hours. The intensity of fluorescence was read with a fluorometric plate reader at 485nm/535nm. Data represent the mean  $\pm$  standard error of three independent experiments performed in triplicate. One-way ANOVA followed by Dunnett's Multiple Comparison Test to compare the mean of treatments with the mean of control. (\*, and \*\*\* represent  $P < 0.05$ , and  $0.001$  respectively). RFU=Relative Fluorescence Units.

Afterwards we investigated the effect of 3BrPA on the mitochondrial dynamics through measuring mitochondrial number, size, volume, and total volume of mitochondrial mass in the cell. For this purpose, we treated cells with 3BrPA for 24hrs then z-stack images were taken using confocal microscopy, and ImageJ was used for analysis data. The results are presented in Figure 5.3 and 5.4.

Results in Figure 5.3 A show that treating cells with 3BrPA changed the number of mitochondria significantly at concentration 250 $\mu$ M and it was increased from 150.18 $\pm$ 5.7 in non-treated control cells to 207.6 $\pm$ 10.6 in mentioned concentration ( $p < 0.001$ ), while, in other concentrations, no significant changes were detected compared to control.

Treating cells with 3BrPA reduced the volume of the mitochondria significantly. As presented in Figure 5.3B, the volume of mitochondria has been decreased from 0.46 $\pm$ 0.038 $\mu$ m<sup>3</sup> in control cells to 0.36 $\pm$ 0.018 $\mu$ m<sup>3</sup> in treated cells with 25mM of 3BrPA ( $p < 0.05$ ), and into 0.29 $\pm$ 0.02, 0.18 $\pm$ 0.012, and 0.11 $\pm$ 0.009 $\mu$ m<sup>3</sup> in treated cells with 50, 100, and 250mM of 3BrPA respectively ( $p < 0.001$ ).

When we measured the size of the mitochondria, we found it was decreased significantly. It was decreased from 5.29 $\pm$ 0.46 $\mu$ m<sup>2</sup> in control cells to 3.69 $\pm$ 0.2, 2.88 $\pm$ 0.18, and 2.1 $\pm$ 0.2 $\mu$ m<sup>2</sup> in treated cells with 50, 100, and 250mM of 3BrPA respectively ( $p < 0.001$ ), while, no significant changes in the mitochondrial size were detected in treated cells with 25mM of 3BrPA compared to the control cells, as shown in Figure 5.3C.

Total mass of the mitochondria was calculated by multiplying volume of mitochondria with the number of the mitochondria, and the results as shown in Figure 5.3D revealed it was decreased significantly from 67.24 $\pm$ 3.73 $\mu$ m<sup>3</sup> in control cells to 47.6 $\pm$ 2.9 $\mu$ m<sup>3</sup> in treated cells with 50 $\mu$ M of 3BrPA ( $p < 0.05$ ), and into 31.94 $\pm$ 2.33, and 23.35 $\pm$ 1.94 $\mu$ m<sup>3</sup> at concentrations 100, and 250 $\mu$ M of 3BrPA respectively ( $p < 0.001$ ), while, in cells treated with 25 $\mu$ M, no significant changes were observed compared to control cells.

These dynamic changes in mitochondria in the cells treated with 3BrPA were presented in Figure 5.4.

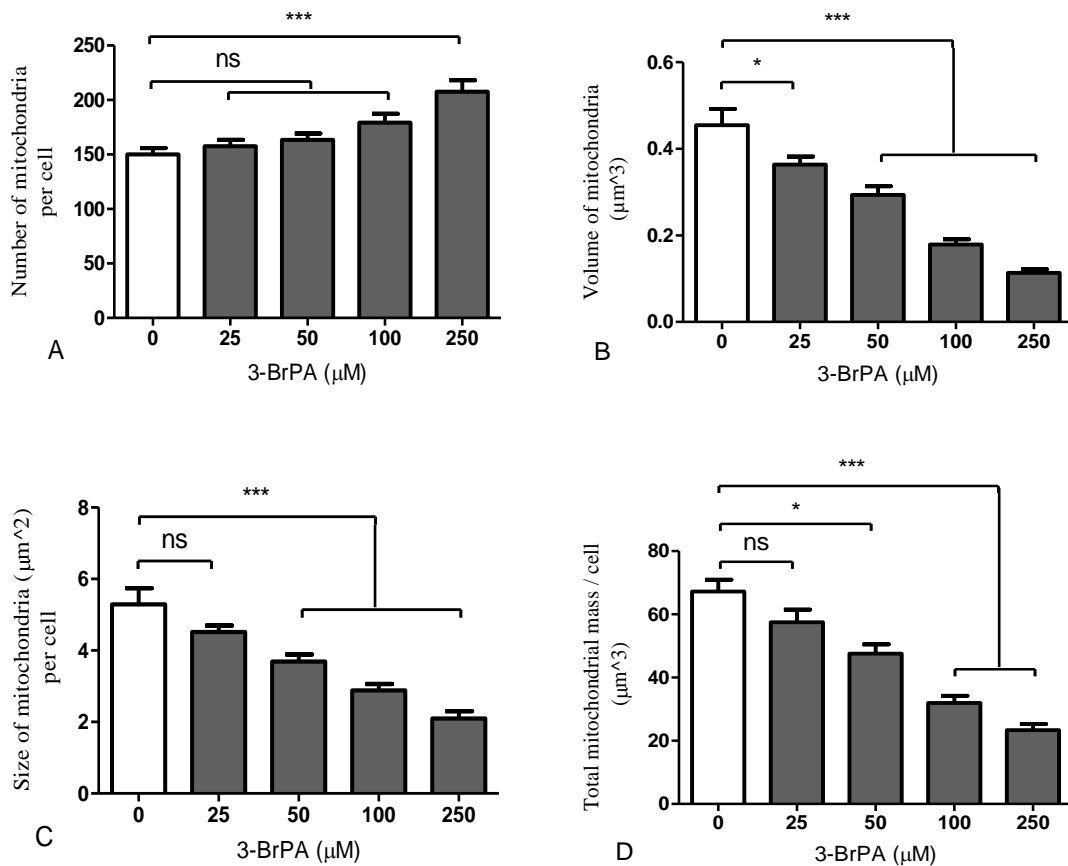


**Figure 5.3: Effect of 3-BrPA on the mitochondrial morphology in MDA-MB-231 cells.** Cells treated with 3-BrPA for 24hrs then mitochondria were stained with MitoTracker probe and DAPI was used to stain nucleus. Z- Stack images were taken by confocal microscopy used to take mitochondrial images. (A) Represent quantification analysis of number of mitochondria, (B) Volume of mitochondria, (C) Size of mitochondria, and (D) represent quantification analysis of total mitochondria mass per cell. Data represent the mean  $\pm$  standard error of three independent experiments performed in triplicate; each experiment contained at least 30 cells. One-way ANOVA followed by Dunnett's Multiple Comparison test to compare between the mean of treatments with the control mean (\* and \*\*\*represent  $P < 0.05$  and  $0.001$  respectively).

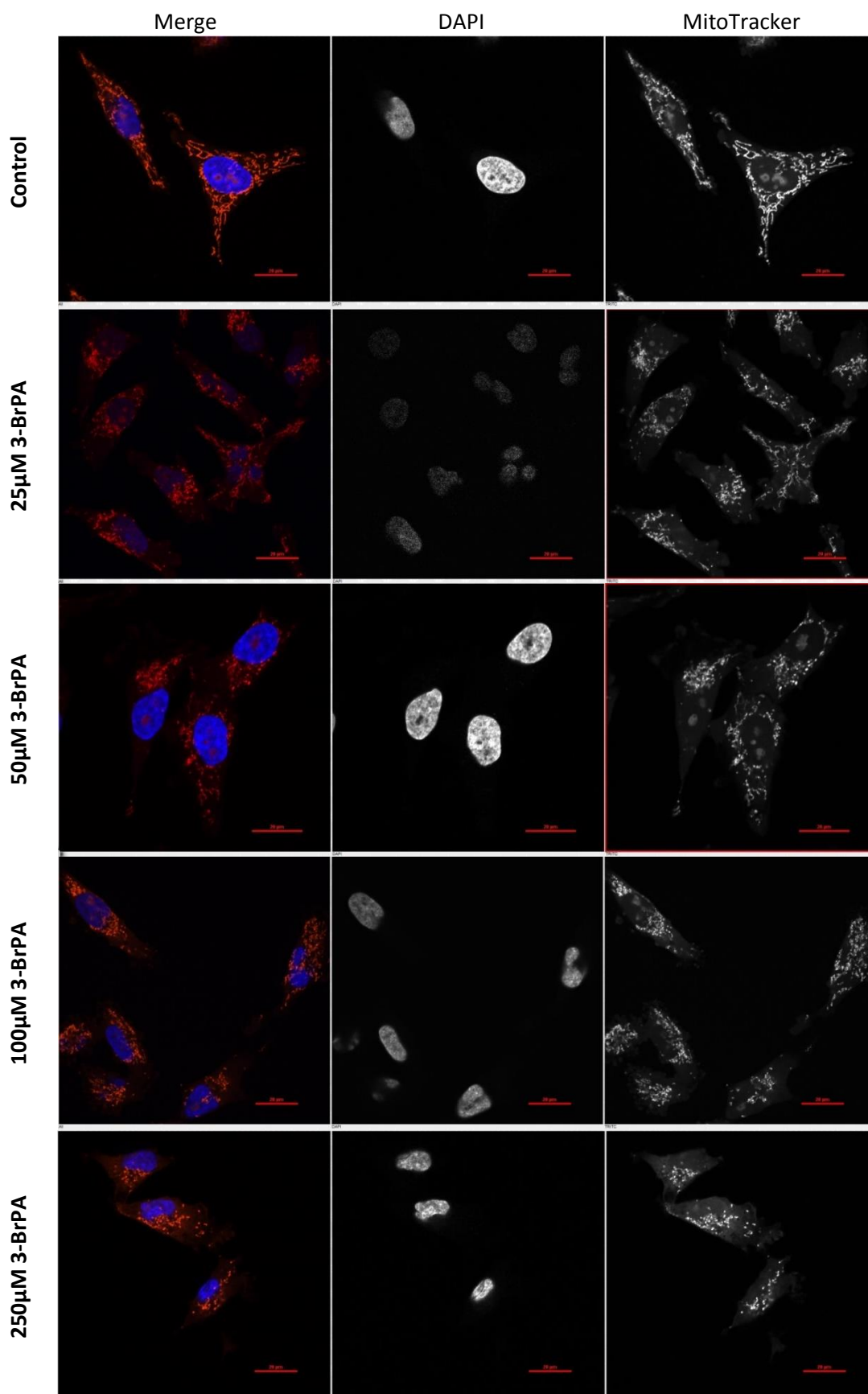


**Figure 5.4:** Micrographs showing the mitochondrial morphology in MDA-MB-231 cells treated with 3BrPA. Mitochondria were stained with MitoTracker orange CMTMRos probe (red colour) and nucleus stained with DAPI (blue colour), for MDA-MB-231 cells treated with different concentrations of 3-BrPA. Images were taken by confocal microscopy. Scale bar = 20 µm.

To discover the effect of AMA on the mitochondrial dynamics, we treated MDA-MB-231 cells with different concentrations 12.5, 25, 50, and 100 $\mu$ M of AMA for 24hrs, and then changes in mitochondrial morphology were measured as shown in Figure 5.5 and 5.6.

The effect of AMA on the mitochondrial numbers was analysed as shown in Figure 5.5A, and it was revealed that AMA statistically did not induce significant changes in the mitochondrial numbers.

Figure 5.5B shows the effect of AMA on the size of the mitochondria. The results found that mitochondrial size was decreased significantly from  $4.78 \pm 1.05 \mu\text{m}^2$  in non-treated control cells to  $1.59 \pm 0.11$ , and  $1.5 \pm 0.09 \mu\text{m}^2$  in treatments 50, and 100 $\mu$ M ( $p < 0.05$ ), while, no significant changes were recorded between cells treated with 12.5, and 25 $\mu$ M of AMA and control cells.

Similar results were obtained when we measured the volume of the mitochondria in treated cells with AMA as shown in Figure 5.5C. Treating cells with 50, and 100 $\mu$ M led to decreases in the mitochondrial volume markedly, it was decreased from  $0.38 \pm 0.11 \mu\text{m}^3$  in control cells to  $0.11 \pm 0.011$ , and  $0.09 \pm 0.007 \mu\text{m}^3$  respectively ( $p < 0.05$ ), whereas, no significant changes were found between treatments 12.5, and 25 $\mu$ M compared to the non-treated control cells.

At the end, total mass of the mitochondria per cell was calculated, and the results in Figure 5.5D, revealed that AMA reduced on it. It declined significantly from  $31.84 \pm 8.94 \mu\text{m}^3$  in control cells to  $9.11 \pm 1.96 \mu\text{m}^3$  in cells treated with 100 $\mu$ M of AMA ( $p < 0.05$ ), while, one way ANOVA results found no significant changes between other treatments with control.

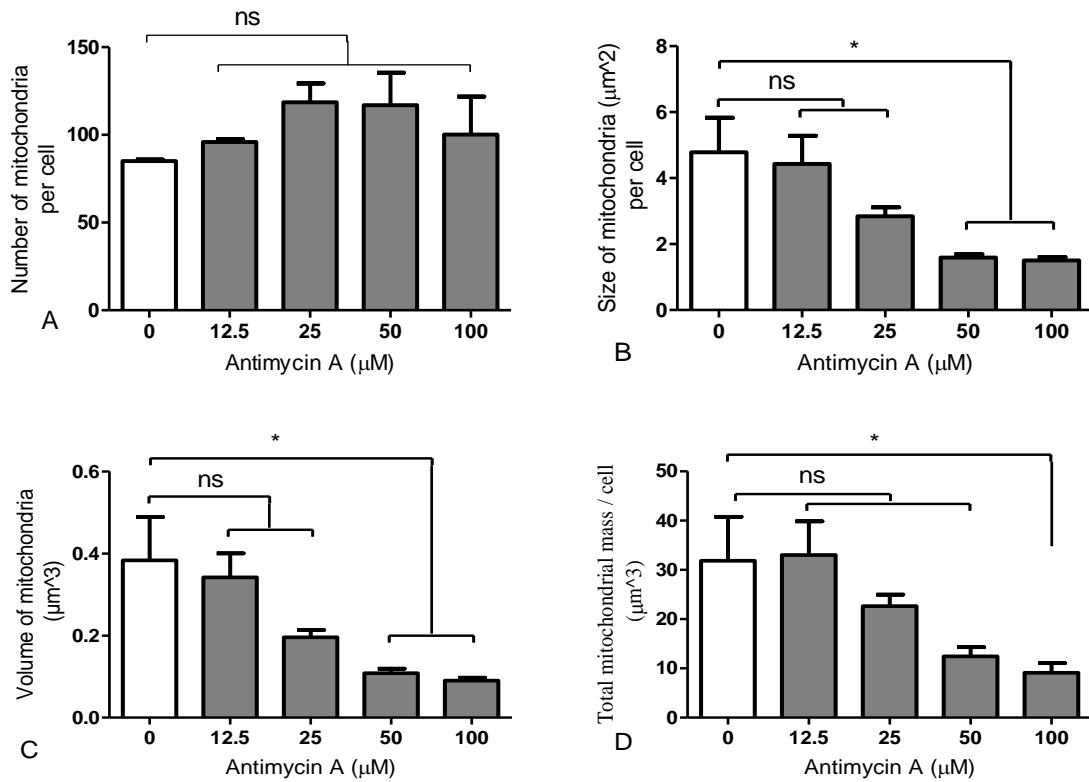


**Figure 5.5: Effect of AMA on mitochondrial morphology in MDA-MB-231 cells.** Cells treated with AMA for 24hrs then mitochondria stained with MitoTracker probe and confocal microscopy used to take z-stack images. (A) Represent quantification analysis of number of mitochondria, (B) Size of mitochondria, (C) Volume of mitochondria, and (D) represent quantification analysis of total mass of mitochondria per cell. Data represent the mean  $\pm$  standard error of three independent experiments performed in triplicate; each experiment contained at least 30 cells. One-way ANOVA and Dunnett's Multiple Comparison test used to compare between the mean of treatments with mean of control (\*represent  $P < 0.05$ ).

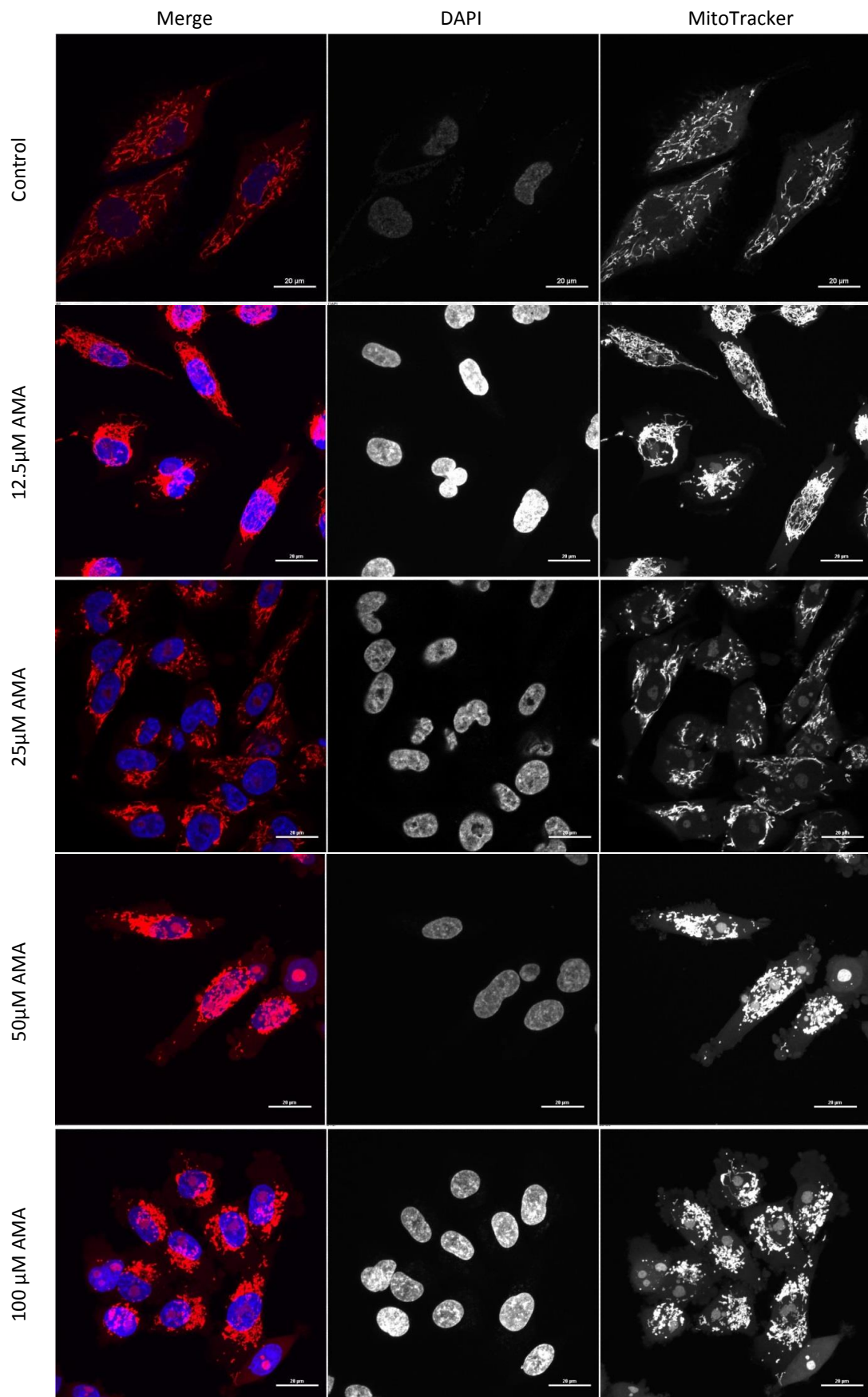
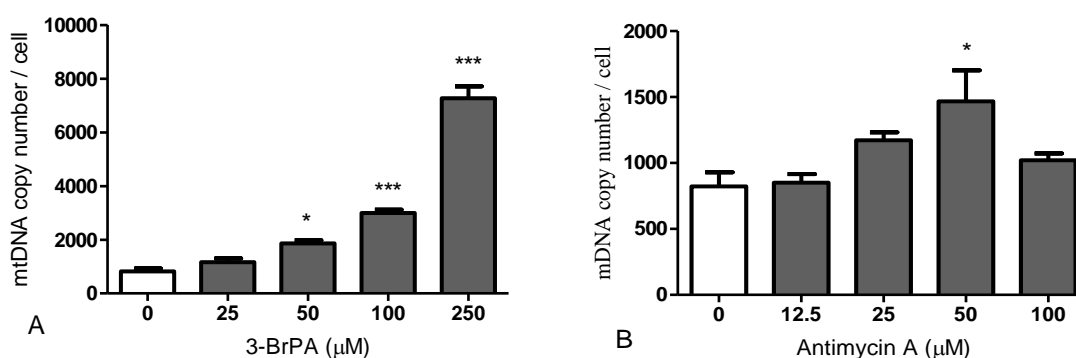


**Figure 5.6:** Micrographs showing the mitochondrial morphology in MDA-MB-231 cells treated with AMA. Mitochondria were stained with MitoTracker probe (red colour) and nucleus stained with DAPI (blue colour), for MDA-MB-231 cells treated with different concentrations of AMA. Images were taken by confocal microscopy. Scale bar = 20 μm.

To confirm our results of mitochondrial morphology obtained by confocal microscopy in MDA-MB-231 cells treated with 3-BrPA, and AMA, we measured mtDNA copy number after treating cells with 3BrPA or AMA for 24hrs.

Figure 5.7A show the results of mtDNA copy number in MDA-MB-231 cells treated with different concentrations of 3BrPA, and it was revealed that mtDNA copy number was increased significantly from  $822.5 \pm 106.4$  in non-treated control cells to  $1863.6 \pm 111.7$  in treatment  $50 \mu\text{M}$  ( $p < 0.05$ ), and into  $2993.6 \pm 129.7$ , and  $7270.3 \pm 440.9$  in treatments 100, and  $250 \mu\text{M}$  respectively ( $p < 0.001$ ), whilst, no differences in mtDNA copy number were detected between the cells treated with  $25 \mu\text{M}$  and control.

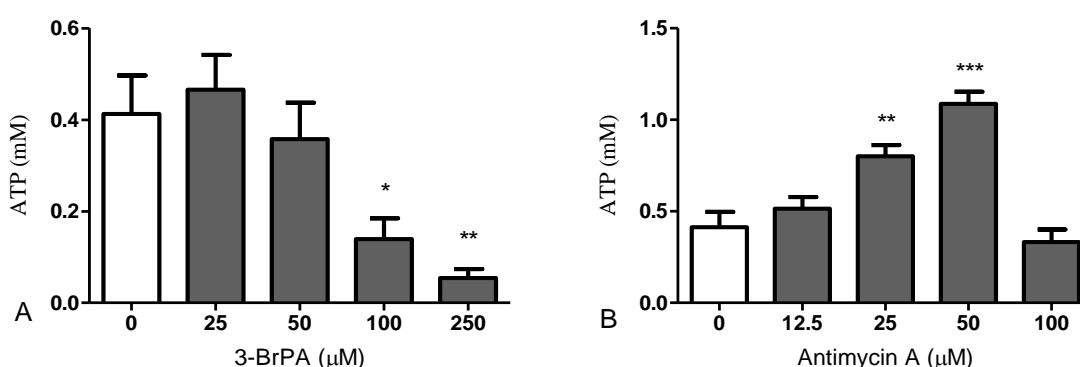
The results presented in Figure 5.7B, show the mtDNA copy number in MDA-MB-231 cells treated with different concentrations of AMA. It appears that treating cells with AMA at concentration  $50 \mu\text{M}$  induced significant increases in the mtDNA copy number, it was increased from  $822.5 \pm 106.4$  in control cells to  $1466.8 \pm 236$  ( $p < 0.05$ ), while, no significant changes in the mtDNA copy number were recorded between other treatments compared to control.



**Figure 5.7: Impact of 3-BrPA and AMA on the mtDNA copy number in MDA-MB-231 cells.** Cells were treated with 3-BrPA or AMA for 24hrs, and then DNA extracted and used to determine mtDNA using quantitative real-time PCR. (A) Represent quantification analysis of mtDNA copy number in cells treated with 3-BrPA, (B) Represent quantification analysis of mtDNA copy number in cells treated with AMA. Data represent the mean  $\pm$  standard error of three independent experiments performed in triplicate. One-way ANOVA followed by Dunnett's Multiple Comparison Test to compare mean of the treatments with mean of control (\*, and \*\*\*represent  $P < 0.05$ , and  $0.001$  respectively).

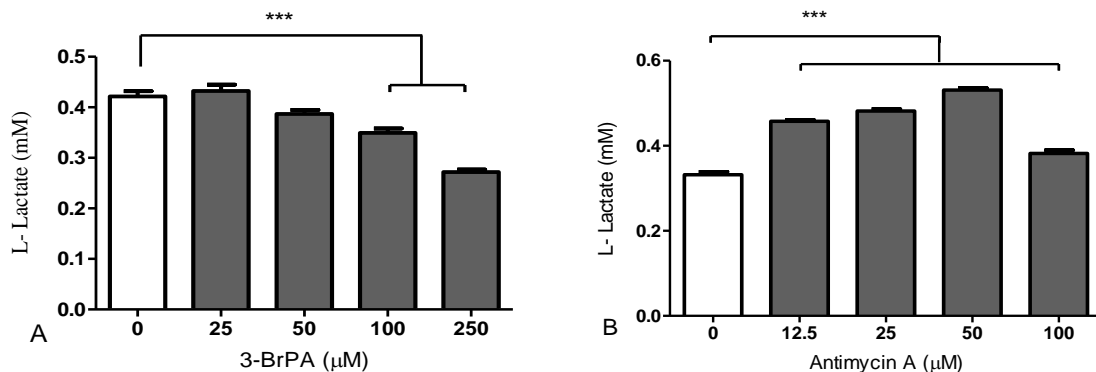
To find out the extent of the impact of 3BrPA and AMA on cellular metabolism, we measured generated ATP and lactate after 24hrs of treated MDA-MB-231 cells with different concentrations of 3BrPA and AMA using specific commercial kits.

Figure 5.8A shows the results of ATP production in the cells treated with 3BrPA. It was revealed that ATP production was decreased significantly from  $0.41 \pm 0.08$  mM in control to  $0.14 \pm 0.05$  mM in treated cells with  $100 \mu\text{M}$  ( $p < 0.05$ ), and into  $0.05 \pm 0.02$  mM in treatment  $250 \mu\text{M}$  ( $p < 0.01$ ); which is mean that ATP production was decreased by 66.25%, and 86.85% in treated cells with 100 and  $250 \mu\text{M}$  of 3BrPA compared to control, whereas, no differences were detected between treatments 25, and  $50 \mu\text{M}$  and control. On the contrary, treating cells with AMA led to increases in ATP production as seen in Figure 5.8B. It was increased markedly from  $0.41 \pm 0.08$  mM in control to  $0.801 \pm 0.06$  mM in treated cells with  $25 \mu\text{M}$  of AMA ( $p < 0.01$ ), and into  $1.09 \pm 0.07$  mM in treatment  $50 \mu\text{M}$  ( $p < 0.001$ ); these mean ATP production was increased by 93.97%, and 163.03% in treated cells with 25 and  $50 \mu\text{M}$  of AMA compared to control, whereas, no significant differences were recorded between treatments 12.5, and  $100 \mu\text{M}$  and control. What is interesting to note is that after increasing ATP production at concentrations 25, and  $50 \mu\text{M}$  of AMA, we found decline of ATP production again at concentration  $100 \mu\text{M}$ .



**Figure 5.8: Quantification of ATP in MDA-MB-231 cells treated with 3-BrPA or AMA.** After treating cells with different concentrations of 3-BrPA or AMA for 24hrs, lysate of  $1 \times 10^6$  cells were used for measuring ATP level by colorimetric ATP assay kit. Graphs represent quantification analysis of ATP production in the cells treated with (A) 3-BrPA, and (B) with AMA. Data represent the mean  $\pm$  standard error of four independent experiments performed in triplicate. One-way ANOVA followed by Dunnett's Multiple Comparison Test to compare mean of treatments with mean of control (\*, \*\* and \*\*\* represent  $P < 0.05$ ,  $0.01$  and  $0.001$  respectively)

When we measured lactate production in MDA-MB-231 cells treated with 3BrPA, results as shown in Figure 5.9A revealed that lactate production was decreased sharply from  $0.42\pm 0.01$  mM in control to  $0.35\pm 0.009$ , and  $0.27\pm 0.005$  mM in treated cells with 100, and 250  $\mu$ M of 3BrPA respectively ( $p < 0.001$ ); which is mean lactate production was decreased by 17.1%, and 35.5% in treated cells with 100 and 250  $\mu$ M of 3BrPA compared to control, whilst, no significant differences in lactate production were found between cells treated with 25, and 50  $\mu$ M of 3BrPA and control cells. On the contrary to 3BrPA, we found treating cells with AMA increased lactate production. As seen in Figure 5.9B, lactate production was increased strongly from  $0.33\pm 0.007$  mM in control cells to  $0.46\pm 0.004$ ,  $0.48\pm 0.005$ ,  $0.53\pm 0.005$ , and  $0.38\pm 0.008$  mM in treated cells with 12.5, 25, 50, and 100  $\mu$ M respectively ( $p < 0.001$ ); these mean that lactate production was increased by 37.7%, 45.02%, 59.95%, and 15.06% in treated cells with 12.5, 25, 50 and 100  $\mu$ M of AMA compared to control.



**Figure 5.9: Effect of 3-BrPA and AMA on lactate production in MDA-MB-231 cells.** After 24 hours of treating cells with 3-BrPA or AMA, supernatants were assayed to determine the L-Lactate concentrations. (A) Represent quantification analysis of L-Lactate production in the cells treated with 3-BrPA, and (B) with AMA. Data represent the mean  $\pm$  standard error of four independent experiments performed in triplicate. One-way ANOVA followed by Dunnett's Multiple Comparison Test to compare mean of treatments with control mean. (\*\*\*)represent  $p < 0.001$ ).

After we found that 3BrPA and AMA induced changes in mitochondrial dynamics and metabolism, we investigated their effects on the cell migration using time-lapse to track cell movements during 24hrs.

Effect of 3BrPA on the cell migration presented in Figure 5.10A revealed that speed of cell migration was decreased significantly at concentrations 100, and 250 $\mu$ M compared to control. It was decreased from 31.1 $\pm$ 0.9 $\mu$ m/h in control to 19.9 $\pm$ 1.6, and 16.1 $\pm$ 0.4 $\mu$ m/h in mentioned concentrations respectively ( $p < 0.001$ ), while, no significant changes were recorded between treatments 25, and 50 $\mu$ M and control.

In the Figure 5.10B, results showed that treating cells with AMA increased the cell migration significantly. It was increased from 19.4 $\pm$ 0.75 $\mu$ m/h in control to 23.9 $\pm$ 0.67, and 24.1 $\pm$ 1.13 $\mu$ m/h in the cells treated with 12.5, and 25 $\mu$ M of AMA respectively ( $p < 0.05$ ), and into 26.27 $\pm$ 1.15, and 24.87 $\pm$ 0.8 $\mu$ m/h in cells treated with 50, and 100 $\mu$ M of AMA respectively ( $p < 0.01$ ).

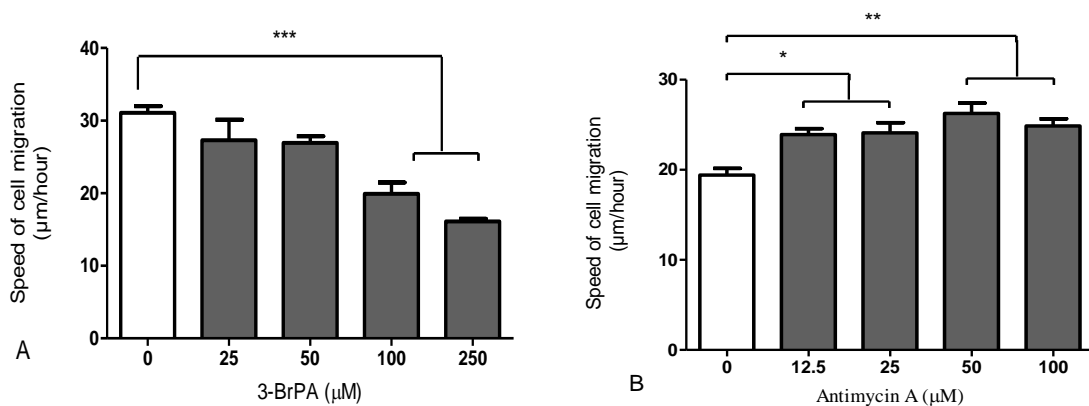


**Figure 5.10: Effect of 3-BrPA and AMA on the cell migration in MDA-MB-231 cells.** Cell migration was monitored by the time-lapse microscopy. Images were taken every 15 minutes over 24 hours, and ImageJ software was used for tracking individual cell. A: represent quantification analysis of speed of cell migration in cells treated with 3BrPA, and B: with AMA. Data represent the mean  $\pm$  standard error of three independent experiments performed in triplicate. One-way ANOVA followed by Dunnett test to compare mean of treatments with control mean (\*, \*\*, and \*\*\* represent  $P < 0.05$ , 0.01 and 0.001 respectively).

#### **5.4 Discussion:**

There is evidence that confirms a relationship between mitochondrial morphology and function (Picard et al., 2013, Nadova et al., 2016). In previous chapters we found that changes in the mitochondrial morphology induced by high ROS can affect cellular metabolism, here we targeted cellular and mitochondrial metabolism with pharmacological treatments to understand the impact of mitochondrial metabolism on mitochondrial morphology and cell migration. Therefore, we used 3-bromopyruvate (3BrPA), which targets glycolysis, and Antimycin A (AMA), which targets oxidative phosphorylation, in sub-lethal concentrations in MDA-MB-231 breast cancer cells. First we measured cell viability after exposing these cells to both 3BrPA and AMA for 24hrs to find sub-lethal concentrations. Our data show that 3BrPA did not affect cell viability with the concentrations used (Figure 5.1A), whereas, AMA led to significant decrease in cell viability at 200 $\mu$ M. In lower concentrations no significant effect on cell viability was observed (Figure 5.1B). These results were confirmed with time-lapse microscopy results for cell migration (Figure 5.10) which showed that treating cells with 250 $\mu$ M 3BrPA and 100 $\mu$ M AMA did not induce apoptosis.

Induction of ROS has been demonstrated as one of the side effects of many cancer treatments on non-cancerous normal cells (Yokoyama et al., 2017), and it has been suggested that anticancer drugs exert their cytotoxic effect on cancer cells through generation of ROS to lethal levels that can kill cancer cells through inducing apoptosis (Conklin, 2004, K. Maiti, 2012, Kasiappan and Safe, 2016). To know whether 3BrPA and AMA induce generation of ROS, we measured intracellular ROS using Dichloro-dihydro fluorescein diacetate (DCFH<sub>2</sub>-DA) as the ROS sensitive probe, and results showed both 3BrPA and AMA can induce production of ROS significantly in all used concentrations (Figure 5.2A and 5.2B for 3BrPA and AMA respectively). This result is in agreement with findings by Lin and co-workers (2016) who found that 3BrPA enhances apoptosis through

inducing ROS production after myeloid cell leukemia-1 (MCL-1) knockdown in MDA-MB-231 cells. Similarly, Zou and co-workers (2015) found that 3BrPA induces non-apoptotic necroptosis by generation of ROS in nasopharyngeal carcinoma. It was reported that 3BrPA in multiple myeloma cells can contribute to the generation of ROS via marked decreases in the glutathione (GSH) concentration (Lis et al., 2016). Whereas, previous observations by Park and co-workers (2007) support the impact of AMA in inducing ROS, they found that in HeLa cells AMA induces apoptosis through significant increases in the production of ROS and depletion of glutathione. It was suggested that AMA induces production of ROS in high rates through binding to the  $Q_i$  site and blocks the oxidation of cytochrome *b* heme, which in turn limits oxidation of semiquinone in the  $Q_o$  site and this promotes reduction of oxygen molecule to generate superoxide (Quinlan et al., 2011).

Previously we found that increased production of ROS can induce mitochondrial fission through activation of Drp1 protein. To know whether targeting metabolism with 3BrPA and AMA (in different concentrations), which have induced ROS production, affected mitochondrial morphology; we measured number, size, volume and total mass of mitochondria through confocal microscopy of MDA-MB-231 cells stained with MitoTracker probe. Markedly reducing of mitochondrial size, volume, and total mass (Figure 5.3 and 5.4) suggest that 3BrPA induces mitochondrial fragmentation. Despite that, mitochondrial number has increased significantly only when the cells treated with highest concentration of 3BrPA (Figure 5.3A), the data obtained from qPCR show significant increases of mtDNA copy number after treating the cells with 3BrPA at 50 $\mu$ M and higher concentrations (Figure 5.7), and this confirms mitochondrial fragmentation in the MDA-MB-231 breast cancer cells treated with 3BrPA. One challenge of counting mitochondrial number using confocal microscopy was mitochondrial overlapping, that is maybe the reason of that data obtained from confocal microscopy of the cells treated with 3BrPA did not show significant differences only at highest concentration.

. Similar results were observed with AMA as data showed that mitochondrial size, volume, and total mass were reduced, whereas, mitochondrial number was not affected (Figure 5.5 and 5.6). This result suggests that AMA has also induced mitochondria fragmentation, which is mainly due to generating high rate of ROS.

In the previous chapter we found a correlation between mitochondrial fragmentation and glycolytic reprogramming, and it was supposed that targeting glycolysis through using 3BrPA would decrease mitochondrial fragmentation. However, due to increased oxidative stress induced by ROS, mitochondrial fragmentation has increased. It was predicted that treating with AMA would induce mitochondrial fragmentation, because inhibition of oxidative phosphorylation by AMA promotes the cancer cells to reprogram their metabolism to glycolysis to obtain required ATP energy. This is in addition to high rate of ROS generation which increases the impact of AMA on mitochondrial morphology, which in turn induces metabolism reprogramming to glycolysis. Pletjushkina and co-workers (2006) report similar results when they inhibited the respiratory chain in HeLa cells and epithelial CV-1 cells, they found that inhibition of complex I and III stimulated generation of ROS which has led to mitochondrial fragmentation.

3BrPA has several targets in cancer cells (Marrache and Dhar, 2015). It can target hexokinase II (HK II), which catalyzes the initial step in glycolysis pathway (Chen et al., 2009), as well as glyceraldehyde-3-phosphate dehydrogenase (GAPDH) (Baghdadi, 2017); which converts glyceraldehyde 3-phosphate to D glycerate 1, 3-bisphosphate in the glycolysis pathway (Krasnov et al., 2013) leading to decrease in the level of ATP production (Sun et al., 2015). Our data show that 3BrPA has a potential effect on ATP production as increased concentration of 3BrPA has increased the decline of ATP production (Figure 5.8A), and this decrease in ATP level was due to the effect of 3BrPA on the glycolysis, as shown in Figure 5.9A, L-lactate production; the end product of glycolysis was markedly decreased with increased concentration of 3BrPA. This result

confirms our previous finding about the role of glycolysis in raising ATP level in MDA-MB-231 cells. The result also confirms that mitochondrial fragmentation leads to increase of ATP via glycolysis, because targeting glycolysis minimized ATP production despite mitochondrial fragmentation. Our results are in agreement with findings by Ihlund and co-workers (2008), who found that 3BrPA led to loss of ATP by 65% and 90% at concentrations 50 and 100 $\mu$ M in HCT116 colon carcinoma cells. Similarly, Zou and co-workers (2015) found decreases in ATP production in HNEI and CNE-2Z cell strains of NPC (Nasopharyngeal carcinoma) cells after 5hrs of treating with 3BrPA.

Despite the fact that many cancer cells rely mainly on glycolysis for ATP production, mitochondrial oxidative phosphorylation in cancer cells is still intact and contributes to ATP production (Zheng, 2012). Targeting the glycolysis pathway leads to reduction of ATP levels as both glycolysis and oxidative phosphorylation will be affected, whilst, targeting oxidative phosphorylation does not affect glycolysis. Therefore, it is expected that targeting oxidative phosphorylation such as by using AMA can induce the cancer cells to reprogram their metabolism to rely more on glycolysis to obtain required ATP for their activity, and because glycolysis generates lower amount of energy compared to oxidative phosphorylation, cancer cells rise glucose uptake to generate higher amount of ATP via acceleration of glycolysis. Obtained data agree with our expectation and showed that treating cells with AMA, which targets complex III in the electron transport chain in mitochondria, led to increase in ATP production (Figure 5.8B) as well as increase in the lactate production (Figure 5.9B). These results suggest that metabolism was altered toward glycolysis for production of ATP due to a defect in mitochondrial metabolism induced by AMA. Kale (2016) found that treating rat L6 cells with AMA did not induce increases in the ATP generation; however, he treated cells with low concentrations of AMA (5, 10, and 25 $\mu$ M) and for 48hrs.

The link between cell migration and metabolism is well documented. Since migration of cells requires high amount of ATP energy, most cancer cells alter their metabolism from oxidative phosphorylation to aerobic glycolysis which known as Warburg effect (Han et al., 2013), however, this does not mean that oxidative phosphorylation does not have a role in generating ATP, as most cancer cells still rely on it by 30-50% (Zheng, 2012). Therefore, targeting metabolism may affect cell migration strongly. In our study, we found that targeting glycolysis with 3BrPA reduced cell migration in MDA-MB-231 cells (Figure 5.10 A). Another explanation of reducing cell migration by 3BrPA is that inhibition of glycolysis leads to decrease of lactate; the end product of glycolysis, which has an important role in the acidification of the tumor microenvironment and in cell migration (Annibaldi and Widmann, 2010, Beckert et al., 2006). Our results agree with finding by Tomizawa and co-workers (2016), who reported that 3BrPA, can suppress cell migration in hepatocellular carcinoma (HCC) cells at 100 $\mu$ M. It was reported also that 3BrPA can potentiate the effect of photodynamic therapy (PDT) of cell migration inhibition in MDA-MB-31 cells (Feng et al., 2015).

In contrast to the effect of 3BrPA, treating cells with AMA promoted cell migration markedly (Figure 5.10B). This change in cell migration may be due to the effect of AMA on reprogramming metabolism toward glycolysis in addition to its effect on rising ROS generation that increases mitochondrial fragmentation, which in turn increase glycolysis. Hung and co-workers (2012) results confirm our finding; they found that treating human gastric cancer SC-M1 cells with AMA induced cell migration due to mitochondrial dysfunction. While Kouvroukoglou and co-workers (1998) suggest that AMA has no effect on cell migration in MatLu cell line; a variant of the Dunning R-3327 rat prostate adenocarcinoma model. This novel finding suggests that targeting mitochondrial oxidative phosphorylation with the anticancer agent AMA in sub-lethal concentration can increase

cancer metastasis, while, fragmentation of mitochondria mediated by AMA can increase resistance to apoptosis.

## **Chapter Six: Role of p66shc and TRAP1 proteins in cancer cell migration.**

### **6.1 Introduction:**

Protein p66shc is one of three shc isoforms and plays an important role in the cellular response to oxidative stress through inducing apoptosis (Pacini et al., 2004). Like the other two shc isoforms, p52shc and p46shc, p66shc has a tyrosine activation site which activates after growth factor receptor activation. However, it has no effect on Ras signaling pathway (Bonfini et al., 1996, Migliaccio et al., 1997, Trinei et al., 2002).

Oxidative stress which is the result of over accumulation of ROS in the cell is due to an imbalance between ROS production and cellular antioxidant system, and it is responsible for cell damage, necrosis, and apoptosis through oxidation and degradation of several macromolecules including lipids, proteins, and DNA (Elahi et al., 2009, De Marchi et al., 2013).

Protein p66shc is localized in different subcellular compartments and can be activated in response to oxidative stress induced by UV radiation, H<sub>2</sub>O<sub>2</sub> treatment, and high glucose (hyperglycaemia) (Migliaccio et al., 1999, Sun et al., 2010, Lebedzinska-Arciszewska et al., 2015). It is activated through phosphorylation at ser36 residue by PKC- $\beta$ , which facilitates its translocation to the intermembrane space (IMS) of mitochondria via TIM/TOM mitochondrial import machinery. In IMS, p66shc oxidizes cytochrome c and catalyzes the reduction of O<sub>2</sub> to generating H<sub>2</sub>O<sub>2</sub>, which leads to elevating mitochondrial ROS level. This ROS can cause opening of mitochondrial permeability transition pore (PTP), which increases permeability of mitochondrial membrane to ions. This leads to swelling and disruption of the outer mitochondrial membrane (OMM) and release of cytochrome c; a pro-apoptotic factor which lead to formation of the apoptosome and activation of caspase proteins triggering cell death (Galimov, 2010, Lebedzinska-Arciszewska et al., 2015), as illustrated in Figure 6.1.

In normal cells high level of glucose causes oxidative stress and in turn triggers p66shc activation and apoptosis (Pagnin et al., 2005, Xi et al., 2010, Hung et al., 2014), while, several types of cancer cells exhibit high expression of p66shc without inducing apoptosis (Lebiedzinska-Arciszewska et al., 2015). On the contrary, high expression of p66shc enhances cell proliferation, migration and invasion (Zhu et al., 2013, Takatani-Nakase et al., 2014).

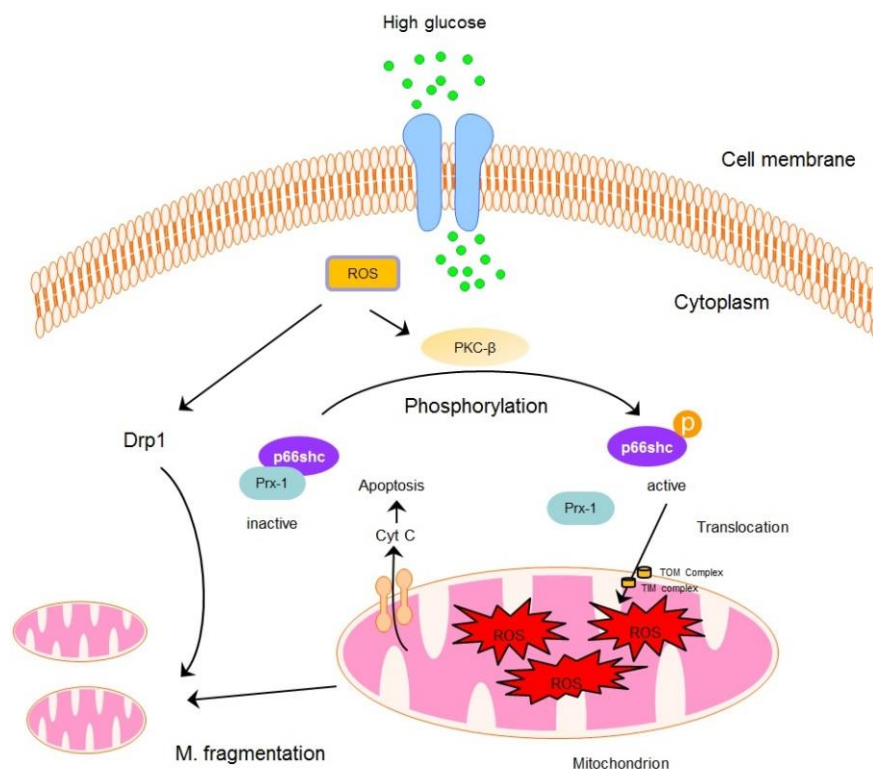


**Figure 6.1: Impact of glucose on mitochondrial dynamics.** Oxidative stress due to high glucose activates protein kinase C-β isoform activate p66Shc via phosphorylation of Ser36, allowing transfer of it from the cytosol to the mitochondrion through TIM-TOM import system. In the mitochondrion, p66Shc can oxidizes cytochrome C and catalyzes the reduction of O<sub>2</sub> to H<sub>2</sub>O<sub>2</sub>, which induces opening of the mitochondrial permeability transition pore (PTP). This increase permeability of mitochondrial membrane to ions, solutes and water, swelling and disruption of the organelle, and consequent release of pro-apoptotic factors into the cytosol.

p66Shc also plays important role in metabolism, in the study by Soliman and co-workers (2014), they concluded that p66Shc has a suppressive effect on cancer cell metabolism through dampening growth factor signalling(Lebiedzinska-Arciszewska et al., 2015).

Although, until now it is not clear how activation of p66shc affects metabolism. However, may be that activated p66shc affects metabolism through disrupting electron transport chain through oxidizing cytochrome c; the small haemoprotein component of the electron transport chain in mitochondria, in which heme group accepts electrons from complex III and transfers electrons to the complex IV.

Recently it was revealed that Tumor Necrosis Factor (TNF) receptor-associated protein 1 (TRAP1); a mitochondrial chaperone protein highly expressed during cellular stress (Liu et al., 2010), especially in cancer cells (Ghosh et al., 2010, Leav et al., 2010), protects cells from apoptosis induced by oxidative stress (Matassa et al., 2011). It was suggested that TRAP1 chaperone protects cells through binding and inhibiting cyclophilin D; a peptidyl-prolyl cis-trans isomerase enzyme which is located in the mitochondrial matrix and it catalyses protein folding. Mitochondrial oxidative stress can induce cyclophilin D to interact with the permeability transition pore (PTP) complex, forming and opening non-selective pores in the mitochondrial inner membrane allowing the release of cytochrome c; a first step in triggering apoptosis (Xiang et al., 2010, Matassa et al., 2011, Su et al., 2013)

Besides the protective effect of TRAP1, it has been suggested that it can promote growth of cancer cells through inhibiting succinate dehydrogenase, complex II of the respiratory chain and switching metabolism to aerobic glycolysis which is important for cancer cell growth (Sciacovelli et al., 2013). However, the mechanism remains unclear.

Despite upregulation of cytoprotective TRAP1 expression in several cancer cells, its relation to p66shc, which is overexpressed under oxidative stress remains unclear, as well as their effect on the metabolism and the cell migration have not been studied well.

We suggest that cancer cells upon exposure to oxidative stress, upregulate expression of TRAP1 to prevent apoptosis which can be induced by activated p66shc. While, generated mitochondrial ROS can inhibit oxidative phosphorylation and thus promote glycolysis that increase cancer cell migration.

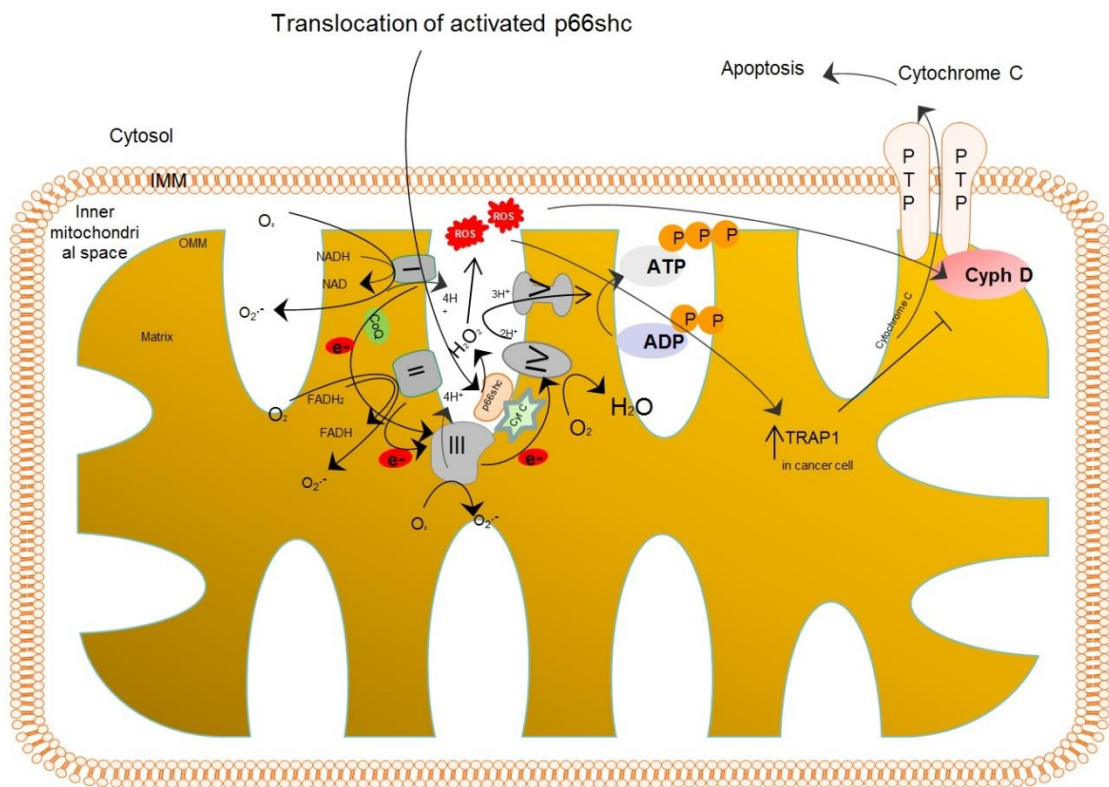


**Figure 6.2: Mitochondrial electron transport chain.** Electrons were passing through complexes I, II, and III, then transferred from cytochrome C to complex IV. Flow of electron is accompanied by proton transfer across the membrane, producing both a chemical gradient ( $\Delta pH$ ) and an electrical gradient ( $\Delta \psi$ ). Protons can reenter the matrix via complex V or ATP synthase providing the energy for ATP synthesis. Translocated activated p66shc oxidize cytochrome c, this rise ROS that induce cytochrome c to bind and open PTP consequently release of cytochrome C and trigger apoptosis. TRAP1 that also induced by high ROS can avoid binding cytochrome c and prevent apoptosis.

In this chapter we aimed to study the impact of silencing p66shc and TRAP1 on the cancer cell migration and metabolism through measuring generated ATP and lactate in three cell lines MDA-MB-231 breast cancer cell, HT1080 fibrosarcoma cell line, and HeLa cell.

## 6.2 Materials and Methods

### 6.2.1 Materials

- On-TARGET plus Human TRAP1 siRNA-Smart pool with following targets were obtained from Dharmacon GE Company.

Target sequence 1    GAGAUGUGGUAACGAAGUA

Target sequence 2    UAACCAGCCUCUCAGAAUA

Target sequence 3    GCUCCAGCGUUGCACUGUA

Target sequence 4    GAUUGCUGCUGGACUUGUU

- On-TARGET plus Non-target TRAP1 siRNA from Dharmacon GE Company with following target sequence

Target sequence      UGGUUUACAUGUCGACUAA

- DharmaFECT 1 Transfection Reagent and DharmaFECT 4 Transfection Reagent were obtained from Thermo Scientific, UK.
- 5X siRNA Buffer, 100ml obtained from Dharmacon GE Company.
- P66shc siRNA were designed depending on instruction by Sigma-Aldrich, UK.

With the following targets.

Target sequence 1    UGAGUCUCUGUCAUCGCUG

Target sequence 2    AUAGUCCCACUACCCUGUG

Target sequence 3    AGCAACCUGAGGCUGGCCA

### 6.2.2 Cell culture

In the present study, we used three cell lines; MDA-MB-231 breast adenocarcinoma cell line, HT1080 fibrosarcoma cells line, and HeLa cells line. MDA-MB-231 cells were continuously cultured in Dulbecco's Modified Eagles Media (DMEM) with relevant glucose levels (5.5, and 25mM) supplemented with 10% FBS, 1% L-glutamine, 100 Unit/ml of penicillin and 100 µg/ml of streptomycin (Gibco), at 37°C in a humidified

atmosphere containing 5% CO<sub>2</sub>. HT1080 and HeLa cells were cultured in Eagle's Minimum Essential Medium (EMEM) instead of DMEM.

Cells were grown in T-75 (75 cm<sup>2</sup>) culture flasks and during experiments cells were grown in T-75 (75 cm<sup>2</sup>) culture flasks for western blot, in twelve wells plate for time-lapse microscope imaging or immunostaining, or in 96 well plates for measuring ROS, ATP, and lactate production.

### **6.2.3 siRNA Transfection**

Small interfering RNA (siRNA) transfection is considered a potent gene silencing method, in which a double-stranded RNA, of short length (21-23 base pairs), is used to inhibit gene expression. The mechanism of siRNA action can explain in brief, the double-strand RNA (dsRNA) is delivered into cultured cells by transfection reagents. We used DharmaFECT reagent from Dharmacon, DharmaFECT 1 for HeLa cells, and DharmaFECT 4 for MDA-MB-231, and HT1080 cells, depending on the manufacturer instructions. The dsRNA is complexed with reagent making packaging particles called liposomes that can be uptake easily by the cells. Once entered into the cell, dsRNA will be processed to siRNA by the RNase III enzyme Dicer. Then the siRNA binds to the RNA inducing silencing complex (RISC), which dissociates and degrades the sense strand. While, the other strand (antisense strand) remains with the RISC complex, and assists in the identification of target mRNA sequence that is complementary to this single stranded siRNA. Upon recognition of the target, it will cleave mRNA by activated RISC, and then it will be degraded by cellular machinery, resulting in of downregulation of gene expression.

We performed a silencing of TRAP1 and p66shc genes using a commercial available TRAP1 siRNA and our designed p66shc siRNA. Cells were transfected with 25 nM of either TRAP1 siRNA, p66shc siRNA, combination of TRAP1& p66shc siRNA, or with scrambled siRNA. Oligonucleotide stock solutions of 20µM were prepared depending to the manufacturer's instructions.

Prior to transfection, cells were seeded at density mentioned in Table 6.1 and incubated overnight under normal growth conditions for cancer cells. In the day of transfection, depending on Dharmacon protocol for siRNA transfection two sets of 4 tubes were prepared. In the first set, oligonucleotides were diluted to the desired concentration (25nM) in antibiotic and serum free high glucose medium. In the second set, transfection reagent was diluted in antibiotic and serum free high glucose medium; DharmaFECT reagent type 1 was diluted to final concentration (1 $\mu$ L / ml), while, DharmaFECT reagent type 4 was diluted to final concentration (0.5 $\mu$ L / ml). Next, all tubes were incubated for 5 minutes in room temperature (RT), then content of each tube in set 2 were mixed with same tube in set1 and incubated for 20 minutes in RT allowing complexes to form. Later, the volume of each tube was completed to the final used volume using complete medium (without antibiotic), then used for treating cells. After 12 hrs of incubation, transfection medium was replaced with complete medium to reduce cytotoxic effects of the transfection reagent, and then cells were incubated again to complete total 48hrs.

#### **6.2.4 Immunostaining**

Immunostaining was performed using specific primary anti-p66Shc antibody (Cell Signaling Technology) to measure activated p66shc after 48hrs of gene silencing as described in section 2.2.8. However, mitochondria were also stained with MitoTracker probe prior to fixation step. Images were taken using confocal microscopy and analysed by ImageJ software as explained in section 2.2.16.

#### **6.2.5 Quantitative Real- Time PCR (qRT-PCR)**

The Quantitative real time polymerase chain reaction (qRT-PCR) was used to measure mtDNA copy number as described in section 2.2.10. DNA was extracted after 48hrs of gene knockdown. Primers for the t-RNA gene (for mitochondrial) and the  $\beta$ -actin gene locus (for nuclear) were used to calculate amount of mtDNA and nucDNA.

**Table 6.1: The cell numbers used in the experiments**

Experiment	Plates (surface area)	Seeding Density
Time-lapse Live imaging	12 well plate (3.9 cm <sup>2</sup> )	0.5X10 <sup>4</sup> /well/ml
Immunostaining	12 well plate (3.9 cm <sup>2</sup> )	1X10 <sup>4</sup> /well/ml
Western blot	T-75 flask (75 cm <sup>2</sup> )	1X10 <sup>6</sup> /flask/10ml
ATP measuring	T-25 flask (25 cm <sup>2</sup> )	3X10 <sup>5</sup> /flask/5ml
ROS, and Lactate measuring	96 well plate (0.3cm <sup>2</sup> )	2.5X10 <sup>3</sup> /well/100μL

### 6.2.6 Analysis of metabolism and ROS

ATP, lactate, and ROS production were measured using specific commercial kits as described in sections 2.2.14, 2.2.13, and 2.2.12 respectively, after 48hrs of gene knockdown.

### 6.2.7 Western Blot

Western blot was used to evaluate protein expression. The total protein was isolated using RIPA lysis buffer containing a cocktail of protease inhibitors (PI), as described in section 2.2.3. Expression of total p66Shc and TRAP1 were assessed, using anti-p66Shc, anti-TRAP1 respectively.

### 6.2.8 Apoptosis

Time-lapse microscopy was used for monitoring cell death after 24hrs of silencing p66shc and TRAP1 genes. NIS-Elements, Nikon's imaging software were used to take a series of images every 15minutes for 24hrs, and ImageJ software was used for data analysis through the cell counter plugin as described in chapter two in section 2.2.18 in page 66.

### 6.2.9 Cell migration

Time-lapse microscopy was used to track single cell migration after 24hrs of silencing genes and for duration of 24hrs, and 24hrs ImageJ (Fiji) software (MtrackJ plugin) was used to measuring the speed of cell movement as described in section 2.2.17.

## 6.3 Results:

### 6.3.1 TRAP1 and p66shc gene silencing efficiency

To evaluate the efficiency of silencing p66shc and TRAP1 genes on the expression of their proteins in the cancer cells, MDA-MB-231, HT1080, and HeLa cells were grown at a density of  $1 \times 10^6$  cells/75cm<sup>2</sup> flask in high glucose (25mM) DMEM medium (except normal glucose control) overnight under humidified condition at 37°C and 5% CO<sub>2</sub>. Then cells were transfected with (25nM) of smart pool of p66shc siRNA and /or TRAP1 siRNA using Dharmacon transfection reagent. Western blot analysis was then performed to measure protein p66shc and TRAP1 expression.

We normalized our data to the high glucose control, as we used high glucose to induce expression of proteins p66shc and TRAP1. Normal glucose control was used to confirm that high glucose induced the expression of these proteins.

Normalized results showed in Figure 6.3A, revealed that expression of protein p66shc in MDA-MB-231 cells was decreased significantly after knockdown of p66shc and TRAP1 genes alone and in combination together. Compared to scrambled treatment in which the expression of p66shc was  $94.4\% \pm 14.9$ , it was decreased to  $46.4\% \pm 1.76$  in p66shc siRNA treatment ( $p < 0.05$ ). Also we found that TRAP1 gene knockdown as well as combination of TRAP1 and p66shc gene knockdown were affected the expression of the protein p66shc which decreased to  $33.2\% \pm 10.4$  and  $28.1\% \pm 4.9$  respectively compared to p66shc protein expression in scrambled treatment ( $p < 0.01$ ).

Then we measured the expression of the protein TRAP1 in MDA-MB-231 cells after silencing p66shc gene and TRAP1 gene alone and in combination together. Normalized results in Figure 6.3B, revealed that expression of protein TRAP1 was reduced markedly from  $81.7\% \pm 3.5$  in scrambled treatment to  $46.5\% \pm 8.9$ ,  $43.8\% \pm 10.7$ , and  $44.8\% \pm 7.4$  in p66shcsiRNA, TRAP1siRNA, and combination of p66siRNA and TRAP1siRNA treatments respectively ( $p < 0.05$ ).

The Figures also showed that in the normal glucose control, expression of p66shc and TRAP1 proteins was lower than in high glucose control, with  $63.3\% \pm 6.83$  and  $49.3\% \pm 8.5$  for p66shc and TRAP1 respectively in normal glucose compared to them in high glucose at ( $p < 0.05$ , and  $p < 0.01$ ) respectively.

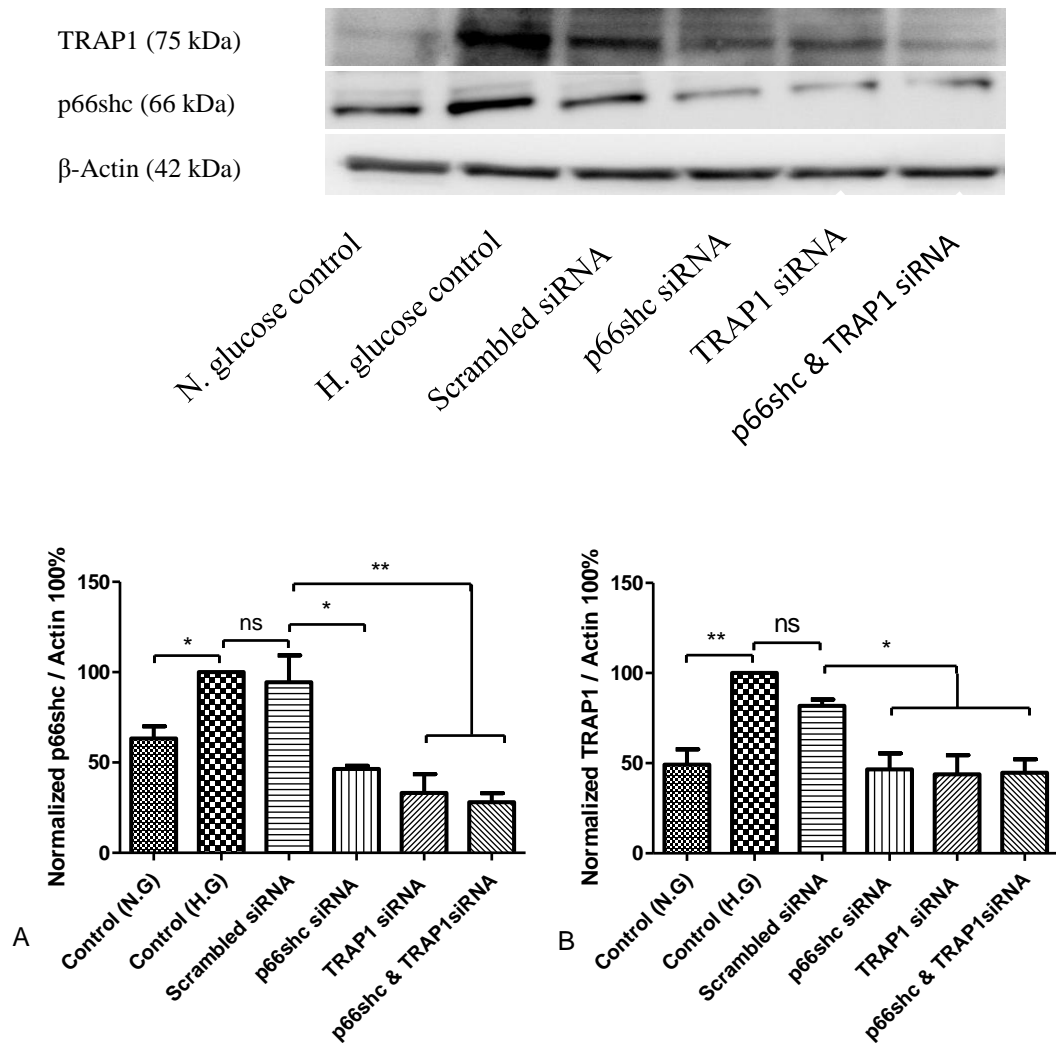


**Figure 6.3: Western blot of p66shc and/or TRAP1 proteins in MDA-MB-231 cells after 48hrs of silencing p66shc and TRAP1 genes.** Cells cultured in high glucose medium overnight then transfected with 25nM of p66shc siRNA and/or TRAP1 siRNA. (A) Western blot analysis of expression of p66shc protein, and (B) Western blots analysis of expression of TRAP1 protein. Data represents the mean  $\pm$  standard error of three independent experiments performed in triplicate. One-way ANOVA followed by Dunnett's Multiple Comparison Test to compare mean of treatments with mean of scrambled siRNA. (\*, and \*\*represent  $P < 0.05$ , and  $0.01$  respectively).

When we measured the expression of the protein p66shc and TRAP1 in HT1080 cells to know the efficiency of silencing p66shc and TRAP1 genes, we found significant decreases in the expression of p66shc from  $92.85\% \pm 5.37$  in non-target siRNA treatment to  $54.95\% \pm 8.2$ , and  $52.5\% \pm 11.46$  in p66shcsiRNA, and TRAP1siRNA treatments ( $p < 0.05$ ), whereas, statistically no significant differences were observed between the treatment where both genes silenced and non-target siRNA treatment, as seen in Figure 6.4A.

Figure 6.4B shows the results of the expression of protein TRAP1 in HT1080 cells after silencing of p66shc and TRAP1 genes, and we found that expression of this protein was reduced significantly. It was reduced from  $106.4\% \pm 5.48$  in scrambled siRNA treatment to  $74.65\% \pm 9.89$ ,  $74.4\% \pm 7.96$ , and  $72.87\% \pm 4.61$  in p66shc siRNA, TRAP1 siRNA, and combination of both genes knockdown treatments respectively ( $p < 0.05$ ).

The results also shows the increases in the expression of both proteins in high glucose control compared to normal glucose control. The expression of p66shc protein was  $52.3\% \pm 7.5$  ( $p < 0.01$ ) and protein TRAP1 was  $72.7\% \pm 5.65$  ( $p < 0.05$ ) in normal glucose control compared to them in high glucose control.

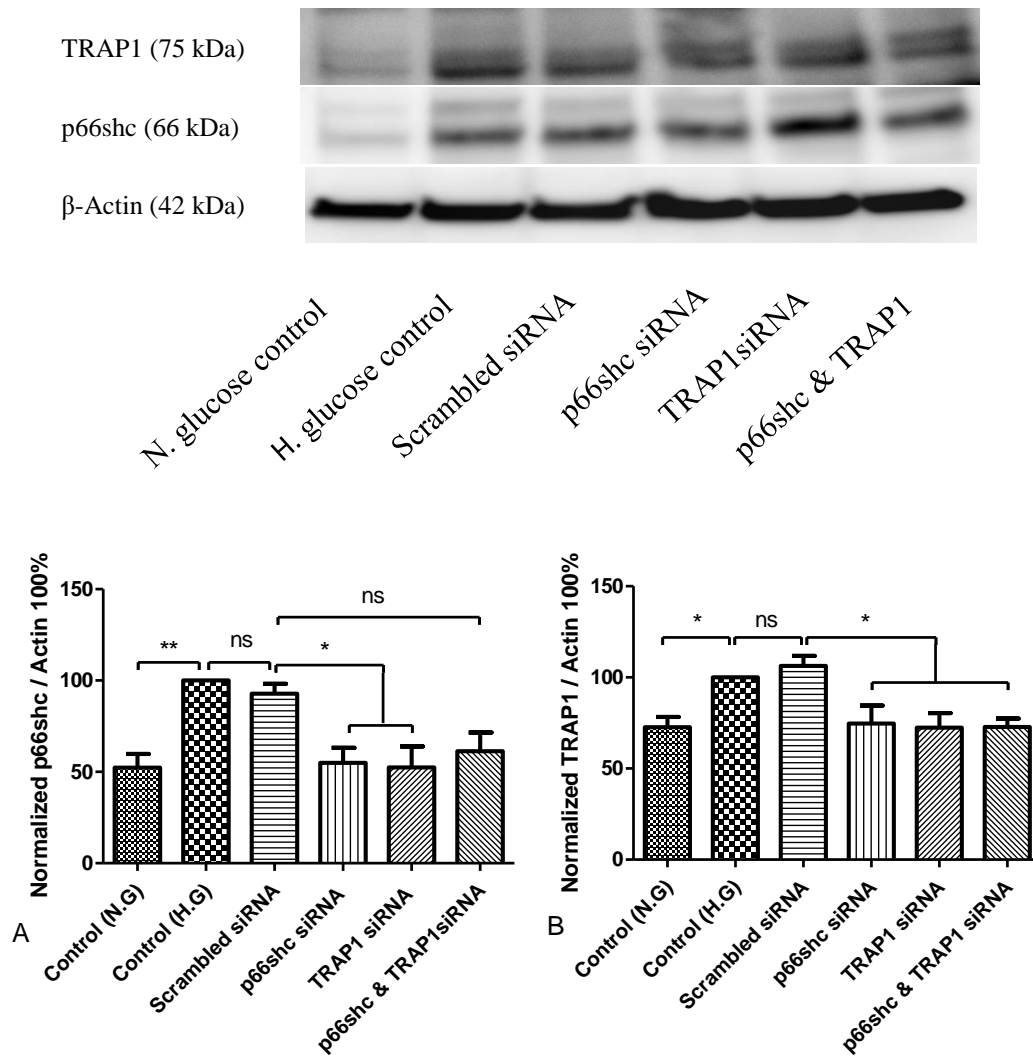


**Figure 6.4: Western blot of p66shc and/or TRAP1 proteins in HT1080 cells after 48hrs of silencing p66shc and TRAP1 genes.** Cells cultured in high glucose medium overnight then transfected with 25nM of p66shc siRNA and/or TRAP1 siRNA. (A) Western blot analysis of expression of p66shc protein, and (B) Western blots analysis of expression of TRAP1 protein. Data represents the mean  $\pm$  standard error of three independent experiments performed in triplicate. One-way ANOVA followed by Dunnett's Multiple Comparison Test to compare mean of treatments with mean of scrambled siRNA. (\*, and \*\*represent  $P < 0.05$ , and  $0.01$  respectively).

Afterward the efficiency of silencing p66shc and TRAP1 genes in HeLa cells on the expression of their protein was measured via western blot. Results in Figure 6.5A, show that p66shc expression was reduced from  $88.4\pm 3.57$  in scrambled siRNA treatment to  $51.4\pm 7.6$ ,  $49.3\pm 8.9$ , and  $58.9\pm 6.68$  in p66shc siRNA, TRAP1siRNA, and both gene knockdown treatments respectively ( $p<0.05$ ). Figure 6.5A also shows that high glucose induced significant increases in the expression of this protein, and its expression in normal glucose was  $50.95\pm 15.2$  of it in high glucose ( $p<0.01$ ).

In Figure 6.5B, results showed that silencing the TRAP1 gene was efficient in reducing expression of protein TRAP1, it was reduced to  $59.8\pm 6.65$  compared to  $95.9\pm 2.76$  in scrambled siRNA treatment ( $p<0.05$ ), while, in other treatments statistically no significant differences were recorded compared to scrambled siRNA treatment. The results also confirm that high glucose enhanced expression of TRAP1 protein, with its expression of  $55\pm 6.64$  in normal glucose compared to high glucose control ( $p<0.001$ ).

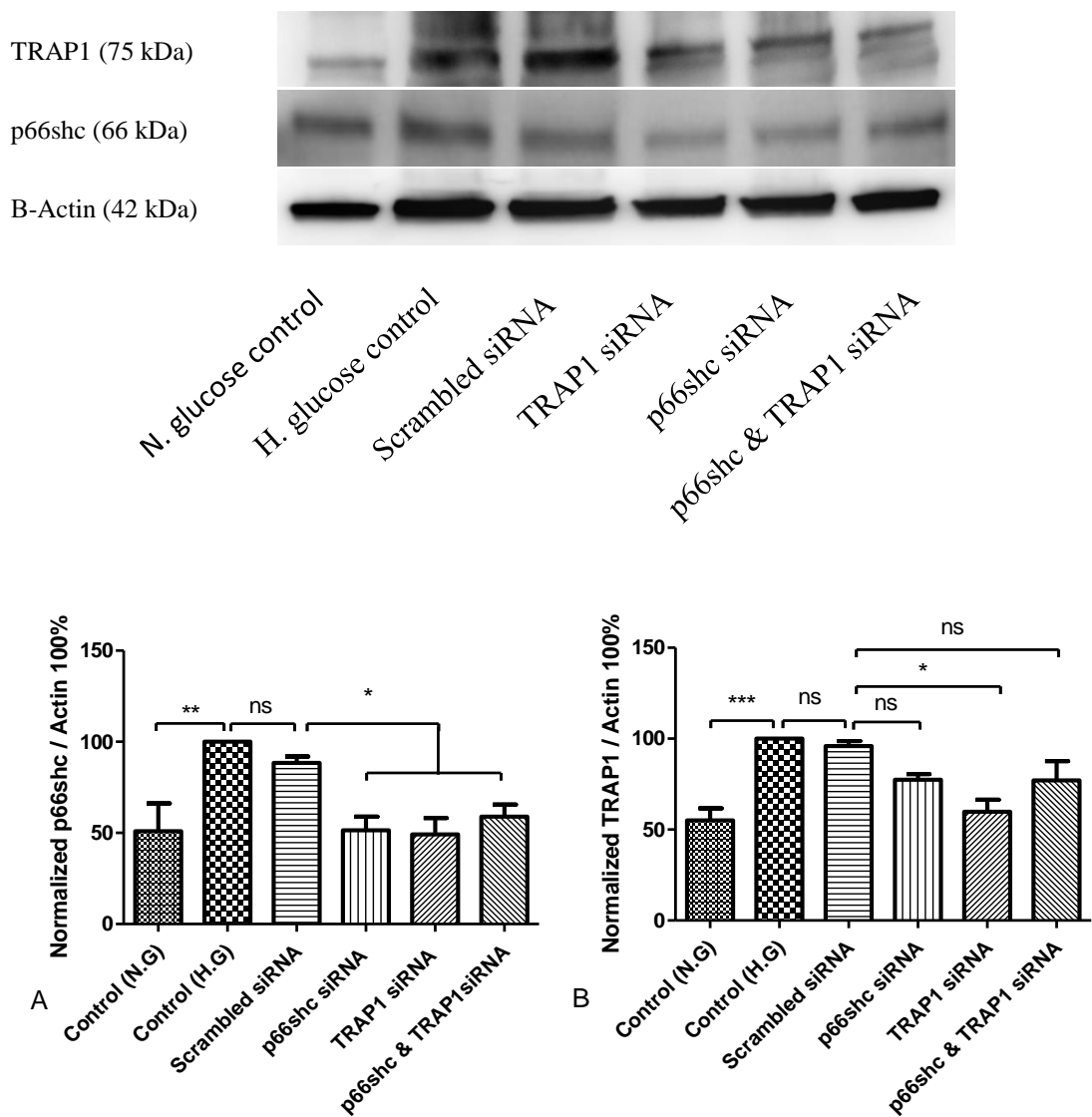


**Figure 6.5: Western blot of p66shc and/or TRAP1 proteins in HeLa cells after 48hrs of p66shc and TRAP1 genes knockdown.** Cells cultured in high glucose medium overnight then transfected with 25nM of p66shc siRNA and/or TRAP1 siRNA. (A) Represent western blot analysis of expression of p66shc protein, and (B) Western blots analysis of expression of TRAP1 protein. Data represents the mean  $\pm$  standard error of three independent experiments performed in triplicate. One-way ANOVA followed by Dunnett's Multiple Comparison Test to compare mean of treatments with mean of scrambled siRNA. (\*, \*\*, and \*\*\*represent  $P < 0.05$ ,  $0.01$ , and  $0.001$  respectively).

### 6.3.2 Effect of silencing p66shc and/or TRAP1 genes on the activation of p66shc in MDA-MB-231 cells.

To evaluate the effect of silencing p66shc and TRAP1 on the activated p66shc, MDA-MB-231 cells were grown in high glucose medium (except normal glucose control) overnight. Cells were then transfected with p66shc siRNA and /or TRAP1siRNA for 48hrs. Next cells were subjected to staining with a mitochondrial probe, and the immunofluorescence analysis with anti-p66shc antibody. Images were taken using confocal microscopy and ImageJ software was used to measure activated p66shc in treated cells compared to scrambled siRNA. Figure 6.6 and micrographs in Figure 6.7 show that silencing of p66shc and TRAP1 genes alone and together led to significant decline of activated p66shc compared to scrambled siRNA. The mean of activated p66shc was decreased to  $140.6 \pm 4.2$ ,  $102.3 \pm 9.9$ , and  $142.7 \pm 7.5$  in p66shc siRNA, TRAP1 siRNA, and combination p66shc & TRAP1 siRNA treatments respectively compared to  $204.5 \pm 2.6$  in scrambled siRNA treatment ( $p < 0.001$ ).

Analysis of data also found that the mean of activated p66shc was increased from  $93.3 \pm 20.7$  in normal glucose control to  $220.2 \pm 14.6$  in high glucose control ( $p < 0.001$ ), whereas, no significant differences in the mean of activated p66shc was detected between high glucose control and scrambled siRNA treatment.

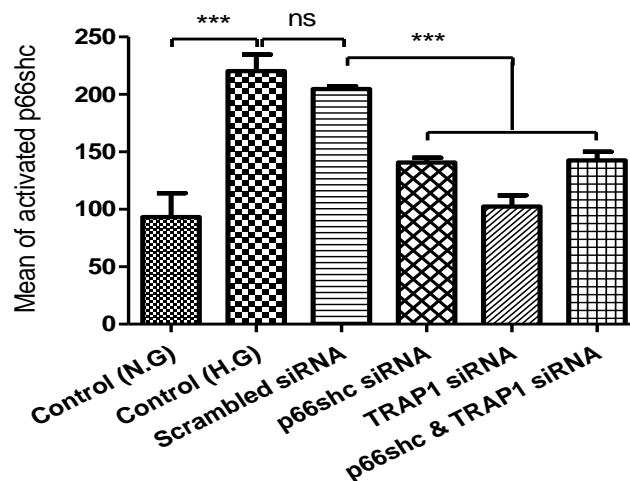


**Figure 6.6:** Effect of silencing p66shc and TRAP1 on the activation of protein p66shc in MDA-MB-231 cells. After transfection cells with p66shc siRNA and/or TRAP1 siRNA, cells subjected to immunofluorescence analysis using anti-p66shc (green) antibody and mitochondrial probe (red). Data represents the mean  $\pm$  standard error of three independent experiments performed in triplicate. One-way ANOVA followed by Dunnett's Multiple Comparison Test to compare mean of treatments with mean of scrambled siRNA. (\*\*\*)represent  $P < 0.001$ .

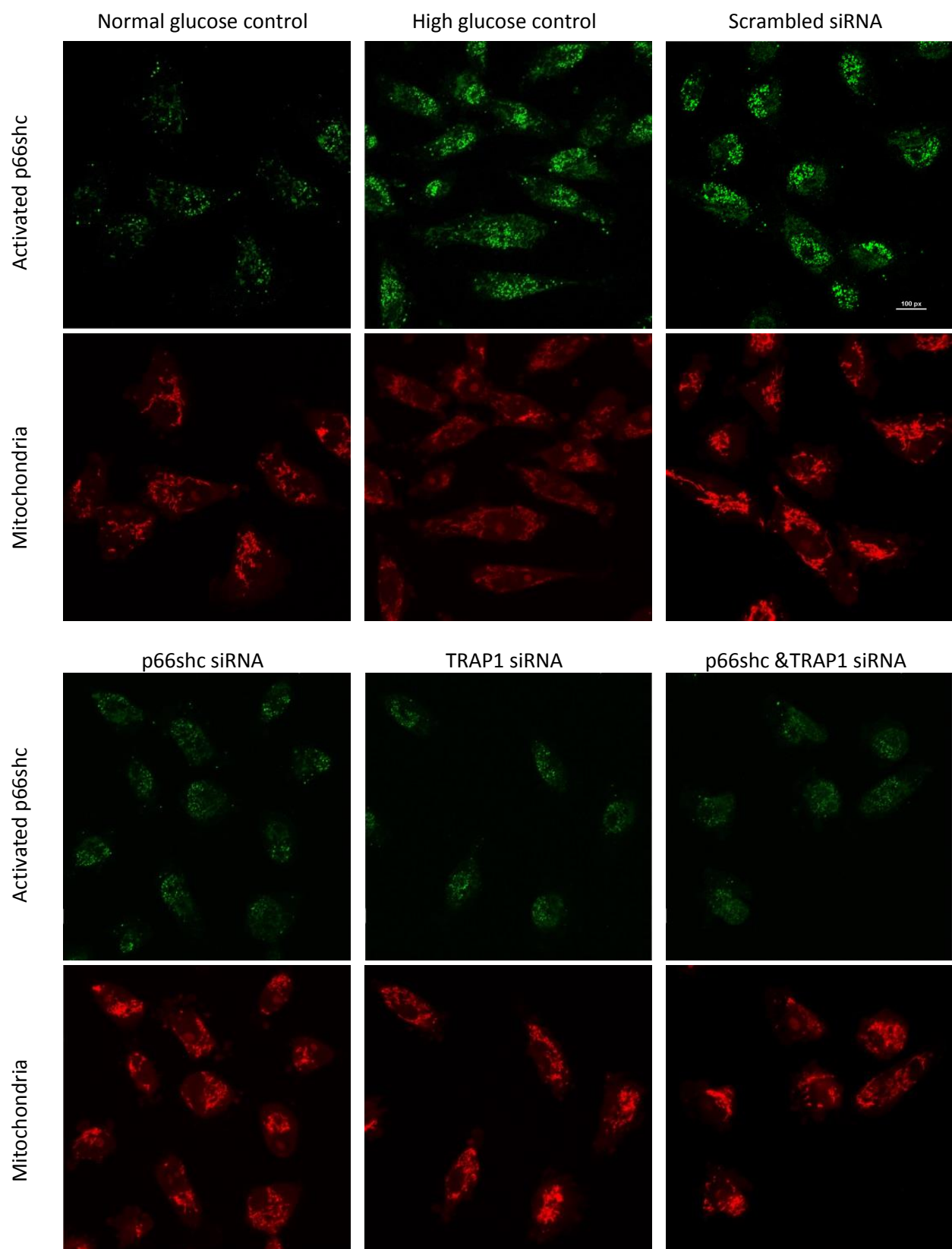


**Figure 6.7:** Microscopic images shows activated p66shc in MDA-MB-231 cells after 48hrs of silencing p66shc or/and TRAP1 genes. Green fluorescence represents activated p66shc, and red fluorescence represents mitochondria. Scale bar= 100pixel

### 6.3.3 Effect of silencing p66shc and/or TRAP1 genes on apoptosis in MDA-MB-231 cells.

TRAP1 prevents opening of mitochondrial permeability transition pores and consequently prevents apoptosis. To investigate its silencing effect on the apoptosis, we grew MDA-MB-231 cells in high glucose (25mM) DMEM medium (except normal glucose control) overnight. Then cells were transfected with (25nM) of smart pool of p66shc siRNA and/or TRAP1 siRNA after 24hrs from transfection, plate transferred to time-lapse microscope for monitoring cell death during next 24hrs. Our results revealed that silencing TRAP1 significantly induced cell death compared to scrambled siRNA; it was increased from  $6.1\% \pm 0.26$  in the scrambled siRNA treatment to  $18.1\% \pm 1.98$  in silencing TRAP1 treatment, while, statistically no significant differences were found in cell death between silencing p66shc alone or together with TRAP1 compared to scrambled siRNA, as shown in figure 6.8

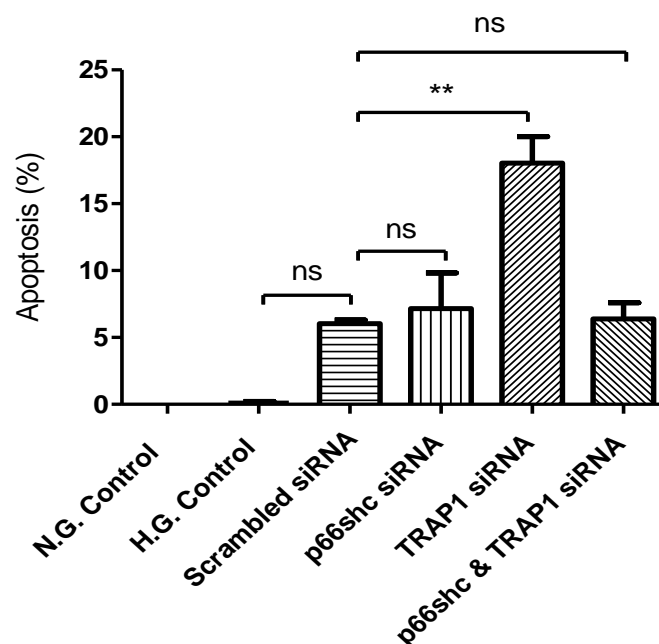


**Figure 6.8: Effect of Silencing p66shc and TRAP1 genes on cell death in MDA-MB-231 cells.** Cells were transfected with 25nM of p66shc siRNA and/or TRAP1 siRNA for 48hrs after have been cultured in high glucose medium overnight. Scrambled siRNA treated with 25nM of non-target siRNA, whereas, N.G and H.G controls were treated only with DharmaFECT reagent. Cell death was measured by time-lapse microscopy for 24hrs (during transfection time). Data represents the mean  $\pm$  standard error of three independent experiments performed in triplicate. One-way ANOVA followed by Dunnett's Multiple Comparison Test used to compare mean of treatments with mean of scrambled siRNA (\*\*represent  $P < 0.01$ ). Dharma-FECT 1

#### **6.3.4 Effect of silencing p66shc and/or TRAP1 genes on the intracellular ROS production.**

To uncover the effect of silencing p66shc and TRAP1 genes alone and together on the ROS production, specific commercial ROS assay kit was used to measuring generated intracellular ROS by cells. The genes, p66shc and TRAP1 were silenced in three cell lines, MDA-MB-231, HT1080, and HeLa cells, and after 48hrs of silencing genes, the intensity of fluorescence DCF which equivalent to generated ROS has been read with fluorometric plate reader at 485nm/535nm. The result in Figure 6.9A shows that in MDA-MB-231 cells silencing of p66shc alone or with TRAP1 led to decreases in the ROS production, it was decreased markedly from a mean of  $32142.3 \pm 2085$  in scrambled siRNA treatment to a mean of  $18237.8 \pm 2427$  in p66shc siRNA treatment ( $p < 0.01$ ), and into a mean of  $20381.8 \pm 2867$  in combination of p66shc siRNA and TRAP1 siRNA treatment ( $p < 0.05$ ); this mean that ROS production was decreased by 43.3%, and 36.6% in p66shc siRNA treatment and in combination of p66shc siRNA and TRAP1 siRNA treatment respectively. No significant differences in the ROS production were observed when the TRAP1 gene silenced alone.

Results for HT1080 cells revealed that silencing of p66shc gene reduced the generation of ROS significantly, while, other treatments did not cause significant differences. As seen in Figure 6.9B, ROS production was decreased to  $17764 \pm 2650$  in p66shc siRNA treatment compared to  $32966.3 \pm 4926$  in scrambled siRNA treatment ( $p < 0.05$ ); which is mean it was decreased by 85.6%.

We found that silencing of p66shc and TRAP1 genes alone and together, statistically did not induce significant changes in the ROS production, as shown in Figure 6.9C.

The results also confirmed that high glucose has induced raised ROS production compared to normal glucose in all cell lines, it was increased significantly from  $17186.3 \pm 3470$  in normal glucose control to  $35115.6 \pm 2816$  in high glucose ( $p < 0.001$ ) in MDA-MB-231; which is mean it was increased by 104.4%, in HT1080 cells it was increased from  $16063 \pm 1860$  to  $34301.5 \pm 4456$  ( $p < 0.01$ ); which is mean it was increased by 113.6%, and

in HeLa cells it was increased from  $15915 \pm 2676$  to  $29664.3 \pm 3726$  ( $p < 0.05$ ); which is mean it was increased by 86.4%, as seen in Figure 6.9 A, B, and C.

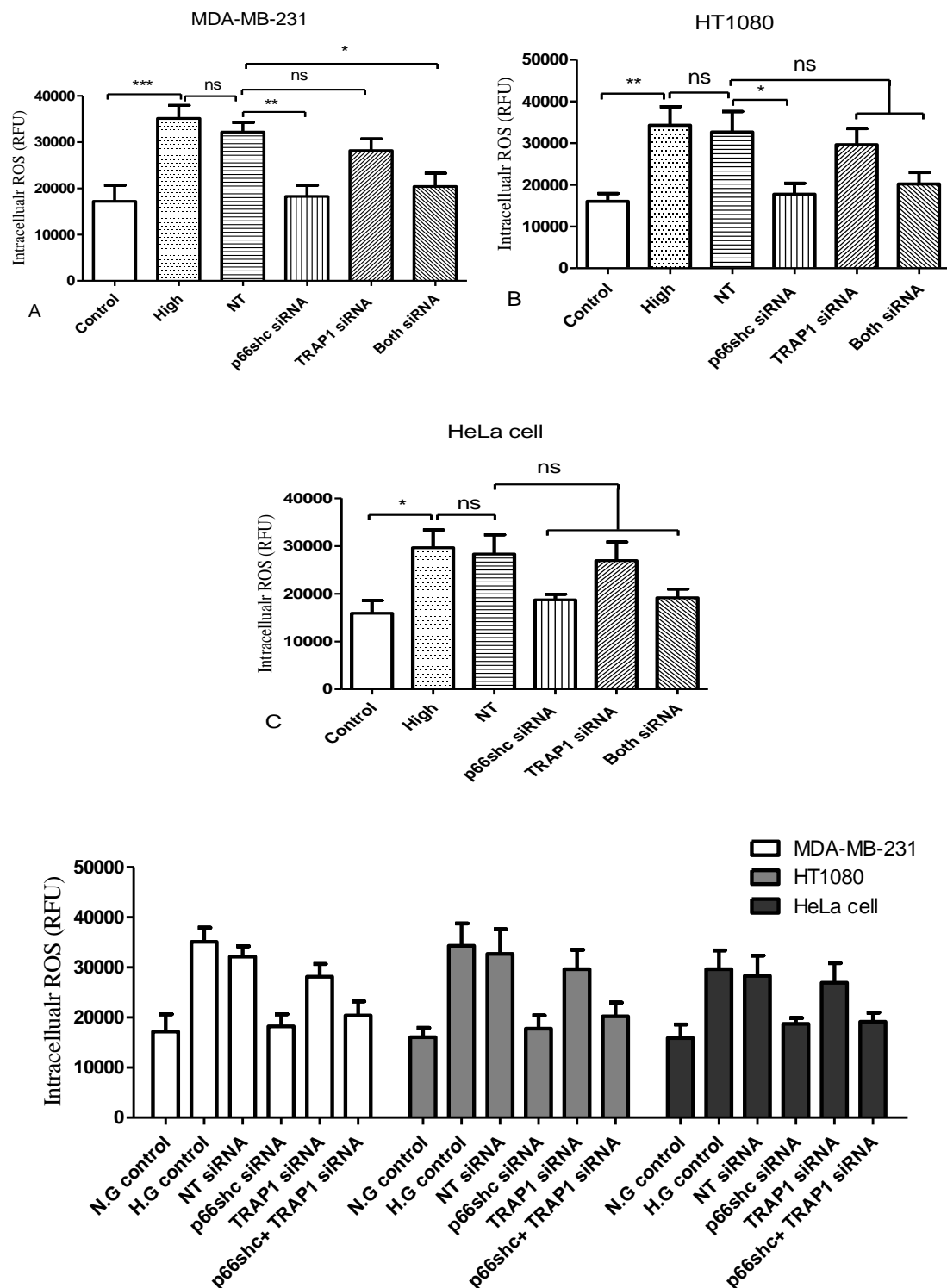


**Figure 6.9: Effect of silencing p66shc or/and TRAP1 genes on the ROS production.** Intracellular ROS production was measured after 48hrs of transfection the cells with p66shc and/or TRAP1 siRNA. A: Represents analysed data of MDA-MB-231 cells, B: data of HT1080 cells, C: data of HeLa cells, and D: graph shows data of all cell lines together. Data represents the mean  $\pm$  standard error of four independent experiments performed in triplicate. One-way ANOVA followed by Dunnett's Multiple Comparison Test to compare mean of treatments with the control mean (\*, \*\*, and \*\*\*represent  $P < 0.05$ ,  $0.01$ , and  $0.001$  respectively).

### 6.3.5 Effect of silencing p66shc and/or TRAP1 genes on cellular metabolism

Activation and translocating of p66shc to mitochondria leads to a rise of ROS level; this can change the mitochondrial microenvironment and affect mitochondrial oxidative phosphorylation enzymes. To investigate the effect of silencing p66shc and TRAP1 genes alone and together on the cellular metabolism, we measured generated ATP and lactate after 48hrs of silencing p66shc and TRAP1 in MDA-MB-231, HT1080, and HeLa cells. The Colorimetric ATP Assay Kit was used to quantify generated ATP in cells, while, The Glycolysis Cell-Based Assay Kit was used to quantify generated L-lactate.

Results of ATP production in MDA-MB-231 cells are shown in Figure 6.10A, and it was revealed that silencing of p66shc and/or TRAP1 genes decreased ATP production significantly. Its production was decreased from  $1.12 \pm 0.15$  mM in scrambled siRNA treatment to  $0.63 \pm 0.098$ , and  $0.59 \pm 0.12$  mM in p66shcsiRNA and TRAP1siRNA treatments respectively ( $p < 0.05$ ), and into  $0.55 \pm 0.08$  mM in treatment of both silenced genes. These mean that ATP production was decreased by 43.2%, 46.5%, and 50.6% in p66shcsiRNA, TRAP1siRNA, and combination of p66shcsiRNA and TRAP1siRNA treatments respectively.

In the HT1080 cells, silencing of p66shc and TRAP1 genes alone or in combination did not cause a significant change in ATP production, as seen in Figure 6.10B.

While, in HeLa cells, ATP production was strongly affected with silencing mentioned genes. Compared to scrambled siRNA treatment, which ATP level was  $1.09 \pm 0.09$  mM, it was decreased sharply to  $0.46 \pm 0.05$  and  $0.43 \pm 0.06$  in p66shcsiRNA treatment and in combination of p66shc siRNA and TRAP1siRNA treatments respectively ( $p < 0.001$ ), and into  $0.54 \pm 0.02$  mM in TRAP1siRNA treatment ( $p < 0.01$ ); which is mean it was decreased by 57.2%, 60.9%, and 50.6% in p66shc siRNA, TRAP1siRNA, and combination of p66shc siRNA and TRAP1 siRNA treatments respectively, as shown in Figure 6.10C.

Figure 6.10 also shows that high glucose increased ATP production compared to normal glucose. In MDA-MB-231 cells ATP production was increased from  $0.42 \pm 0.08 \text{mM}$  in normal glucose control to  $1.29 \pm 0.14 \text{mM}$  in high glucose control ( $p < 0.001$ ); which is mean it was increased by 213.07% in high glucose control, in HT1080 it was increased from  $1.03 \pm 0.2 \text{mM}$  to  $2 \pm 0.22 \text{mM}$  ( $p < 0.05$ ); which is mean it was increased by 95.3% in high glucose control, and in HeLa cells it was increased from  $0.56 \pm 0.09 \text{mM}$  to  $1.02 \pm 0.12 \text{mM}$  ( $p < 0.05$ ); which means it was increased by 82.8% in high glucose control compared to normal glucose control.

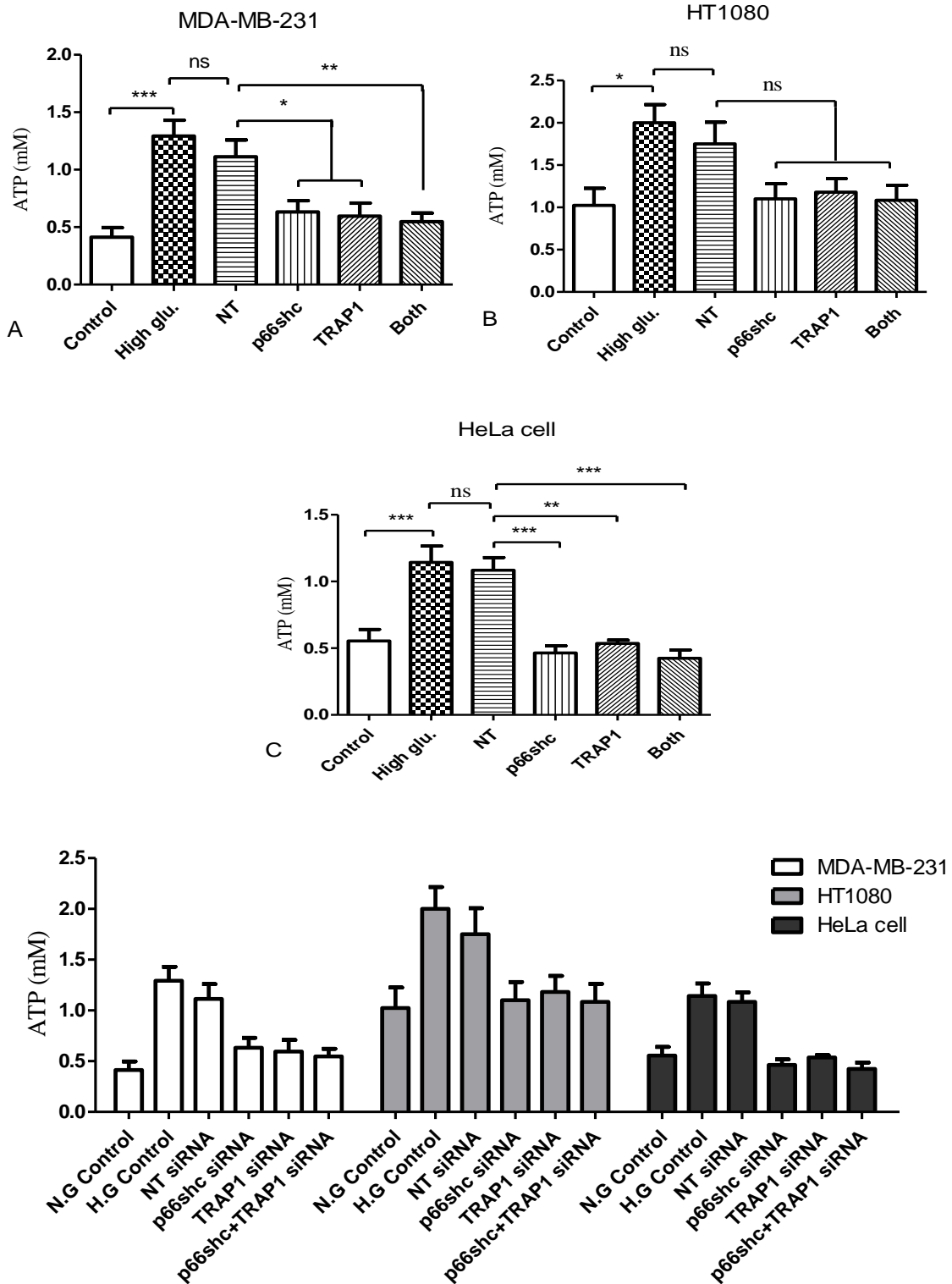


**Figure 6.10: Effect of silencing p66shc and/or TRAP1 genes on the ATP production.** ATP production was measured after 48hrs of transfection the cells with p66shc and/or TRAP1 siRNA using colorimetric ATP assay kit. A: Represents analysed data of MDA-MB-231 cells, B: data of HT1080 cells, C: data of HeLa cells, and D: a graph shows data of all cell lines together. Data represents the mean  $\pm$  standard error of four independent experiments performed in triplicate. One-way ANOVA followed by Dunnett's post hoc test to compare mean of treatments with the mean of scrambled siRNA treatment (\*, \*\* and \*\*\*represent  $P < 0.05$ , 0.01, and 0.001 respectively).

The results of lactate production presented in Figure 6.11 revealed that silencing p66shc and TRAP1 genes alone and together have a strong effect on the production of lactate. In MDA-MB-231 cells, it was decreased from  $0.31\pm 0.0055$  mM in scrambled siRNA treatment to  $0.25\pm 0.004$ ,  $0.21\pm 0.003$ , and  $0.27\pm 0.004$  mM in p66shcsiRNA, TRAP1 siRNA, and in combination of p66shcsiRNA and TRAP1siRNA treatments respectively ( $p < 0.001$ ); which means it decreased by 19.4%, 32.9%, and 13.9% respectively, as seen in Figure 6.11A. Similar results were found when we measured lactate production in HT1080 cells, as shown in Figure 6.11B. It was reduced from  $0.46\pm 0.007$  mM in scrambled siRNA treatment to  $0.42\pm 0.005$ , and  $0.42\pm 0.006$  mM in p66shc siRNA, and combination of p66shc siRNA and TRAP1siRNA treatments respectively ( $p < 0.01$ ), and into  $0.35\pm 0.007$  mM in TRAP1siRNA treatment respectively ( $p < 0.001$ ); which is mean it was decreased by 10.2%, 23.7%, and 8.9% in p66shc siRNA, TRAP1 siRNA, and combination of p66shc siRNA and TRAP1siRNA treatments respectively.

In HeLa cells, results shown in Figure 6.11C confirm that silencing of mentioned genes led to decrease in lactate production. Compared to scrambled siRNA treatment, in which lactate level was  $0.27\pm 0.004$  mM, it decreased to  $0.2\pm 0.003$ ,  $0.16\pm 0.002$ , and  $0.17\pm 0.002$  mM in p66shcsiRNA, TRAP1siRNA, and combination of p66shcsiRNA and TRAP1 siRNA treatments respectively ( $p < 0.001$ ); this means it decreased by 27.3%, 39.9%, and 38% in p66shc siRNA, TRAP1 siRNA, and combination of p66shcsiRNA and TRAP1 siRNA treatments respectively.

The results also showed that lactate production was higher in high glucose compared with normal glucose in all three cell lines. In MDA-MB-231 cells it was increased from  $0.28\pm 0.03$  mM in normal glucose control to  $0.33\pm 0.006$  mM in high glucose control ( $p < 0.001$ ); which means it increased by 20.85%, in HT1080 it was increased from  $0.42\pm 0.007$  mM to  $0.47\pm 0.005$  mM ( $p < 0.01$ ); which means it increased by 9.8%, and in HeLa cells it was increased from  $0.21\pm 0.003$  mM to  $0.29\pm 0.004$  mM ( $p < 0.001$ ); which means it increased by 36.5%.

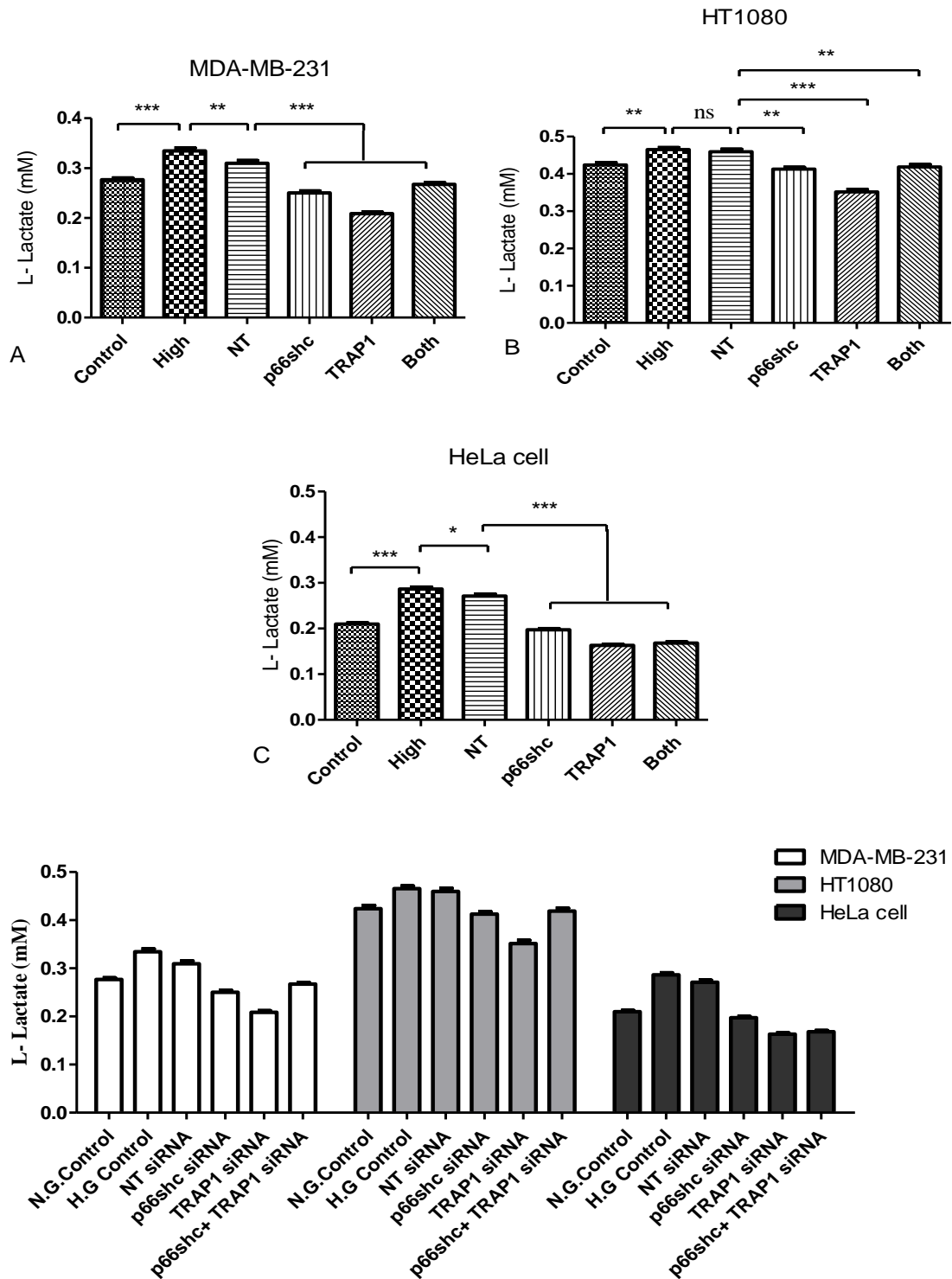


**Figure 6.11: Effect of silencing p66shc and/or TRAP1 genes on lactate production.** Lactate production was measured after 48hrs of transfection the cells with p66shc and/or TRAP1 siRNA using colorimetric lactate assay kit. A: Represents analysed data of MDA-MB-231 cells, B: data of HT1080 cells, C: data of HeLa cells, and D: a graph shows data of all cell lines together. Data represents the mean  $\pm$  standard error of three independent experiments performed in triplicate. One-way ANOVA followed by Dunnett's post hoc test to compare mean of treatments with the mean of scrambled siRNA treatment (\*, \*\* and \*\*\* represent  $P < 0.05$ , 0.01, and 0.001 respectively).

### **6.3.6 Effect of silencing p66shc and/or TRAP1 genes on the cancer cell migration.**

From time-lapse microscopy, cell migration was tracked during 24hrs of MDA-MB-231, HT1080, and HeLa cells on a plastic surface and ImageJ software was used to measure speed of cell movement. Cells were grown in high glucose medium (except normal glucose control) overnight, and then cells were transfected with p66shc siRNA and/or TRAP1 siRNA. 24hrs post transfection; we started imaging of cell migration.

The analysed data in Figure 6.12A shows that silencing p66shc and TRAP1 alone or in combination, led to decreases in cell migration significantly in MDA-MB-231 cells. It was decreased from  $23.6 \pm 0.79 \mu\text{m}/\text{hour}$  in scrambled siRNA treatment to  $10.8 \pm 1.33$ ,  $12.1 \pm 1.35$ , and  $14.1 \pm 0.74 \mu\text{m}/\text{hour}$  in p66shc siRNA, TRAP1 siRNA, and combination of p66shc siRNA and TRAP1 siRNA treatments respectively ( $p < 0.001$ ). Similar results were found for HT1080 cells, as shown in Figure 6.12B. It was decreased from  $26.98 \pm 1.65 \mu\text{m}/\text{hour}$  in scrambled siRNA treatment to  $15.78 \pm 0.22$ ,  $15.47 \pm 0.89$ , and  $16.29 \pm 1.1 \mu\text{m}/\text{hour}$  in p66shc siRNA, TRAP1 siRNA, and combination of p66shc siRNA and TRAP1 siRNA treatments respectively ( $p < 0.001$ ).

Whereas, in HeLa cells, only silencing p66shc gene led to significant decreases in the cell migration. It was decreased from  $12.6 \pm 0.44 \mu\text{m}/\text{hour}$  in scrambled siRNA treatment to  $8.1 \pm 0.34 \mu\text{m}/\text{hour}$  in p66shc siRNA treatment ( $p < 0.001$ ), while, statistically no significant differences were detected between other treatments with scrambled siRNA treatment, as shown in Figure 6.12C

Data also show that high glucose induced cell migration compared to normal glucose in all three cell lines. It was increased from  $16.4 \pm 1.39 \mu\text{m}/\text{hour}$  in normal glucose to  $29.85 \pm 0.33 \mu\text{m}/\text{hour}$  in high glucose ( $p < 0.001$ ) in MDA-MB-231 cells, from  $13.66 \pm 1.3 \mu\text{m}/\text{hour}$  to  $28.24 \pm 0.6 \mu\text{m}/\text{hour}$  in HT1080 ( $p < 0.001$ ), and from  $5.9 \pm 0.24 \mu\text{m}/\text{hour}$  to  $12.49 \pm 1.2 \mu\text{m}/\text{hour}$  in HeLa cells also ( $p < 0.001$ ).

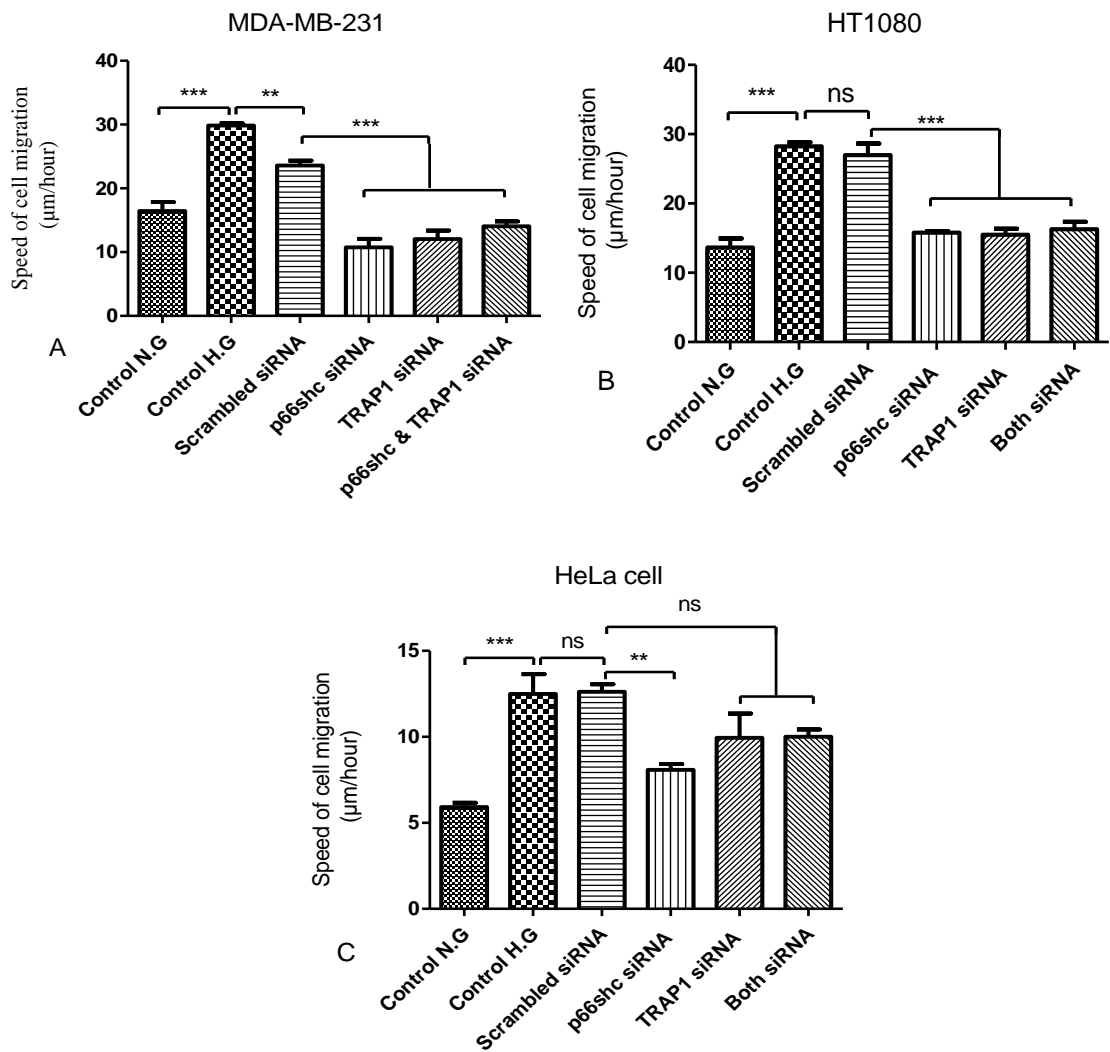


**Figure 6.12: Effect of silencing p66shc and/or TRAP1 genes on the cell migration.** Time-lapse microscopy was used to monitor cell migration for 24 hrs after 24hrs of transfection cells with p66shc and TRAP1 siRNA alone and together. A: Represents analysed data of MDA-MB-231 cells, B: data of HT1080 cells, C: data of HeLa cells, and D: a graph shows data of all cell lines together. Data represents the mean  $\pm$  standard error of three independent experiments performed in triplicate. One-way ANOVA followed by Dunnett test to compare mean of treatments with the mean of scrambled siRNA treatment (\*, \*\*and \*\*\* represent  $P < 0.05$ ,  $0.01$  and  $0.001$  respectively).

## 6.4 Discussion

There are several studies that report increasing p66shc expression in high metastatic cancer (Rajendran et al., 2010, Ma et al., 2007, Bhat et al., 2014, Jackson et al., 2000). In normal cells p66shc, which is recognized as a pro-apoptotic protein, can be activated in response to oxidative stress induced by different pro-apoptotic stimuli such as H<sub>2</sub>O<sub>2</sub>, UV exposure (Migliaccio et al., 1999, Straface et al., 2015), and hyperglycaemia (Fadini et al., 2010, Minami et al., 2018). Upon activation, p66shc translocate from cytoplasm to mitochondria through TOM/TIM complex where it oxidizes cytochrome c and transfers electrons from reduced cytochrome c to oxygen (Galimov, 2010, Giorgio et al., 2005) leading to generation of H<sub>2</sub>O<sub>2</sub> which can induce apoptosis (Giorgio et al., 2005, Galimov, 2010). In contrast, cancer cells can avoid apoptosis induced by activated p66shc; however, the mechanism is still unclear.

Interestingly, TRAP1, which is present in very small amounts or nearly absent in normal cells is highly expressed and activated in various cancer cells under oxidative stress (Kang et al., 2007, Pak et al., 2017). It can minimize the apoptotic effect mediated by ROS through inhibition of oxidative phosphorylation (Sciacovelli et al., 2013), and inducing glycolysis (Yoshida et al., 2013). It can protect cells also through binding to cyclophilin D (CypD) to prevents formation and opening of mitochondrial permeability transition pore (mPTP) and therefore apoptosis (Matassa et al., 2011). However, the link between p66shc and TRAP1 in cancer cells has not been investigated.

Previously our data showed that oxidative stress induced by high glucose, H<sub>2</sub>O<sub>2</sub>, and anti-cancer agents trigger several changes in MDA-MB-231 cells including fragmentation of mitochondria and reprogramming metabolism from oxidative phosphorylation to glycolysis which promoted cell migration. This chapter investigated the role of p66shc, which can be activated under oxidative stress, on cell migration and cellular metabolism as

well as its relationship with TRAP1 in preventing apoptosis in MDA-MB-231, HT1080, and HeLa cells, grown under high glucose level that can induce oxidative stress.

It was found that silencing p66shc and TRAP1 genes reduced the expression of their proteins; p66shc and TRAP1 in MDA-MB-231 (Figure 6.3), HT1080 (Figure 6.4), and HeLa cells (Figure 6.5). However, there was an unexpected decrease in the expression of protein p66shc after silencing TRAP1 gene in all three cell lines (Figures 6.3A, 6.4A, and 6.5A), as well as decreases in the expression of protein TRAP1 after silencing p66shc gene in both MDA-MB-231 and HT1080 cell lines (Figures 6.3B, and 6.5B). This finding suggests a strong correlation between the function of p66shc and TRAP1 proteins under oxidative stresses. The data from the cells that both p66shc and TRAP1 genes were silenced, showed significant decreases in the expression of p66shc protein in MDA-MB-231 (Figure 6.3A) and HeLa cells (Figure 6.5A) and the expression of TRAP1 in MDA-MB-231 (Figure 6.3B) and HT1080 (Figure 6.4B) without inducing apoptosis (Figure 6.8). This is because silencing p66shc gene will reduce generated ROS which is critical for activation TRAP1 that protect cells from its apoptotic effect. Thus, silencing TRAP1 gene in combination with p66shc gene confirms this strong relation between the function of p66shc and TRAP1 proteins. The data obtained from confocal microscopy that show reducing activated p66shc protein after silencing TRAP1 separately and in combination with p66shc (Figure 6.6) also confirm the relation between the p66shc and TRAP1 proteins.

The mechanism by which silencing p66shc leads to decreasing TRAP1 expression maybe due to reducing production of ROS by activated p66shc which promotes expression of TRAP1. While the mechanism by which silencing TRAP1 leads to decreasing p66shc expression remains unknown. This is the first time that a link between the expression of p66shc and TRAP1 has been reported.

Increasing expression of p66shc protein in all cell lines under high glucose level (25mM) (Figures 6.3A, 6.4A, and 6.5A), along with increased activation (Figure 6.6) were predicted as high glucose can induce oxidative stress which leads to increasing ROS generation (Figure 6.9). This study supports evidence from previous observations (Xi et al., 2010, Camici et al., 2007, Pagnin et al., 2005, Song et al., 2014) which reported that increasing p66shc expression is promoted by hyperglycaemia and diabetes mellitus (which is characterized by high glucose conditions) leads to increasing production of ROS and apoptosis. Declining levels of intracellular ROS production after silencing p66shc gene (Figure 6.9) confirms the important role of p66shc protein in enhancing ROS production. This result is in agreement with findings by Migliaccio and co-workers (1999) who found that treating mutant mice lacking the p66shc gene with hydrogen peroxide or irradiation with UV light did not induce a stress response and their life span was increased by 30% compared with wild-type mouse expressing the p66shc gene. Similarly, Galimov and co-workers (2011) reported that knockout of p66shc gene using lentiviral vector pLSLP in RKO cell line (colon cancer cell line) decreased response to oxidative stress induced by hydrogen peroxide or serum starvation.

Surprisingly, despite the strong relationship between TRAP1 and p66shc expression (Figure 6.3), silencing TRAP1 did not lead to decreases in the intracellular ROS in any of the three cell lines (Figure 6.9). One explanation of this finding is that ROS production may not be restricted to mitochondria, other organelles such as peroxisomes and endoplasmic reticulum also have role in generation of ROS (Brown and Borutaite, 2012, Yoboue et al., 2018).

In agreement with previous studies, our data suggest that TRAP1 plays an essential role in prevention of apoptosis induced by high generated ROS by activating p66shc. Whereas, silencing of TRAP1 induced apoptosis (Figure 6.8), silencing of p66shc gene separately

and in combination with TRAP1 gene did not induce apoptosis. One explanation of this finding is that TRAP1 protein in mitochondria suppresses pro-apoptotic activity of CypD, which is activated in response to ROS induced by p66shc, and prevents opening of mPTP and apoptosis. Therefore, silencing of TRAP1 leads to increasing apoptosis, whilst, silencing p66shc did not affect apoptosis as a result of decreasing ROS production. Moreover, increased generation of ROS in all three cell lines (Figure 6.9) with silenced TRAP1 may be an additional factor that enhanced cell apoptosis. These results reflect those of Basit and co-workers (2017) who also found that overexpression of TRAP1 led to inhibition of the opening of mPTP and therefore of apoptosis in melanoma cell line through lowering ROS levels. It was demonstrated that TRAP1 minimizes ROS via inhibition of succinate dehydrogenase (SDH) activity and avoiding mPTP opening and apoptosis (Sciacovelli et al., 2013, Guzzo et al., 2014). Accordingly, targeting TRAP1 in cancer cells in order to induce apoptosis can represent a valuable strategy for cancer therapy.

The present study revealed that in response to oxidative stress induced by high glucose levels, p66shc will be activated leading to generation of H<sub>2</sub>O<sub>2</sub>. It was documented that oxidation of cytochrome c by p66shc, which leads to H<sub>2</sub>O<sub>2</sub> generation, inhibits ATP production via oxidative phosphorylation (Hüttemann et al., 2011). Moreover, there is evidence that TRAP1, whose expression increases in response to the oxidative stress, inhibits succinate dehydrogenase; respiratory complex II in ETC (Guzzo et al., 2014), and triggers reprogramming of metabolism from oxidative phosphorylation to glycolysis (Yoshida et al., 2013). Indeed, previously our data provided evidence that high glucose levels alter metabolism from oxidative phosphorylation towards glycolysis. Therefore, it was very interesting to know whether silencing of p66shc and TRAP1 alone and in combination affects cellular metabolism and ATP production or not. This is because metabolism and ATP production may determine cancer cell migration.

Results revealed that high glucose levels led to increasing ATP production (Figure 6.10) due to increases in aerobic glycolysis (Figure 6.11) in all three cell lines. Silencing of p66shc and TRAP1 alone and together lead to decline of ATP production and slowing down of glycolysis in MDA-MB-231 cells (Figure 6.10A and 6.11A) and in HeLa cells (Figure 6.10C and 6.11C). This result suggests that activation of p66shc as well as TRAP1 plays important roles in rising glycolysis pathway in order to increase ATP production. Despite activated p66shc in mitochondria oxidizing cytochrome c as well as TRAP1 inhibiting SDH (Cosentino et al., 2008, Guzzo et al., 2014), there is evidence that the mitochondrial defect in many cancer cells is not permanent and oxidative phosphorylation function can be recovered with removing inhibitory factors (Smolková et al., 2011, Lu et al., 2015). Therefore, silencing of p66shc and/or TRAP1 can enhance cells to reverse metabolism from glycolysis to oxidative phosphorylation for compensation of required ATP.

Surprisingly, the results show that despite decreasing glycolysis in HT1080 due to knockdown of p66shc, TRAP1, and the combination of them, the decreases in the ATP production was nonsignificant (Figure 6.10B and 6.11B). One possibility is maybe due to high metastatic ability of this cell, and as documented that high metastatic cells are more dependent on the glycolysis (Zheng, 2012, Simões et al., 2015), therefore, it may be despite decreases of p66shc and TRAP1 expression, cancer cells still rely on glycolysis for generating ATP, however, our data cannot confirm this hypothesis as there is a need to measure oxidative phosphorylation activity.

This finding supports the work of other studies in this area linking dysfunction of mitochondria with expression of p66shc. Hagopain and co-workers (2016) reported decreases in glycolysis in Shc knockout mice, while,  $\beta$ -oxidation enzyme activities were increased, which means oxidative phosphorylation is active to generate ATP. They also

found that skeletal muscle with low levels of shc proteins have decreased glycolysis activities (Hagopian et al., 2015, Hagopian et al., 2016). Similarly, Edwards and co-workers (2016) reported that increasing expression of p66shc level alters metabolism in cultured embryos, they found that ATP production decreased due to defects in oxidative phosphorylation as a result of increased superoxide production. While, this finding is contrary to previous study by Soliman and co-workers (2014) which have suggested that depletion of p66shc in murine embryonic fibroblasts enhanced glycolysis and restoring its expression inhibited glycolytic metabolism. They related the effect of p66shc partially to inhibition of the mammalian target of rapamycin (mTOR) signaling in response to insulin. However, it was shown that Ras/MAPK signaling which has been activated by insulin, growth factors, cytokines, and hormones and upstream of mTOR (Carriere et al., 2011, Posada et al., 2017), was not affected by p66shc protein (Bonfini et al., 1996, Migliaccio et al., 1997, Trinei et al., 2002), and that it is possible that other isoforms of shc1 protein have the effect activated by insulin.

In regard to the effect of silencing TRAP1 on ATP production and glycolysis metabolism, a similar result was reported in murine fibroblast TRAP1 knockout cells. It has been found that overexpression of TRAP1 negatively regulates mitochondrial oxidative phosphorylation and reducing its expression will deregulate mitochondrial respiration (Yoshida et al., 2013, Lisanti et al., 2014). The same result was also documented in glioblastoma cell line by Chae and co-workers (2012). They suggested that TRAP1 silencing leads to a variety of metabolic changes including declining glycolysis and reduced secretion of lactic acid. Whereas, Guzzo and co-workers (2014) provide more detail about TRAP1 function. They suggest that TRAP1 affects respiration through inhibition of SDH which leads to reduced ROS generation and protection of cancer cells from apoptosis. The results suggest that overproduction of TRAP1 under oxidative stress induced by activated and translocated p66shc protect cancer cells by reducing ROS

generated via oxidation of cytochrome c and by inhibiting SDH and the activation of CypD, which prevents opening of the mPTP.

Cell migration is strongly affected by changes in the metabolism (Marelli-Berg and Jangani, 2018), and because expression of p66shc and TRAP1 induced reprogramming metabolism to glycolysis, it was interesting to investigate the role of them on cell migration. As expected, silencing of p66shc and TRAP1 alone and in combination reduced cell migration (Figure 6.12) in MDA-MB-231 and HT1080 cell lines, whereas, in HeLa cells, only silencing p66shc led to decreasing cell migration. The reason may be due to generated ROS and glycolytic metabolism, and as we mentioned above that high metastatic cancer cells are more glycolytic (Simões et al., 2015), therefore, silencing of these genes in high metastatic cancer cells will markedly affect cell migration. In accordance with the present result, a previous study by Jackson and co-workers (2000) demonstrated that increased p66shc expression in response to EGF led to increasing metastasis. Ou and co-workers (2014) found that expression of TRAP1 protein in oesophageal squamous cell cancer (ESCC) promoted cell migration, and silencing of it reduced ability of migration. This finding is contrary to a previous study by Agliarulo and co-workers (2015) which suggested that knockdown of TRAP1 enhanced cell migration in human colorectal tumours through modulation of the expression of genes involved in cell migration. It should be mentioned here that despite of silencing TRAP1 led to increase in apoptosis (Figure 6.8); we have monitored cell migration only in the intact cells.

## **Chapter Seven: Investigation role of mitochondria in 3D migration using Collagen gels, decellularised lung tissue, and Alvetex**

### **7.1 Introduction**

It has been well documented that the tumor microenvironment (TME) plays a vital role in the initiation, progression, and metastasis of cancer cells via interactions between cells and its microenvironment (Weber and Kuo, 2012, Kamińska et al., 2015). TME includes stromal cells, signaling molecules, immune cells, extracellular matrix (ECM), and blood vessels that surround cancer cells and supply them with nutrients and oxygen and remove waste. It can affect the cancer cells through deregulation of ECM, activation of proliferative signalling, inhibition of cell death, inducing invasion and metastasis, deregulation of cell metabolism, and deactivation of immune systems (Spano and Zollo, 2012, Kamińska et al., 2015). Cancer cells in turn can affect their microenvironment through secreting factors that remodel ECM which leads to alteration in their microenvironment making it more suitable for their growth, progression, migration and colonization at distant organs (Lu et al., 2012, Xiong and Xu, 2016). Moreover, stromal cells and stroma can promote cancer cell migration through reprogramming metabolism. It was reported that secretion of  $H_2O_2$  by metastatic cancer cells induces neighbouring stromal cell to initiate aerobic glycolysis and efflux by-products such as L-lactate to the microenvironment which is taken and used by cancer cells (Sotgia et al., 2012, Xing et al., 2015). These links and interactions which exist between cancer cells and their micro-environment pose a challenge in cancer cell studies in the artificial micro-environments.

For several decades two-dimensional (2D) cell culture techniques served as an essential tool in cell and molecular biology studies. In this technique, monolayers of cells adhere to a thin flat surface such as glass, and polystyrene plastic, which provides easier environmental control, observation of the cells, and measurement and treatment of the cells (Lee et al., 2008, Edmondson et al., 2014, Antoni et al., 2015). However, it cannot mimic

the true microenvironment that is present *in vivo*, where cell-cell and cell-extracellular matrix (ECM) interaction occurs which is important in the cell survival, growth, and migration (Aljitawi et al., 2014, Edmondson et al., 2014).

3D cell culture models allow the cells to grow and interact with surrounding artificial microenvironment that resembles to some extent human tissues and tumors (Vinci et al., 2012). Despite that 3D cell culture lacks the vascular systems which are essential to support tissues with oxygen, nutrients, and to remove waste as *in vivo* when compared to 2D cell culture, it is much more effective in studying several biological mechanisms such as; cell viability, morphology, drug resistance, cytotoxicity, gene expression and protein synthesis, immune system evasion, migration and invasion of cancer cells into surrounding tissues, cell metabolism and apoptosis (Edmondson et al., 2014, Antoni et al., 2015, Ravi et al., 2015).

In the previous chapters, we investigated the impact of the mitochondrial dynamics on cell migration. However, there are many studies that found that cells in 3D environments exhibit different characteristics, at both morphological and molecular levels that can induce cell growth and migration, from monolayer cells in 2D environment (Even-Ram and Yamada, 2005, Fried and Gilmour, 2009, Song et al., 2015). Therefore, it was important to investigate the impact of mitochondria in 3D environments (Collagen, Alvetex, and Decellularised lung tissue) on cell migration.

### **7.1.1 Collagen I gel as 3D cell culture:**

In tissues, cells exist in 3D - extracellular matrix which is rich in collagen especially type I. *In vitro*, cells can be cultured in/on 3D collagen matrices that reflect 3D microenvironment *in vivo*, it provides simple and fast method to study and analysis cell migration, cell proliferation, and apoptosis (Wolf et al., 2009, Edmondson et al., 2014). It was found that cell migration in 3D matrices is different from that on a 2D surface (Fraley et al., 2010), because cells grown on collagen rich 3D matrix form a dendritic protrusion instead of

lamellipodia and filopodia which display on 2D surface (Giri et al., 2013). As well as cell migration in 3D collagen matrix depending on the expression of matrix metalloproteinases (MMPs) enzyme which initiates the breakdown of matrix and release of the back of the cell (trailing edge) that in turn allows the front of the cell to move forward (Bloom et al., 2008).

### **7.1.2 Alvetex scaffold as 3D cell culture:**

Alvetex is a highly porous, cross-linked polystyrene scaffold that allows invasion and proliferation of cells. It is designated as a thin disc that can be located at the bottom of wells or suspended in it, with a thickness of 200  $\mu\text{m}$  that allow diffusion of medium and removal of waste products, as shown in Figure 7.1. It provides a suitable niche environment for proliferation, and migration of cancer cells and allows the cells to maintain their 3D shape and interactions with adjacent cells, and can be used to study cells in both short and long time experiments (Reinnervatecom, 2017).

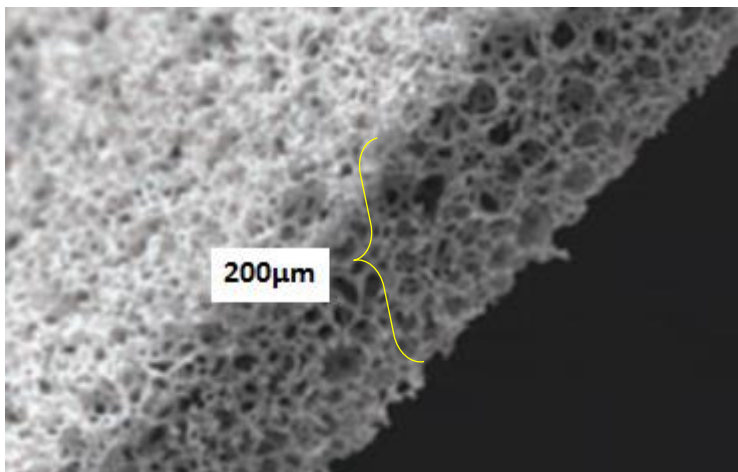


**Figure 7.1: Alvetex Scaffold.** Electron Microscope image of alvetex scaffold viewing its highly porous structure with a thick of 200 $\mu\text{m}$ . Cited from Rigby.,2011.

Mitochondria are highly dynamic organelles; their shape and size are changed upon exposure of the cells to stresses. It has been well known that microenvironment plays an important role in cell response to the stresses, in the study by Bai and co-workers (2015); they found that cell response to the external stress induced by radiation or chemotherapy agents, is influenced by cell culture system. They concluded that expression of genes and proteins that participate in regulation of ECM, cell proliferation, cell adhesion, cell

signaling, and apoptosis in 3D cell culture is different significantly compared to 2D cell culture. However, impact of 3D microenvironment on changes in the mitochondrial dynamics as a response to stress is not well studied.

### **7.1.3 Decellularised lung tissue as 3D cell culture**

The ECM matrix composition is complex and different from one tissue to another. Mixing specific single ECM molecules, for example collagen obtained from rat tail, to make 3D cell culture in vitro cannot recreate the same ECM composition in vivo exactly. Recently, several studies have suggested using decellularised tissue that is used in organ engineering and cancer cell studies (O'Neill et al., 2013, Mazza et al., 2015, Xiang et al., 2016). Tissue of interest can be taken in vivo and decellularised to be used as an in vitro ECM matrix (Gilbert et al., 2006, Hoshiba et al., 2010). Different tissues can be used for this purpose such as lung (Mishra et al., 2012), liver (Mazza et al., 2015), kidney (Bonandrini et al., 2014), brain (De Waele et al., 2015) and pancreatic tissue (Goh et al., 2013).

Decellularised lung tissue has been used for studying several cancer cells especially lung cancers and breast cancer cells (Mishra et al., 2012, Lu et al., 2014), due to the relevance of these decellularised tissues to cancer cell tissues. Xiong and co-workers (2016) used decellularised lung tissue for studying invasion and colonization of MDA-MB-231 breast cancer cells and 4T1 mouse mammary carcinoma cells (which mimic human breast cancer cells). Also, Mishra and co-workers (2012) studied the formation of perfusable tumor nodules by A549, H460, and H1299 lung cancer cells on decellularised lung tissue. However, until today there is no study on the mitochondria in 3D decellularised tissue.

## **7.2 Aim**

In this chapter we aimed to study the effect of mitochondrial dynamics on cell migration in 3D environments; collagen I gel, Alvetex scaffolds, and decellularised rat lung tissue.

### **7.3 Material and methods:**

#### **7.3.1 3D collagen I gel cell culture**

- **Coating with collagen I gel**

Collagen type 1 was obtained from Merck Millipore at 3.9mg/ml. It was stored at 4°C and kept on ice during preparation. For preparing collagen gels, 1:10 volume of 10X DMEM with phenol red (Gibco, Fisher Scientific) was mixed with collagen stock solution, then pH neutralized with 1 M sodium hydroxide solution to reach pH 7.4, and completing the volume with 1X DMEM to final required volume. Each step was conducted on ice to avoid collagen polymerization. The final collagen concentration was 2mg/ml; 400µL of prepared solution was spread into 10 cm<sup>2</sup> well (6-well plates) to make a thin film. For immunostaining, clean coverslips were placed in each well and 100µL of prepared solution spread over them to make a thin film. Collagen was polymerized by incubating plates for 30 minutes at 37°C and wells rinsed with PBS and allowed to dry before use.

- **Culture of cells on collagen I gel**

MDA-MB-231 cells that are grown in different glucose concentrations for more than one week on 2D plastic surface were trypsinized with 0.05% Trypsin and 0.02 % EDTA and 2.5X10<sup>4</sup> cells were seeded in DMEM medium with different glucose concentrations (1, 5.5, and 25mM) on 3D collagen gel for 48hrs, then subjected to live imaging with Nikon time-lapse microscope for tracking cell migration as explained in section 2.2.17, staining with MitoTracker probe for staining mitochondria as described in section 2.2.7. For studying mtDNA copy number through real-time PCR technique, we seeded 5X10<sup>5</sup> cells on 3D collagen gel in each well for 48hrs, then total cell DNA was extracted as described in section 2.2.10.

### **7.3.2 3D Alvetex cell culture**

- **Preparation of Alvetex scaffolds for cell seeding**

Alvetex 12-well plates (AVP002) were obtained from AMS Biotechnology. The sterile Alvetex scaffold discs were kept in transwell and placed in 12-well plates, before seeding of cells. Scaffolds were treated with 70% ethanol for 15 minutes to allow wetting of polymer followed by three washings in sterile PBS. MDA-MB-231 cells were grown in DMEM medium with different glucose concentrations were trypsinized with 0.05% Trypsin and 0.02 % EDTA then each scaffold was seeded with 100  $\mu$ l of medium containing  $2 \times 10^5$  cells. The cells were allowed to settle down for 1 hour in the incubator then 4ml of DMEM medium with different glucose concentrations added to each well. The culture plates were incubated at 37°C and 5% CO<sub>2</sub>, medium was changed every 2-3 days for 10 days to allow the cells to penetrate and proliferate into maximum cell number. Then cells were processed for mitochondrial staining and DNA extraction for real-time PCR as described in section 2.2.7 and 2.2.10 respectively.

#### **Staining and Sectioning of Alvetex scaffolds**

The 3D alvetex scaffolds were washed twice with PBS after removal of medium, then 2mL of pre-warmed serum and antibiotic free growth medium that contains reduced Mito-Tracker® Orange probe with a final concentration 300 nM was placed into each well. The plates were incubated at 37 °C and 5% CO<sub>2</sub> for 20-30minutes, then medium was removed and alvetex scaffolds washed twice with PBS and fixed with 3ml of 4% (w/v) Paraformaldehyde (PFA) for 30 minutes in the incubator at 37°C. After three washings in PBS, alvetex scaffold disc were cut to small pieces of 15mm length and 5mm width then embedded in OCT (Fisher) to make blocks. The OCT blocks were sectioned at 10-14 $\mu$ m thickness using a Cryostat (Bright Model OTF) and sections were transferred to glass slides. Images of mitochondria were taken using confocal microscope at 100X.

### 7.3.3 Decellularised lung tissue as 3D cell culture

- **Decellularization of rat lung**

Decellularised lung (dLung) was prepared based on the protocol (Tris-Trypsin-Triton) described by Lu and colleagues for modeling of 3D tumor microenvironments (Lu et al., 2014). We obtained lungs from 12 week old Sprague Dawley rats. Prepared decellularised rat lung was used as 3D microenvironment tissue for seeding cells after testing it with confocal microscope to confirm tissue is free from the cells, as shown in Figure 7.2.

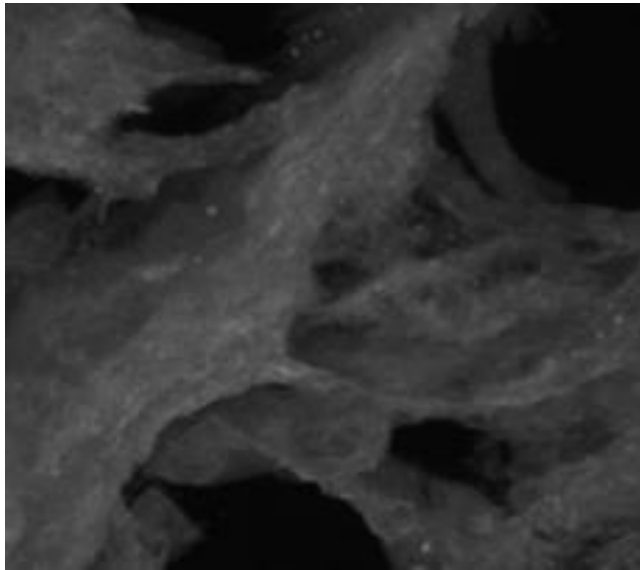


**Figure 7.2: Decellularised rat lung tissue.** Cells removed from lung tissue using Tris-Trypsin-Triton technique

- **Culture of cells on dLung**

Decellularised rat lung tissue was prepared for use as a 3D culture matrix. It was cut into small sizes and placed in 35mm tissue culture dishes under a UV lamp for at least 15-20 minutes for UV sterilisation. Sterile PBS was added and dLung /PBS placed into a tissue culture incubator at 37°C and 5% CO<sub>2</sub> for 24hrs. Then PBS was carefully removed and replaced with DMEM culture medium; the tissue was re-incubated for at least 2 days before adding the cells. After removing the medium, 2X10<sup>5</sup> cells were suspended in 100µL of DMEM medium with different glucose concentrations and added to the tissue surface and incubated for 3hrs to allow the cells to attach to the matrix before flooding the wells with a further 3ml of medium. The plates were incubated for 10 days with changes of

medium every 2-3 days, this allowed the cells to penetrate the dLung tissue and grow to the maximum cell numbers that will be enough for generation of required high yields.

- **Fixing and staining colonized decellularised tissue**

The colonized decellularised tissue (cells and decellularised tissue) were washed twice with pre-warmed PBS after the removal of medium, then 3mL of pre-warmed serum-antibiotic free growth medium containing reduced Mito-Tracker® Orange probe with a final concentration of 300 nM was added into each well. The plates were incubated at 37°C and 5% CO<sub>2</sub> for 20-30minutes, the medium then was removed and colonized decellularised tissue washed twice with pre-warmed PBS and fixed with 3ml of 4% PFA for 30 minutes in incubator at 37°C. After one washing with PBS, colonized decellularised tissue was permeabilized and blocked with 1% Triton X100/PBS / 10% Goat Serum (Fisher Scientific) overnight. Later the colonized decellularised tissue was placed in solution of DAPI (Sigma)/PBS for staining nucleus for 1hrs, and then washed twice with PBS buffer to remove excess stain on it.

- **Embedding and sectioning colonized decellularised tissue**

Colonized decellularised tissue was soaked in sucrose solution (5% overnight at 4°C, then 15% and 30% for 2hrs each at room temperature) then embedded in OCT (Fisher). OCT blocks were sectioned in thick between 10-14µm using a Cryostat (Bright Model OTF), then sections were transferred to clean glass slide.

- **Confocal microscopy**

Nikon A1 confocal microscope was used to take a series of images (Z-stack) captured every 0.250 µm of the focal plane. Then obtained 3D series images, as shown in Figure 7.3, was analysed using ImageJ software as mentioned in section 2.2.16.

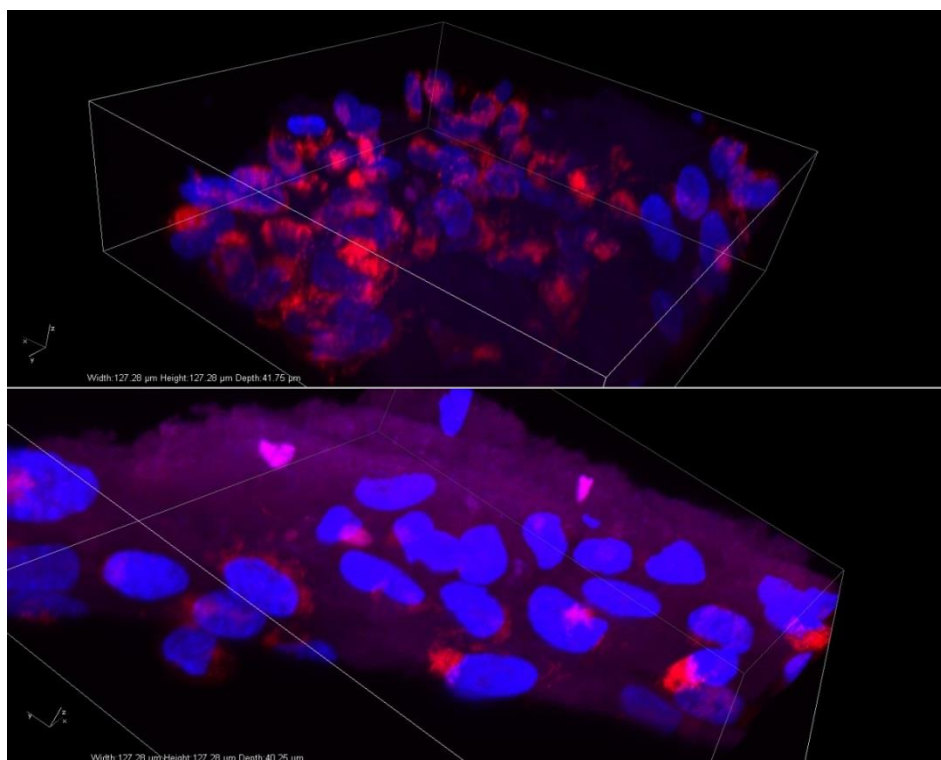


Figure 7.3: Micrographs showing 3D image of MDA-MB-231 cells cultured in decellularised lung tissue. Mitochondria stained with MitoTracker probe (Red), and nucleus Stained with DAPI. Z-stack images were taken by confocal microscope and ImageJ was used for analysing it.

- **Extraction of total DNA**

Total DNA (genomic and mitochondrial DNA) was extracted using DNeasy Blood & Tissue Kit (QIAGEN) according to the protocol for purification of total DNA from animal cells as described in section 2.2.10

## 7.4 Results:

### 7.4.1 Impact of the glucose levels on the mitochondrial number in 3D cell culture

Unlike 2D surfaces, measuring the changes in the mitochondrial dynamics especially mitochondrial number was not accurate in 3D environment. Therefore, we measured mtDNA copy number in MDA-MB-231 cells via real-time PCR to investigate the effect of the glucose on the mitochondrial number in different 3D cell cultures. In this study, MDA-MB-231 cells were cultured on collagen coated surfaces for 48hrs, and for 10 days in dLung tissue and alvetex scaffolds. Next, total DNA was extracted for measuring of mtDNA copy number. Results revealed that increasing glucose concentrations has a positive effect on the mtDNA copy number. Figure 7.4A that shows the mtDNA copy number in cells cultured on collagen and in different glucose levels was increased to  $2531.9 \pm 121.8$  in high glucose compared to  $1884.98 \pm 46.8$ , and  $1637.1 \pm 53.6$  in normal glucose ( $p < 0.01$ ) and in low glucose ( $p < 0.001$ ) respectively. Whereas, no significant changes in mtDNA copy number were found between normal and low glucose treatments.

Similar results were found when we measured mtDNA copy number in the cells cultured in Alvetex scaffolds. The mean of the copy number of mtDNA in cells grown in high glucose was  $2348.4 \pm 106.5$ , and it was significantly higher than it in the normal glucose and in low glucose which was  $1912.3 \pm 54.3$  ( $p < 0.05$ ) and  $1650.9 \pm 77.8$  ( $p < 0.01$ ) respectively, and no significant differences were recorded between normal and low glucose treatments, as shown in Figure 7.4B.

Figure 7.4C that shows the mtDNA copy number in cells cultured in decellularised lung tissue, revealed that mtDNA copy number in cells grown in high glucose was markedly higher than in low glucose, the mean of it was  $2530.7 \pm 171.8$  in high glucose treatment compared to  $1744.1 \pm 52.01$  in low glucose treatment ( $p < 0.01$ ). Statistically no significant differences were observed between high glucose and normal glucose or between normal glucose and low glucose treatments.

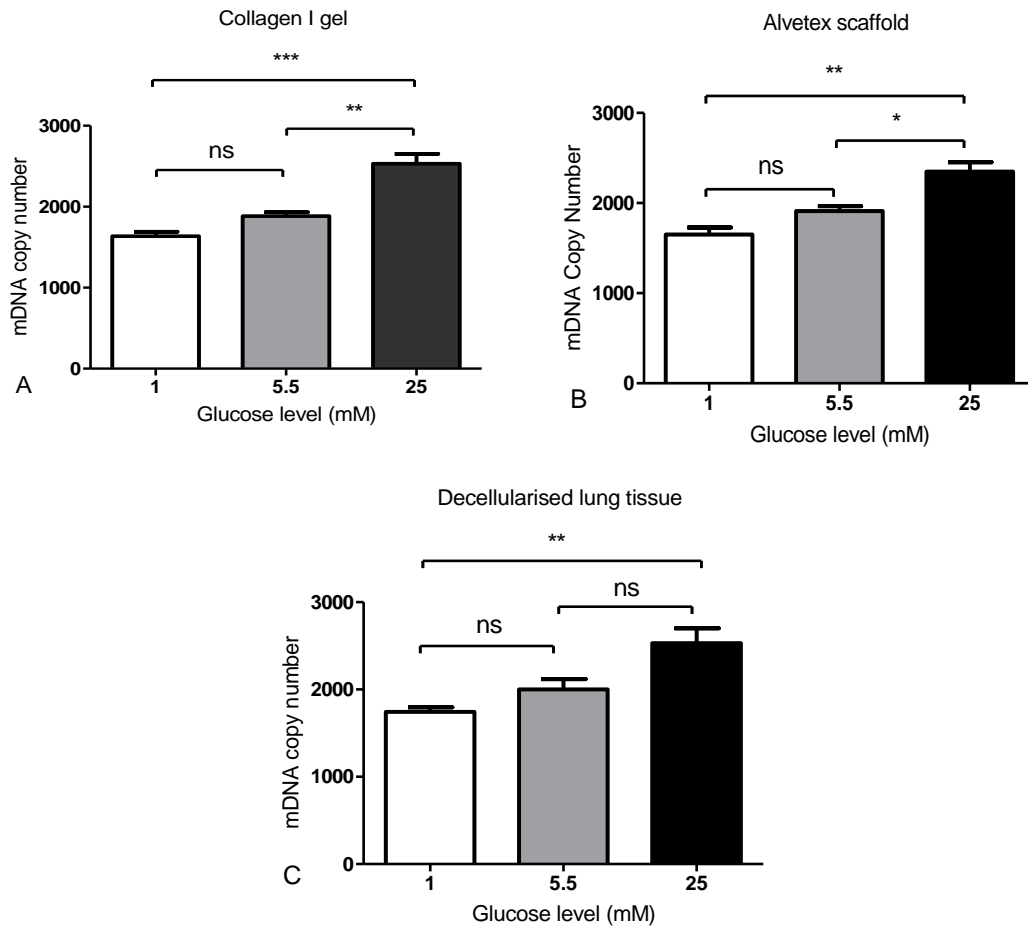


**Figure 7.4: Quantification of mtDNA copy number in MDA-MB-231 cells cultured in different glucose levels and in different 3D cell cultures.** Cells seeded in decellularised lung tissue and Alvetex scaffold for 10 days and for 48hrs on collagen I gel in DMEM medium with different glucose concentrations (1, 5.5, and 25 mM). Then total cell DNA extracted, mtDNA copy number was determined using quantitative real-time PCR. A: Represents data from Collagen I gel, B: from Alvetex, C: from Decellularised lung tissue. Data represent the mean  $\pm$  standard error of three independent experiments performed in triplicate. One-way ANOVA followed by Tukey's Multiple Comparison Test to compare mean of treatments. (\*, \*\*, and \*\*\*represent  $P < 0.05$ , 0.01, and 0.001 respectively).

#### **7.4.2 Impact of the glucose level on the mitochondrial dynamics in 3D cell culture**

Although the changes in the mitochondrial morphology can be noticed using confocal microscopy, however, if we do not say it is impossible to measure these changes, it is certainly not easy and not accurate. In the previous experiment we revealed that mtDNA copy number in MDA-MB-231 cells has been affected with different glucose levels in 3D cell cultures. To show these changes in the mitochondrial morphology, cells were grown on the coverslip coated with the collagen, and in the Alvetex scaffolds, and in the dLung tissue. After the incubation period, mitochondria were stained with MitoTracker probe and the nucleus with DAPI.

The micrograph images show that in low glucose levels, mitochondria in the cells appear in elongated shape that forms tubular network-like structures throughout the cell. In the normal glucose, cells possess mitochondria which have an elongated shape and resemble to some extent the mitochondrial morphology of cells grown in the low glucose medium. While, the mitochondria in the cells cultured in high glucose have been fragmented to small size shape, as they can be seen in Figure 7.5 for cells cultured on collagen gel , Figure 7.6 for cells cultured in Alvetex, and 7.7 for cells cultured in dLung tissue in different glucose levels

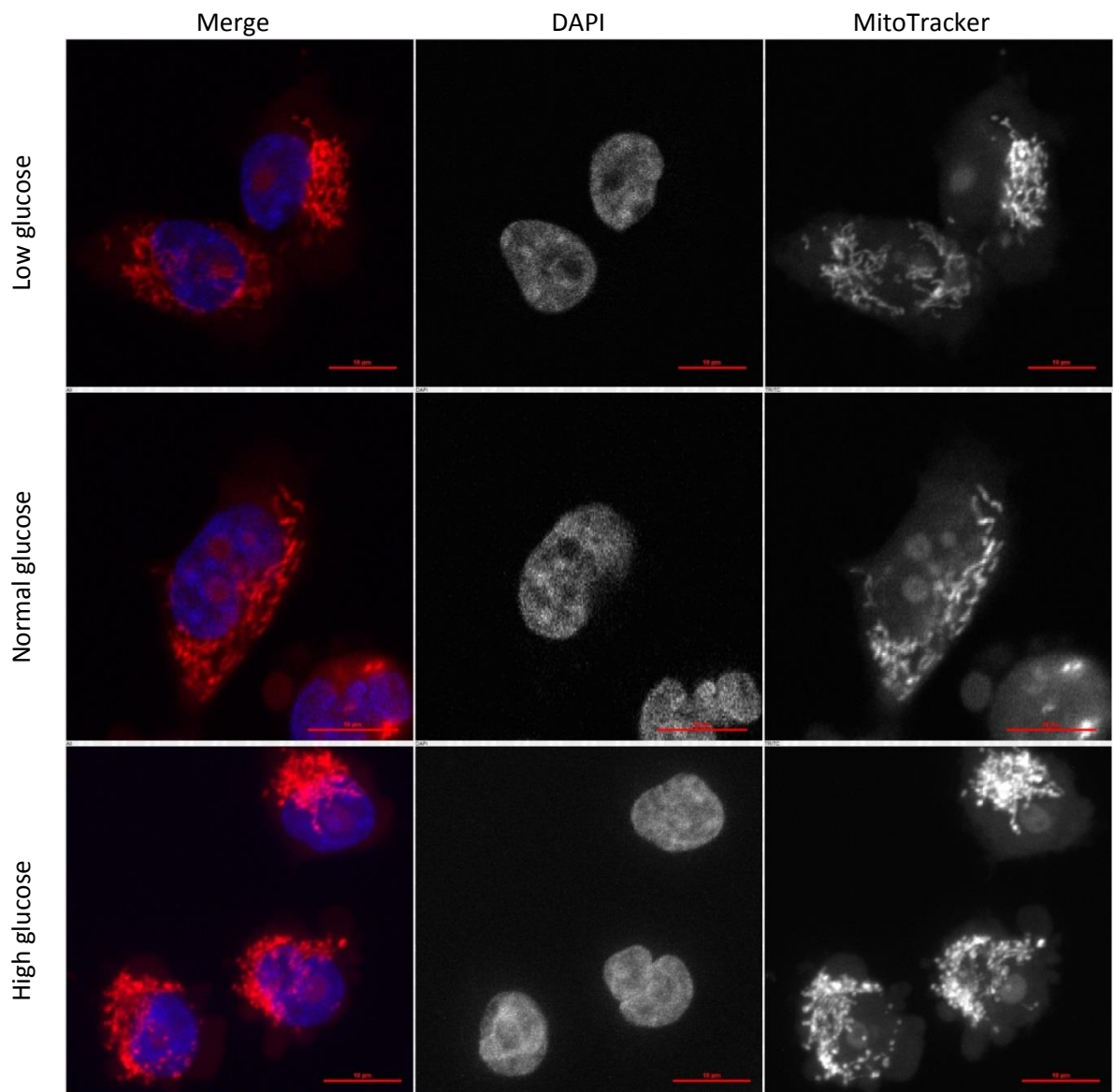


**Figure 7.5:** Micrographs showing mitochondria in MDA-MB-231 cells cultured in different glucose levels on collagen gel. In low glucose (1mM), mitochondria have an elongated, network like shape. In normal glucose (5.5mM), mitochondria showing elongated shape. In high glucose (25mM), mitochondria appear as small fragmented shape. Cells were cultured for 48hrs on 2mg/ml collagen gel. Mitochondria stained with MitoTracker probe (Red), and nucleus Stained with DAPI. Scale bar=10 $\mu$ m

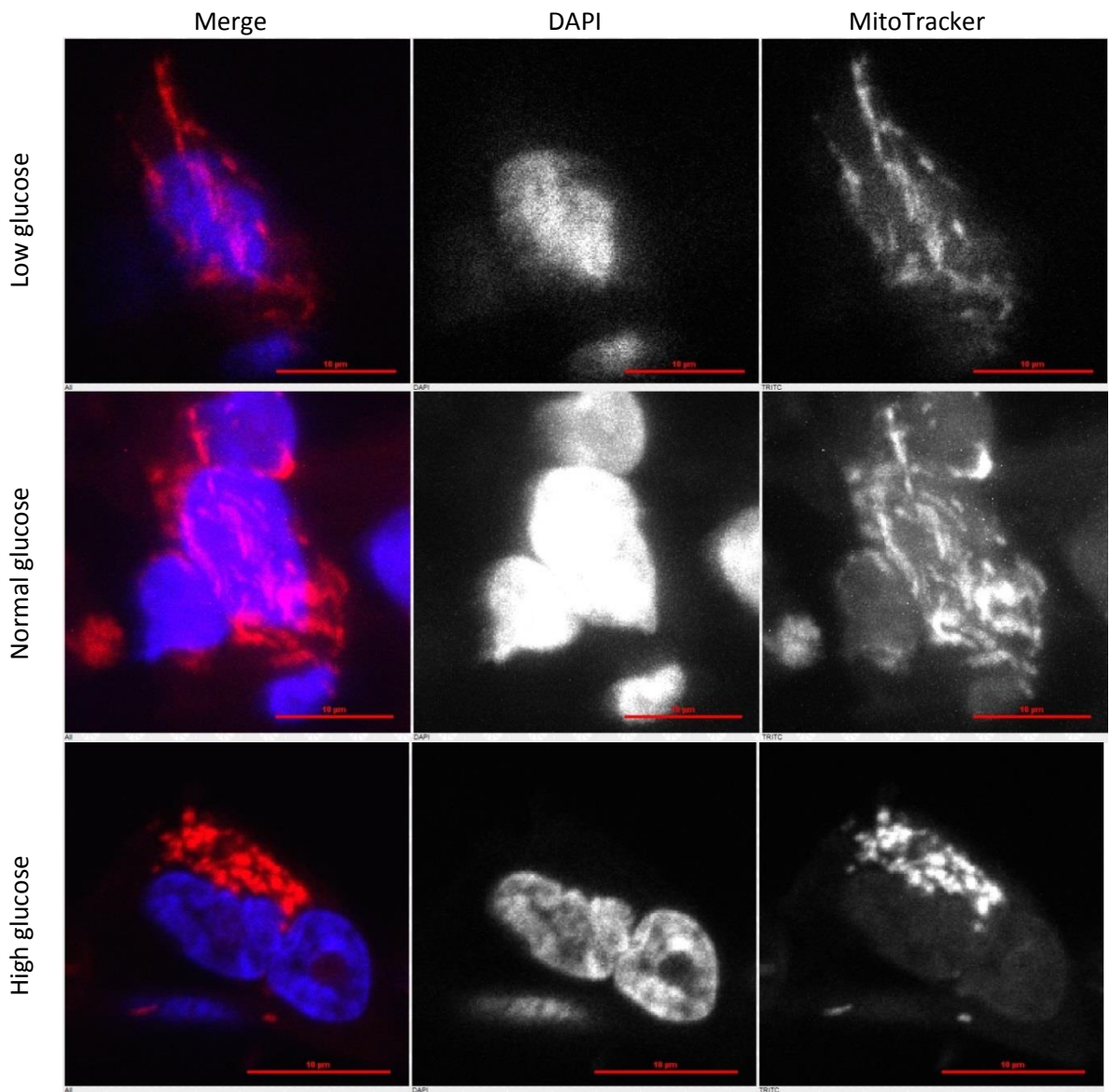


**Figure 7.6:** Micrographs showing mitochondria in MDA-MB-231 cells cultured in different glucose levels in Alvetex scaffold. In low glucose (1mM), mitochondria have an elongated, network like shape. In normal glucose (5.5mM), mitochondria showing elongated shape. In high glucose (25mM), mitochondria appear as small fragmented shape. Cells were cultured for 10 days in Alvetex scaffolds. Mitochondria stained with MitoTracker probe (Red), and nucleus Stained with DAPI. Scale bar=10μm

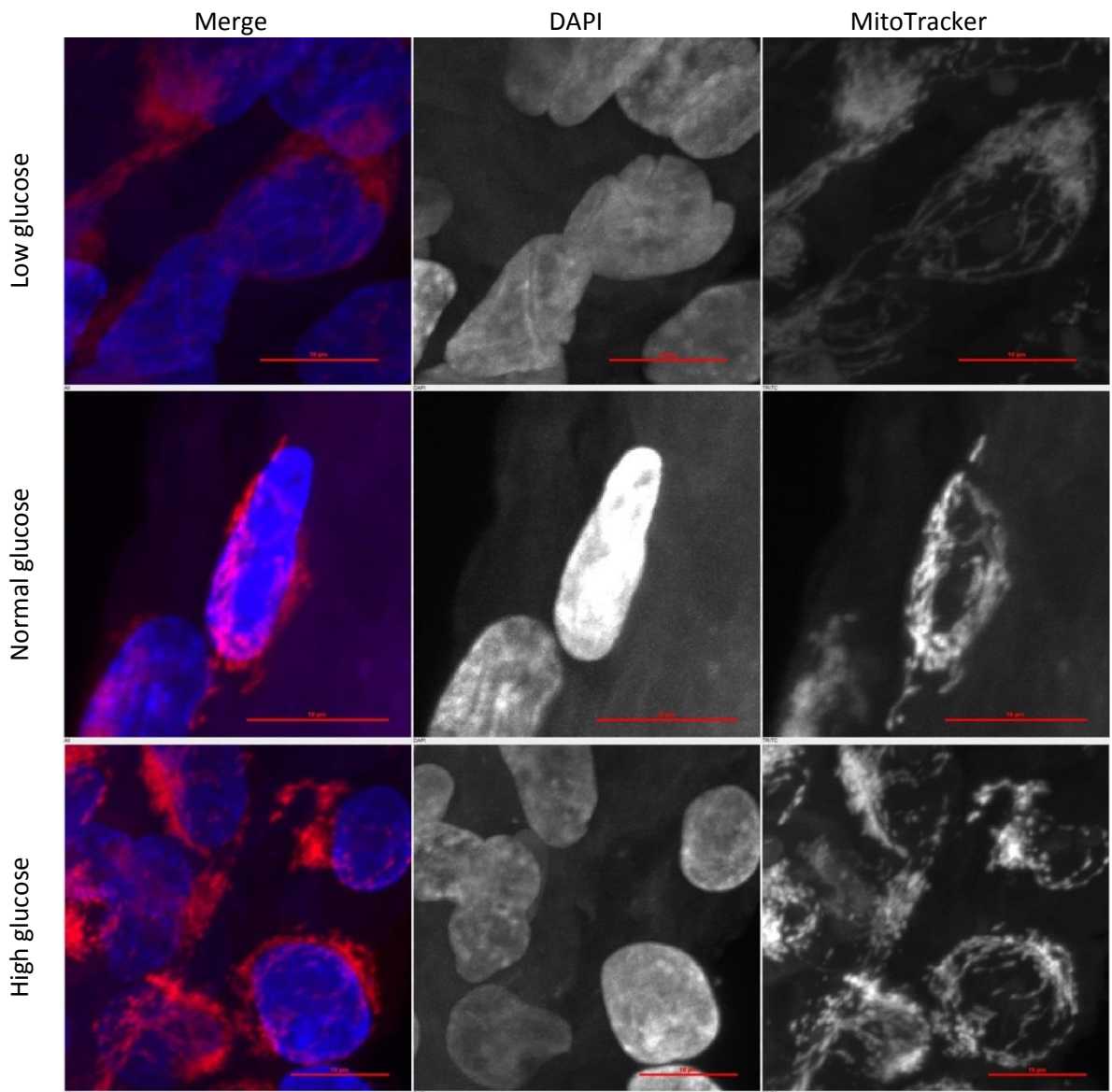


**Figure 7.7:** Micrographs showing mitochondria in MDA-MB-231 cells cultured in different glucose level in decellularised lung tissue. In low glucose (1mM), mitochondria have an elongated, network like shape. In normal glucose (5.5mM), mitochondria showing elongated shape. In high glucose (25mM), mitochondria appear as small fragmented shape. Cells were cultured for 10 days in decellularised lung tissue. Mitochondria stained with MitoTracker probe (Red), and nucleus Stained with DAPI. Scale bar=10 $\mu$ m

### 7.4.3 Impact of mitochondrial dynamics on 3D cell migration in MDA-MB-231

In previous experiments as well as in section 3.3.1, we found that increasing the glucose level in the medium increased mitochondrial fragmentation, and we also found it led to increase in cell migration in 2D plastic surfaces. To know the effects of the mitochondrial shape on the cell migration in 3D cell culture, we cultured MDA-MB-231 cells on collagen coated surfaces for 48hrs, and different concentrations of glucose were used to induce changes in mitochondrial shape. Then through time-lapse microscopy cell movement have been tracked for 24hrs. Cell movement was measured using ImageJ-MtrackJ plugin.

The analysed data showed that cell migration significantly increased with increasing glucose level. As shown in Figure 7.8, mean of cell movement was increased from  $25.4 \pm 0.6 \mu\text{m/h}$  in low glucose to  $31 \pm 1.06 \mu\text{m/h}$  in normal glucose ( $p < 0.01$ ), and into  $34.4 \pm 0.68 \mu\text{m/h}$  in high glucose ( $p < 0.001$ ), whilst, no significant differences were detected in the cell movements between cells cultured in the normal glucose and cells cultured in the high glucose.

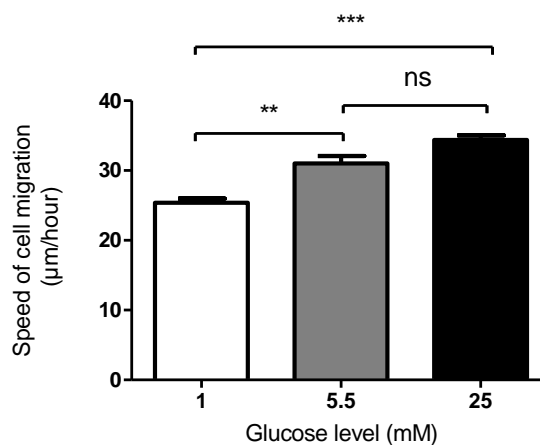


**Figure 7.8: Effect of glucose level on 3D cell migration.** Cells were seeded in different glucose concentrations on pre-coated collagen surface for 48hrs. Then cell movement was monitored using time-lapse microscopy, and ImageJ software used for tracking cell movement every 15 minutes over 24 hours. Data represent the mean  $\pm$  standard error of three independent experiments performed in triplicate. One-way ANOVA followed by Tukey's test to compare mean of treatments (\*\*and \*\*\* represent  $P < 0.01$  and  $0.001$  respectively).

#### 7.4.4 Impact of the mitochondrial division inhibitor on 3D cell migration

The previous results suggested that mitochondrial fission increased with increasing glucose level, may be linked with cell migration. We also found in section 3.3.3 that inhibiting mitochondrial fission affected cell migration on 2D plastic surface negatively. To uncover the effect of inhibiting mitochondrial fission on 3D cell migration, we treated pre-cultured cells on the collagen coated surfaces in high glucose medium with different concentrations 10, 30, 50 $\mu$ M of mitochondrial division-1(mdivi-1) inhibitor for 24hrs. Then, for 24hrs cell migration was monitored using time-lapse microscopy and ImageJ-MtrackJ plugin used for measuring cell movement.

The analysed data showed that cell migration declined significantly after inhibition of mitochondrial division with mdivi-1 inhibitor. It was decreased sharply from  $34.38\pm 0.68\mu\text{m/h}$  in non-treated control cells to  $23.52\pm 0.34$ ,  $18.6\pm 1.2$ , and  $13.76\pm 0.57\mu\text{m/h}$  in treated cells with 10, 30, and 50 $\mu$ M of mdivi-1 inhibitor respectively ( $p < 0.001$ ), as shown in Figure 7.9.

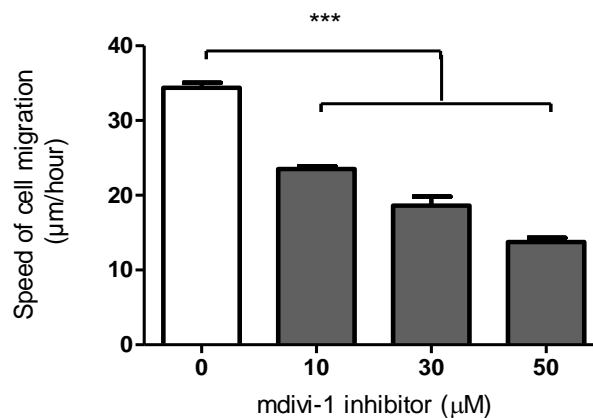


**Figure 7.9: Effect of mdivi-1 inhibitor on 3D cell migration.** MDA-MB-231 cells were grown in high glucose medium on pre-coated collagen surface before treated with mdivi-1 inhibitor for 24hrs. Then through time-lapse microscopy, cell migration was monitored and images were taken every 15 minutes over 24 hours. The cell movement was measured using ImageJ software. Data represent the mean  $\pm$  standard error of three independent experiments performed in triplicate. One-way ANOVA followed by Dunnett's test to compare mean of treatments with control mean (\*\*\*) represent  $P < 0.001$ ).

## 7.5 Discussion

Since the tumour microenvironment (TME) plays an important role in cancer cell migration and metastasis (Quail and Joyce, 2013, Wang et al., 2017a) we investigated the impact of mitochondrial dynamics under different glucose levels on cell migration in various 3D environments. Collagen has been used in cancer research for a long time (Di Lullo et al., 2002, Song et al., 2015, Gu et al., 2016), while, using alvetex scaffolds and decellularised lung tissue as 3D culture matrix environments are more recent developments (Kramer et al., 2013, Mazza et al., 2015, Ravi et al., 2015). Herein, for the first time they were used in mitochondrial study.

In the present study, MDA-MB-231 cells were seeded on collagen, in Alvetex scaffold, and in decellularised tissue, in different glucose levels to quantify mitochondrial DNA copy number (mtDNA) through qPCR as an indicator of changes in the mitochondrial number. Our data showed that mtDNA increased significantly in high glucose compared to low glucose in all three environments as well as compared to normal glucose level in collagen and in alvetex scaffold, whereas, no significant changes were observed between normal and low glucose levels in all three environments( Figure 7.4). These results suggest that increasing glucose level increases fragmentation of the mitochondria, and they are in agreement with our previous finding on 2D plastic surface. Mitochondria are highly sensitive to oxidative stress such as when induced by high glucose as a result of generated ROS which promotes their fragmentation through activation of mitochondrial fission protein; Drp1, and inhibition of mitochondrial fusion (Wu et al., 2011, Trudeau et al., 2011).

In an attempt to give further insight on mitochondrial morphology under the effect of different glucose levels in various 3D environments, a series of images were taken by confocal microscope using MitoTracker to stain mitochondria. Results show that mitochondria appear as an elongated shape in low glucose and normal glucose, whereas, in

high glucose, it has small fragmented shape (Figure 7.5 on collagen, 7.6 in Alvetex, and 7.7 in decellularised lung tissue), suggesting that the changes in the mitochondrial morphology has been induced by increasing glucose level. This result confirm real-time qPCR finding as well as support our previous results on 2D plastic surface.

These findings in 3D environments may help to understand better the changes in the mitochondria in response to stress induced by high glucose, as these environments mimic to natural scaffold in vivo (Lu et al., 2014). However, they were more complex than 2D culture systems to measure the number, size, and volume of mitochondria due to their background which prevented accuracy of these measurements by microscopy.

Cell migration in 3D environments differ from their 2D counterparts as the cell often display a high dendritic pseudopodial protrusions for their migration instead of lamellipodia and filopodia, which are displayed in 2D migration (Wu et al., 2014). It has been reported that production of matrix metalloproteinases (MMPs); matrix degrading enzymes, which play a fundamental role in cancer cell migration and metastasis, increased in acidic TME (Kato et al., 2005, Amaral et al., 2018). Previously, we demonstrated that mitochondrial fragmentation induces metabolic reprogramming to glycolysis, which leads to increases in production of lactic acid, and it is well known that lactic acid contributes to acidification of microenvironment (Romero-Garcia et al., 2016, Jiang, 2017). In the present study we investigated whether changes in mitochondrial morphology induced by different glucose levels can affect cell migration in 3D environments or not. Contrary to expectations, this study did not find a significant difference in cell migration between cells cultured in high glucose and normal glucose levels (Figure 7.8), despite of significant fragmentation of mitochondria in high glucose compared to normal glucose (Figure 7.4A, and 7.5). However, there was increased cell migration in high glucose and normal glucose compared to low glucose (Figure 7.8) confirming that changes in mitochondrial morphology affect cell migration.

This result is in agreement with those obtained by Zanotelli and co-workers (2017), who documented that generation of ATP in cancer cells seeded in three-dimensional collagen environments is correlated with speed of cell migration.

Motility of cells depend on the production of ATP (Campello et al., 2007, Zanotelli et al., 2017), which can be affected by mitochondrial morphology (Anesti and Scorrano, 2006). In low glucose level where mitochondria appear in elongated network-like shape, cells generate ATP via oxidative phosphorylation (Li et al., 2017), whereas, fragmentation of mitochondria such as when induced by high glucose, reduces its function for ATP production (Mannella, 2006), and this forces the cells to alter metabolism to aerobic glycolysis for production of ATP energy (Jiang, 2017). The end product of aerobic glycolysis, lactate, which is released into extracellular microenvironment, changes the pH to acidity (Zheng, 2012). In low pH, activated matrix metalloproteinase enzymes can enhance cell migration through degradation of matrix and non-matrix proteins (Nagase et al., 2006).

To confirm whether mitochondrial fragmentation leads to increases in cell migration, we targeted mitochondrial fission through inhibition of Drp1 protein which mediates mitochondrial division with different concentrations of mdivi-1 inhibitor in MDA-MB-231 cells grown in high glucose level on collagen. Previously we have demonstrated that the mdivi-1 inhibitor prevents fragmentation of mitochondria leading to decreases in glycolysis as well as ATP generation. Herein, as expected, the result showed significant decreases in cell migration in all concentrations of the mdivi-1 inhibitor (Figure 7.9). This outcome has supported above results as well as our previously finding in 2D plastic surfaces related to the role of mitochondrial dynamic in regulation of cell migration.

Altogether, these results in 3D environment agree with our previous finding in 2D plastic surface that mitochondrial morphology affects cell migration. Alvetex and decellularised lung tissue were used for the first time in mitochondrial studies revealed that stress induced by high glucose led to fragmentation of mitochondria, whereas, low glucose enhanced elongation of mitochondria.

we are more confident about our results obtained on 2D surface since it were in agreement with obtained results on 3D environment, which are mimic to human tissues and tumors. This mean that the mitochondrial changes and their effect on the cancer cells observed in 2D surface can be used as a scientific basis in in vivo cancer treatments.

## **Chapter Eight: General Discussion**

Mitochondria play a central role in many cellular pathways including ATP generation, lipid metabolism, calcium homeostasis, aging, and apoptosis, as well as being a main source for ROS production (Giorgi et al., 2012, Osellame et al., 2012, Payne and Chinnery, 2015, Sas et al., 2018). It has been documented that mitochondria contribute in many disorders and diseases such as diabetes mellitus (Kwak et al., 2010), cardiovascular disease (Marzetti et al., 2013), neurodegenerative diseases such as Alzheimer and Parkinson diseases (Keogh and Chinnery, 2015), autism (Rose et al., 2014), and cancer (Singleterry et al., 2014). They are highly dynamic organelles (Yin and Cadenas, 2015, Mishra and Chan, 2016) and continuously undergo fission and fusion processes in response to different cellular signals (Suárez-Rivero et al., 2017). The balance between these two events is critical for maintaining mitochondrial function and efficiency (Yin and Cadenas, 2015, Mishra and Chan, 2016). Many factors such as hyperglycaemia, hypoxemia, heat, H<sub>2</sub>O<sub>2</sub>, U.V., and chemotherapy can disrupt this balance and shift mitochondria toward fragmentation (Yu et al., 2006, Yu et al., 2011, Van Beersel et al., 2013, Aung et al., 2017, Fan et al., 2010).

The relationship between mitochondrial morphology and function has been well studied (Picard et al., 2013), and there are reports that mitochondrial fragmentation can lead to mitochondrial dysfunction (Anesti and Scorrano, 2006, Giedt et al., 2016, Wai and Langer, 2016). Cell migration, which is a fundamental characteristic of metastasis, can be affected by changes in mitochondrial function (Han et al., 2013, Ma et al., 2013). However, the link between mitochondrial morphology and their metabolism with cell migration is not yet clear.

Our aim in this study was to determine the link between mitochondrial morphology and their metabolism with cell migration through investigating the effect of different glucose

levels, H<sub>2</sub>O<sub>2</sub>, ZLN005 activator (PGC-1 $\alpha$  coactivator), and anti-cancer drugs on mitochondrial morphology, mitochondrial metabolism, and cell migration as well as studying the role of p66shc and TRAP1, which activated by oxidative stress, alone and in combination, on metabolism reprogramming and cell migration.

To investigate the impact of mitochondrial morphologic changes on the cellular metabolism and cell migration, we seeded MDA-MB-231 cells in different glucose concentrations (1, 5.5, and 25mM). These concentrations were chosen depending on reports that related hyperglycaemia with progression of several mitochondria associated diseases including cancer initiation (Saha et al., 2017, Chang and Yang, 2016) Indeed, there is increasing evidence confirming progression of several types of cancer among obesity, and diabetic patients, which are characterized by high glucose rate in the blood, albeit the exact reason is not known (Gristina et al., 2015, Wang et al., 2015c). While, in low glucose level, down regulation of Drp1 has been reported which leads to mitochondria elongation (Rambold et al., 2011)

Our findings demonstrated that increasing glucose levels led to fragmentation of mitochondria, and induced the cells to reprogram their metabolism to be more glycolytic and generate higher amount of ATP, which has promoted speed of cell migration.

Mitochondrial morphology has been affected significantly with increasing oxidative stress induced by high glucose, leading to significant fragmentation of mitochondria. This change reduced mitochondrial outer membrane and mitochondrial inner membrane, which can increase apoptotic resistance and change cell metabolism.

Despite that changes in mitochondrial morphology depend on the oxidative stress which can be induced by several factors, duration of exposure consider another factor that can determine the changes in mitochondrial morphology, since it is not stable and it can be reversed as oxidative stress decreased by time. Therefore, it is possible that real

fragmentation rates of mitochondria induced for example by high glucose concentration or elongation of mitochondria induced by low glucose concentration, could be higher than obtained data. Moreover, mitochondrial overlapping that can occur may impede correct counting of mitochondrial number, however, we measured mitochondrial number via real time PCR as confirmation test.

Metabolism reprogramming in high glucose level was expected, because, reduced inner membrane surface in small fragmented mitochondria cannot support ETC enzyme function to generate ATP (Mannella, 2006). Therefore, cells reprogram their metabolism to aerobic glycolysis. In contrary, in low glucose level due to decreases in mitochondrial division protein; Drp1, mitochondria elongate with sufficient inner membrane surface for production of ATP via ETC. Despite generated ATP /molecule of glucose through oxidative phosphorylation is higher compared to generated ATP via aerobic glycolysis, however, it is much slower by 10-100 times(Lunt and Vander Heiden, 2011, Liberti and Locasale, 2016). Therefore, total generated ATP is lower.

It was important to measure O<sub>2</sub> consumption since it can show changes in oxidative phosphorylation rates. However, unavailability of suitable commercial kit and Seahorse XF Analyzer, limits the measurement of O<sub>2</sub> consumption as an important indicator for metabolic reprogramming in cancer cells.

Data for cell migration was obtained from two techniques; wound healing assay and tracking cell during 24hrs, confirm that speed of cell migration increases significantly with increasing concentrations of glucose. This finding shows the importance of glucose in controlling cell migration and thereby spreading of tumours. Cancer cells rely on glucose not only for generating ATP, but also for cell migration through the end product of glycolysis; lactate, which changes acidity of tumour microenvironment and induce enzymes for degradation ECM (Rofstad et al., 2006, Kato et al., 2013).

This finding of this study may explain the reason for progression of several types of cancer among obesity and diabetic patients, which characterised by excessive glucose level in their blood hyperglycaemia (Ryu et al., 2014, Martyn et al., 2008, Ozougwu, 2013).

In diabetes mellitus, glucose concentration in the blood increases significantly either due to an insufficient amount of insulin in the body or due to insulin resistance by body cells (Hu et al., 2017). Persistent hyperglycaemic condition causes several complications including tissue necrosis, retinopathy (vision loss), neuropathy (peripheral nerve injury), and nephropathy (kidney damage) , cancer progression and metastasis (Yagihashi et al., 2011, Levigne et al., 2013, Kang et al., 2015, Sayin et al., 2015, Volpe et al., 2018).

Obesity, which is a metabolic disease and can be defined as a massive accumulation of adipose tissue, is strongly implicated with progression of several types of cancers (Iyengar et al., 2015, De Marchi et al., 2013). Adipose tissue can secrete several adipokines, including tumor necrosis factor- $\alpha$  (TNF- $\alpha$ ), interleukin-6 (IL-6), resistin, adiponectin, and adiponectin that can change the metabolic, immunologic, and endocrine state and promote insulin resistance (John et al., 2006), and hyperglycaemia associated with type-2 diabetes (Martyn et al., 2008). It also secretes growth factors such as insulin-like growth factor-1(IGF-1), chemokines, and vascular endothelial growth factor (VEGF), which is seen to increase in metastatic cancer (Silha et al., 2005). It was reported that obesity can induce systemic oxidative stress as a result of high accumulation of fat and increasing glucose level in the circulatory bloods (De Marchi et al., 2013).

Oxidative stress induced due to high glucose level can regulate development and progression of several cancers including liver, pancreatic, lung, breast, colon, prostate, ovary, and brain cancers (Saha et al., 2017, Duan et al., 2014) through modification and mutation in mtDNA, genomic DNA, and several proteins and signaling pathways (Al-Kafaji and Golbahar, 2013, Lee and Chan, 2015), including tumor suppressor protein, p53, which

plays a crucial role in the regulation of the cell cycle and programmed cell death (Bates and Vousden, 1999), This protein controls expression of glucose transporter 1 and 4 (GLU1 and GLU4) through suppression of the promoter activity of GLUT1 and GLUT4 genes, thereby controls glucose uptake by the cells (Matsuura et al., 2016). Moreover, p53 inhibits metabolism reprogramming through downregulating the gene expression of hexokinase-2 (HK II), first enzyme in glycolysis pathway that converts glucose to glucose-6-phosphate, and high expressed and required for tumor initiation (Patra et al., 2013, Matsuura et al., 2016), as well as through regulation of cytochrome c oxidase (COX) complex in ETC (Puzio-Kuter, 2011).

Hyperglycaemia can make a major challenge during cancer treatment. Moreover, corticosteroids, which are usually used with chemotherapy to lesson nausea, can increase glucose levels in the blood dramatically (Hwangbo and Lee, 2017, Clore and Thurby-Hay, 2009). Using anti-diabetes drugs such as metformin and insulin, which are usually used in treatment for type-2 and type-1 diabetes respectively, in combination with chemotherapy, can solve hyperglycaemic conditions through decreasing glucose level in the blood, mainly through increasing glucose uptake. However, using these drugs continuously and for long time, can increase glucose flux to the cells more than they tolerate (Sonksen and Sonksen, 2000) inducing intracellular oxidative stress similar to metabolic stress (Ben Sahra et al., 2008, Ben Sahra et al., 2010, Giacco and Brownlee, 2010) that can induce fragmentation of mitochondria (Lefevre et al., 2012), and impairing mitochondrial oxidative phosphorylation (Suárez-Rivero et al., 2017), which can lead to apoptosis autophagy, and cell cycle arrest (Brooks and Dong, 2007).

Our results in regards to treating MDA-MB-231 cells with H<sub>2</sub>O<sub>2</sub> as an exogenous ROS source, which led to fragmentation of mitochondria, reprogramming metabolism to

glycolysis, and increases in cell migration, confirmed that the effect of high glucose on the cells was likely due to increased oxidative stress.

Inhibition of mitochondrial fragmentation using mitochondrial division inhibitor1, which targets Drp1 protein in MDA-MB-231 cells, show significant decreases in glycolysis and cell migration. Fission and fusion are important for biogenesis, mitophagy, and mitochondria dynamics and it appears that targeting mitochondrial fission may be effective in reducing cancer cell progression and metastasis. Moreover, prevention of mitochondrial fragmentation can decrease resistance to apoptosis. Therefore, using mitochondrial division inhibitor in cancer treatment in combination with other anti-cancer therapy could increase effectiveness of anti-cancer treatments significantly as it increases cancer cell sensitivity to apoptosis.

The missing point in previous studies on cancer progression among diabetes mellitus and obesity patients were p66shc and TRAP1 proteins. Protein p66shc activated and translocated from cytoplasm to mitochondria in response to oxidative stress such as that exerted by high glucose, U.V , and exogenous H<sub>2</sub>O<sub>2</sub> (Migliaccio et al., 1999, Sun et al., 2010, Lebedzinska-Arciszewska et al., 2015) and contributes to increasing mitochondrial ROS through oxidizing of cytochrome c (Giorgio et al., 2005). Its expression has been linked to defects in mitochondrial metabolism (Soliman et al., 2014) and apoptosis (Galimov, 2010). It was shown that oxidative stress induced in obesity and diabetes can lead to phosphorylation of p66Shc and triggers mitochondrial apoptosis (De Marchi et al., 2013).

Cancer cells can avoid apoptosis induced by p66shc through raising expression of cytoprotective protein TRAP1, which is located in the mitochondria and its expression increased in response to oxidative stress, can protect the cells from apoptosis through inhibition of Cyp D, which is essential in the formation of mPTP channel for release of

cytochrome c (Sinha and D'Silva, 2014). It also can inhibit oxidative phosphorylation through binding to and inhibiting SDH (Sciacovelli et al., 2013). It appears that cancer cells under oxidative stress can avoid themselves from apoptosis as one hallmark through increasing expression of TRAP1 and fragmentation of mitochondria. Therefore, preventing and inhibition of them can be a key for therapy of several types of cancer.

A novel finding in our study is that the strong correlation between p66shc and TRAP1 function may explain how they contribute in cell transformation to cancerous cells in diabetic and obesity patients, which characterized by hyperglycaemic and high oxidative stress state, through increasing cell resistance to apoptosis and to reprogram mitochondrial metabolism to aerobic glycolysis, which is important for initiation, proliferation, and success cancer metastasis.

Despite that p66shc can play a protective role from the consequences of the damaged oxidative stress on the normal cells by inducing apoptosis, targeting p66shc as well as TRAP1 separately can be effective for treatment of several types of cancers. Targeting p66shc protects oxidative phosphorylation and inhibits its reprogramming to glycolysis, which is crucial for cancer cell proliferation and increasing cell migration (Galimov, 2010). While, targeting TRAP1, which is expressed in very small amounts or nearly absent (Kang et al., 2007, Pak et al., 2017), will decline apoptotic resistance significantly, as well as maintain oxidative phosphorylation and prevent reprogramming metabolism. Therefore, targeting TRAP1 with specific inhibitor in cancer therapy can be in a great value especially if combined with other anti-cancer agents that induce apoptosis.

PGC-1 $\alpha$  is a powerful transcription factor involved in the regulation of mitochondrial biogenesis, oxidative metabolism (Austin and St-Pierre, 2012), and mitochondrial fission/fusion through controlling Drp1 expression (Dabrowska et al., 2015). It is also considered a powerful regulator of ROS removal through increasing expression of several

ROS-detoxifying enzymes (Austin and St-Pierre, 2012). ZLN005 has been designed as selective transcriptional regulator of PGC-1 $\alpha$  (Zhang et al., 2013). We were inspired to investigate the possibility that overexpression of PGC-1 $\alpha$  can induce mitochondrial fission independent from oxidative stress, therefore, we treated MDA-MB-231 cells with ZLN005. The results revealed that ZLN005 can induce mitochondrial fragmentation. However, western blotting analysis revealed that increases in expression of PGC-1 $\alpha$  and its downstream protein Drp1 were limited (only at 10 $\mu$ M of ZLN005). This finding is quite interesting, since, it was supposed that expression of mitochondrial division protein Drp1 will be increased even if it is not affected by upstream protein regulator; PGC-1 $\alpha$ , as mitochondria has fragmented significantly in all used concentrations of ZLN005. This result can suggest that ZLN005 may be interacting with other unknown proteins and pathways that induce fragmentation of mitochondria.

To further investigate the relationship between mitochondrial morphology and their metabolism with cell migration, we targeted glycolysis with 3BrPA inhibitor, which inhibits glycolysis through inhibition of HKII and GAPDH (Ganapathy-Kanniappan et al., 2009, Ho et al., 2016), and oxidative phosphorylation was targeted with AMA, which inhibits cytochrome c oxidoreductase complex (complex III) in ETC (Ma et al., 2011). The findings show that treating MDA-MB-231 cells with both 3BrPA and AMA led to fragmentation of mitochondria, with significant increases in ROS production. Our results show that targeting cells with AMA induce reprogramming metabolism to glycolysis, with increases in speed of cell migration. Whereas, treating the cells with 3BrPA inhibitor led to declining glycolysis with slowdown of cell migration speed.

This novel finding demonstrates that using AMA in cancer therapy can promote cancer cell migration and metastasis as it inhibits oxidative phosphorylation and promotes redirection of metabolism to aerobic glycolysis, whereas, fragmentation of mitochondria

mediated by AMA can increase resistance to apoptosis. In contrast, using 3BrPA inhibitor for targeting cancer cells may reduce cancer progression and metastasis significantly. However, cytotoxic effect of 3BrPA inhibitor on the normal cells can limit its usage as anti-cancer therapy in vivo. Since normal cells also rely on glycolysis for generating either ATP as in muscle and cardiac cells (Conley et al., 2001, Doenst et al., 2013) or acetyl Co-A, which enters TCA cycle in mitochondria in most body cells (DeBerardinis and Chandel, 2016). Recently, it has been reported that metabolic profiles of both T lymphocytes and cancer cells are similar, and this increases the risk of targeting cancer cell metabolism with 3BrPA inhibitor on immune system (Allison et al., 2017).

Moreover, elevated levels of generated ROS accompanied to 3BrPA inhibitor treatment lead to hyperfragmentation of mitochondria, which can increase resistance of cancer cells to treatments including 3BrPA inhibitor itself (Renault et al., 2015, Han et al., 2018), as well as it can affect and interact with several other pathways, proteins, and enzymes (Görlach et al., 2015; Liou and Storz, 2010; Nicco and Batteux, 2017). Although it has been suggested a fragmentation of mitochondria as an initial step of apoptosis (Parone and Martinou, 2006), many studies suggested that mitochondrial fragmentation have no role in apoptosis (Parone et al., 2006, Suen et al., 2008). Furthermore, there are reports found that in some conditions mitochondrial fragmentation can inhibit apoptosis (Arnoult, 2007, Renault et al., 2015). Therefore; targeting glycolysis using 3BrPA for cancer treatment would not be a good choice to recommend.

Although targeting metabolism as strategy for cancer treatment has been developed for long time (Tran et al., 2016), depending on our result, AMA and 3BrPA are not recommended to be used as anti-cancer therapy. However, targeting glucose transporter (GLUTs), lactate dehydrogenase A (LDHA), which catalyzes the conversion of pyruvate to L-lactate and back, pyruvate dehydrogenase kinase (PDK), inactivate the enzyme pyruvate

dehydrogenase, and hexokinase II (Zhao et al., 2013b), which is specific to cancer cells, may be more effective in cancer treatment.

### **Limitation and challenges in this study**

One of limitation of the present study was inability to investigate O<sub>2</sub> consumption, which is powerful test to know oxidative phosphorylation rates, due to unavailability of Seahorse XF Analyzer, which can measure O<sub>2</sub> consumption directly in live cells, during studying time. Although we measured ATP and lactate using specific kits, which are high accurate for determination ATP and lactate, however, they can show changes in glycolysis but not oxidative phosphorylation.

Another challenge in this study was in counting mitochondrial number using confocal microscopy. Due to mitochondrial overlapping it was difficult to measuring mitochondrial number in some non-metastatic cell line such as MCF-10A breast cancer cell and HeLa cell, which are characterized by high mitochondrial number in contrast to high metastatic MDA-MB-231 breast cancer cell line, which characterized by low number of mitochondria.

Since the mitochondria are highly dynamic and the fusion-fission can be occur very fast in response to any changes in the medium and temperature, it made a challenge especially during staining. We fix this issue through adding paraformaldehyde to culture medium directly to fix cells before changing medium and washing the cells with PBS.

### **Future study**

This thesis has contributed new insights into the role of mitochondrial morphology and their metabolism in regulating cancer cell migration through studying the effect of high glucose levels, which feature in several diseases including diabetes, obesity, neurodegenerative diseases, and many types of cancers, on mitochondrial dynamics in vitro on 2D plastic surface and several 3D cell cultures. Despite this, to confirm the

hyperglycaemic effect on mitochondrial morphology and their metabolism, we are interested in repeating this investigation on cells biopsy samples from patients with diabetes (type 1 and type 2) to study changes in mitochondrial morphology in comparison with same type of cells taking from cancer patients and healthy control individuals. Furthermore, this study will allow us to know the mechanism that makes the diabetic cells to avoid cytotoxic effect of accumulated ROS, since generated and accumulated ROS in the cells that can be induced by factors such as hyperglycaemia, which is common characteristic in many diseases and disorders such as diabetes, obesity, cardiovascular diseases, and neurodegenerative diseases, can transform cells to neoplasia and cancer cells. Actually, there are reports that referred to cancer progression among diabetes type 2 and obesity, which are characterized by severe insulin resistance (Gristina et al., 2015; Iyengar et al., 2015; Wang et al., 2015c). Unfortunately, overdose or prolonged use of insulin therapy can decline glucose level in the blood to dangerous low levels and at the same time induce high uptake of glucose by cells that can causes several health complications such as heart attack, stroke, cancer and eye complications (Duan et al., 2014; Sayin et al., 2015; Tseng, 2015).

Since p66shc plays an important role in reprogramming metabolism and its function and expression is strongly related with TRAP1, which preventing apoptosis, it will be interesting to repeat this investigation in other cell lines especially nerve cells as it has been reported that many neurodegenerative diseases are linked to hyperglycaemia and mitochondrial fragmentation (Rajamani, 2014, Gao et al., 2017), as well as nerve cell death due to that high ROS production could be responsible on several complications including dementia (Rossen et al., 2009, Gella and Durany, 2009).

The effect of ZLN0005, which activates expression of PGC-1 $\alpha$  and its downstream protein Drp1, was limited to low concentrations, while, at high concentrations it did not show any

effect on expression of PGC-1 $\alpha$  or on its downstream protein Drp1, despite significant effect of ZLN0005 on the mitochondrial fragmentation, metabolism, and cell migration. Recently,  $\alpha$ -synuclein, which localizes in cytosol and is present in mitochondria-associated endoplasmic reticulum membranes, has been linked to fragmentation of mitochondria without expression of Drp1 protein (Guardia-Laguarta et al., 2014, Nakamura et al., 2011). Therefore, it will be interesting to study its effect on mitochondrial morphology and function in regulating cancer cell migration under hyperglycaemic conditions.

Finally, It is recommended to use Seahorse XF Analyzer for measuring ATP, lactate, and O<sub>2</sub> consumption directly in live cells since the results will be more accurate and solve technical limitation encountered in the present study. Also it is preferred to study changes in mitochondrial morphology at different times as mitochondrial fusion-fission is a dynamic process and reversible during the time.

## References:

- Aguiar, D.P., de Farias, G.C., de Sousa, E.B., de Mattos Coelho-Aguiar, J., Lobo, J.C., Casado, P.L., Duarte, M.E.L., and Abreu, J.G.R. (2014). New strategy to control cell migration and metastasis regulated by CCN2/CTGF. *Cancer Cell Int* *14*, 61-61.
- Akita, M., Suzuki-Karasaki, M., Fujiwara, K., Nakagawa, C., Soma, M., Yoshida, Y., Ochiai, T., Tokuhashi, Y., and Suzuki-Karasaki, Y. (2014). Mitochondrial division inhibitor-1 induces mitochondrial hyperfusion and sensitizes human cancer cells to TRAIL-induced apoptosis. *International journal of oncology* *45*, 1901-1912.
- Al-Gubory, K.H. (2005). Fibered confocal fluorescence microscopy for imaging apoptotic DNA fragmentation at the single-cell level in vivo. *Exp Cell Res* *310*, 474-481.
- Al-Kafaji, G., and Golbahar, J. (2013). High Glucose-Induced Oxidative Stress Increases the Copy Number of Mitochondrial DNA in Human Mesangial Cells. *BioMed Research International* *2013*, 754946.
- Alecu, I., Tedeschi, A., Behler, N., Wunderling, K., Lamberz, C., Lauterbach, M.A.R., Gaebler, A., Ernst, D., Van Veldhoven, P.P., Al-Amoudi, A., *et al.* (2017). Localization of 1-deoxysphingolipids to mitochondria induces mitochondrial dysfunction. *Journal of Lipid Research* *58*, 42-59.
- Alexandre, A., and Lehninger, A.L. (1984). Bypasses of the antimycin A block of mitochondrial electron transport in relation to ubisemiquinone function. *Biochimica et Biophysica Acta (BBA) - Bioenergetics* *767*, 120-129.
- Allison, K.E., Coomber, B.L., and Bridle, B.W. (2017). Metabolic reprogramming in the tumour microenvironment: a hallmark shared by cancer cells and T lymphocytes. *Immunology* *152*, 175-184.

- Alsarraj, J., and Hunter, K. (2012). Bromodomain-Containing Protein 4: A Dynamic Regulator of Breast Cancer Metastasis through Modulation of the Extracellular Matrix, Vol 2012.
- Amaral, S.F., Scaffa, P.M.C., Rodrigues, R.D.S., Nesadal, D., Marques, M.M., Nogueira, F.N., and Sobral, M.A.P. (2018). Dynamic Influence of pH on Metalloproteinase Activity in Human Coronal and Radicular Dentin. *Caries Research* 52, 113-118.
- Amoroso, M.R., Matassa, D.S., Sisinni, L., Lettini, G., Landriscina, M., and Esposito, F. (2014). TRAP1 revisited: novel localizations and functions of a 'next-generation' biomarker (review). *International journal of oncology* 45, 969-977.
- Amundson, S.A., Myers, T.G., and Fornace, A.J., Jr. (1998). Roles for p53 in growth arrest and apoptosis: putting on the brakes after genotoxic stress. *Oncogene* 17, 3287-3299.
- Ananthakrishnan, R., and Ehrlicher, A. (2007). The forces behind cell movement. *Int J Biol Sci* 3, 303-317.
- Anesti, V., and Scorrano, L. (2006). The relationship between mitochondrial shape and function and the cytoskeleton. *Biochimica et Biophysica Acta (BBA) - Bioenergetics* 1757, 692-699.
- Antico Arciuch, V.G., Elguero, M.E., Poderoso, J.J., and Carreras, M.C. (2012). Mitochondrial Regulation of Cell Cycle and Proliferation. *Antioxidants & redox signaling* 16, 1150-1180.
- Aravamudan, B., Kiel, A., Freeman, M., Delmotte, P., Thompson, M., Vassallo, R., Sieck, G.C., Pabelick, C.M., and Prakash, Y.S. (2014). Cigarette smoke-induced mitochondrial fragmentation and dysfunction in human airway smooth muscle. *Am J Physiol Lung Cell Mol Physiol* 306, L840-854.
- Arnoult, D. (2007). Mitochondrial fragmentation in apoptosis. *Trends in cell biology* 17, 6-12.

- Aung, L.H.H., Li, R., Prabhakar, B.S., Maker, A.V., and Li, P. (2017). Mitochondrial protein 18 (MTP18) plays a pro-apoptotic role in chemotherapy-induced gastric cancer cell apoptosis. *Oncotarget* 8, 56582-56597.
- Austin, S., and St-Pierre, J. (2012). PGC1alpha and mitochondrial metabolism--emerging concepts and relevance in ageing and neurodegenerative disorders. *J Cell Sci* 125, 4963-4971.
- Ayala, A., Munoz, F.M., and Argguelles, S. (2014). Lipid Peroxidation: Production, Metabolism, and Signaling Mechanisms of Malondialdehyde and 4-Hydroxy-2-Nonenal. *Oxidative medicine and cellular longevity* 2014, 31.
- Balaban, R.S., Nemoto, S., and Finkel, T. (2005). Mitochondria, oxidants, and aging. *Cell* 120, 483-495.
- Baldelli, S., Aquilano, K., and Ciriolo, M.R. (2014). PGC-1alpha buffers ROS-mediated removal of mitochondria during myogenesis. *Cell Death Dis* 5, e1515.
- Barazzoni, R. (2012). Modulating mitochondrial fission to lower diabetic oxidative stress. *Diabetes* 61, 1915-1917.
- Bates, S., and Vousden, K.H. (1999). Mechanisms of p53-mediated apoptosis. *Cell Mol Life Sci* 55, 28-37.
- Beckert, S., Farrahi, F., Aslam, R., Scheuenstuhl, H., Königsrainer, A., Zamirul Hussain, M., and Hunt, T. (2006). Lactate stimulates endothelial cell migration, Vol 14.
- Ben Sahra, I., Laurent, K., Loubat, A., Giorgetti-Peraldi, S., Colosetti, P., Auberger, P., Tanti, J.F., Le Marchand-Brustel, Y., and Bost, F. (2008). The antidiabetic drug metformin exerts an antitumoral effect in vitro and in vivo through a decrease of cyclin D1 level. *Oncogene* 27, 3576-3586.
- Ben Sahra, I., Le Marchand-Brustel, Y., Tanti, J.F., and Bost, F. (2010). Metformin in cancer therapy: a new perspective for an old antidiabetic drug? *Mol Cancer Ther* 9, 1092-1099.

- Benischke, A.-S., Vasanth, S., Miyai, T., Katikireddy, K.R., White, T., Chen, Y., Halilovic, A., Price, M., Price, F., Liton, P.B., *et al.* (2017). Activation of mitophagy leads to decline in Mfn2 and loss of mitochondrial mass in Fuchs endothelial corneal dystrophy. *Scientific Reports* 7, 6656.
- Berniakovich, I., Trinei, M., Stendardo, M., Migliaccio, E., Minucci, S., Bernardi, P., Pelicci, P.G., and Giorgio, M. (2008). p66(Shc)-generated Oxidative Signal Promotes Fat Accumulation. *The Journal of Biological Chemistry* 283, 34283-34293.
- Bhat, S.S., Anand, D., and Khanday, F.A. (2015). p66Shc as a switch in bringing about contrasting responses in cell growth: implications on cell proliferation and apoptosis. *Molecular cancer* 14, 76.
- Bhattacharyya, A., Chattopadhyay, R., Mitra, S., and Crowe, S.E. (2014). Oxidative Stress: An Essential Factor in the Pathogenesis of Gastrointestinal Mucosal Diseases. *Physiological Reviews* 94, 329-354.
- Bhatti, J.S., Kumar, S., Vijayan, M., Bhatti, G.K., and Reddy, P.H. (2017). Chapter Two - Therapeutic Strategies for Mitochondrial Dysfunction and Oxidative Stress in Age-Related Metabolic Disorders. In *Progress in Molecular Biology and Translational Science*, P.H. Reddy, ed. (Academic Press), pp. 13-46.
- Bordi, M., Nazio, F., and Campello, S. (2017). The Close Interconnection between Mitochondrial Dynamics and Mitophagy in Cancer. *Frontiers in Oncology* 7, 81.
- Boroughs, L.K., and DeBerardinis, R.J. (2015). Metabolic pathways promoting cancer cell survival and growth. *Nat Cell Biol* 17, 351-359.
- Bradford, M.M. (1976). A rapid and sensitive method for the quantitation of microgram quantities of protein utilizing the principle of protein-dye binding. *Analytical Biochemistry* 72, 248-254.

- Bratic, A., and Larsson, N.-G. (2013). The role of mitochondria in aging. *The Journal of Clinical Investigation* *123*, 951-957.
- Bratton, D.L., Fadok, V.A., Richter, D.A., Kailey, J.M., Guthrie, L.A., and Henson, P.M. (1997). Appearance of phosphatidylserine on apoptotic cells requires calcium-mediated nonspecific flip-flop and is enhanced by loss of the aminophospholipid translocase. *J Biol Chem* *272*, 26159-26165.
- Braut, C., and Schulze, A. (2016). The Role of Glucose and Lipid Metabolism in Growth and Survival of Cancer Cells. *Recent Results Cancer Res* *207*, 1-22.
- Briere, J.J., Favier, J., Benit, P., El Ghouzzi, V., Lorenzato, A., Rabier, D., Di Renzo, M.F., Gimenez-Roqueplo, A.P., and Rustin, P. (2005). Mitochondrial succinate is instrumental for HIF1alpha nuclear translocation in SDHA-mutant fibroblasts under normoxic conditions. *Human molecular genetics* *14*, 3263-3269.
- Broertjes, J. (2015). The Ten Hallmarks of Cancer in Cutaneous Malignant Melanoma.
- Brooks, C., and Dong, Z. (2007). Regulation of Mitochondrial Morphological Dynamics During Apoptosis by Bcl-2 family proteins: A Key in Bak? *Cell cycle (Georgetown, Tex)* *6*, 3043-3047.
- Burte, F., Carelli, V., Chinnery, P.F., and Yu-Wai-Man, P. (2015). Disturbed mitochondrial dynamics and neurodegenerative disorders. *Nature reviews Neurology* *11*, 11-24.
- Cai, L., Li, W., Wang, G., Guo, L., Jiang, Y., and Kang, Y.J. (2002). Hyperglycemia-Induced Apoptosis in Mouse Myocardium; Mitochondrial Cytochrome Mediated Caspase-3 Activation Pathway. *American Diabetes Association* *51*, 1938-1948.
- Caino, M.C., and Altieri, D.C. (2015). Cancer cells exploit adaptive mitochondrial dynamics to increase tumor cell invasion. *Cell cycle (Georgetown, Tex)* *14*, 3242-3247.

- Caino, M.C., Chae, Y.C., Vaira, V., Ferrero, S., Nosotti, M., Martin, N.M., Weeraratna, A., O'Connell, M., Jernigan, D., Fatatis, A., *et al.* (2013). Metabolic stress regulates cytoskeletal dynamics and metastasis of cancer cells. *J Clin Invest* *123*, 2907-2920.
- Campello, S., Lacalle, R., Bettella, M., Mañes, S., Scorrano, L., and Viola, A. (2007). Orchestration of lymphocyte chemotaxis by mitochondrial dynamics, Vol 203.
- Campello, S., and Scorrano, L. (2010). Mitochondrial shape changes: orchestrating cell pathophysiology. *EMBO reports* *11*, 678-684.
- Cantor, J.R., and Sabatini, D.M. (2012). Cancer Cell Metabolism: One Hallmark, Many Faces. *Cancer discovery* *2*, 881-898.
- Cao, J.-J., Tan, C.-P., Chen, M.-H., Wu, N., Yao, D.-Y., Liu, X.-G., Ji, L.-N., and Mao, Z.-W. (2017). Targeting cancer cell metabolism with mitochondria-immobilized phosphorescent cyclometalated iridium(iii) complexes. *Chemical Science* *8*, 631-640.
- Cassidy-Stone, A., Chipuk, J.E., Ingerman, E., Song, C., Yoo, C., Kuwana, T., Kurth, M.J., Shaw, J.T., Hinshaw, J.E., Green, D.R., *et al.* (2008). Chemical inhibition of the mitochondrial division dynamin reveals its role in Bax/Bak-dependent mitochondrial outer membrane permeabilization. *Developmental cell* *14*, 193-204.
- Chang, S.C., and Yang, W.V. (2016). Hyperglycemia, tumorigenesis, and chronic inflammation. *Crit Rev Oncol Hematol* *108*, 146-153.
- Chen, B., Kumar, G., Co, C.C., and Ho, C. C. (2013). Geometric Control of Cell Migration. *Scientific Reports* *3*, 2827.
- Chen, H., Vermulst, M., Wang, Y.E., Chomyn, A., Prolla, T.A., McCaffery, J.M., and Chan, D.C. (2010). Mitochondrial fusion is required for mtDNA stability in skeletal muscle and tolerance of mtDNA mutations. *Cell* *141*, 280-289.

- Chen, W., Wang, Q., Bai, L., Chen, W., Wang, X., Tellez, C.S., Leng, S., Padilla, M.T., Nyunoya, T., Belinsky, S.A., *et al.* (2014). RIP1 maintains DNA integrity and cell proliferation by regulating PGC-1 $\alpha$ -mediated mitochondrial oxidative phosphorylation and glycolysis. *Cell Death and Differentiation* 21, 1061-1070.
- Chipuk, J.E., and Green, D.R. (2008). How do BCL-2 proteins induce mitochondrial outer membrane permeabilization? *Trends in cell biology* 18, 157-164.
- Ciron, C., Zheng, L., Bobela, W., Knott, G.W., Leone, T.C., Kelly, D.P., and Schneider, B.L. (2015). PGC-1 $\alpha$  activity in nigral dopamine neurons determines vulnerability to alpha-synuclein. *Acta neuropathologica communications* 3, 16.
- Clore, J.N., and Thurby-Hay, L. (2009). Glucocorticoid-induced hyperglycemia. *Endocrine practice : official journal of the American College of Endocrinology and the American Association of Clinical Endocrinologists* 15, 469-474.
- Cogliati, S., Enriquez, J.A., and Scorrano, L. (2016). Mitochondrial Cristae: Where Beauty Meets Functionality. *Trends Biochem Sci* 41, 261-273.
- Cogliati, S., Frezza, C., Soriano, M.E., Varanita, T., Quintana-Cabrera, R., Corrado, M., Cipolat, S., Costa, V., Casarin, A., Gomes, L.C., *et al.* (2013). Mitochondrial cristae shape determines respiratory chain supercomplexes assembly and respiratory efficiency. *Cell* 155, 160-171.
- Conley, K.E., Kemper, W.F., and Crowther, G.J. (2001). Limits to sustainable muscle performance: interaction between glycolysis and oxidative phosphorylation. *The Journal of experimental biology* 204, 3189-3194.
- Cosentino, F., Francia, P., Camici, G.G., Pelicci, P.G., Luscher, T.F., and Volpe, M. (2008). Final common molecular pathways of aging and cardiovascular disease: role of the p66Shc protein. *Arterioscler Thromb Vasc Biol* 28, 622-628.

- Coskun, P., Wyrembak, J., Schriener, S.E., Chen, H.W., Marciniack, C., Laferla, F., and Wallace, D.C. (2012). A mitochondrial etiology of Alzheimer and Parkinson disease. *Biochimica et biophysica acta* 1820, 553-564.
- Cree, I.A., and Charlton, P. (2017). Molecular chess? Hallmarks of anti-cancer drug resistance. *Bmc Cancer* 17, 10.
- Cribbs, J.T., and Strack, S. (2007). Reversible phosphorylation of Drp1 by cyclic AMP-dependent protein kinase and calcineurin regulates mitochondrial fission and cell death. *EMBO Reports* 8, 939-944.
- Dabrowska, A., Venero, J.L., Iwasawa, R., Hankir, M.-k., Rahman, S., Boobis, A., and Hajji, N. (2015). PGC-1 $\alpha$  controls mitochondrial biogenesis and dynamics in lead-induced neurotoxicity. *Aging (Albany NY)* 7, 629-643.
- De Marchi, E., Baldassari, F., Bononi, A., Wieckowski, M.R., and Pinton, P. (2013). Oxidative stress in cardiovascular diseases and obesity: role of p66Shc and protein kinase C. *Oxidative medicine and cellular longevity* 2013, 564961.
- de Visser, K.E., Eichten, A., and Coussens, L.M. (2006). Paradoxical roles of the immune system during cancer development. *Nat Rev Cancer* 6, 24-37.
- DeBerardinis, R.J., and Chandel, N.S. (2016). Fundamentals of cancer metabolism. *Science Advances* 2.
- Di Lullo, G.A., Sweeney, S.M., Korkko, J., Ala-Kokko, L., and San Antonio, J.D. (2002). Mapping the ligand-binding sites and disease-associated mutations on the most abundant protein in the human, type I collagen. *J Biol Chem* 277, 4223-4231.
- DiMilla, P.A., Stone, J.A., Quinn, J.A., Albelda, S.M., and Lauffenburger, D.A. (1993). Maximal migration of human smooth muscle cells on fibronectin and type IV collagen occurs at an intermediate attachment strength. *The Journal of cell biology* 122, 729-737.

- Din, S., Mason, M., Völkers, M., Johnson, B., Cottage, C.T., Wang, Z., Joyo, A.Y., Quijada, P., Erhardt, P., Magnuson, N.S., *et al.* (2013). Pim-1 preserves mitochondrial morphology by inhibiting dynamin-related protein 1 translocation. *Proceedings of the National Academy of Sciences of the United States of America* *110*, 5969-5974.
- Doenst, T., Nguyen, T.D., and Abel, E.D. (2013). Cardiac Metabolism in Heart Failure - Implications beyond ATP production. *Circulation research* *113*, 709-724.
- Doherty, J.R., and Cleveland, J.L. (2013). Targeting lactate metabolism for cancer therapeutics. *J Clin Invest* *123*, 3685-3692.
- Duan, W., Shen, X., Lei, J., Xu, Q., Yu, Y., Li, R., Wu, E., and Ma, Q. (2014). Hyperglycemia, a Neglected Factor during Cancer Progression. *BioMed Research International* *2014*, 10.
- Elmore, S. (2007). Apoptosis: A Review of Programmed Cell Death. *Toxicologic pathology* *35*, 495-516.
- Elustondo, P.A., Nichols, M., Negoda, A., Thirumaran, A., Zakharian, E., Robertson, G.S., and Pavlov, E.V. (2016). Mitochondrial permeability transition pore induction is linked to formation of the complex of ATPase C-subunit, polyhydroxybutyrate and inorganic polyphosphate. *Cell Death Discovery* *2*, 16070.
- Eyassu, F., and Angione, C. (2017). Modelling pyruvate dehydrogenase under hypoxia and its role in cancer metabolism. *Royal Society Open Science* *4*, 170360.
- Fabian, S.-G., Jose Luis, G.-G., Mari Carmen, G.-C., and Federico, V.P. (2014). Mitochondrial Biogenesis in Health and Disease. *Molecular and Therapeutic Approaches. Current Pharmaceutical Design* *20*, 5619-5633.
- Fan, X., Hussien, R., and Brooks, G.A. (2010). H<sub>2</sub>O<sub>2</sub>-induced mitochondrial fragmentation in C2C12 myocytes. *Free radical biology & medicine* *49*, 1646-1654.

- Fantin, V.R., St-Pierre, J., and Leder, P. (2006). Attenuation of LDH-A expression uncovers a link between glycolysis, mitochondrial physiology, and tumor maintenance. *Cancer Cell* 9, 425-434.
- Feitelson, M.A., Arzumanyan, A., Kulathinal, R.J., Blain, S.W., Holcombe, R.F., Mahajna, J., Marino, M., Martinez-Chantar, M.L., Nawroth, R., Sanchez-Garcia, I., *et al.* (2015). Sustained proliferation in cancer: Mechanisms and novel therapeutic targets. *Seminars in Cancer Biology* 35, S25-S54.
- Ferguson, L.R., Chen, H., Collins, A.R., Connell, M., Damia, G., Dasgupta, S., Malhotra, M., Meeker, A.K., Amedei, A., Amin, A., *et al.* (2015). Genomic instability in human cancer: Molecular insights and opportunities for therapeutic attack and prevention through diet and nutrition. *Seminars in Cancer Biology* 35, S5-S24.
- Fernald, K., and Kurokawa, M. (2013). Evading apoptosis in cancer. *Trends in cell biology* 23, 620-633.
- Ferree, A., and Shirihai, O. (2012). Mitochondrial dynamics: the intersection of form and function. *Adv Exp Med Biol* 748, 13-40.
- Fiaschi, T., and Chiarugi, P. (2012). Oxidative stress, tumor microenvironment, and metabolic reprogramming: a diabolic liaison. *Int J Cell Biol* 2012, 762825.
- Filippi, B.M., Abraham, M.A., Silva, P.N., Rasti, M., LaPierre, M.P., Bauer, P.V., Rocheleau, J.V., and Lam, T.K.T. (2017). Dynamin-Related Protein 1-Dependent Mitochondrial Fission Changes in the Dorsal Vagal Complex Regulate Insulin Action. *Cell Rep* 18, 2301-2309.
- Finck, B.N., and Kelly, D.P. (2006). PGC-1 coactivators: inducible regulators of energy metabolism in health and disease. *Journal of Clinical Investigation* 116, 615-622.
- Finley, L.W.S., and Thompson, C.B. (2015). 13 - The Metabolism of Cell Growth and Proliferation. In *The Molecular Basis of Cancer (Fourth Edition)* (Philadelphia: Content Repository Only!), pp. 191-208.e192.

- Fouad, Y.A., and Aanei, C. (2017). Revisiting the hallmarks of cancer. *American Journal of Cancer Research* 7, 1016-1036.
- Frank, S., Gaume, B., Bergmann-Leitner, E.S., Leitner, W.W., Robert, E.G., Catez, F., Smith, C.L., and Youle, R.J. (2001). The Role of Dynamin-Related Protein 1, a Mediator of Mitochondrial Fission, in Apoptosis. *Developmental cell* 1, 515-525.
- Franz, C.M., Jones, G.E., and Ridley, A.J. (2002). Cell Migration in Development and Disease. *Developmental cell* 2, 153-158.
- Fulda, S. (2010). Evasion of Apoptosis as a Cellular Stress Response in Cancer. *International Journal of Cell Biology* 2010, 6.
- Galimov, E.R. (2010). The Role of p66shc in Oxidative Stress and Apoptosis. *Acta Naturae* 2, 44-51.
- Gan, X., Huang, S., Yu, Q., Yu, H., and Yan, S.S. (2015). Blockade of Drp1 rescues oxidative stress-induced osteoblast dysfunction. *Biochemical and Biophysical Research Communications* 468, 719-725.
- Ganapathy-Kanniappan, S., and Geschwind, J.F. (2013). Tumor glycolysis as a target for cancer therapy: progress and prospects. *Molecular cancer* 12, 152.
- Gao, J.Y., Song, B.R., Peng, J.J., and Lu, Y.M. (2012). Correlation between mitochondrial TRAP-1 expression and lymph node metastasis in colorectal cancer. *World journal of gastroenterology* 18, 5965-5971.
- Gao, L., Laude, K., and Cai, H. (2008). Mitochondrial Pathophysiology, Reactive Oxygen Species, and Cardiovascular Diseases. *The Veterinary clinics of North America Small animal practice* 38, 137-vi.
- Ge, Y., and Xu, K. (2016). Alpha-synuclein contributes to malignant progression of human meningioma via the Akt/mTOR pathway. *Cancer Cell Int* 16, 86.

- Georgieva, E., Ivanova, D., Zhelev, Z., Bakalova, R., Gulubova, M., and AOKI, I. (2017). Mitochondrial Dysfunction and Redox Imbalance as a Diagnostic Marker of “Free Radical Diseases”. *Anticancer Res* 37, 5373-5381.
- Gerweck, L.E., and Seetharaman, K. (1996). Cellular pH gradient in tumor versus normal tissue: potential exploitation for the treatment of cancer. *Cancer Res* 56, 1194-1198.
- Giacco, F., and Brownlee, M. (2010). Oxidative stress and diabetic complications. *Circulation research* 107, 1058-1070.
- Giampazolias, E., and Tait, S.W. (2016). Mitochondria and the hallmarks of cancer. *FEBS J* 283, 803-814.
- Giedt, R.J., Fumene Feruglio, P., Pathania, D., Yang, K.S., Kilcoyne, A., Vinegoni, C., Mitchison, T.J., and Weissleder, R. (2016). Computational imaging reveals mitochondrial morphology as a biomarker of cancer phenotype and drug response. *Scientific Reports* 6, 32985.
- Giorgi, C., Agnoletto, C., Bononi, A., Bonora, M., De Marchi, E., Marchi, S., Missiroli, S., Patergnani, S., Poletti, F., Rimessi, A., *et al.* (2012). Mitochondrial calcium homeostasis as potential target for mitochondrial medicine. *Mitochondrion* 12, 77-85.
- Giorgio, M., Migliaccio, E., Orsini, F., Paolucci, D., Moroni, M., Contursi, C., Pelliccia, G., Luzi, L., Minucci, S., Marcaccio, M., *et al.* (2005). Electron transfer between cytochrome c and p66Shc generates reactive oxygen species that trigger mitochondrial apoptosis. *Cell* 122, 221-233.
- Girnun, G.D. (2012). The diverse role of the PPARgamma coactivator 1 family of transcriptional coactivators in cancer. *Semin Cell Dev Biol* 23, 381-388.

- Görlach, A., Dimova, E.Y., Petry, A., Martínez-Ruiz, A., Hernansanz-Agustín, P., Rolo, A.P., Palmeira, C.M., and Kietzmann, T. (2015). Reactive oxygen species, nutrition, hypoxia and diseases: Problems solved? *Redox biology* 6, 372-385.
- Gou, H., Zhao, M., Xu, H., Yuan, J., He, W., Zhu, M., Ding, H., Yi, L., and Chen, J. (2017). CSFV induced mitochondrial fission and mitophagy to inhibit apoptosis. *Oncotarget* 8, 39382-39400.
- Gough, D.R., and Cotter, T.G. (2011). Hydrogen peroxide: a Jekyll and Hyde signalling molecule. *Cell Death & Disease* 2, e213.
- Gredilla, R. (2011). DNA Damage and Base Excision Repair in Mitochondria and Their Role in Aging. *Journal of Aging Research* 2011, 257093.
- Griffiths, G.J., Dubrez, L., Morgan, C.P., Jones, N.A., Whitehouse, J., Corfe, B.M., Dive, C., and Hickman, J.A. (1999). Cell damage-induced conformational changes of the pro-apoptotic protein Bak in vivo precede the onset of apoptosis. *The Journal of cell biology* 144, 903-914.
- Gristina, V., Cupri, M.G., Torchio, M., Mezzogori, C., Cacciabue, L., and Danova, M. (2015). Diabetes and cancer: A critical appraisal of the pathogenetic and therapeutic links. *Biomed Rep* 3, 131-136.
- Grivennikov, S.I., Greten, F.R., and Karin, M. (2010). Immunity, inflammation, and cancer. *Cell* 140, 883-899.
- Gu, Q., Zhu, H., Chen, L., Shuai, L., Fang, J., Wu, J., Liu, L., Li, W., Dai, J., Hao, J., *et al.* (2016). Three dimensional collagen scaffolds promote iPSC induction with higher pluripotency. *Protein & Cell* 7, 844-848.
- Guardia-Laguarta, C., Area-Gomez, E., Rüb, C., Liu, Y., Magrané, J., Becker, D., Voos, W., Schon, E.A., and Przedborski, S. (2014).  $\alpha$ -Synuclein Is Localized to Mitochondria-Associated ER Membranes. *The Journal of Neuroscience* 34, 249-259.

- Guido, C., Whitaker-Menezes, D., Lin, Z., Pestell, R.G., Howell, A., Zimmers, T.A., Casimiro, M.C., Aquila, S., Ando, S., Martinez-Outschoorn, U.E., *et al.* (2012). Mitochondrial fission induces glycolytic reprogramming in cancer-associated myofibroblasts, driving stromal lactate production, and early tumor growth. *Oncotarget* 3, 798-810.
- Guitart-Mampel, M., Hernandez, A.S., Moren, C., Catalan-Garcia, M., Tobias, E., Gonzalez-Casacuberta, I., Juarez-Flores, D.L., Gatell, J.M., Cardellach, F., Milisenda, J.C., *et al.* (2017). Imbalance in mitochondrial dynamics and apoptosis in pregnancies among HIV-infected women on HAART with obstetric complications. *The Journal of antimicrobial chemotherapy* 72, 2578-2586.
- Guo, C., Sun, L., Chen, X., and Zhang, D. (2013). Oxidative stress, mitochondrial damage and neurodegenerative diseases. *Neural Regeneration Research* 8, 2003-2014.
- Guo, K., Lu, J., Huang, Y., Wu, M., Zhang, L., Yu, H., Zhang, M., Bao, Y., He, J.C., Chen, H., *et al.* (2015). Protective Role of PGC-1 $\alpha$  in Diabetic Nephropathy Is Associated with the Inhibition of ROS through Mitochondrial Dynamic Remodeling. *PLoS ONE* 10, e0125176.
- Gupta, G.P., and Massagué, J. (2006). Cancer Metastasis: Building a Framework. *Cell* 127, 679-695.
- Guzzo, G., Sciacovelli, M., Bernardi, P., and Rasola, A. (2014). Inhibition of succinate dehydrogenase by the mitochondrial chaperone TRAP1 has anti-oxidant and anti-apoptotic effects on tumor cells. *Oncotarget* 5, 11897-11908.
- Hall, L., and Martinus, R.D. (2013). Hyperglycaemia and oxidative stress upregulate HSP60 & HSP70 expression in HeLa cells. *Springerplus* 2, 431.
- Hamacher-Brady, A., and Brady, N.R. (2016). Mitophagy programs: mechanisms and physiological implications of mitochondrial targeting by autophagy. *Cellular and Molecular Life Sciences* 73, 775-795.

- Han, T., Kang, D., Ji, D., Wang, X., Zhan, W., Fu, M., Xin, H.B., and Wang, J.B. (2013). How does cancer cell metabolism affect tumor migration and invasion? *Cell Adh Migr* 7, 395-403.
- Han, Y., Cho, U., Kim, S., Park, I.S., Cho, J.H., Dhanasekaran, D.N., and Song, Y.S. (2018). Tumour microenvironment on mitochondrial dynamics and chemoresistance in cancer. *Free Radical Research*, 1-17.
- Han, Y.H., Kim, S.H., Kim, S.Z., and Park, W.H. (2008). Antimycin A as a mitochondrial electron transport inhibitor prevents the growth of human lung cancer A549 cells. *Oncology reports* 20, 689-693.
- Hanahan, D., and Weinberg, R.A. (2000). The Hallmarks of Cancer. *Cell* 100, 57-70.
- Hanahan, D., and Weinberg, R.A. (2011). Hallmarks of cancer: the next generation. *Cell* 144, 646-674.
- Hata, A.N., Engelman, J.A., and Faber, A.C. (2015). The BCL-2 family: key mediators of the apoptotic response to targeted anti-cancer therapeutics. *Cancer discovery* 5, 475-487.
- Herzig, S., Long, F., Jhala, U.S., Hedrick, S., Quinn, R., Bauer, A., Rudolph, D., Schutz, G., Yoon, C., Puigserver, P., *et al.* (2001). CREB regulates hepatic gluconeogenesis through the coactivator PGC-1. *Nature* 413, 179-183.
- Hood, D.A. (2009). Mechanisms of exercise-induced mitochondrial biogenesis in skeletal muscle This paper is one of a selection of papers published in this Special Issue, entitled 14th International Biochemistry of Exercise Conference – Muscles as Molecular and Metabolic Machines, and has undergone the Journal's usual peer review process. *Applied Physiology, Nutrition, and Metabolism* 34, 465-472.
- Horwitz, R., and Webb, D. (2003). Cell migration. *Current Biology* 13, R756-R759.

- Hou, Q., Lei, M., Hu, K., and Wang, M. (2015). The effects of high glucose levels on reactive oxygen species-induced apoptosis and involved signaling in human vascular endothelial cells. *Cardiovascular toxicology* *15*, 140-146.
- Hou, Y., Zhou, M., Xie, J., Chao, P., Feng, Q., and Wu, J. (2017). High glucose levels promote the proliferation of breast cancer cells through GTPases. *Breast Cancer : Targets and Therapy* *9*, 429-436.
- Hsu, C.C., Tseng, L.M., and Lee, H.C. (2016). Role of mitochondrial dysfunction in cancer progression. *Experimental biology and medicine (Maywood, NJ)* *241*, 1281-1295.
- Hsu, P.P., and Sabatini, D.M. (2008). Cancer Cell Metabolism: Warburg and Beyond. *Cell* *134*, 703-707.
- Hu, C., Huang, Y., and Li, L. (2017). Drp1-Dependent Mitochondrial Fission Plays Critical Roles in Physiological and Pathological Progresses in Mammals. *International Journal of Molecular Sciences* *18*, 144.
- Hu, L., Yao, X., and Shen, Y. (2016). Altered mitochondrial DNA copy number contributes to human cancer risk: evidence from an updated meta-analysis. *Scientific Reports* *6*, 35859.
- Huber, V., Camisaschi, C., Berzi, A., Ferro, S., Lugini, L., Triulzi, T., Tuccitto, A., Tagliabue, E., Castelli, C., and Rivoltini, L. (2017). Cancer acidity: An ultimate frontier of tumor immune escape and a novel target of immunomodulation. *Seminars in Cancer Biology* *43*, 74-89.
- Huh, S., Ker, D.F., Su, H., and Kanade, T. (2012). Apoptosis detection for adherent cell populations in time-lapse phase-contrast microscopy images. *Med Image Comput Comput Assist Interv* *15*, 331-339.
- Hüttemann, M., Lee, I., Samavati, L., Yu, H., and Doan, J.W. (2007). Regulation of mitochondrial oxidative phosphorylation through cell signaling. *Biochimica et Biophysica Acta (BBA) - Molecular Cell Research* *1773*, 1701-1720.

- Hwangbo, Y., and Lee, E.K. (2017). Acute Hyperglycemia Associated with Anti-Cancer Medication. *Endocrinology and Metabolism* 32, 23-29.
- Iacovelli, J., Rowe, G.C., Khadka, A., Diaz-Aguilar, D., Spencer, C., Arany, Z., and Saint-Geniez, M. (2016). PGC-1alpha Induces Human RPE Oxidative Metabolism and Antioxidant Capacity. *Invest Ophthalmol Vis Sci* 57, 1038-1051.
- Igney, F.H., and Krammer, P.H. (2002). Immune escape of tumors: apoptosis resistance and tumor counterattack. *J Leukoc Biol* 71, 907-920.
- Iqbal, S., and Hood, D.A. (2014). Oxidative stress-induced mitochondrial fragmentation and movement in skeletal muscle myoblasts. *American Journal of Physiology - Cell Physiology* 306, C1176-C1183.
- Itoh, K., Nakamura, K., Iijima, M., and Sesaki, H. (2013). Mitochondrial dynamics in neurodegeneration. *Trends in cell biology* 23, 64-71.
- Iyengar, N.M., Hudis, C.A., and Dannenberg, A.J. (2015). Obesity and cancer: local and systemic mechanisms. *Annual review of medicine* 66, 297-309.
- Jayappa, K.D., Kovi, R.C., and Chatterjee, S. (2016). Interplay between Tumor Microenvironment and Cancer Cells. *Biomed Res Int* 2016, 4650498.
- Jeong, S.Y., and Seol, D.W. (2008). The role of mitochondria in apoptosis. *BMB reports* 41, 11-22.
- Ježek, J., Cooper, K.F., and Strich, R. (2018). Reactive Oxygen Species and Mitochondrial Dynamics: The Yin and Yang of Mitochondrial Dysfunction and Cancer Progression. *Antioxidants* 7, 13.
- Jheng, H.F., Tsai, P.J., Guo, S.M., Kuo, L.H., Chang, C.S., Su, I.J., Chang, C.R., and Tsai, Y.S. (2012). Mitochondrial fission contributes to mitochondrial dysfunction and insulin resistance in skeletal muscle. *Mol Cell Biol* 32, 309-319.
- Jiang, B. (2017). Aerobic glycolysis and high level of lactate in cancer metabolism and microenvironment. *Genes & Diseases* 4, 25-27.

- Jiang, P., Du, W., and Wu, M. (2014). Regulation of the pentose phosphate pathway in cancer. *Protein Cell* 5, 592-602.
- Jin, H., Kanthasamy, A., Ghosh, A., Anantharam, V., Kalyanaraman, B., and Kanthasamy, A.G. (2014). Mitochondria-Targeted Antioxidants For Treatment Of Parkinson's Disease: Preclinical And Clinical Outcomes. *Biochimica et biophysica acta* 1842, 1282-1294.
- Jin, Z., and El-Deiry, W.S. (2005). Overview of cell death signaling pathways. *Cancer Biol Ther* 4, 139-163.
- John, B.J., Irukulla, S., Abulafi, A.M., Kumar, D., and Mendall, M.A. (2006). Systematic review: adipose tissue, obesity and gastrointestinal diseases. *Alimentary pharmacology & therapeutics* 23, 1511-1523.
- Jones, A.W., Yao, Z., Vicencio, J.M., Karkucinska-Wieckowska, A., and Szabadkai, G. (2012). PGC-1 family coactivators and cell fate: roles in cancer, neurodegeneration, cardiovascular disease and retrograde mitochondria-nucleus signalling. *Mitochondrion* 12, 86-99.
- Jornayvaz, F.R., and Shulman, G.I. (2010). Regulation of mitochondrial biogenesis. *Essays in biochemistry* 47, 10.1042/bse0470069.
- Jose, C., Bellance, N., and Rossignol, R. (2011). Choosing between glycolysis and oxidative phosphorylation: A tumor's dilemma? *Biochimica et Biophysica Acta (BBA) - Bioenergetics* 1807, 552-561.
- Kadye, R., Kramer, A.H., Joos-Vandewalle, J., Parsons, M., Njengele, Z., Hoppe, H., and Prinsloo, E. (2014). Guardian of the furnace: mitochondria, TRAP1, ROS and stem cell maintenance. *IUBMB Life* 66, 42-45.
- Kang, B.H. (2012). TRAP1 regulation of mitochondrial life or death decision in cancer cells and mitochondria-targeted TRAP1 inhibitors. *BMB reports* 45, 1-6.

- Kang, J., and Pervaiz, S. (2012). Mitochondria: Redox Metabolism and Dysfunction. *Biochemistry Research International* 2012, 14.
- Kang, X., Kong, F., Wu, X., Ren, Y., Wu, S., Wu, K., Jiang, Z., and Zhang, W. (2015). High glucose promotes tumor invasion and increases metastasis-associated protein expression in human lung epithelial cells by upregulating heme oxygenase-1 via reactive oxygen species or the TGF-beta1/PI3K/Akt signaling pathway. *Cell Physiol Biochem* 35, 1008-1022.
- Karamanlidis, G., Lee, C.F., Garcia-Menendez, L., Kolwicz, S.C., Jr., Suthammarak, W., Gong, G., Sedensky, M.M., Morgan, P.G., Wang, W., and Tian, R. (2013). Mitochondrial complex I deficiency increases protein acetylation and accelerates heart failure. *Cell Metab* 18, 239-250.
- Kato, Y., Lambert, C.A., Colige, A.C., Mineur, P., Noel, A., Frankenne, F., Foidart, J.M., Baba, M., Hata, R., Miyazaki, K., *et al.* (2005). Acidic extracellular pH induces matrix metalloproteinase-9 expression in mouse metastatic melanoma cells through the phospholipase D-mitogen-activated protein kinase signaling. *J Biol Chem* 280, 10938-10944.
- Kato, Y., Ozawa, S., Miyamoto, C., Maehata, Y., Suzuki, A., Maeda, T., and Baba, Y. (2013). Acidic extracellular microenvironment and cancer. *Cancer Cell Int* 13, 89-89.
- Keogh, M.J., and Chinnery, P.F. (2015). Mitochondrial DNA mutations in neurodegeneration. *Biochimica et biophysica acta* 1847, 1401-1411.
- Khan, N., and Mukhtar, H. (2010). Cancer and metastasis: prevention and treatment by green tea. *Cancer metastasis reviews* 29, 435-445.
- Kim, H., Rafiuddin-Shah, M., Tu, H.C., Jeffers, J.R., Zambetti, G.P., Hsieh, J.J., and Cheng, E.H. (2006). Hierarchical regulation of mitochondrion-dependent apoptosis by BCL-2 subfamilies. *Nat Cell Biol* 8, 1348-1358.

- Kim, S., Kim, C., and Park, S. (2017). Mdivi-1 Protects Adult Rat Hippocampal Neural Stem Cells against Palmitate-Induced Oxidative Stress and Apoptosis. *International Journal of Molecular Sciences* *18*, 1947.
- Knez, J., Winckelmans, E., Plusquin, M., Thijs, L., Cauwenberghs, N., Gu, Y., Staessen, J.A., Nawrot, T.S., and Kuznetsova, T. (2016). Correlates of Peripheral Blood Mitochondrial DNA Content in a General Population. *Am J Epidemiol* *183*, 138-146.
- Knott, A.B., Perkins, G., Schwarzenbacher, R., and Bossy-Wetzel, E. (2008). Mitochondrial Fragmentation In Neurodegeneration. *Nature reviews Neuroscience* *9*, 505-518.
- Koff, J.L., Ramachandiran, S., and Bernal-Mizrachi, L. (2015). A time to kill: targeting apoptosis in cancer. *Int J Mol Sci* *16*, 2942-2955.
- Kornfeld, O.S., Hwang, S., Disatnik, M.-H., Chen, C.-H., Qvit, N., and Mochly-Rosen, D. (2015). Mitochondrial Reactive Oxygen Species at the Heart of the Matter. *Circulation Research* *116*, 1783.
- Kramer, N., Walzl, A., Unger, C., Rosner, M., Krupitza, G., Hengstschlager, M., and Dolznig, H. (2013). In vitro cell migration and invasion assays. *Mutation research* *752*, 10-24.
- Kroemer, G., and Pouyssegur, J. (2008). Tumor cell metabolism: cancer's Achilles' heel. *Cancer Cell* *13*, 472-482.
- Kühlbrandt, W. (2015). Structure and function of mitochondrial membrane protein complexes. *BMC Biology* *13*, 89.
- Kumari, S., Anderson, L., Farmer, S., Mehta, S.L., and Li, P.A. (2012). Hyperglycemia alters mitochondrial fission and fusion proteins in mice subjected to cerebral ischemia and reperfusion. *Translational stroke research* *3*, 296-304.

- Kuwana, T., and Newmeyer, D.D. (2003). Bcl-2-family proteins and the role of mitochondria in apoptosis. *Curr Opin Cell Biol* 15, 691-699.
- Kwak, S.H., Park, K.S., Lee, K.U., and Lee, H.K. (2010). Mitochondrial metabolism and diabetes. *J Diabetes Investig* 1, 161-169.
- Labelle, M., and Hynes, R.O. (2012). The initial hours of metastasis: the importance of cooperative host-tumor cell interactions during hematogenous dissemination. *Cancer discovery* 2, 1091-1099.
- Landes, T., and Martinou, J.-C. (2011). Mitochondrial outer membrane permeabilization during apoptosis: The role of mitochondrial fission. *Biochimica et Biophysica Acta (BBA) - Molecular Cell Research* 1813, 540-545.
- Lauffenburger, D.A., and Horwitz, A.F. (1996). Cell Migration: A Physically Integrated Molecular Process. *Cell* 84, 359-369.
- Lebiedzinska-Arciszewska, M., Oparka, M., Vega-Naredo, I., Karkucinska-Wieckowska, A., Pinton, P., Duszynski, J., and Wieckowski, M.R. (2015). The interplay between p66Shc, reactive oxygen species and cancer cell metabolism. *Eur J Clin Invest* 45 Suppl 1, 25-31.
- LeBleu, V.S., O'Connell, J.T., Gonzalez Herrera, K.N., Wikman, H., Pantel, K., Haigis, M.C., de Carvalho, F.M., Damascena, A., Domingos Chinen, L.T., Rocha, R.M., *et al.* (2014). PGC-1alpha mediates mitochondrial biogenesis and oxidative phosphorylation in cancer cells to promote metastasis. *Nat Cell Biol* 16, 992-1003, 1001-1015.
- Lee, S.C., and Chan, J.C.N. (2015). Evidence for DNA Damage as a Biological Link Between Diabetes and Cancer. *Chinese Medical Journal* 128, 1543-1548.
- Lefevre, S., Sliwa, D., Rustin, P., Camadro, J.M., and Santos, R. (2012). Oxidative stress induces mitochondrial fragmentation in frataxin-deficient cells. *Biochem Biophys Res Commun* 418, 336-341.

- Leni, Z., Parakkal, G., and Arcaro, A. (2013). Emerging Metabolic Targets in the Therapy of Hematological Malignancies. *BioMed Research International* 2013, 946206.
- Lennicke, C., Rahn, J., Lichtenfels, R., Wessjohann, L.A., and Seliger, B. (2015). Hydrogen peroxide – production, fate and role in redox signaling of tumor cells. *Cell Communication and Signaling : CCS* 13, 39.
- Levigne, D., Tobalem, M., Modarressi, A., and Pittet-Cuenod, B. (2013). Hyperglycemia Increases Susceptibility to Ischemic Necrosis. *BioMed Research International* 2013, 5.
- Li, C., Zhang, G., Zhao, L., Ma, Z., and Chen, H. (2016). Metabolic reprogramming in cancer cells: glycolysis, glutaminolysis, and Bcl-2 proteins as novel therapeutic targets for cancer. *World journal of surgical oncology* 14, 15.
- Li, C., and Zhou, H.M. (2011). The role of manganese superoxide dismutase in inflammation defense. *Enzyme Res* 2011, 387176.
- Li, J., Huang, Q., Long, X., Guo, X., Sun, X., Jin, X., Li, Z., Ren, T., Yuan, P., Huang, X., *et al.* (2017). Mitochondrial elongation-mediated glucose metabolism reprogramming is essential for tumour cell survival during energy stress. *Oncogene* 36, 4901-4912.
- Li, T., Liu, M., Feng, X., Wang, Z., Das, I., Xu, Y., Zhou, X., Sun, Y., Guan, K.-L., Xiong, Y., *et al.* (2014). Glyceraldehyde-3-phosphate Dehydrogenase Is Activated by Lysine 254 Acetylation in Response to Glucose Signal. *Journal of Biological Chemistry* 289, 3775-3785.
- Liang, H., and Ward, W.F. (2006). PGC-1alpha: a key regulator of energy metabolism. *Adv Physiol Educ* 30, 145-151.
- Liberti, M.V., and Locasale, J.W. (2016). The Warburg Effect: How Does it Benefit Cancer Cells? *Trends in biochemical sciences* 41, 211-218.

- Lin, C.-Y., Lee, C.-H., Huang, C.-C., Lee, S.-T., Guo, H.-R., and Su, S.-B. (2015). Impact of high glucose on metastasis of colon cancer cells. *World Journal of Gastroenterology : WJG* 21, 2047-2057.
- Lin, J., Handschin, C., and Spiegelman, B.M. (2005). Metabolic control through the PGC-1 family of transcription coactivators. *Cell Metab* 1, 361-370.
- Lin, J., Tarr, P.T., Yang, R., Rhee, J., Puigserver, P., Newgard, C.B., and Spiegelman, B.M. (2003). PGC-1beta in the regulation of hepatic glucose and energy metabolism. *J Biol Chem* 278, 30843-30848.
- Liou, G.-Y., and Storz, P. (2010). Reactive oxygen species in cancer. *Free radical research* 44, 10.3109/10715761003667554.
- Lopez-Lazaro, M. (2007). Dual role of hydrogen peroxide in cancer: possible relevance to cancer chemoprevention and therapy. *Cancer letters* 252, 1-8.
- Lopez-Lazaro, M. (2008). The warburg effect: why and how do cancer cells activate glycolysis in the presence of oxygen? *Anti-cancer agents in medicinal chemistry* 8, 305-312.
- Lopez-Saez, J.F., de la Torre, C., Pincheira, J., and Gimenez-Martin, G. (1998). Cell proliferation and cancer. *Histology and histopathology* 13, 1197-1214.
- Lopez, J., and Tait, S.W.G. (2015). Mitochondrial apoptosis: killing cancer using the enemy within. *British Journal Of Cancer* 112, 957.
- Lu, P., Takai, K., Weaver, V.M., and Werb, Z. (2011). Extracellular Matrix Degradation and Remodeling in Development and Disease. *Cold Spring Harbor perspectives in biology* 3, 10.1101/cshperspect.a005058 a005058.
- Lu, W.D., Zhang, L., Wu, C.L., Liu, Z.G., Lei, G.Y., Liu, J., Gao, W., and Hu, Y.R. (2014). Development of an acellular tumor extracellular matrix as a three-dimensional scaffold for tumor engineering. *PLoS One* 9, e103672.

- Lunt, S.Y., and Vander Heiden, M.G. (2011). Aerobic glycolysis: meeting the metabolic requirements of cell proliferation. *Annu Rev Cell Dev Biol* 27, 441-464.
- Lushchak, V.I. (2012). Glutathione Homeostasis and Functions: Potential Targets for Medical Interventions. *Journal of Amino Acids* 2012, 26.
- Ma, J., Zhang, Q., Chen, S., Fang, B., Yang, Q., Chen, C., Miele, L., Sarkar, F.H., Xia, J., and Wang, Z. (2013). Mitochondrial Dysfunction Promotes Breast Cancer Cell Migration and Invasion through HIF1 $\alpha$  Accumulation via Increased Production of Reactive Oxygen Species. *PLOS ONE* 8, e69485.
- Ma, X., Jin, M., Cai, Y., Xia, H., Long, K., Liu, J., Yu, Q., and Yuan, J. (2011). Mitochondrial Electron Transport Chain Complex III Is Required for Antimycin A to Inhibit Autophagy. *Chemistry & biology* 18, 1474-1481.
- MacDonald, C., Finlay, D., Javed, A., Glass, M., and Graham, E. (2014). Development of positive control tissue for in situ hybridisation using Alvetex scaffolds, Vol 238.
- Maguire, J.J., Kagan, V.E., and Packer, L. (1992). Electron transport between cytochrome c and alpha tocopherol. *Biochem Biophys Res Commun* 188, 190-197.
- Mai, S., Klinkenberg, M., Auburger, G., Bereiter-Hahn, J., and Jendrach, M. (2010). Decreased expression of Drp1 and Fis1 mediates mitochondrial elongation in senescent cells and enhances resistance to oxidative stress through PINK1. *J Cell Sci* 123, 917-926.
- Maiuri, M.C., and Kroemer, G. (2015). Essential role for oxidative phosphorylation in cancer progression. *Cell Metab* 21, 11-12.
- Mannella, C.A. (2006). Structure and dynamics of the mitochondrial inner membrane cristae. *Biochimica et biophysica acta* 1763, 542-548.
- Marchi, S., Giorgi, C., Suski, J.M., Agnoletto, C., Bononi, A., Bonora, M., De Marchi, E., Missiroli, S., Patergnani, S., Poletti, F., *et al.* (2012). Mitochondria-Ros Crosstalk in the Control of Cell Death and Aging. *Journal of Signal Transduction* 2012, 17.

- Marelli-Berg, F.M., and Jangani, M. (2018). Metabolic regulation of leukocyte motility and migration. *J Leukoc Biol.*
- Marquez, R., Tsao, W.-c., Faust, N., and Xu, L. (2013). Drug Resistance and Molecular Cancer Therapy: Apoptosis Versus Autophagy.
- Martin-Guerrero, S.M., Munoz-Gamez, J.A., Carrasco, M.C., Salmeron, J., Martin-Estebane, M., Cuadros, M.A., Navascues, J., and Martin-Oliva, D. (2017). Poly(ADP-ribose)polymerases inhibitors prevent early mitochondrial fragmentation and hepatocyte cell death induced by H<sub>2</sub>O<sub>2</sub>. *PLoS One* *12*, e0187130.
- Martin, T., Ye, L., Aj, S., Lane, J., and Jiang, W. (2013). Cancer Invasion and Metastasis: Molecular and Cellular perspective.
- Martyn, M.D.F.R.C.A.F.C.C.M.J A.J., Kaneki, M.D.P.D.M., and Yasuhara, M.D.P.D.S. (2008). Obesity-induced Insulin Resistance and Hyperglycemia Etiologic Factors and Molecular Mechanisms. *Anesthesiology* *109*, 137-148.
- Marzetti, E., Csiszar, A., Dutta, D., Balagopal, G., Calvani, R., and Leeuwenburgh, C. (2013). Role of mitochondrial dysfunction and altered autophagy in cardiovascular aging and disease: from mechanisms to therapeutics. *American Journal of Physiology - Heart and Circulatory Physiology* *305*, H459-H476.
- Marzo, I., Brenner, C., Zamzami, N., Susin, S.A., Beutner, G., Brdiczka, D., Rémy, R., Xie, Z.-H., Reed, J.C., and Kroemer, G. (1998). The Permeability Transition Pore Complex: A Target for Apoptosis Regulation by Caspases and Bcl-2-related Proteins. *The Journal of Experimental Medicine* *187*, 1261-1271.
- Matsuo, Y., and Kamitani, T. (2010). Parkinson's disease-related protein, alpha-synuclein, in malignant melanoma. *PLoS One* *5*, e10481.

- Matsuura, K., Canfield, K., Feng, W., and Kurokawa, M. (2016). Metabolic Regulation of Apoptosis in Cancer. In *International Review of Cell and Molecular Biology*, K.W. Jeon, and L. Galluzzi, eds. (Academic Press), pp. 43-87.
- McCarron, J.G., Wilson, C., Sandison, M.E., Olson, M.L., Girkin, J.M., Saunter, C., and Chalmers, S. (2013). From Structure to Function: Mitochondrial Morphology, Motion and Shaping in Vascular Smooth Muscle. *Journal of Vascular Research* *50*, 357-371.
- McInnes, J. (2013). Mitochondrial-associated metabolic disorders: foundations, pathologies and recent progress. *Nutrition & Metabolism* *10*, 63-63.
- Mei, H., Sun, S., Bai, Y., Chen, Y., Chai, R., and Li, H. (2015). Reduced mtDNA copy number increases the sensitivity of tumor cells to chemotherapeutic drugs. *Cell Death & Disease* *6*, e1710.
- Memon, A.A., Zöller, B., Hedelius, A., Wang, X., Stenman, E., Sundquist, J., and Sundquist, K. (2017). Quantification of mitochondrial DNA copy number in suspected cancer patients by a well optimized ddPCR method. *Biomolecular Detection and Quantification* *13*, 32-39.
- Miriyala, S., Spasojevic, I., Tovmasyan, A., Salvemini, D., Vujaskovic, Z., St. Clair, D., and Batinic-Haberle, I. (2012). Manganese superoxide dismutase, MnSOD and its mimics. *Biochimica et biophysica acta* *1822*, 794-814.
- Mishra, N., Kar, R., Singha, P.K., Venkatachalam, M.A., McEwen, D.G., and Saikumar, P. (2010). Inhibition of mitochondrial division through covalent modification of Drp1 protein by 15 Deoxy-  $\Delta(12,14)$  - Prostaglandin J(2). *Biochemical and biophysical research communications* *395*, 17-24.
- Mishra, P., and Chan, D.C. (2014). Mitochondrial dynamics and inheritance during cell division, development and disease. *Nature reviews Molecular cell biology* *15*, 634-646.

- Mishra, P., and Chan, D.C. (2016). Metabolic regulation of mitochondrial dynamics. *The Journal of cell biology* 212, 379-387.
- Mitra, K., Wunder, C., Roysam, B., Lin, G., and Lippincott-Schwartz, J. (2009). A hyperfused mitochondrial state achieved at G1-S regulates cyclin E buildup and entry into S phase. *Proc Natl Acad Sci U S A* 106, 11960-11965.
- Mokhtari-Jafari, F., Amoabediny, G., Haghighipour, N., Zarghami, R., Saatchi, A., Akbari, J., and Salehi-Nik, N. (2015). Mathematical modeling of cell growth in a 3D scaffold and validation of static and dynamic cultures.
- Molavian, H.R., Goldman, A., Phipps, C.J., Kohandel, M., Wouters, B.G., Sengupta, S., and Sivaloganathan, S. (2016). Drug-induced reactive oxygen species (ROS) rely on cell membrane properties to exert anticancer effects. *Scientific Reports* 6, 27439.
- Montesano Gesualdi, N., Chirico, G., Pirozzi, G., Costantino, E., Landriscina, M., and Esposito, F. (2007). Tumor necrosis factor-associated protein 1 (TRAP-1) protects cells from oxidative stress and apoptosis. *Stress (Amsterdam, Netherlands)* 10, 342-350.
- Moreno-Sanchez, R., Rodriguez-Enriquez, S., Marin-Hernandez, A., and Saavedra, E. (2007). Energy metabolism in tumor cells. *Febs j* 274, 1393-1418.
- Nabeshima, K., Inoue, T., Shima, Y., and Sameshima, T. (2002). Matrix metalloproteinases in tumor invasion: role for cell migration. *Pathology international* 52, 255-264.
- Nagase, H., Visse, R., and Murphy, G. (2006). Structure and function of matrix metalloproteinases and TIMPs. *Cardiovascular research* 69, 562-573.
- Nahta, R., Al-Mulla, F., Al-Temaimi, R., Amedei, A., Andrade-Vieira, R., Bay, S.N., Brown, D.G., Calaf, G.M., Castellino, R.C., Cohen-Solal, K.A., *et al.* (2015).

- Mechanisms of environmental chemicals that enable the cancer hallmark of evasion of growth suppression. *Carcinogenesis* 36, S2-S18.
- Nakamura, K., Nemani, V.M., Azarbal, F., Skibinski, G., Levy, J.M., Egami, K., Munishkina, L., Zhang, J., Gardner, B., Wakabayashi, J., *et al.* (2011). Direct membrane association drives mitochondrial fission by the Parkinson disease-associated protein alpha-synuclein. *J Biol Chem* 286, 20710-20726.
- Negrini, S., Gorgoulis, V.G., and Halazonetis, T.D. (2010). Genomic instability — an evolving hallmark of cancer. *Nature Reviews Molecular Cell Biology* 11, 220.
- Ni, H.-M., Williams, J.A., and Ding, W.-X. (2015). Mitochondrial dynamics and mitochondrial quality control. *Redox Biology* 4, 6-13.
- Nicco, C., and Batteux, F. (2017). ROS Modulator Molecules with Therapeutic Potential in Cancers Treatments. *Molecules* 23.
- Nita, M., and Grzybowski, A. (2016). The Role of the Reactive Oxygen Species and Oxidative Stress in the Pathomechanism of the Age-Related Ocular Diseases and Other Pathologies of the Anterior and Posterior Eye Segments in Adults. *Oxidative medicine and cellular longevity* 2016, 23.
- Nogueira, V., Park, Y., Chen, C.-C., Xu, P.-Z., Chen, M.-L., Tonic, I., Unterman, T., and Hay, N. (2008). Akt determines replicative senescence and oxidative or oncogenic premature senescence and sensitizes cells to oxidative apoptosis. *Cancer cell* 14, 458-470.
- Novak, I. (2012). Mitophagy: a complex mechanism of mitochondrial removal. *Antioxidants & redox signaling* 17, 794-802.
- Ong, S.B., and Hausenloy, D.J. (2010). Mitochondrial morphology and cardiovascular disease. *Cardiovascular research* 88, 16-29.
- Orsini, F., Migliaccio, E., Moroni, M., Contursi, C., Raker, V.A., Piccini, D., Martin-Padura, I., Pelliccia, G., Trinei, M., Bono, M., *et al.* (2004). The life span

determinant p66Shc localizes to mitochondria where it associates with mitochondrial heat shock protein 70 and regulates trans-membrane potential. *J Biol Chem* 279, 25689-25695.

Osellame, L.D., Blacker, T.S., and Duchen, M.R. (2012). Cellular and molecular mechanisms of mitochondrial function. *Best Practice & Research Clinical Endocrinology & Metabolism* 26, 711-723.

Otera, H., Ishihara, N., and Mihara, K. (2013). New insights into the function and regulation of mitochondrial fission. *Biochimica et biophysica acta* 1833, 1256-1268.

Otera, H., and Mihara, K. (2011). Molecular mechanisms and physiologic functions of mitochondrial dynamics. *The Journal of Biochemistry* 149, 241-251.

Ott, M., Gogvadze, V., Orrenius, S., and Zhivotovsky, B. (2007). Mitochondria, oxidative stress and cell death. *Apoptosis* 12, 913-922.

Ou, Y., Liu, L., Xue, L., Zhou, W., Zhao, Z., Xu, B., Song, Y., and Zhan, Q. (2014). TRAP1 shows clinical significance and promotes cellular migration and invasion through STAT3/MMP2 pathway in human esophageal squamous cell cancer. *Journal of genetics and genomics = Yi chuan xue bao* 41, 529-537.

Ozougwu, O. (2013). The pathogenesis and pathophysiology of type 1 and type 2 diabetes mellitus, Vol 4.

Palorini, R., Simonetto, T., Cirulli, C., and Chiaradonna, F. (2013). Mitochondrial Complex I Inhibitors and Forced Oxidative Phosphorylation Synergize in Inducing Cancer Cell Death. *International Journal of Cell Biology* 2013, 14.

Pan, Q., Qiu, W.Y., Huo, Y.N., Yao, Y.F., and Lou, M.F. (2011). Low levels of hydrogen peroxide stimulate corneal epithelial cell adhesion, migration, and wound healing. *Invest Ophthalmol Vis Sci* 52, 1723-1734.

- Panduri, V., Weitzman, S.A., Chandel, N.S., and Kamp, D.W. (2004). Mitochondrial-derived free radicals mediate asbestos-induced alveolar epithelial cell apoptosis. *Am J Physiol Lung Cell Mol Physiol* 286, L1220-1227.
- Pani, G., Galeotti, T., and Chiarugi, P. (2010). Metastasis: cancer cell's escape from oxidative stress. *Cancer metastasis reviews* 29, 351-378.
- Park, W.H. (2016). Exogenous H<sub>2</sub>O<sub>2</sub> induces growth inhibition and cell death of human pulmonary artery smooth muscle cells via glutathione depletion. *Molecular medicine reports* 14, 936-942.
- Parone, P.A., James, D.I., Da Cruz, S., Mattenberger, Y., Donze, O., Barja, F., and Martinou, J.C. (2006). Inhibiting the mitochondrial fission machinery does not prevent Bax/Bak-dependent apoptosis. *Mol Cell Biol* 26, 7397-7408.
- Pascual, G., Domínguez, D., and Benitah, S.A. (2018). The contributions of cancer cell metabolism to metastasis. *Disease Models & Mechanisms* 11.
- Patra, K.C., and Hay, N. (2014). The pentose phosphate pathway and cancer. *Trends Biochem Sci* 39, 347-354.
- Patra, K.C., Wang, Q., Bhaskar, P.T., Miller, L., Wang, Z., Wheaton, W., Chandel, N., Laakso, M., Muller, W.J., Allen, E.L., *et al.* (2013). Hexokinase 2 is required for tumor initiation and maintenance and its systemic deletion is therapeutic in mouse models of cancer. *Cancer cell* 24, 213-228.
- Payne, B.A.I., and Chinnery, P.F. (2015). Mitochondrial dysfunction in aging: Much progress but many unresolved questions. *Biochimica et Biophysica Acta (BBA) - Bioenergetics* 1847, 1347-1353.
- Peiris-Pagès, M., Bonuccelli, G., Sotgia, F., and Lisanti, M.P. (2018). Mitochondrial fission as a driver of stemness in tumor cells: mDIVI1 inhibits mitochondrial function, cell migration and cancer stem cell (CSC) signalling. *Oncotarget* 5.

- Peng, K., Yang, L., Wang, J., Ye, F., Dan, G., Zhao, Y., Cai, Y., Cui, Z., Ao, L., Liu, J., *et al.* (2017). The Interaction of Mitochondrial Biogenesis and Fission/Fusion Mediated by PGC-1alpha Regulates Rotenone-Induced Dopaminergic Neurotoxicity. *Molecular neurobiology* *54*, 3783-3797.
- Perfettini, J.L., Roumier, T., and Kroemer, G. (2005). Mitochondrial fusion and fission in the control of apoptosis. *Trends in cell biology* *15*, 179-183.
- Pham, N.A., Robinson, B.H., and Hedley, D.W. (2000). Simultaneous detection of mitochondrial respiratory chain activity and reactive oxygen in digitonin-permeabilized cells using flow cytometry. *Cytometry* *41*, 245-251.
- Phan, L.M., Yeung, S.C., and Lee, M.H. (2014). Cancer metabolic reprogramming: importance, main features, and potentials for precise targeted anti-cancer therapies. *Cancer Biol Med* *11*, 1-19.
- Picard, M., Shirihai, O.S., Gentil, B.J., and Burrelle, Y. (2013). Mitochondrial morphology transitions and functions: implications for retrograde signaling? *American journal of physiology Regulatory, integrative and comparative physiology* *304*, R393-406.
- Pinton, P., Rimessi, A., Marchi, S., Orsini, F., Migliaccio, E., Giorgio, M., Contursi, C., Minucci, S., Mantovani, F., Wieckowski, M.R., *et al.* (2007). Protein kinase C beta and prolyl isomerase 1 regulate mitochondrial effects of the life-span determinant p66Shc. *Science (New York, NY)* *315*, 659-663.
- Pridgeon, J.W., Olzmann, J.A., Chin, L.S., and Li, L. (2007). PINK1 protects against oxidative stress by phosphorylating mitochondrial chaperone TRAP1. *PLoS biology* *5*, e172.
- Puzio-Kuter, A.M. (2011). The Role of p53 in Metabolic Regulation. *Genes & Cancer* *2*, 385-391.

- Qi, X., Qvit, N., Su, Y.-C., and Mochly-Rosen, D. (2013). A novel Drp1 inhibitor diminishes aberrant mitochondrial fission and neurotoxicity. *Journal of Cell Science* *126*, 789-802.
- Qian, B.Z., and Pollard, J.W. (2010). Macrophage diversity enhances tumor progression and metastasis. *Cell* *141*, 39-51.
- Qian, W., Wang, J., and Van Houten, B. (2013). The role of dynamin-related protein 1 in cancer growth: a promising therapeutic target? *Expert opinion on therapeutic targets* *17*, 997-1001.
- Quail, D.F., and Joyce, J.A. (2013). Microenvironmental regulation of tumor progression and metastasis. *Nature medicine* *19*, 1423-1437.
- Quinlan, C.L., Gerencser, A.A., Treberg, J.R., and Brand, M.D. (2011). The mechanism of superoxide production by the antimycin-inhibited mitochondrial Q-cycle. *J Biol Chem* *286*, 31361-31372.
- Rajendran, M., Thomes, P., Zhang, L., Veeramani, S., and Lin, M.F. (2010). p66Shc--a longevity redox protein in human prostate cancer progression and metastasis : p66Shc in cancer progression and metastasis. *Cancer metastasis reviews* *29*, 207-222.
- Rakhmatullina, D., Ponomareva, A., Gazizova, N., and Minibayeva, F. (2016). Mitochondrial morphology and dynamics in *Triticum aestivum* roots in response to rotenone and antimycin A. *Protoplasma* *253*, 1299-1308.
- Rambold, A.S., Kostecky, B., Elia, N., and Lippincott-Schwartz, J. (2011). Tubular network formation protects mitochondria from autophagosomal degradation during nutrient starvation. *Proc Natl Acad Sci U S A* *108*, 10190-10195.
- Ravichandran, K.S. (2001). Signaling via Shc family adapter proteins. *Oncogene* *20*, 6322-6330.

- Ray, M.R., and Jablons, D.M. (2010). Hallmarks of Metastasis. In Lung Cancer Metastasis: Novel Biological Mechanisms and Impact on Clinical Practice, V. Keshamouni, D. Arenberg, and G. Kalemkerian, eds. (New York, NY: Springer New York), pp. 29-46.
- Reddy, P.H. (2014). Inhibitors of mitochondrial fission as a therapeutic strategy for diseases with oxidative stress and mitochondrial dysfunction. *Journal of Alzheimer's disease : JAD* 40, 245-256.
- Redza-Dutordoir, M., and Averill-Bates, D.A. (2016). Activation of apoptosis signalling pathways by reactive oxygen species. *Biochimica et Biophysica Acta (BBA) - Molecular Cell Research* 1863, 2977-2992.
- Renault, T.T., Floros, K.V., Elkholi, R., Corrigan, K.A., Kushnareva, Y., Wieder, S.Y., Lindtner, C., Serasinghe, M.N., Asciolla, J.J., Buettner, C., *et al.* (2015). Mitochondrial shape governs BAX-induced membrane permeabilization and apoptosis. *Molecular cell* 57, 69-82.
- Ridge, P.G., and Kauwe, J.S.K. (2018). Mitochondria and Alzheimer's Disease: the Role of Mitochondrial Genetic Variation. *Current Genetic Medicine Reports* 6, 1-10.
- Riganti, C., Gazzano, E., Polimeni, M., Aldieri, E., and Ghigo, D. (2012). The pentose phosphate pathway: an antioxidant defense and a crossroad in tumor cell fate. *Free Radical Biology and Medicine* 53, 421-436.
- Rivas-Arancibia, S., Gallegos-Riños, C., Gómez, N., Ferreira, E., Flores Brisenño, D., Navarro, L., and Rodríguez-Martínez, E. (2011). Oxidative Stress and Neurodegenerative Disease. In
- Rodríguez-Enríquez, S., Carreño-Fuentes, L., Gallardo-Pérez, J.C., Saavedra, E., Quezada, H., Vega, A., Marín-Hernández, A., Olín-Sandoval, V., Torres-Márquez, M.E., and Moreno-Sánchez, R. (2010). Oxidative phosphorylation is impaired by

- prolonged hypoxia in breast and possibly in cervix carcinoma. *The International Journal of Biochemistry & Cell Biology* 42, 1744-1751.
- Rofstad, E.K., Mathiesen, B., Kindem, K., and Galappathi, K. (2006). Acidic extracellular pH promotes experimental metastasis of human melanoma cells in athymic nude mice. *Cancer Res* 66, 6699-6707.
- Rolo, A.P., and Palmeira, C.M. (2006). Diabetes and mitochondrial function: role of hyperglycemia and oxidative stress. *Toxicology and applied pharmacology* 212, 167-178.
- Romero-Garcia, S., Moreno-Altamirano, M.M.B., Prado-Garcia, H., and Sánchez-García, F.J. (2016). Lactate Contribution to the Tumor Microenvironment: Mechanisms, Effects on Immune Cells and Therapeutic Relevance. *Frontiers in Immunology* 7, 52.
- Rooney, J.P., Ryde, I.T., Sanders, L.H., Howlett, E.H., Colton, M.D., Germ, K.E., Mayer, G.D., Greenamyre, J.T., and Meyer, J.N. (2015). PCR Based Determination of Mitochondrial DNA Copy Number in Multiple Species. *Methods in molecular biology (Clifton, NJ)* 1241, 23-38.
- Rosdah, A.A., J, K.H., Delbridge, L.M., Disting, G.J., and Lim, S.Y. (2016). Mitochondrial fission - a drug target for cytoprotection or cytodestruction? *Pharmacol Res Perspect* 4, e00235.
- Rose, S., Frye, R.E., Slattery, J., Wynne, R., Tippett, M., Pavliv, O., Melnyk, S., and James, S.J. (2014). Oxidative stress induces mitochondrial dysfunction in a subset of autism lymphoblastoid cell lines in a well-matched case control cohort. *PLoS One* 9, e85436.
- Röth, D., Krammer, P.H., and Gülow, K. (2014). Dynamin related protein 1-dependent mitochondrial fission regulates oxidative signalling in T cells. *FEBS Letters* 588, 1749-1754.

- Röttgermann, P.J.F., Dawson, K.A., and Rädler, J.O. (2016). Time-Resolved Study of Nanoparticle Induced Apoptosis Using Microfabricated Single Cell Arrays. *Microarrays (Basel, Switzerland)* 5, 8.
- Rovira-Llopis, S., Bañuls, C., Diaz-Morales, N., Hernandez-Mijares, A., Rocha, M., and Victor, V.M. (2017). Mitochondrial dynamics in type 2 diabetes: Pathophysiological implications. *Redox Biology* 11, 637-645.
- Russell, J.W., Golovoy, D., Vincent, A.M., Mahendru, P., Olzmann, J.A., Mentzer, A., and Feldman, E.L. (2002). High glucose-induced oxidative stress and mitochondrial dysfunction in neurons. *Faseb J* 16, 1738-1748.
- Ryu, T.Y., Park, J., and Scherer, P.E. (2014). Hyperglycemia as a Risk Factor for Cancer Progression. *Diabetes & Metabolism Journal* 38, 330-336.
- Saha, S.K., Lee, S.B., Won, J., Choi, H.Y., Kim, K., Yang, G.M., Dayem, A.A., and Cho, S.G. (2017). Correlation between Oxidative Stress, Nutrition, and Cancer Initiation. *Int J Mol Sci* 18.
- Sakai, R., Henderson, J.T., O'Bryan, J.P., Elia, A.J., Saxton, T.M., and Pawson, T. (2000). The mammalian ShcB and ShcC phosphotyrosine docking proteins function in the maturation of sensory and sympathetic neurons. *Neuron* 28, 819-833.
- Salem, A.F., Whitaker-Menezes, D., Howell, A., Sotgia, F., and Lisanti, M.P. (2012). Mitochondrial biogenesis in epithelial cancer cells promotes breast cancer tumor growth and confers autophagy resistance. *Cell cycle (Georgetown, Tex)* 11, 4174-4180.
- Sanborn, B.M., Felberg, N.T., and Hollocher, T.C. (1971). The inactivation of succinate dehydrogenase by bromopyruvate. *Biochimica et Biophysica Acta (BBA) - Enzymology* 227, 219-231.

- Sanchis-Gomar, F., Garcia-Gimenez, J.L., Gomez-Cabrera, M.C., and Pallardo, F.V. (2014). Mitochondrial biogenesis in health and disease. Molecular and therapeutic approaches. *Curr Pharm Des* 20, 5619-5633.
- Sanjuán Szklarz, L.K., and Scorrano, L. (2012). The antiapoptotic OPA1/Parl couple participates in mitochondrial adaptation to heat shock. *Biochimica et Biophysica Acta (BBA) - Bioenergetics* 1817, 1886-1893.
- Sano, M., and Fukuda, K. (2008). Activation of Mitochondrial Biogenesis by Hormesis. *Circulation Research* 103, 1191-1193.
- Santel, A., and Fuller, M.T. (2001). Control of mitochondrial morphology by a human mitofusin. *J Cell Sci* 114, 867-874.
- Santos, D., Esteves, A.R., Silva, D.F., Januario, C., and Cardoso, S.M. (2015). The Impact of Mitochondrial Fusion and Fission Modulation in Sporadic Parkinson's Disease. *Molecular neurobiology* 52, 573-586.
- Sas, K., Szabo, E., and Vecsei, L. (2018). Mitochondria, Oxidative Stress and the Kynurenine System, with a Focus on Ageing and Neuroprotection. *Molecules* 23.
- Saunier, E., Antonio, S., Regazzetti, A., Auzeil, N., Laprévotte, O., Shay, J.W., Coumoul, X., Barouki, R., Benelli, C., Huc, L., *et al.* (2017). Resveratrol reverses the Warburg effect by targeting the pyruvate dehydrogenase complex in colon cancer cells. *Scientific Reports* 7, 6945.
- Sayin, N., Kara, N., and Pekel, G. (2015). Ocular complications of diabetes mellitus. *World Journal of Diabetes* 6, 92-108.
- Schafer, Z.T., and Kornbluth, S. (2006). The Apoptosome: Physiological, Developmental, and Pathological Modes of Regulation. *Developmental cell* 10, 549-561.
- Schmidt, C.E., Horwitz, A.F., Lauffenburger, D.A., and Sheetz, M.P. (1993). Integrin-cytoskeletal interactions in migrating fibroblasts are dynamic, asymmetric, and regulated. *The Journal of cell biology* 123, 977-991.

- Scholar, E. (2007). Antimetabolites. In *xPharm: The Comprehensive Pharmacology Reference* (New York: Elsevier), pp. 1-4.
- Schumacker, P.T. (2006). Reactive oxygen species in cancer cells: Live by the sword, die by the sword. *Cancer Cell* *10*, 175-176.
- Sciacovelli, M., Guzzo, G., Morello, V., Frezza, C., Zheng, L., Nannini, N., Calabrese, F., Laudiero, G., Esposito, F., Landriscina, M., *et al.* (2013). The mitochondrial chaperone TRAP1 promotes neoplastic growth by inhibiting succinate dehydrogenase. *Cell Metab* *17*, 988-999.
- Scott, D.A., Richardson, A.D., Filipp, F.V., Knutzen, C.A., Chiang, G.G., Ronai, Z.e.A., Osterman, A.L., and Smith, J.W. (2011). Comparative Metabolic Flux Profiling of Melanoma Cell Lines: BEYOND THE WARBURG EFFECT. *Journal of Biological Chemistry* *286*, 42626-42634.
- Scott, I., and Youle, R.J. (2010). Mitochondrial fission and fusion. *Essays in biochemistry* *47*, 85-98.
- Sever, R., and Brugge, J.S. (2015). *Signal Transduction in Cancer*. Cold Spring Harbor Perspectives in Medicine *5*, a006098.
- Shamas-Din, A., Kale, J., Leber, B., and Andrews, D.W. (2013). Mechanisms of Action of Bcl-2 Family Proteins. *Cold Spring Harbor perspectives in biology* *5*, a008714.
- Sheridan, C., and Martin, S.J. (2010). Mitochondrial fission/fusion dynamics and apoptosis. *Mitochondrion* *10*, 640-648.
- Shin, J.W., Park, S.H., Kang, Y.G., Wu, Y., Choi, H.J., and Shin, J.-W. (2016). Changes, and the Relevance Thereof, in Mitochondrial Morphology during Differentiation into Endothelial Cells. *PLoS ONE* *11*, e0161015.
- Siddiqui, A., Chinta, S.J., Mallajosyula, J.K., Rajagopalan, S., Hanson, I., Rane, A., Melov, S., and Andersen, J.K. (2012). Selective binding of nuclear alpha-synuclein to the PGC1alpha promoter under conditions of oxidative stress may

- contribute to losses in mitochondrial function: implications for Parkinson's disease. *Free radical biology & medicine* 53, 993-1003.
- Silha, J.V., Krsek, M., Sucharda, P., and Murphy, L.J. (2005). Angiogenic factors are elevated in overweight and obese individuals. *International Journal Of Obesity* 29, 1308.
- Simula, L., Nazio, F., and Campello, S. (2017). The mitochondrial dynamics in cancer and immune-surveillance. *Seminars in Cancer Biology* 47, 29-42.
- Singleterry, J., Sreedhar, A., and Zhao, Y. (2014). Components of cancer metabolism and therapeutic interventions. *Mitochondrion* 17, 50-55.
- Sinha, D., and D'Silva, P. (2014). Chaperoning mitochondrial permeability transition: regulation of transition pore complex by a J-protein, DnaJC15. *Cell Death & Disease* 5, e1101.
- Smolkova, K., Plecita-Hlavata, L., Bellance, N., Benard, G., Rossignol, R., and Jezek, P. (2011). Waves of gene regulation suppress and then restore oxidative phosphorylation in cancer cells. *Int J Biochem Cell Biol* 43, 950-968.
- Sonksen, P., and Sonksen, J. (2000). Insulin: understanding its action in health and disease. *BJA: British Journal of Anaesthesia* 85, 69-79.
- Sotgia, F., Martinez-Outschoorn, U.E., and Lisanti, M.P. (2013). Cancer metabolism: new validated targets for drug discovery. *Oncotarget* 4, 1309-1316.
- Sradhanjali, S., and Reddy, M.M. (2018). Inhibition of Pyruvate Dehydrogenase Kinase as a Therapeutic Strategy against Cancer. *Current topics in medicinal chemistry*.
- Sreedhar, A., and Zhao, Y. (2018). Dysregulated metabolic enzymes and metabolic reprogramming in cancer cells. *Biomed Rep* 8, 3-10.
- Stanczyk, M., Gromadzinska, J., and Wasowicz, W. (2005). Roles of reactive oxygen species and selected antioxidants in regulation of cellular metabolism.

International journal of occupational medicine and environmental health *18*, 15-26.

Stincone, A., Prigione, A., Cramer, T., Wamelink, M.M., Campbell, K., Cheung, E., Olin-Sandoval, V., Gruning, N.M., Kruger, A., Tauqeer Alam, M., *et al.* (2014). The return of metabolism: biochemistry and physiology of the pentose phosphate pathway. *Biol Rev Camb Philos Soc* *90*, 927-963.

Stratton, M.R., Campbell, P.J., and Futreal, P.A. (2009). The cancer genome. *Nature* *458*, 719-724.

Suárez-Rivero, J.M., Villanueva-Paz, M., de la Cruz-Ojeda, P., de la Mata, M., Cotán, D., Oropesa-Ávila, M., de Laveria, I., Álvarez-Córdoba, M., Luzón-Hidalgo, R., and Sánchez-Alcázar, J.A. (2017). Mitochondrial Dynamics in Mitochondrial Diseases. *Diseases* *5*, 1.

Sudheer Shenoy P, B.B. (2014). Stem Cell versus Cancer and Cancer Stem Cell: Intricate Balance Decides Their Respective Usefulness or Harmfulness in the Biological System. *Journal of Stem Cell Research & Therapy* *04*.

Suen, D.F., Norris, K.L., and Youle, R.J. (2008). Mitochondrial dynamics and apoptosis. *Genes Dev* *22*, 1577-1590.

Summermatter, S., Santos, G., Perez-Schindler, J., and Handschin, C. (2013). Skeletal muscle PGC-1alpha controls whole-body lactate homeostasis through estrogen-related receptor alpha-dependent activation of LDH B and repression of LDH A. *Proc Natl Acad Sci U S A* *110*, 8738-8743.

Takatani-Nakase, T., Matsui, C., Maeda, S., Kawahara, S., and Takahashi, K. (2014). High Glucose Level Promotes Migration Behavior of Breast Cancer Cells through Zinc and Its Transporters. *PLOS ONE* *9*, e90136.

- Tan, Z., Luo, X., Xiao, L., Tang, M., Bode, A.M., Dong, Z., and Cao, Y. (2016). The Role of PGC1alpha in Cancer Metabolism and its Therapeutic Implications. *Mol Cancer Ther* 15, 774-782.
- Thorpe, G.W., Fong, C.S., Alic, N., Higgins, V.J., and Dawes, I.W. (2004). Cells have distinct mechanisms to maintain protection against different reactive oxygen species: Oxidative-stress-response genes. *Proceedings of the National Academy of Sciences of the United States of America* 101, 6564.
- Tian, X., Ma, P., Sui, C.G., Meng, F.D., Li, Y., Fu, L.Y., Jiang, T., Wang, Y., and Jiang, Y.H. (2014). Suppression of tumor necrosis factor receptor-associated protein 1 expression induces inhibition of cell proliferation and tumor growth in human esophageal cancer cells. *Febs j* 281, 2805-2819.
- Tiberi, L., Faisal, A., Rossi, M., Di Tella, L., Franceschi, C., and Salvioli, S. (2006). p66(Shc) gene has a pro-apoptotic role in human cell lines and it is activated by a p53-independent pathway. *Biochem Biophys Res Commun* 342, 503-508.
- Tomita, K., Teratani, T., Suzuki, T., Oshikawa, T., Yokoyama, H., Shimamura, K., Nishiyama, K., Mataka, N., Irie, R., Minamino, T., *et al.* (2012). p53/p66Shc-mediated signaling contributes to the progression of non-alcoholic steatohepatitis in humans and mice. *Journal of hepatology* 57, 837-843.
- Tondera, D., Santel, A., Schwarzer, R., Dames, S., Giese, K., Klippel, A., and Kaufmann, J. (2004). Knockdown of MTP18, a novel phosphatidylinositol 3-kinase-dependent protein, affects mitochondrial morphology and induces apoptosis. *J Biol Chem* 279, 31544-31555.
- Tran, Q., Lee, H., Park, J., Kim, S.H., and Park, J. (2016). Targeting Cancer Metabolism - Revisiting the Warburg Effects. *Toxicol Res* 32, 177-193.
- Trepat, X., Chen, Z., and Jacobson, K. (2012). Cell migration. *Comprehensive Physiology* 2, 2369-2392.

- Trewin, A.J., Berry, B.J., and Wojtovich, A.P. (2018). Exercise and Mitochondrial Dynamics: Keeping in Shape with ROS and AMPK. *Antioxidants (Basel)* 7.
- Trinei, M., Giorgio, M., Cicalese, A., Barozzi, S., Ventura, A., Migliaccio, E., Milia, E., Padura, I.M., Raker, V.A., Maccarana, M., *et al.* (2002). A p53-p66Shc signalling pathway controls intracellular redox status, levels of oxidation-damaged DNA and oxidative stress-induced apoptosis. *Oncogene* 21, 3872-3878.
- Trudeau, K., Molina, A.J., and Roy, S. (2011). High glucose induces mitochondrial morphology and metabolic changes in retinal pericytes. *Invest Ophthalmol Vis Sci* 52, 8657-8664.
- Tseng, C.-H. (2015). Prolonged use of human insulin increases breast cancer risk in Taiwanese women with type 2 diabetes. *Bmc Cancer* 15, 846-846.
- Tsouko, E., Khan, A.S., White, M.A., Han, J.J., Shi, Y., Merchant, F.A., Sharpe, M.A., Xin, L., and Frigo, D.E. (2014). Regulation of the pentose phosphate pathway by an androgen receptor-mTOR-mediated mechanism and its role in prostate cancer cell growth. *Oncogenesis* 3, e103.
- Tsujimoto, Y., Nakagawa, T., and Shimizu, S. (2006). Mitochondrial membrane permeability transition and cell death. *Biochimica et Biophysica Acta (BBA) - Bioenergetics* 1757, 1297-1300.
- Tsukihara, T., Aoyama, H., Yamashita, E., Tomizaki, T., Yamaguchi, H., Shinzawa-Itoh, K., Nakashima, R., Yaono, R., and Yoshikawa, S. (1996). The whole structure of the 13-subunit oxidized cytochrome c oxidase at 2.8 Å. *Science (New York, NY)* 272, 1136-1144.
- Uddin, M.H. (2014). Anticancer Strategy Targeting Mitochondrial Biogenesis in Ovarian Cancer. *Journal of Cancer Science & Therapy* 06.
- Um, J.-H., and Yun, J. (2017). Emerging role of mitophagy in human diseases and physiology. *BMB reports* 50, 299-307.

- Vaarmann, A., Mandel, M., Zeb, A., Wareski, P., Liiv, J., Kuum, M., Antsov, E., Liiv, M., Cagalinec, M., Choubey, V., *et al.* (2016). Mitochondrial biogenesis is required for axonal growth. *Development* *143*, 1981-1992.
- Valastyan, S., and Weinberg, R.A. (2011). Tumor Metastasis: Molecular Insights and Evolving Paradigms. *Cell* *147*, 275-292.
- Van Beersel, G., Tihon, E., Demine, S., Hamer, I., Jadot, M., and Arnould, T. (2013). Different molecular mechanisms involved in spontaneous and oxidative stress-induced mitochondrial fragmentation in tripeptidyl peptidase-1 (TPP-1)-deficient fibroblasts. *Bioscience reports* *33*, e00023.
- van der Blik, A.M., Shen, Q., and Kawajiri, S. (2013). Mechanisms of mitochondrial fission and fusion. *Cold Spring Harbor perspectives in biology* *5*.
- Vandecasteele, G., Szabadkai, G., and Rizzuto, R. (2001). Mitochondrial calcium homeostasis: mechanisms and molecules. *IUBMB Life* *52*, 213-219.
- Vander Heiden, M.G., Cantley, L.C., and Thompson, C.B. (2009). Understanding the Warburg Effect: The Metabolic Requirements of Cell Proliferation. *Science (New York, NY)* *324*, 1029-1033.
- Verschoor, M.L., Ungard, R., Harbottle, A., Jakupciak, J.P., Parr, R.L., and Singh, G. (2013). Mitochondria and Cancer: Past, Present, and Future. *BioMed Research International* *2013*, 10.
- Vinci, M., Gowan, S., Boxall, F., Patterson, L., Zimmermann, M., Court, W., Lomas, C., Mendiola, M., Hardisson, D., and Eccles, S.A. (2012). Advances in establishment and analysis of three-dimensional tumor spheroid-based functional assays for target validation and drug evaluation. *BMC Biology* *10*, 29.
- Volpe, C.M.O., Villar-Delfino, P.H., dos Anjos, P.M.F., and Nogueira-Machado, J.A. (2018). Cellular death, reactive oxygen species (ROS) and diabetic complications. *Cell Death Dis* *9*, 119.

- Vyas, S., Zaganjor, E., and Haigis, M.C. (2016). Mitochondria and Cancer. *Cell* 166, 555-566.
- Wai, T., and Langer, T. (2016). Mitochondrial Dynamics and Metabolic Regulation. *Trends Endocrinol Metab* 27, 105-117.
- Wallace, D.C. (2012). Mitochondria and cancer. *Nature reviews Cancer* 12, 685-698.
- Wang, C., and Youle, R.J. (2009). The Role of Mitochondria in Apoptosis. *Annual review of genetics* 43, 95-118.
- Wang, L., Duan, Q., Wang, T., Ahmed, M., Zhang, N., Li, Y., Li, L., and Yao, X. (2015a). Mitochondrial Respiratory Chain Inhibitors Involved in ROS Production Induced by Acute High Concentrations of Iodide and the Effects of SOD as a Protective Factor. *Oxidative medicine and cellular longevity* 2015, 14.
- Wang, L., Yu, T., Lee, H., O'Brien, D.K., Sesaki, H., and Yoon, Y. (2015b). Decreasing mitochondrial fission diminishes vascular smooth muscle cell migration and ameliorates intimal hyperplasia. *Cardiovascular research* 106, 272-283.
- Wang, M., Hu, R.-Y., Wu, H.-B., Pan, J., Gong, W.-W., Guo, L.-H., Zhong, J.-M., Fei, F.-R., and Yu, M. (2015c). Cancer risk among patients with type 2 diabetes mellitus: a population-based prospective study in China. *Scientific Reports* 5, 11503.
- Wang, M., Zhao, J., Zhang, L., Wei, F., Lian, Y., Wu, Y., Gong, Z., Zhang, S., Zhou, J., Cao, K., *et al.* (2017). Role of tumor microenvironment in tumorigenesis. *Journal of Cancer* 8, 761-773.
- Wang, W., Wang, Y., Long, J., Wang, J., Haudek, S.B., Overbeek, P., Chang, B.H.J., Schumacker, P.T., and Danesh, F.R. (2012). Mitochondrial Fission Triggered by Hyperglycemia Is Mediated by ROCK1 Activation in Podocytes and Endothelial Cells. *Cell Metabolism* 15, 186-200.
- Wang, X., and Moraes, C.T. (2011). Increases in mitochondrial biogenesis impair carcinogenesis at multiple levels. *Molecular Oncology* 5, 399-409.

- Waters, A., Zhdanov, A., and Papkovsky, D. (2014). Regulation of pyruvate dehydrogenase phosphorylation by hypoxia (572.4). *The FASEB Journal* 28, 572.574.
- Weaver, V.M. (2017). Cell and tissue mechanics: the new cell biology frontier. *Mol Biol Cell* 28, 1815-1818.
- Westermann, B. (2012). Bioenergetic role of mitochondrial fusion and fission. *Biochimica et biophysica acta* 1817, 1833-1838.
- Willis, S.N., Fletcher, J.I., Kaufmann, T., van Delft, M.F., Chen, L., Czabotar, P.E., Ierino, H., Lee, E.F., Fairlie, W.D., Bouillet, P., *et al.* (2007). Apoptosis initiated when BH3 ligands engage multiple Bcl-2 homologs, not Bax or Bak. *Science (New York, NY)* 315, 856-859.
- Winklhofer, K.F., and Haass, C. (2010). Mitochondrial dysfunction in Parkinson's disease. *Biochimica et Biophysica Acta (BBA) - Molecular Basis of Disease* 1802, 29-44.
- Wu, P.H., Giri, A., Sun, S.X., and Wirtz, D. (2014). Three-dimensional cell migration does not follow a random walk. *Proc Natl Acad Sci U S A* 111, 3949-3954.
- Wu, S., Zhou, F., Zhang, Z., and Xing, D. (2011). Mitochondrial oxidative stress causes mitochondrial fragmentation via differential modulation of mitochondrial fission-fusion proteins. *Febs j* 278, 941-954.
- Xi, G., Shen, X., Radhakrishnan, Y., Maile, L., and Clemmons, D. (2010). Hyperglycemia-induced p66shc inhibits insulin-like growth factor I-dependent cell survival via impairment of Src kinase-mediated phosphoinositide-3 kinase/AKT activation in vascular smooth muscle cells. *Endocrinology* 151, 3611-3623.
- Xie, W., and Chung, K.K. (2012). Alpha-synuclein impairs normal dynamics of mitochondria in cell and animal models of Parkinson's disease. *J Neurochem* 122, 404-414.

- Xiong, S., Mu, T., Wang, G., and Jiang, X. (2014). Mitochondria-mediated apoptosis in mammals. *Protein & Cell* 5, 737-749.
- Xiong, Y., Yu, Y., Montani, J.P., Yang, Z., and Ming, X.F. (2013). Arginase-II induces vascular smooth muscle cell senescence and apoptosis through p66Shc and p53 independently of its l-arginine ureahydrolase activity: implications for atherosclerotic plaque vulnerability. *Journal of the American Heart Association* 2, e000096.
- Yagihashi, S., Mizukami, H., and Sugimoto, K. (2011). Mechanism of diabetic neuropathy: Where are we now and where to go? *Journal of Diabetes Investigation* 2, 18-32.
- Yamada, K.M., and Cukierman, E. (2007). Modeling tissue morphogenesis and cancer in 3D. *Cell* 130, 601-610.
- Yan, S., Du, F., Wu, L., Zhang, Z., Zhong, C., Yu, Q., Wang, Y., Lue, L.F., Walker, D.G., Douglas, J.T., *et al.* (2016). F1F0 ATP Synthase-Cyclophilin D Interaction Contributes to Diabetes-Induced Synaptic Dysfunction and Cognitive Decline. *Diabetes* 65, 3482-3494.
- Yaswen, P., MacKenzie, K.L., Keith, W.N., Hentosh, P., Rodier, F., Zhu, J., Firestone, G.L., Matheu, A., Carnero, A., Bilslund, A., *et al.* (2015). Therapeutic targeting of replicative immortality. *Seminars in Cancer Biology* 35, S104-S128.
- Ye, Q., Wang, T.F., Peng, Y.F., Xie, J., Feng, B., Qiu, M.Y., Li, L.H., Lu, A.G., Liu, B.Y., and Zheng, M.H. (2010). Expression of alpha-, beta- and gamma-synuclein in colorectal cancer, and potential clinical significance in progression of the disease. *Oncology reports* 23, 429-436.
- Yin, F., and Cadenas, E. (2015). Mitochondria: The Cellular Hub of the Dynamic Coordinated Network. *Antioxidants & redox signaling* 22, 961-964.

- Yokoyama, C., Sueyoshi, Y., Ema, M., Mori, Y., Takaishi, K., and Hisatomi, H. (2017). Induction of oxidative stress by anticancer drugs in the presence and absence of cells. *Oncol Lett* *14*, 6066-6070.
- Yoshida, S., Tsutsumi, S., Muhlebach, G., Sourbier, C., Lee, M.-J., Lee, S., Vartholomaiou, E., Tatokoro, M., Beebe, K., Miyajima, N., *et al.* (2013). Molecular chaperone TRAP1 regulates a metabolic switch between mitochondrial respiration and aerobic glycolysis. *Proceedings of the National Academy of Sciences of the United States of America* *110*, E1604-E1612.
- Youle, R.J., and Karbowski, M. (2005). Mitochondrial fission in apoptosis. *Nature reviews Molecular cell biology* *6*, 657-663.
- Young, K.W., Pinon, L.G., Bampton, E.T., and Nicotera, P. (2010). Different pathways lead to mitochondrial fragmentation during apoptotic and excitotoxic cell death in primary neurons. *Journal of biochemical and molecular toxicology* *24*, 335-341.
- Yu, M. (2011). Generation, function and diagnostic value of mitochondrial DNA copy number alterations in human cancers. *Life sciences* *89*, 65-71.
- Yu, T., Jhun, B.S., and Yoon, Y. (2011). High-glucose stimulation increases reactive oxygen species production through the calcium and mitogen-activated protein kinase-mediated activation of mitochondrial fission. *Antioxidants & redox signaling* *14*, 425-437.
- Yu, T., Robotham, J.L., and Yoon, Y. (2006). Increased production of reactive oxygen species in hyperglycemic conditions requires dynamic change of mitochondrial morphology. *Proc Natl Acad Sci U S A* *103*, 2653-2658.
- Yu, T., Sheu, S.-S., Robotham, J.L., and Yoon, Y. (2008). Mitochondrial fission mediates high glucose-induced cell death through elevated production of reactive oxygen species. *Cardiovascular research* *79*, 341-351.

- Zanotelli, M.R., Goldblatt, Z.E., Miller, J.P., Bordeleau, F., Li, J., VanderBurgh, J.A., Lampi, M.C., King, M.R., and Reinhart-King, C.A. (2017). Regulation of ATP utilization during metastatic cell migration by collagen architecture. *Mol Biol Cell* 29, 1-9.
- Zemirli, N., Morel, E., and Molino, D. (2018). Mitochondrial Dynamics in Basal and Stressful Conditions. *Int J Mol Sci* 19.
- Zeviar, D.D., Gonzalez, M., Miranda-Massari, J., Duconge, J., Mikirova, N., and Zeviar Edd Lac Mphcph Msln, D. (2014). The role of mitochondria in cancer and other chronic diseases, Vol 29.
- Zhang, B., Wang, J., Huang, Z., Wei, P., Liu, Y., Hao, J., Zhao, L., Zhang, F., Tu, Y., and Wei, T. (2015). Aberrantly upregulated TRAP1 is required for tumorigenesis of breast cancer. *Oncotarget* 6, 44495-44508.
- Zhang, L.N., Zhou, H.Y., Fu, Y.Y., Li, Y.Y., Wu, F., Gu, M., Wu, L.Y., Xia, C.M., Dong, T.C., Li, J.Y., *et al.* (2013). Novel small-molecule PGC-1alpha transcriptional regulator with beneficial effects on diabetic db/db mice. *Diabetes* 62, 1297-1307.
- Zhao, J., Zhang, J., Yu, M., Xie, Y., Huang, Y., Wolff, D.W., Abel, P.W., and Tu, Y. (2013). Mitochondrial dynamics regulates migration and invasion of breast cancer cells. *Oncogene* 32, 4814-4824.
- Zheng, J. (2012). Energy metabolism of cancer: Glycolysis versus oxidative phosphorylation (Review). *Oncol Lett* 4, 1151-1157.
- Zhu, L., Sun, G., Zhang, H., Zhang, Y., Chen, X., Jiang, X., Jiang, X., Krauss, S., Zhang, J., Xiang, Y., *et al.* (2009). PGC-1alpha is a key regulator of glucose-induced proliferation and migration in vascular smooth muscle cells. *PLoS One* 4, e4182.
- Zhu, M., Li, W., and Lu, C. (2012). Role of Alpha-Synuclein Protein Levels in Mitochondrial Morphology and Cell Survival in Cell Lines. *PLoS ONE* 7, e36377.

- Zu, X.L., and Guppy, M. (2004). Cancer metabolism: facts, fantasy, and fiction. *Biochemical and Biophysical Research Communications* 313, 459-465.
- World Health Organization (Aguilar et al.) Global battle against cancer won't be won with treatment alone Effective prevention measures urgently needed to prevent cancer crisis Retrieved from <http://www.who.int/mediacentre/factsheets/fs297/en/>
- Parker, M. (2017). Mitochondrial dynamics in the radiation response of cancer cells. Ph.D. University Of Cape Town.
- Reinnervatecom. (Ahmed and Prigent). Reinnervatecom. Retrieved 12 December, 2017, from <http://reinnervate.com/alvetex/alv>
- Rigby, Hannah, Frances (2011) An investigation of 2D and 3D substrates for embryonic facial process culture , Durham theses, Durham University. Available at Durham E-Theses Online: <http://etheses.dur.ac.uk/3565/>
- Shc A isoforms. <http://www.atlasgeneticsoncology.org>